Secondary materials in cement-based products

Treatment, modelling and environmental interaction

Miruna V. A. Florea

/ Department of the Built Environment

bouwstenen 192

Secondary materials applied in cement-based products

Treatment, modelling and environmental interaction

De promotiecommissie is als volgt samengesteld:

Voorzitter:	
prof.dr.ir. B. De Vries	Eindhoven University of Technology
Promotor:	
prof.dr.ir. H.J.H. Brouwers	Eindhoven University of Technology

Leden (in alfabetische volgorde):

prof.dr.ir. N. De Belie	Ghent University
prof.dr. sc. D. Bjegović	University of Zagreb
prof.dr. H. Justnes	Norwegian University of Science and Technology
prof.dr.dr. H. Pöllmann	Martin Luther University of Halle-Wittenberg
prof.dr.ir. T.A.M. Salet	Eindhoven University of Technology
prof.dr.ir. D.M.J. Smeulders	Eindhoven University of Technology

TU/e Technische Universiteit Eindhoven University of Technology

CIP-DATA LIBRARY TECHNISCHE UNIVERSITEIT EINDHOVEN

Secondary materials applied in cement-based products- Treatment, modelling and environmental interaction/ by Miruna V.A. Florea

A catalogue record is available from the Eindhoven University of Technology Library
ISBN: 978-90-386-3609-2

Bouwstenen 192

NUR 955

Ph.D. Thesis, Eindhoven University of Technology, the Netherlands

Cover design: Miruna V.A. Florea

Cover photographs supplied by the author.

Printed by: Ipskamp Drukkers, Enschede, The Netherlands

Secondary materials applied in cement-based products

Treatment, modelling and environmental interaction

PROEFSCHRIFT

ter verkrijging van de graad van doctor aan de
Technische Universiteit Eindhoven, op gezag van de
rector magnificus, prof.dr.ir. C.J. van Duijn, voor een
commissie aangewezen door het College voor
Promoties in het openbaar te verdedigen
op dinsdag 29 april 2014 om 16.00 uur

door

Miruna Victoria Alexandra Florea

geboren te Boekarest, Roemenië

Dit proefschrift is goedgekeurd door de promotor:

prof.dr.ir. H.J.H. Brouwers

Preface

This thesis is the mirror of my learning process in the last five years, and as I write these words I am beginning to realize that my study years have now come to an end. This book contains the results of all research steps I took along the way, and I invite you to discover them; this journey has not come to an end yet, as there are still open questions left to investigate and new directions to follow. However, this period in my life does come to an end now, and there are so many aspects of it that the chapters of this thesis will not reveal. I would like to take this brief space in the beginning to give thanks where thanks are due, because the overpowering feeling I get when I look back is not only one of accomplishment, but primarily one of deep gratitude.
I had help, support and advice of so many people every step of the way, it would take another volume to even briefly discuss each one; please know that my gratitude extends far deeper than the few words on these pages.

My supervisor and promotor, Jos Brouwers, deserves the first mention on this list. Jos, you offered me the PhD position the day after I defended my Engineering Diploma. It's been a journey through so many research interests and ideas, through modelling, theory, practical aspects and applications that you have guided me through. You have offered me resources, connections, your time, creativity and knowledge, for which I will always be grateful. You are still a source of information and advice I value and respect.
I would like to thank prof.dr.ir. N. De Belie, prof.dr.sc. D. Bjegović, prof.dr. H. Justnes, prof. dr.dr. H. Pöllmann, prof.dr.ir. T.A.M. Salet and prof.dr.ir. D.M.J. Smeulders for accepting to be members in my PhD committee. Thank you for offering your time and attention to this thesis; I am grateful to have you as advisors in this stage.
Two people deserve special thanks for their contribution to the research in this thesis. Koos Schenk, for your novel ideas, help with so many aspects in the laboratory, enthusiasm and humour, thank you! Arno Keulen- you have taught me so much about waste materials, about their interactions and impact, about practical aspects and overcoming challenges. Thank you for all these, for years of collaboration and sharing ideas, data, stories and laughs!
The Cement-Concrete-Immobilisates sponsor group has contributed to my research with resources and advice; I wish I had the space here to thank you all properly. I can only hope to continue and grow our collaborations in the future.
This thesis would have been very different without the contributions of Zuokui Ning and Guillaume Doudart de la Grée. You brought a focus on practical aspects, generated results and ideas, tested hypothesis and, through the whole process, taught me so much! Being the supervisor of your graduation projects made me a better teacher and a better colleague; I appreciated your enthusiasm and dedication, and it has been a joy to work with you. Pei Tang, and later also Guillaume- I have learnt a lot through supervising your

PhD projects from the beginning. To me, teaching is a joy and working with the three of you and seeing your progress brought me incredible pride- thank you!
I have had support both in the laboratory and in the office, which has made my work efficient and pleasant. I would like to thank the whole laboratory staff of BPS for so many hours of help, and especially to Peter Cappon, for the generous time and attention he invested in my project. The secretary's office and the reception staff of Vertigo- you have also made so many things run smoothly and efficiently for me- thank you! and especially to Renée van Geene, who has been a friend every step of the way and Janet Smolders who is always there to offer help and a smile.
My gratitude extends also to the Science and Engineering of Oxidic Materials and Nanomaterials department of the Faculty of Applied Chemistry and Materials Science of the University "Politehnica" of Bucharest- to the professors who have kindled my passion for the world of materials science and paved the way towards this PhD.

I am grateful for the role that the PhD Network Bouwkunde has played in my life in Eindhoven- all the members, and especially my fellow board members have become an important part of my life as a PhD student. Thank you Bart, Oliver, Lisje, Daniel, Aida, Rubina, Roel, Zara, Zahra, Ifigenia, Widi- and so many others- for your friendship, enthusiasm and the good times we shared!
A special word of thanks goes to Wolfram Schmidt and the whole SPIN consortium- it has been an honour and a pleasure to work with you. Our collaboration has taught me so many wonderful lessons, and I only hope we will stay in contact in the future.
The group of Building Materials has many members, and my fellow PhDs and researchers have shared almost every day of the last 5.5 years with me. Alberto, Ariën, Azee, Bo, Chris, George, Götz, Guillaume, Katrin, Martin, Milagros, Qingliang, Pei, Perry, Przemek, Rui, Štěpán, Xu- we have worked, talked, travelled, laughed and partied together, and I am grateful to each and every one of you for more things that I can list here. Przemek and Qingliang- I have worked with you the longest and the closest, and you have been a great help during the writing of this thesis- you deserve your own acknowledgement and thanks.

I am extremely lucky to have a group of friends that have stayed with me through time and distance, through ups and downs- through everything. I am immensely thankful for your friendship, patience and love, for your encouragement when I needed it and for braving the distances repeatedly to be at my side for all happy occasions. You are my family and having you in my life makes all the difference in the world. Thank you!
My parents would deserve their own acknowledgements section; they have supported my every ambition and provided all help humanly possible every day of my life. You have sacrificed so much to always be next to me and I will never be able to show the extent of my love and my gratitude. All my achievements are a tribute to you, this thesis included.

It contains also your time, your love and your patience throughout all my study years and I see your contribution on every page. Thank you!

I have not started my PhD journey alone. I have had next to me, for the past 12 years, the most caring, patient, trustful and supportive person in the world. Dany, you are my strength and my courage, the gentle love that guides my whole life. You wrote your thesis at the same time with me, and now we will embark on a new adventure together- with all the love and trust, sincerely, from the heart and forever.
I must confess now that this thesis has a second author, who has thought and written each word together with me. Andy, the first completed draft of this thesis is merely one day older than you. You are my greatest gift and joy and your laugh lights up each one of my days- and nights. You are the heart of my heart, and you have given me the enthusiasm and perspective needed every day of writing and correcting this thesis, which should really have your name on the cover as well.

Miruna Florea

Eindhoven, December 2013

Contents

Chapter 1

Introduction

1.1 Environmental impact of concrete

The most produced material worldwide is concrete - twice as much is used in construction around the world than the total of all other produced materials, including wood, steel, plastic and aluminium. The annual global production of concrete is about 3.8 billion cubic meters [1]. The main constituents of concrete are cement, aggregates (sand and gravel) and water. Ordinary Portland Cement (OPC) and natural aggregates (limestone, quartz etc.) are considered primary materials for concrete mixes. Streams of secondary materials can be used to replace primary materials; these include supplementary cementitious materials for the replacement of cement (ground granulated blast furnace slag and coal combustion fly ash being the most common ones) or of the aggregates (recycled concrete particles, mining waste streams etc.). The manufacture of concrete requires ~ 0.7 GJ/ton of energy, when only the cement production, aggregate use and plant operation are taken into consideration [2]. Transport costs, for instance, will further increase this value. Around 8-12% of the concrete composition is cement, with an global production of 3.6 billion t in 2011 [3]. Producing one ton of cement requires about 2 tons of raw materials (limestone and shale) and consumes about 4 GJ of energy in electricity, process heat, and transport (the energy equivalent to 131 cubic meters of natural gas). Moreover, producing one ton of cement generates approximately one ton of CO_2, 3 kg of NO_x and ~ 0.4 kg of PM10 – an airborne particulate matter that is harmful to the respiratory tract when inhaled. It is estimated [4] that cement contributes ~ 4% of global CO_2 emissions just through the decomposition of limestone, and another 4% from fuel combustion, adding to roughly 8% of global CO_2 production. Therefore, the replacement of cement with other supplementary cementitious materials in concrete mixes is beneficial for the environment. Moreover, using waste products to replace concrete components brings a new dimension besides environmental impact- the sustainability of the material, by reducing the amount of natural raw materials needed. Examples of such replacement materials are recycled concrete aggregates and municipal solid waste incineration bottom ash for the larger particles needed for concrete, and fly ashes, ground granulated blast furnace slags, sludges and recycled concrete fines for the replacement of the cement. One of the drawbacks of using industrial by-products in concrete is the possible introduction of unwanted constituents, like chlorides, sulphates, or some heavy metals. While the latter are known to be bound by the cementitious matrix sufficiently, chlorides are the main cause of structural damage in reinforced concrete

structures. Therefore, a number of ways in which the environmental impact of concrete production can be reduced become apparent:

1. Employing sustainable energy sources;
2. Increasing the durability of concrete structures;
3. Upgrading recycled concrete as a new building material;
4. Incorporating industrial by-products in new concrete recipes;

All these approaches can come together in more ways than one. Alternative energy-generating processes, for instance the incineration of municipal wastes or biomass, also produce materials which can be used as additions in concrete. Intelligent processing of the construction and demolition waste can generate new materials for the production of clinker and also recycled aggregates that can replace the natural gravel in concrete and thus contributing to its sustainability. The use of industrial by-products can contribute to the durability of concrete, by increasing its mechanical properties or its resistance to aggressive environments, like for instance chloride attack in coastal areas. The aim of this thesis is to bring together all these aspects and show their benefits in lowering the environmental impact of concrete.

1.2 Sustainable energy production

The macroeconomic survey "bio based economy" performed in the Netherlands on behalf of the Energy Transition Platform for Green Materials concludes that large scale application of biomass for power generation might have a huge environmental benefit and longer-term positive economic impact of 5 and 8 billion Eur per annum. Biomass is considered a sustainable and renewable resource that can replace fossil fuels like coal and gas. Being a part of the CO_2 cycle, it reduces the CO_2-emission because of its "carbon neutral" origin. Thus, CO_2 released in converting biomass into energy does not contribute to the increase of the greenhouse effect. Therefore, biomass complies with the objective of the government for the reduction of the CO_2 emission and increased independency from fossil fuels. Furthermore, using waste as fuel, instead of using it as landfill, is more favourable for the environment because of preventing the emission of methane from landfills. The landfill generated gas methane is a greenhouse gas which is about 20 times more harmful than CO_2. Therefore, the amount of the land filling with biodegradable waste and hence, the landfill gas emissions are being reduced in recent years. Between 1990 and 2006 the annual emission of landfill methane has decreased by more than 300 kton, from 572 kton methane in 1990 to 257.6 kton in 2006. This corresponds to about 6 Mt CO_2 in equivalent [5].
The Copernicus Institute (Utrecht University), in cooperation with the Agricultural Economics Institute LEI (Wageningen UR), conducted a study on the economic effects of biomass. The survey provides some long-term macroeconomic scenarios for the use of

biomass for bio-fuels, chemistry and electricity generation [6]. The scenarios are designed for situations with high and low amount of biomass imported to the Netherlands from European countries and for situations with high and low levels of technological development. The study encourages the ministry to pursue the scenario of high technology developments in the large-scale import of biomass. The predicted effects of such a scenario by 2030 are: an additional annual turnover of 5 and 8 billion Eur, 25% of the fossil fuels are being replaced by biomass, reducing greenhouse gas emissions by about 25%.

Every year the potential of bio-power plants is increased due to the reasons stated above. According to the recent Energy Report 2011 [7], the Netherlands is less dependent on fossil fuels and gradually switching to renewable energy. Figure 1.1 illustrates the breakdown by source of the total renewable energy production between 1990 and 2010.

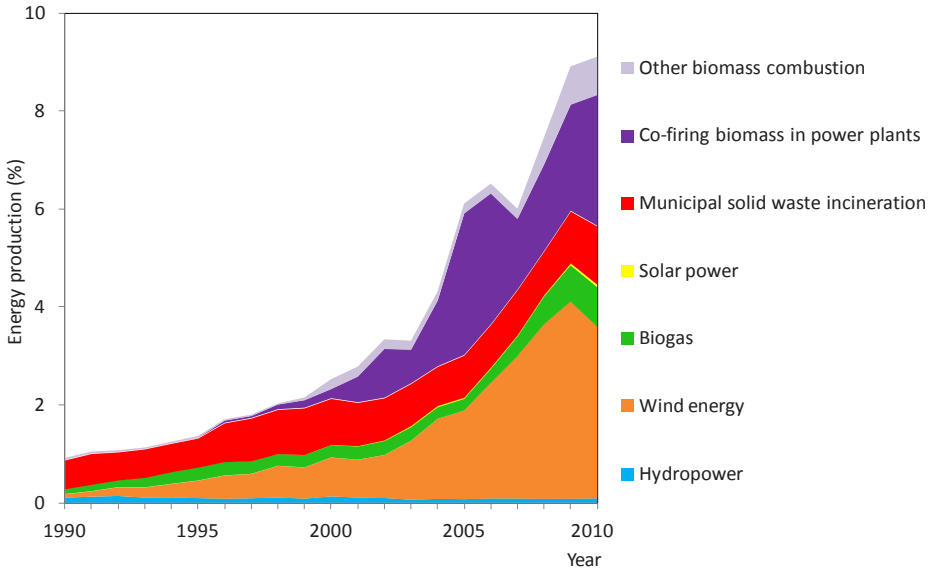

Figure 1.1. Renewable electricity between 1991 and 2010 [7].

The incineration of biomass produces bio-energy fly ashes, which are investigated in this thesis. Another incineration process, of paper sludge from the paper recycling industry, produces paper sludge fly ash, which is also the focus of one of the chapters. Municipal solid waste incineration also generates a type of ashes which can be a beneficial addition in concrete recipes and is also addressed in this thesis.

1.3 Durability of concrete

Reinforced concrete structures in coastal areas or which are periodically exposed to de-icing salts mainly deteriorate because of the attack of chloride ions. The chloride ions, responsible for the initiation of the corrosion mechanism, intrude from the external medium into the concrete. Another possibility is the so-called "internal chlorides"- chloride ions added to the concrete at the time of mixing. The source of such internal chlorides can be industrial by-products used to replace either the cement or the aggregates in the concrete mixture, since brackish water is not allowed to be used in concrete. Regardless of the way the chlorides enter the concrete matrix, a part of these chloride ions will be retained by the hydration products of the binder in concrete, either through chemical binding or by physical adsorption. These retained chloride ions are generically referred to as "bound chlorides". Chloride ions that are not bound by hydration products (termed "free chlorides") are able to travel through the pore solution of the binder matrix to the level of the rebars.

Chloride binding is a research topic of interest for various reasons, the most important being evaluation of corrosion of steel reinforcement due to chloride ingress in concrete structures. Other reasons include studying the hydration rate of cement in the presence of chloride ions and expansion caused by chloride reactions with hydration products. Another purpose for this kind of investigation is to accumulate data in order to be able to predict the chloride ingress into concrete, using different numerical methods.

When a certain threshold concentration of chlorides is reached at the concrete-reinforcement interface, the corrosion of the steel rebars is initiated. A part of the intruding chloride ions will be retained by the hydration products of the binder in concrete, either through chemical binding or by physical adsorption. Therefore, chloride binding can delay the achieving of the threshold chloride concentration at the level of the reinforcement by removing chloride ions from the pore solution.

Quantifying the chloride binding process helps predict the service-life of reinforced concrete structures exposed to chloride attack, and allows for a better planning of their maintenance and repair periods. Another important purpose of studying chloride binding is the design of new cement mixes that are able to slow down chloride intrusion, thus improving the durability of future marine structures.

Since the hydration products of cement are responsible for the chloride binding in concrete, this study will focus on the chloride binding in hardened cement paste. A new reaction model will be used in order to predict the hydration products and their relative amounts in a hardened OPC paste. The final scope is to develop an algorithm in order to evaluate the chloride binding capacity of a given cement paste. Two main chloride binding mechanisms – through physical adsorption and through chemical reactions- will be taken into account.

The second part of the study deals with the chloride binding in ground blast furnace slag-blended cements, which are the most used cement types in the Netherlands. Due to the

use of this by-product, this cement has a lower energy footprint. The impact of the different phase assembly of the hydration products on the chloride binding will be evaluated. The amount of slag mixed with Portland cement is one of the main parameters taken into consideration. This is yet another example of how industrial by-products have a beneficial impact on the durability of concrete.

1.4 Recycled materials

The disposal of wastes can be categorized by environmental impact levels into 6 levels, according to [8]. These levels are, in order starting with the most important: reduce, reuse, recycle, compost, incinerate and landfill. Three most important levels (reduce, reuse, recycle) are referred to as ”the 3Rs”. The rates of waste recycling vary greatly across the globe. As it can be seen from Table 1.1 [9], construction and demolition waste (C&DW) are among the least recycled materials within the European Union, while in the US or Japan the rate of recycling is much (more than 2.5 times) higher.

Table 1.1. The recycling rate of different materials in Europe, the US and Japan [9].

Material	Recycling rate Europe (%)	Recycling rate US (%)	Recycling rate Japan (%)
Concrete/ C&DW	30	82	80
Aluminium beverage cans	58	52	93
Aluminium in buildings	96	N/A	80
Glass containers	61	22	90
Lead acid batteries	95	99	99
Paper/cardboard	63	56	66
PET bottles	39	24	66
Tires	84	86	85
Steel containers	66	63	88

1.4.1 Construction and demolition waste

When comparing recycled concrete aggregate (RCA) to new aggregate, a number of factors need to be taken into account [9]. A first factor is the land use impact – the use of recycled aggregate means that less waste goes to landfill, while also reducing the need of producing primary aggregates. Another important factor is the transportation cost

(including fuel usage and CO_2 emissions), which can be much lower than in the case of new aggregates, if the C&DW is located close to the construction site. New aggregates are usually transported from distant quarries to the construction site. Also to be mentioned are the useful life expectations- using recycled aggregates meaning that the concrete itself has a longer period of use than the structure it was initially part of.

Table 1.2. The total and recovered construction and demolition waste (C&DW) in Mt, (N/A= not available) and the percentage of recovery of CD&W [9].

Country	**Total C&DW (Mt)**	**Total C&DW Recovery (Mt)**	**%C&DW Recovery**
Australia	14	8	57
Belgium	14	12	86
Canada	N/A	8 (recycled concrete)	N/A
Czech Republic	9 (incl. 3 of concrete)	1 (recycled concrete)	45 (concrete)
England	90	64	50-90
France	309	195	63
Germany	201	179	89
Ireland	17	13	80
Japan	77	62	80
Netherlands	26	25	95
Norway	N/A	N/A	50-70
Portugal	4	Minimal	Minimal
Spain	39	4	10
Switzerland	7 (incl. 2 of concrete)	2	Near 100
Taiwan	63	58	91
Thailand	10	N/A	N/A
US	317	127 (recycled concrete)	82

The economic benefits of recycling and minimizing waste volumes are mentioned in [8]:

1. Reducing the volume of materials going to landfills;
2. Free removal of the waste from site;

3. Selling the new recycled products.

Tam [8] also identifies the main reasons for the increase of the volume of demolition concrete waste:

1. old structures have overcome their use expectancy and need to be demolished;
2. new requirements and necessities lead to the demolition of otherwise still viable structures;
3. natural destructive phenomena (earthquakes, storms).

In the report on "Recycled concrete" [9] there is a breakdown of C&DW recycling on European countries, between others. Table 1.2 shows the total C&DW in Mt, the recovered C&DW and the percentage of recovery for these countries. Among the total C&DW recovery, recycled aggregate accounts for 6% to 8% of aggregate use in Europe [9]. The greatest users are the United Kingdom, the Netherlands, Belgium, Switzerland and Germany (data from 2005 and 2006, published in 2008 [9]).

1.4.2 Recycled concrete aggregates

The different sources for recycled concrete aggregate are identified by Oikonomou [10] as either recycled precast elements and cubes after testing or demolished concrete buildings. In the first case, the aggregate should be relatively clean, with only the cement paste adhering to it. In the latter case, the aggregate could be contaminated with salts, bricks and tiles, sand and dust, timber, plastics, cardboard and paper, and metals. It has been shown that even contaminated aggregate, after separation from other waste, and sieving, can be used as a substitute for natural coarse aggregates in concrete.
The RILEM specifications for RCAs are given in [10]. There are three types of RCAs, depending on their origin:

1. Type I which consists primarily from masonry rubble;
2. Type II which consists primarily from concrete rubble;
3. Type III which consists of a blend of recycled aggregates (max. 20%) and natural aggregates (min. 80%).

BRE Digest 433 specifies similar classes, based on the RILEM categories:

1. RCA (I), origin: brickwork, brick content: 0–100% mass;
2. RCA (II), origin: concrete, brick content: 0–10% mass;
3. RCA (III), origin: concrete and brickwork, brick content: 0–50% mass.

Besides the recycled aggregates, also the recycled concrete fines can be re-used as building material, especially when cement paste and aggregates can be better separated.

This thesis shows how, through a smart crushing method, the quality of both the recycled concrete fines and larger particles can be improved. The possibility of using recycled concrete fines as cement replacement is also investigated, in order to complete the cycle of concrete recycling into new concrete.

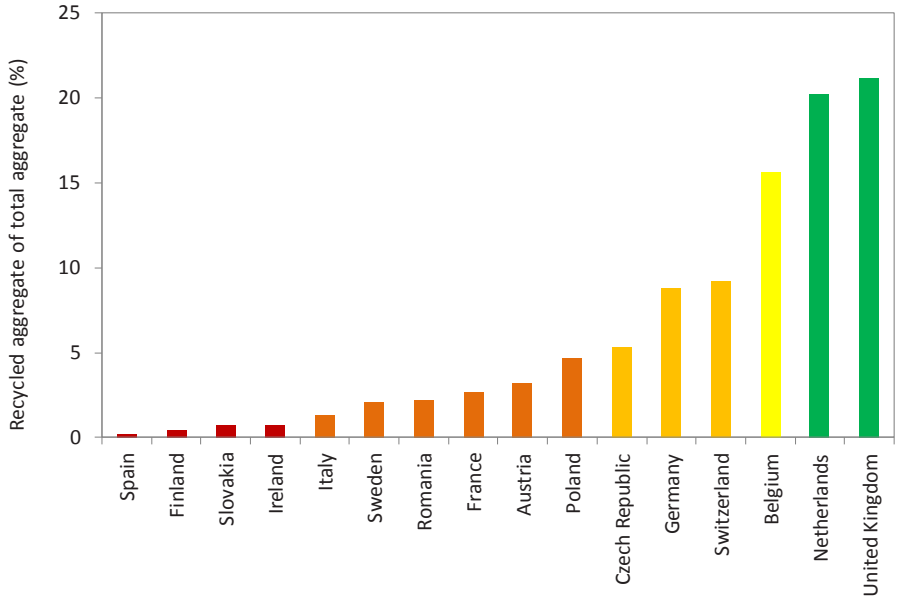

Figure 1.2. Recycled aggregate fraction of total aggregate use in European countries [9].

1.5 Supplementary materials in concrete

Both Portland cement and blended cements are used in the Netherlands, with more than 75% of the total consisting of blended cements (mainly CEM II, CEM III and CEM V). The strength classes produced are 32.5N and R, 42.5N and R and 52.5N and R. Table 1.3 gives the breakdown for cement use in the Netherlands, both locally produced and imported. The most used cement types in this thesis are CEM I 42.5N and CEM I 52.5N, CEM III/B 42.5N which contains 20-34%clinker and 66-80% ground granulated blast furnace slag, according to EN 197-1 [11]. A Cem I- fly ash blend containing 21% fly ash is also employed, which is similar to a CEM II/B composition.

1.5.1 Supplementary cementitious materials

Fly ash and granulated blast furnace slag are two kinds of industrial by-products; both of them are being used in construction industry as cement replacement materials. Fly ash and slag have some common characteristics with Portland cement. For instance, their

particle size range is similar to or smaller than that of the Portland cement; they can be involved in the hydration reactions; their chemical compositions are similar to that of Portland cement but with different proportions. Based on the similarities, they can be added to the cement clinker to make fly ash cement or slag cement. Moreover, they can be dosed as individual materials directly to the concrete at mixing [12].

Table 1.3. Breakdown of cement types sold in the Netherlands (data from 2008, provided by ENCI BV).

Cement type	**ENCI BV**	**Cemex, Dyckerhoff, Holcim, CCB**
CEM I (95-100% clinker)	1122995 t	663518 t
CEM II (65-95% clinker)	92612 t	64928 t
CEM III (5-64% clinker) Blast furnace slag cement	2053403 t	1079813 t
CEM V (20-64% clinker)	74901 t	0 t
Total	3343911 t	1808259 t
	5152170 t	

Fly ash and slag can display pozzolanic behaviour, while slag is also latent hydraulic. Illston [13] defines that "a pozzolanic material is one which contains active silica (SiO_2) and is cementitious in itself but will, in a finely divided form and in the presence of moisture, chemically reacts with calcium hydroxide at ordinary temperatures to form cementitious compounds." The key to the pozzolanic behaviour is the structure of the silica; this must be in a glassy or amorphous form with a disordered structure, which is formed in a rapid cooling from a molten state. A uniform crystalline structure which is formed in slower cooling, such as is found in silica sand, is not chemically active. Fly ash and slag are usually used to partly replace Portland cement to make the binder materials for construction industry (Table 1.3).

Both fly ash and slag have lower specific gravities than Portland cement, and when used to substitute cement on a weight-for-weight basis will result in a greater volume of paste. Both high lime fly ash and slag contain significant quantities of CaO which also take part in the hydration reactions. Therefore, both of them are to a certain extent self-cementing, thus they are more hydraulic than pozzolanic [13]. The presence of cement acts in a way like a catalyst to speed up the hydrations of fly ash and slag. When fly ash and slag are

used to replace Portland cement, sufficient Portland cement has to be in the mixture in order to supply enough calcium hydroxide for the secondary reactions.

Ground granulated blast furnace slag

Slag, or ground granulated blast furnace slag, is the unwanted part of pig iron from the steel industry suddenly cooled down by water. It is ground to a similar fineness as Portland cement. Slag has a higher silica content and a lower calcium content than Portland cement.

In order to be used in concrete the molten blast furnace slag is cooled with water to produce a glassy state solid. After drying it is crushed and ground in to very powder which is called ground-granulated blast-furnace slag (GGBFS). The composition and properties of the blast furnace slag are dependent on the process and products of the pig iron production process, and mainly consists of silica, alumina, calcium oxide, and magnesia. In Europe EN 15167-1 [14] regulates the properties (chemical and physical requirements, finess, moisture content, durability requirements and emissions) of ground granulated blast furnace slag in concrete, mortar and grout. In the US, three classes of GGBFS are distinguished according to the ASTM C989 [15] by their respective mortar strength when they are mixed with equal mass of Portland cement. The three grades are 80, 100, and 120, depending on the impact on the compressive strength of the concrete. GGBFS use results in slower strength development of the concrete and therefore also lower heat evolution and early strength [16], but an increased strength over a long time period is achieved. Slag-blended cements are investigated in this thesis in several ways. Initially, their impact on the chloride binding ability of hardened cement pastes is studied. Further, the blending of slag, Portland cement and recycled concrete fines is studied.

Fly ashes

Since ancient times, Romans, Chinese and Indians have used volcanic ashes and other similar natural and man-made materials to produce cementing materials by mixing with lime, volcanic ashes and pulverized burned bricks. In this way they produced cementitious mortars for the construction of ancient monuments that are still in existence today [17]. The term “fly ash” first appeared in literature in 1937. However, from 1914, data about the use of finely pulverized powdered coal (fly ash) as a pozzolan in concrete had been already published [17].

Fly ash can be described as a fine material precipitated from the stack gases of burning solid fuels. In Europe the ash was always referred to as pulverized fuel ash, but in the United States this ash was termed fly ash because it escaped with the flue gasses of coal-fuelled power plants and “flew” into the atmosphere.

There are many types of fly ash produced from different installations:

1. Coal combustion fly ash, from 1882, design Thomas Edison [18];
2. Bio-energy fly ash, since 1971 [19];
3. Paper-sludge fly ash, since 1990 [20];
4. Municipal Solid Waste Incineration (Destructor) fly ash, since 1874 [21].

All these types of fly ashes are studied within this thesis and their impact on the properties of mortars is evaluated. Blending of these fly ashes, Portland cement and recycled concrete fines is also investigated.

The current annual production of coal combustion fly ash is about 600 million tons (in 2000) and forms 75-80% of the total ash production worldwide. Only ~ 9% of this production is recycled worldwide [22]. The rest is landfilled, but this is not economically desirable because of high landfill costs, and environmental risks such as leaching to the ground, thereby creating water and also air pollution. However, the government of the Netherlands aimed to reuse the produced coal combustion fly ash from the beginning. This goal was achieved in 1988, when from the annual production of 712400 tons fly ash, 98% was reused. This percentage represents the highest amount in the world [23]. In 2007, 814717 tons of fly ash were produced: 506139 tons of fly ash were used as cement filler and concrete mixtures and 88054 t of fly ash were used in the production of pozzolanic cements. In total, this forms 73% of fly ash production [24].

Fly ash is generated in combustion processes and rises with the flue gasses after combustion, the ashes that do not rise with these flue glasses are called bottom ashes and can also be used in concrete mixtures. Fly ash can contain various substances; therefore the exact origin of the fly ash is of great influence on its performance when added in the concrete. The European standard EN 450 [25] gives the criteria for the selection of fly ash; only fly ash with certain particle size, (maximum 40% retention on the 45 μm sieve for class N and respectively 12% for class S) and chemical composition and loss on ignition values (under 5% for class A, between 2 and 7% for class B and between 4 and 9% for class C) can be used in concrete production. The ASTM C618 [26] classify fly ash based on the lime content. Two classifications of fly ash are produced, fly ash type C and type F, where the key difference between these classes is the amount of calcium, silica, alumina, and iron content in the ashes. Class C fly ash contains more than 20% lime, where it is less than 20% in type F fly ash, keeping in mind that the origin and properties of the combustion material are key factors that determine the parameters of the fly ash, and therefore its performance when added to the concrete mixture. Finally, the amount of fly ash determines the class of cement according to the EN 197-1 [11] standard. Fly ash addition to concrete results in increased workability and similar to GGBFS a slow reaction time and increased strength over a long time. Also, the w/c ratio is reduced when fly ash is applied to the concrete mix.

Using fly ash in new concrete can be beneficial for the environment, since landfilling is not required and less cement needs to be produced. The other advantage of using fly ash

in concrete is that it slows down the hydration process and so reduces the hydration heat accumulation, which makes it good for bulky constructions to reduce heat related cracking. However, the hydration of fly ash does take a longer time to start than Portland cement. In the construction industry often a high construction speed is desired, which often corresponds with rapid hardening.
In the case of both fly ashes and bottom ashes, the main issue to be taken into consideration before their application in concrete mixtures is their environmental impact. Leaching standards have been devised for quantifying the emissions of unwanted contaminants from waste materials (EN 12457 [27]). In the Netherlands, there are two legislative documents that regulate the use of waste materials – Landfill Ban Decree [5] and the Soil Quality Regulation [28]. The Landfill Ban Decree classifies waste streams into inert, non-hazardous, hazardous and no landfill materials, according to their emission level. The Soil Quality Regulation uses similar criteria to divide materials destined to be used in the built sector into non-shaped, shaped and IBC materials (which need to undergo insulation, management and control measures). These requirements will be detailed in Chapter 6 and will be applied to all incineration waste streams applied throughout this thesis.

1.6 Hypotheses and structure of the thesis

This thesis brings together a number of approaches for lowering the environmental impact of concrete. The topics of durability, sustainable energy, reuse of industrial by-products and the recycling of demolished concrete are studied both individually and then used in combination for a more complete image of their influence in cement-based recipes.
The following hypothesis and sub-hypotheses are formulated for this thesis:

"How can supplementary materials be applied in cement-based products in order to lead to sustainable development in the Netherlands?"

- Is the composition and amount of ground granulated blast furnace slag in blended cement a key factor for the chloride binding ability?
- How can the aggregate recycling process be further developed and optimized?
- Which type of incineration by-products from the Netherlands can be used as cement replacement?

The questions to all these hypotheses can be found in Chapter 10, as well as in more detail throughout the contents of this thesis. Figure 1.3 presents the connections between all chapters of the thesis.
Chapter 2 deals with the binding of chloride ions. The case of the chloride attack is considered through modelling, correlating the total amount of chloride bound in concrete

with the amounts bound by different hydration products. New insights in the quantities of the hydration products formed during the hydration of Ordinary Portland Cement are used in order to predict the phase assemblage of hardened cement pastes. The two main chloride binding mechanisms were considered – through physical adsorption and through chemical reactions are considered.

Chapter 3 is a continuation in the binding assessment. The OPC chloride binding model is extended to slag-blended cements, which are known for their superior capacity to bind chlorides. An improved hydration model of slag-blended cements, taking into account new insights, is to estimate and quantify the hydration products of slag-blended cements. Individual chloride binding isotherms were used to correlate these amounts of hydration products with the amount of bound chlorides.

Chapter 4 deals with the lifecycle of concrete, by considering the reuse of demolished concrete. Recycled concrete aggregates are mainly used for road construction, but another interesting application would be their incorporation into concrete mixes. So far, such an application is hindered by the loss of mechanical properties of recycled aggregates concrete. However, through an efficient crushing technique (termed "smart crushing"), recycled concrete can be a beneficial addition. This study deals with properties (particle size distribution, density, thermal treatment reaction, oxide and mineralogical composition) of a large number of recycled concrete fractions, obtained through three crushing methods.

Chapter 5 focuses on the upgrading of recycled concrete fines (RCF) obtained from smart crushing to replace part of the cement in new mortar recipes through a thermal treatment method. If a certain amount of cement can be replaced by recycled concrete fines, it will increase the recycled material application level and thus help CO_2 environment protection and natural resources preservation. Mortar samples are tested by following the European standard EN 196-1 [29] to keep the test conditions constant. RCF treated with different temperatures are used to replace part of the cement in the standard mortar samples containing either OPC or slag- or fly-ash blended cements.

Chapter 6 continues the study on supplementary cementitious materials, this time using incineration by-products from sustainable energy production. The first aim is to combine four different bio-energy fly ashes from bio-energy power plants in concrete mixtures. In order to do this, the bio-energy fly ashes are extensively characterized, and their environmental impact evaluated.

Chapter 7 deals with the roles of the previously studied bio-energy fly ashes in a concrete mixture as a binder (partly or totally replacing cement) or filler. By using different treatment techniques like crushing, thermally and water treating, bio-energy fly ash is upgraded to a material comparable with commercial fly ash. After assessing their leaching behaviour, the bio-energy fly ashes are extensively tested in terms of their effect on the mechanical properties of mortars in which they are used as cement replacement.

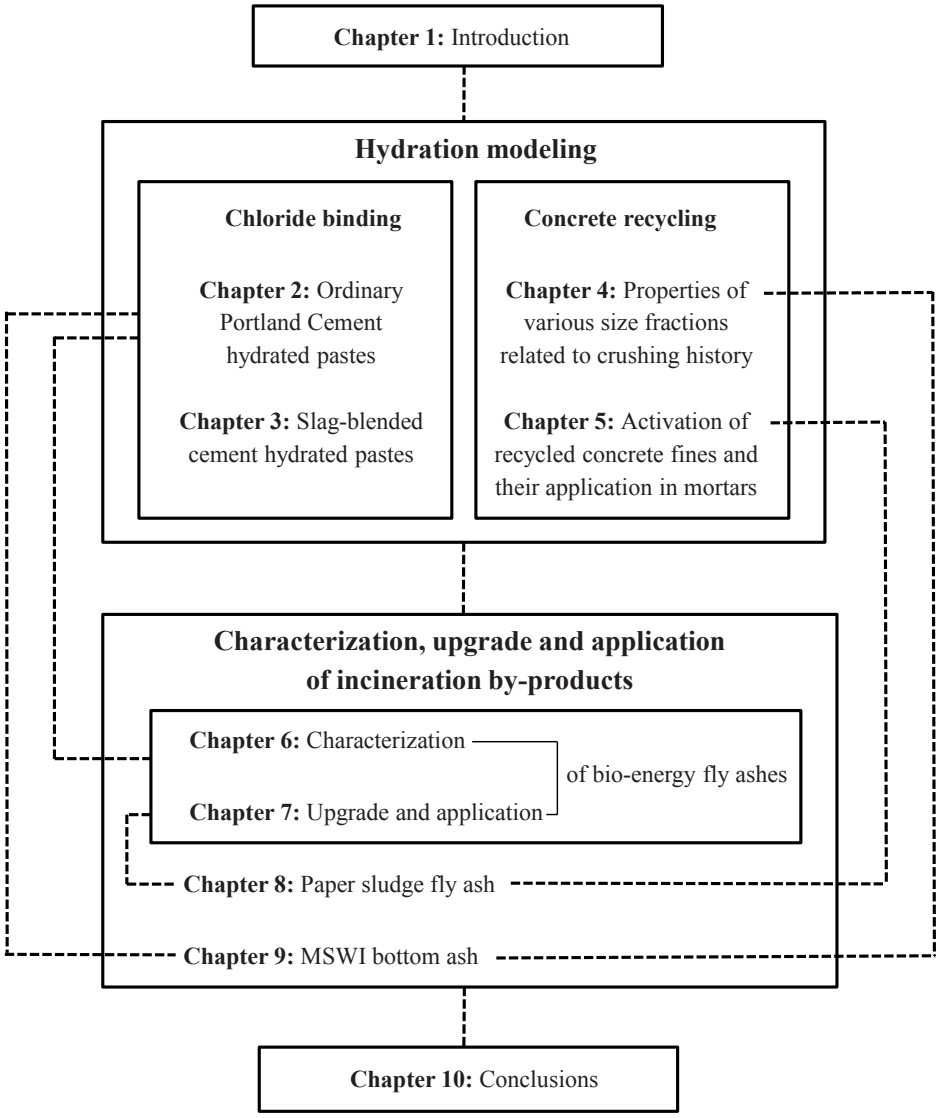

Figure 1.3. Structure of the thesis.

Chapter 8 focuses on yet another type of fly ash - paper sludge fly ash, which is a by-product from the recycling of paper. Challenges for its use in concrete are the increased water demand and content of free lime, which may reduce the properties of concrete. The upgrading of the paper sludge fly ash is attempted through two different methods. It is

found that paper sludge fly ash has a positive effect on the hydration of coal combustion fly ash and can by this increase its own utilization.
Chapter 9 approaches another incineration waste stream, MSWI bottom ashes. Several materials, generated from various MSWI incinerators in the Netherlands are investigated. Three treatment lines were used to generate materials that would comply with the requirements of the Soil Quality Regulation [28]. Successive test programs lead to the application of MSWI bottom ash from laboratory-made concrete to industrial applications on the waste treatment plant, to a kerb stones pilot test.
Chapter 10 concludes this thesis, by summarizing the main conclusions and proposing further research topics which can advance the understanding in the field of reducing the environmental impact of concrete.

Chapter 2

Chloride binding related to hydration products - Ordinary Portland Cement*

2.1 Introduction

Chloride attack is the main cause of structural damage in reinforced concrete buildings exposed to marine environments or de-icing salts. The corrosion of the rebars is triggered by the propagation of the chloride ions through the pore solution to the reinforcement level. The intruding chloride ions can be either bound by the hydration products of the binder in concrete, or they can exist as free ions in the pore solution. Therefore, the ability of a concrete structure to resist chloride attack depends among others on its capacity to bind chloride ions [30–32].

There are several factors that influence chloride binding. Perhaps the most important one is the way chloride ions are added to the concrete mix. Using this criteria, chloride ions can be divided in two categories: internal chlorides (when the chloride solution is intermixed with the cement powder [33–35]), or external chlorides (when chloride ions intrude in already hardened cement paste or concrete [35–38]). Since the amount of internal chlorides is restricted and their use is currently discouraged, this study will focus on external chlorides, as the more frequent situation in practice.

There is an important distinction to be made between the different sources of chloride ions. The most studied two salts are calcium chloride and sodium chloride, which give different results due to their differences in the binding mechanisms of the Cl^- ion [35,39,40]. This study deals with NaCl as the source of the intruding chloride ions, for several reasons. The first reason for this choice is that NaCl is the source of chloride ions in marine environments, the most frequent environment for chloride attack on reinforced concrete structures. The typical concentration of NaCl in seawater is fairly constant (e.g. the Atlantic Ocean: 3.6% mass, the North Sea: 3.3%, the Persian Gulf: 4.3%) [41]. These concentrations (between 3.3 and 4.3%) correspond to a range of 0.6-0.7 mol Cl^-/l seawater. Another reason for investigating NaCl as a source of chloride ions is its use in the rapid chloride migration (RCM) test. This widely-used accelerated test for determining chloride ingress into concrete uses a value for the concentration of the external solution of 1.83 mol NaCl/l immersion solution [38,42–44]. Furthermore, in the case of salty lakes, the chloride concentration can be over 3 mol/l [45]. In order to

*The content of this chapter was published in *Cement and Concrete Research* **42**, 282-290 (2012).

incorporate all values mentioned above, the range of NaCl concentration used in this study is 0-3 mol/l.

Researchers have studied chloride binding using various approaches. Some studies dealt with existing concrete structures [46,47], while others preferred the use of mortars, due to their less complicated structure [38,48]. The method that produces the best results is to use cement paste, in which the presence of aggregates cannot interfere with the measurements [38,49,50]. Another approach was to study pure hydration products [36,37,51,52]. Through this method important information about the mechanisms through which single hydration products bind chlorides were gathered. This study will use data collected in literature through most of these methods to predict the chloride binding of cement pastes.

Ordinary Portland Cement (OPC) is chosen as binder throughout the study, since it is the most abundantly used cement type and the most basic system in terms of hydration modelling that still contains all phases involved in chloride binding. Other cementitious materials studied in literature include grounded blast furnace slag, fly-ash or silica fume [31,35,45,53,54]. All these materials have different hydration mechanisms and will not be considered in the present chapter, but will be addressed in Chapter 3.

The two main chloride binding mechanisms – through physical adsorption and through chemical substitution- were considered, along with estimating the amount of chloride in the pore solution. Out of the considered hydration products in OPC hardened pastes, two hydrated phases are best known to be able to bind chloride ions - the calcium silicate hydrate ($C-S-H$) phase [36,38] and the AFm phase [34,36,37,55,56]. Beside these, the chloride binding capacity of portlandite and ettringite are debated in literature [37,48,57,58]. Friedel's salt, a compound formed through the interaction of AFm phases and chloride, is considered to be also able to physically adsorb chlorides on its surface [59].

2.2 The paste model

The three main phases of a hardened cement paste (unreacted cement, unreacted water and its hydration products) and the porosity can be studied in terms of mass and volume for a given hydration degree. When clinker phases hydrate individually, so not in combination with others, their degree of hydration can vary significantly. This is important when considering the hydration degree of individual phases rather than OPC. On the other side, for longer curing times, clinker minerals can be considered to react more or less congruently when hydrating together in cement pastes [60]. For the hydration of OPC pastes, a global degree of hydration can be assumed for all clinker minerals, when hydration has progressed over 50% [61,62]. Typical hydration kinetics at ambient temperature for pure clinker minerals (C_3S, C_2S, C_3A with and without added gypsum, C_4AF), as well as for an OPC, are given in [60]. Another important point to

consider is that the hydration degree will increase with the increase of the water to binder (w_0/b_0) ratio used for the hydration of an OPC paste [63].
In order to predict the hydration products formed, a recent model proposed by Brouwers [61,62] will be used. The reactions that apply to the saturated hydration of OPC are presented in Table 2.1.
These reactions assume no carbonation of the paste has taken place. While the model of Brouwers [61,62] allows for different carbonation degrees, this option has not been taken into consideration in the current study, as explained further in Section 2.4.1. The relations in Table 2.2, which are deduced from the chemical equations in Table 2.1, can be used to calculate the molar amounts of hydration products.
These are the maximum amounts that can be formed after a complete hydration of cement. Since this is usually not the case, each amount has to be multiplied by the degree of hydration, α.
The mass of reacted cement, b, can be calculated using the following relation:

$$b^{OPC} = \alpha(b_0^{OPC} - m_{UO}^{OPC}) \tag{2.2.1}$$

where b_0^{OPC} is the initial mass of cement before the start of hydration and m_{UO}^{OPC} are the unreacted oxides.

Table 2.1. The chemical equations describing the saturated hydration of OPC [61,62].

$$C_3S + 4.5H \rightarrow C_{1.7}SH_{3.2} + 1.3CH$$

$$C_2S + 3.5H \rightarrow C_{1.7}SH_{3.2} + 0.3CH$$

$$C_3A + C\bar{S} + 14H \rightarrow C_4A\bar{S}H_{14}$$

$$C_3A + CH + 21H \rightarrow C_4AH_{22}$$

$$C_3A + 3C\bar{S} + 36H \rightarrow C_6A\bar{S}_3H_{36}$$

$$C_4AF + 2C_3S + 22H \rightarrow C_6AFS_2H_{18} + 4CH$$

$$C_4AF + 2C_2S + 20H \rightarrow C_6AFS_2H_{18} + 2CH$$

The initial mass of cement is made out of clinker minerals (m_{C_3S}, m_{C_2S} etc.) and unreacted oxides, m_{UO}^{OPC}:

$$b_0^{OPC} = m_{C_3S} + m_{C_2S} + m_{C_3A} + m_{C_4AF} + m_{C\bar{S}} + m_{UO}^{OPC} \tag{2.2.2}$$

These equations are used when the hydration of individual phases is considered, in Section 2.5.
The mass of the hydration products can also be expressed as a function of the mass fractions of clinker minerals in the binder. These mass fractions by mass of binder for the clinker minerals have the following expressions:

$$x_{C_3S} = m_{C_3S} / b_0^{OPC} = \alpha\, m_{C_3S} / b^{OPC}; \quad x_{C_2S} = \alpha\, m_{C_2S} / b^{OPC}; \quad \text{etc.} \tag{2.2.3}$$

where Eq. (2.2.1) has been inserted.

Table 2.2. Molar relations between the amounts of hydration products and the mineral composition of OPC, as described in [61,62].

$$n_{C_4A\bar{S}H_{14}}^{OPC} = \alpha \cdot 0.5 n_{C\bar{S}}$$

$$n_{C_4AH_{22}}^{OPC} = \alpha\left(n_{C_3A} - 0.5 n_{C\bar{S}}\right)$$

$$n_{C_6A\bar{S}_3H_{36}}^{OPC} = \alpha \cdot 0.25 n_{C\bar{S}}$$

$$n_{C_{1.7}SH_{3.2}}^{OPC} = \alpha\left(n_{C_3S} + n_{C_2S} - 2n_{C_4AF}\right)$$

$$n_{C_6AFS_2H_{18}}^{OPC} = \alpha \cdot n_{C_4AF}$$

$$n_{CH}^{OPC} = \alpha\left(1.3\, n_{C_3S} + 0.3 n_{C_2S} - n_{C_3A} + 1.4 n_{C_4AF} + 0.5 n_{C\bar{S}}\right)$$

Knowing how many moles of each hydration product were formed (see Table 2.2), their masses can also be computed from their molecular mass and number of moles:

$$m_{C_4A\bar{S}H_{14}}^{OPC} = n_{C_4A\bar{S}H_{14}}^{OPC} M_{C_4A\bar{S}H_{14}}; \quad m_{CH}^{OPC} = n_{CH}^{OPC} M_{CH} \tag{2.2.4}$$

The molecular masses for the hydration products formed under saturated conditions are listed in Table 2.3.
Using these molecular masses, the molecular masses of the clinker minerals from Table 2.4 and Eq. (2.2.4), the mass relations can be computed for the molar relations as shown in Table 2.2.

For ease of use, Table 2.5 lists the modified formulas for computing the mass of hydration products formed, relative to the mass of reacted binder, for saturated conditions, meaning 100% relative humidity (r.h.).
Most experimental studies found in literature [37,38] determine the chloride binding capacity of hardened cement paste on samples dried at 11% r.h..
When a saturated hardened cement paste sample is dried to 11% r.h., some of the hydration products modify their water content [64]. The corresponding hydration stages and molecular masses can also be found in the second column of Table 2.3.

Table 2.3. Formula and molecular mass for several hydration products of OPC and slag-blended cements formed in saturated state and after drying at 11% r.h. [61,62,64,65]. The names of all mentioned compounds can be found in Appendix 2.

Saturated state (100% r.h.)		**Dried state (11% r.h.)**	
Formula	(g/mol)	Formula	(g/mol)
$C_6A\bar{S}_3H_{36}$	1327.34	$C_6A\bar{S}_3H_{12}$	894.98
C_4AH_{22}	722.72	C_4AH_{13}	560.58
$C_{1.7}SH_{3.2}$	213.09	$C_{1.7}SH_{2.1}$	193.27
CH	74.00	CH	74.00
$C_6AFS_2H_{18}$	1042.67	$C_6AFS_2H_8$	862.47
$C_4A\bar{S}H_{14}$	658.62	$C_4A\bar{S}H_{10}$	586.56
M_5AH_{19}	645.50	M_5AH_7	429.50

Upon 11% r.h. drying, the mass of the hydration products changes due to the water loss, but the molar quantities remain the same. Therefore, the mass of the hydration products after 11% r.h. drying can be calculated using the equations listed in Table 2.2 and the molecular masses from Table 2.3, Eq. (2.2.4) thus becoming:

$$m^{OPC}_{C_{1.7}SH_{2.1}} = n^{OPC}_{C_{1.7}SH_{3.2}} M_{C_{1.7}SH_{2.1}}; \quad m^{OPC}_{C_6A\bar{S}_3H_{12}} = n^{OPC}_{C_6A\bar{S}_3H_{36}} M_{C_6A\bar{S}_3H_{12}} \quad \text{etc.} \qquad (2.2.5)$$

Table 2.4. The formula and molecular mass for each clinker mineral considered [64].

Formula	Molecular mass (g/mol)
C_3S	228.33
C_2S	172.25
C_3A	270.20
C_4AF	485.97
$C\bar{S}$	136.14

Table 2.5. Relations between the mass of hydration products and the mass fractions of OPC minerals, as described in [61,62].

$$m^{OPC}_{C_6AFS_2H_{18}} / b^{OPC} = 2.146\, x_{C_4AF}$$

$$m^{OPC}_{C_6A\bar{S}_3H_{36}} / b^{OPC} = 2.437\, x_{C\bar{S}}$$

$$m^{OPC}_{C_4A\bar{S}H_{14}} / b^{OPC} = 1.209\, x_{C\bar{S}}$$

$$m^{OPC}_{C_4AH_{22}} / b^{OPC} = 2.675\, x_{C_3A} - 2.654\, x_{C\bar{S}}$$

$$m^{OPC}_{C_{1.7}SH_{3.2}} / b^{OPC} = 0.933\, x_{C_3S} + 1.237\, x_{C_2S} - 0.877\, x_{C_4AF}$$

$$m_{CH} / b^{OPC} = 0.422\, x_{C_3S} + 0.129\, x_{C_2S} - 0.274\, x_{C_3A} + 0.213\, x_{C_4AF} + 0.271\, x_{C\bar{S}}$$

$$m^{OPC}_{UO} / b^{OPC} = 1 - x_{C_3S} - x_{C_2S} - x_{C_3A} - x_{C_4AF} - x_{C\bar{S}}$$

Knowing the hydration degree and the mass of the formed hydration products, the mass of the whole sample dried to 11% r.h. can be calculated. The sample dried to 11% r.h. consists of dried hydration products (see Table 2.3), unreacted cement minerals and uncombined oxides. The formula for the mass of the whole sample after drying to 11% r.h. is given as:

$$m_{spl}^{OPC} = m_{C_{1.7}SH_{2.1}}^{OPC} + m_{C_4A\bar{S}H_{10}}^{OPC} + m_{C_6AFS_2H_8}^{OPC} + m_{C_6A\bar{S}_3H_{12}}^{OPC} + m_{C_4AH_{13}}^{OPC} + m_{CH}^{OPC} + (1-\alpha)(b_0^{OPC} - m_{UO}^{OPC}) + m_{UO}^{OPC} \quad (2.2.6)$$

where b_0^{OPC} can be determined from Eq. (2.2.2).

2.3 Chloride ions in cement paste

2.3.1 Binding isotherms

Chloride ions ingressed in the hardened cement paste can be divided into two main groups: free chloride ions, present in the pore solution, and bound chloride ions, attached to various hydration products. The relationship between the concentration of free chloride ions in the pore solution, c, and expressed in mol Cl/l of pore solution, and bound chlorides can be described using chloride binding isotherms. Tang and Nilsson [38] have concluded that Freundlich isotherms can be used at concentrations of external chlorides greater than 0.01 mol/l, while Langmuir isotherms are better suited for lower concentrations, below 0.05 mol/l (therefore, an overlap may exist between the two). Zibara [37] also employed both Freundlich and Langmuir isotherms in describing the experimental results, and preferred the Freundlich isotherm expression throughout the study. Hirao et al. [57] have chosen both Freundlich and Langmuir isotherms to describe the chloride binding capacity of hydrated phases. Since both types of isotherms are used in different studies, also here both correlations will be addressed.

2.3.2 Chloride binding – experimental data used in this study

All chloride binding isotherms presented in this study were obtained under laboratory conditions using the equilibrium method [37,38,57]. All experiments were conducted at ambient temperature (around 22ºC).

Several OPC compositions have been selected from [37] and [38] in order to test the accuracy of the chloride binding predictions. These compositions have been selected following some guidelines mentioned for OPC in literature. According to the standard EN 197-1 [11], there are a few compulsory requirements (Table 2.6).

Hewlett [60] mentions usual composition ranges for OPC, while [41] gives the typical values of compound composition of OPC, in terms of clicker minerals percentages (Table 2.7). OPC compositions not complying with the values mentioned in Tables 2.6 and 2.7 were not considered in this study, as being atypical of commercially available compositions. Another important reason for the exclusion of certain cement compositions was the expected change in the phase assemblage of the hydration products, when the considered cement does not comply with usual compositional ranges.

Zibara [37] has fitted Freundlich isotherms for hardened pastes obtained from the OPC1÷OPC3 compositions (see Table 2.8) with different w_0/b_0 ratios: 0.3, 0.5 and 0.7. In

[38], the authors present three Freundlich-type binding isotherms for the OPC4 paste, for three different w_0/b_0 ratios, of 0.4, 0.6 and 0.8.

Table 2.6. Requirements for OPC composition mentioned in the EN 197-1 standard [11].

$$x_{C_2S} + x_{C_3S} \geq 0.67$$

$$\frac{x_{CaO}}{x_{SiO_2}} \geq 2$$

$$x_{MgO} \leq 5\%$$

Table 2.7. Compositional range for Ordinary Portland Cements [41,60].

Oxide	**Hewlett** [60] **(% mass)**	**Neville** [41] **(% mass)**
CaO	58.10-68.00	43.12-85.22
SiO_2	18.4-24.5	13.84-28.44
Al_2O_3	3.10-5.04	3.15-7.80
Fe_2O_3	0.16-5.78	2-4
SO_3	0-5.35	1.5-2

The composition of all these hardened cement pastes are given in Table 2.9, together with their estimated hydration degree at the end of the sorption experiment and their initial mass of sample dried at 11% r.h., m_{spl}, calculated using Eq. (2.2.6).

The hydration degree is estimated based on the w_0/b_0 ratio and the age of sample at the time of immersion in the chloride solution for the HCP1÷HCP5 compositions. The hydration degree values for HCP6÷HCP8 are taken from [38]. Also mentioned in Table 2.9 are the fitted α_F and β_F values for these isotherms. Figures 2.1a and 2.1b show the experimental binding isotherms of all eight compositions.

2.4 The chloride binding ability of OPC hydration products

The AFm phases are generally known to be able to bind chloride ions through chemical substitution [30,31,34,36,37,55]. The C−S−H phase is considered to physically bind chloride due to its high specific surface areas [36,66–68]. The role of ettringite in chloride binding is highly debated [48,55,57], the same being true for portlandite [57,59]. Friedel's salt (FS) is a hydrated phase formed under the attack of chloride ions, but which is, in its turn, considered in [59] to be able to physically bind chlorides.

Table 2.8. The oxide and mineral compositions of all binders considered in Chapters 2 and 3, from [37,38] (N/A = not available, the value in *italics* is estimated).

Oxide	**OPC 1 (% mass)**	**OPC 2 (% mass)**	**OPC 3 (% mass)**	**OPC 4 (% mass)**	**Slag (%mass)**
CaO	62.38	61.33	63.58	62.10	35.49
SiO_2	18.89	18.43	21.26	19.90	36.18
Al_2O_3	5.51	5.36	4.09	5.30	10.02
Fe_2O_3	2.55	2.64	2.89	2.80	0.50
SO_3	4.12	4.43	2.79	*3.50*	1.51
MgO	2.75	2.61	2.47	1.3	0.66
Na_2O	1.19	1.19	0.58	N/A	0.77
K_2O	1.04	1.06	0.62	1.3	0.50
Mn_2O_3	0.11	0.10	0.06	N/A	13.58
SrO	0.30	0.28	0.12	N/A	0.04
TiO_2	0.25	0.24	0.20	N/A	0.67
P_2O_5	0.30	0.28	0.07	N/A	0.01
RO	0.61	2.05	1.27	1.49	0.07
LOI	1.02	2.44	0.99	2.31	1.72
C_3S	58.00	57.23	57.63	51.95	N/A
C_2S	10.50	9.76	17.60	18.01	N/A
C_3A	10.26	9.71	5.93	9.27	N/A
C_4AF	7.72	8.00	8.74	8.47	N/A
$C\overline{S}$	6.99	7.52	4.73	5.93	N/A

Table 2.9. Parameters of all hardened cement pastes selected from [37,38]. Cement compositions OPC1÷OPC4 are described in Table 2.8.

	Type of cement	w_0 / b_0^{OPC}	Age at time of immersion (weeks)	α	m_{spl}^{OPC} (g)	α_F	β_F
HCP1	OPC 1	0.5	8	0.8	113.26	11.11	0.37
HCP2	OPC 2	0.5	8	0.8	110.87	9.37	0.39
HCP3	OPC 3	0.3	8	0.75	113.79	7.60	0.31
HCP4	OPC 3	0.5	8	0.8	114.70	8.20	0.26
HCP5	OPC 3	0.7	8	0.85	115.62	8.43	0.29
HCP6	OPC 4	0.4	6	0.58	109.55	8.03	0.28
HCP7	OPC 4	0.6	6	0.66	110.87	9.50	0.37
HCP8	OPC 4	0.8	6	0.67	111.03	10.32	0.40

2.4.1 The chloride binding ability of the AFm phase

Justnes [31,41] concluded, based on an extensive literature review, that the chloride binding capacity of cementitious materials is dominated by the content of calcium aluminates and calcium aluminoferrites (through the formation of Friedel's salt, $3CaO•Al_2O_3•CaCl_2•10H_2O$). However, Neville [41,60] argued that the hypothesis according to which the content of aluminates in cement is proportional to its chloride binding ability is only valid in the case of intermixed chlorides. His study states that the formation of Friedel's salt or chloroferrite from the aluminates takes place rapidly during hydration; in the case of external chlorides, a smaller amount of chloroaluminates is formed, and these may dissociate under certain circumstances, releasing chloride ions in order to replenish those removed from the pore water by transport mechanisms. This approach suggested that more insights into the chloride binding ability of the AFm phase are needed in order to explain these observations.

Even though AFm is usually considered in cement literature to be only one phase, this generalization cannot be used when studying the microstructure of the cement paste. The AFm family consists of a great number of compounds, the most important being monosulphate (SO_4-AFm) $C_3A•CaSO_4•14H_2O$, hydroxy-AFm ($HO-AFm$) $C_3A•Ca(OH)_2•12H_2O$ and monocarbonate $C_3A•CaCO_3•10H_2O$. Moreover, intermediary compounds and solid solutions can form between these end-products. The carbonated AFm phases (monocarbonate, hemicarbonate and any of their solid solutions) will not be

considered further. As stated in Section 2.2, the cement pastes studied are considered not to be carbonated.

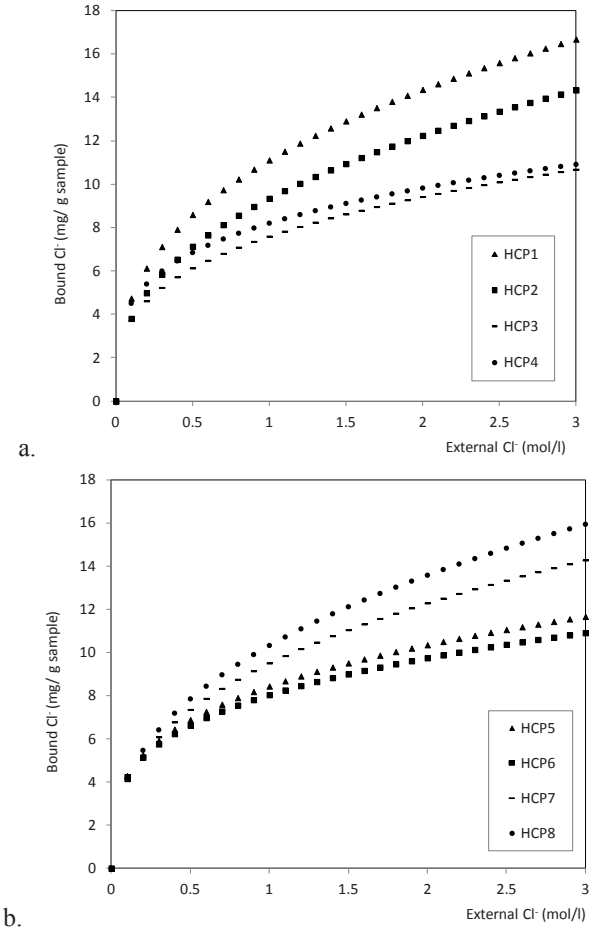

Figure 2.1. Experimental binding isotherms of cement paste samples (11% r.h.) for compositions a. HCP1÷HCP4, b. HCP5÷HCP8 (see Table 2.9), from [37].

The chloride ion is able to substitute the sulphate or hydroxyl groups in the structure of different AFm-type compounds, forming chloride-containing phases, Friedel's salt and Kuzel's salt among other possible compositions with a varying degree of anion substitution by the chloride ions. Different solid solutions can occur between these compounds and chloride-free AFm compounds.

Despite the wide range of compositions of the AFm family, the difference in their chloride binding ability has never been detailed and quantified. Excepting the case of

carbonated AFm phases, as well as the formation of solid solution between various members, an important distinction can still be made. Henceforth, the chloride binding abilities of monosulphate and hydroxy-AFm will be distinguished from each other.

Hirao et al. [57] has studied the chloride binding capacity of AFm, obtained from the hydration of C_3A in the presence of gypsum, in a ratio of C_3A:gypsum:water = 1:1:5. Given these synthesis conditions, only the formation of monosulphate can be expected because of the high gypsum content of the mix. The chloride binding capacity of this compound was found to obey a Freundlich-type isotherm, for the whole range of external chloride concentrations (up to over 4 mol/l). The formation of Friedel's salt was clearly shown by XRD measurements, and the chloride binding isotherm was corrected by the amount of Friedel's salt determined by DSC measurements. An uncertainty in these measurements is mentioned for free chloride concentrations under 1 mol/l, because of the formation of the monosulphate-Friedel's salt solid solution with undetermined proportions of sulphate and chloride ions.

Birnin-Yauri and Glasser [58] synthesized hydroxy-AFm-Friedel's salt solid solutions of different compositions, with the general formula $C_3A\bullet(1\text{-}x)CaCl_2\bullet xCa(OH)_2\bullet 10H_2O$, where x satisfies the condition $0 \leq x \leq 0.9$. Birnin-Yauri and Glasser [58] concluded that intruding chlorides can react with the chloride-free AFm in the hardened cement paste. In the case of hydroxy-AFm, the reaction of intruding chlorides with aluminates is considered to begin at ~ 2 mmol/l [Cl]. Buffering is considered to be provided by the AFm, through changes in composition in order to incorporate chlorides in its structure. The buffering is considered to be exhausted above ~ 14.5 mmol/l, at which point the AFm phase is virtually pure Friedel's salt.

Nielsen [69] applied the phase rule for predicting the stable or metastable phase equilibrium assemblage in hydrated Portland cement paste. Nielsen suggests an overall global reaction taking place in hydrated Portland cement pastes, accounting for the total content of alkalis and the relative amount of solution to solid paste. The reaction describes the distribution of chlorides between the $C-S-H$, AFm solid solution and pore solution and the change in Ca^{2+}, OH^- and alkali concentrations in the pore solution. For a constant concentration of alkalis in the pore solution (550 mmol/l), a relation between the amount of chlorides adsorbed by $C-S-H$ and the fraction of Friedel's salt in the AFm phase is described. The relationship found to describe this dependency is linear, because the alkali concentration is always the same as the chloride concentration. The linear dependency between the amount of chlorides adsorbed by $C-S-H$ and the fraction of Friedel's salt in the AFm phase also suggests that the two chloride binding mechanisms take place with approximately the same rate.

A more recent article [70] brings new insights into the interactions between various AFm phases: $HO-AFm$, monosulphate, monocarbonate and Friedel's salt. Only the carbonate-free system will be discussed here, as explained above. In [70], chloride is introduced through intermixing of the phases (and not from an external solution) and the

used compound is $CaCl_2$ and not NaCl. Differences between intermixed and external chlorides, as well as the effect of the associated cation were discussed in Section 2.1. However, the findings are in good agreement with other literature reviews [37,51,57]. The chloride ions are found to displace sulphate from a $SO_4 - AFm - HO - AFm$ solid solution, with the formation of Kuzel's salt for low $CaCl_2$ concentrations and Friedel's salt for higher concentrations, either in solid solution with $HO - AFm$. The sulphate ions which are thus released from monosulphate will form additional ettringite. This assumption will be incorporated in Section 2.5.2. When considering the chloride binding capacity of a commercial Portland cement, it is concluded in [70] that Friedel's salt is the only hydrated phase formed that incorporated chlorides into its structure, up to an external chloride concentration of 3 mol/l. This is the assumption on which also the model in this chapter will be based.

There are a number of different mechanisms proposed in literature for the chemical conversion of AFm phases to Friedel's salt or Kuzel's salt ($C_3A•1/2CaCl_2•1/2CaSO_4•10H_2O$). There are also two different mechanism proposed in literature for the formation of Friedel's salt. The first one is the ion exchange mechanism [34,71]. This mechanism implies that chloride is bound by replacing hydroxyl ions present in the interlayers of the hydroxy AFm phase. Suryavanshi et al. [34] propose the following reaction for the formation of Friedel's salt:

$$R\text{-}OH + Na^+ + Cl^- \rightarrow R\text{-}Cl + Na^+ + OH^- \qquad (2.4.7)$$

where R is the principal layer of the hydroxy-AFm, $[Ca_2Al(OH)_6 \cdot nH_2O]^+$, and the value of n is related to the type of hydroxy-AFm. This reaction was based on the fact that the AFm phases have layered structures derived from the structure of portlandite by the ordered replacement of one Ca^{2+} ion out of three in a $Ca(OH)_2$ layer by an Al^{3+} ion. This substitution would cause a charge imbalance in each principal layer, which is corrected by the adsorption of a Cl^- in the interlayer space.

The second mechanism for the transformation of the AFm phase into Friedel's salt implies a reconstructive process: one phase dissolves while another, differing in composition and structure, nucleates and crystallizes. This mechanism has been proposed by Matschei et al. [56] and Putnis et al. [72] for the transformation of hydroxy-AFm to hemicarboaluminate and monocarboaluminate. In Matschei et al. [56] it is also suggested the transformation between AFm phases can occur by ion exchange but with some simultaneous reordering and rearrangement within the $[Ca_2Al(OH)_6]^+$ layers avoiding, or partly avoiding the need for a nucleation and crystallization step. This mechanism could also be responsible for the transformation of the AFm phase to Friedel's salt.

The difference between the chloride binding abilities of monosulphate and hydroxy-AFm, as summarized above, will be quantified in Section 2.5.1.

2.4.2 The role of ettringite, portlandite and Friedel's salt in chloride binding

Ekolu et al. [48] concluded that at intermediate levels of chloride concentrations (including 0.5 mol/l NaCl) monosulphate is destroyed while most ettringite ($C_3A•3CaSO_4•36H_2O$, the AFt phase) remains stable and that at high chloride levels both monosulphate and ettringite are destroyed with the release of Friedel's salt and gypsum as main final products. Birnin-Yauri and Glasser [58] propose that ettringite may play a role in chloride binding, even at lower free chloride concentrations, but this assumption is not sustained by any experimental data. However, Hirao et al. [57] experimentally tested the chloride binding capacity of the AFt phase and found that ettringite does not bind any chloride ions from an external solution. Elakneswaran et al. [59] consider the chloride binding capacity of ettringite to be intermediary between the one of Friedel's salt and the one of $C-S-H$, which is a very low binding capacity. In this case, AFt is considered to bind chlorides not through a chemical process, but through physical adsorption on the hydrate's surface. Moreover, due to the small amounts of ettringite formed in the cement paste, when compared to the one of $C-S-H$, the effect of the chloride adsorption on the surface of ettringite would be minimal. Still, considering the findings of Baloni et al. [70], that the ettringite amount formed increases because of the release of sulphate ions from monosulphate, the chloride binding ability of ettringite will also be estimated in Section 5.2.

Elakneswaran et al. [59] also give chloride binding isotherms of portlandite (CH) and Friedel's salt, proposing that Friedel's salt can, in its turn, adsorb chloride ions on its surface. Portlandite is believed to behave in the same way. It is stated that the dissociation processes of both Friedel's salt and portlandite give positive surfaces. According to the same study, Friedel's salt dissociates in water and its surface charge (which is due to $[Ca_2Al(OH)_6]^+$ groups) is compensated by chloride ions in the solution. Chlorides can also be adsorbed on the positive surface of dissociated portlandite and form CaOHCl, its crystal structure being detectable by XRD. However, Hirao et al. [57] measured the chloride binding capacity of CH and found that it does not bind chloride ions.

2.4.3 The chloride binding ability of the $C-S-H$ phase

The $C-S-H$ phase is known to physically bind chlorides, due to its high specific surface. There are several studies about the binding capacity of the $C-S-H$ phase, some of which will be summarized here. Beaudoin et al. [66] have suggested three states of chloride bound to $C-S-H$: free, adsorbed and interlayer chloride. It is suggested that the chemisorbed and interlayer species can be removed by water, while lattice substituted chloride cannot be removed by leaching. The authors believe that the most of the chloride ions are chemisorbed on the surface of $C-S-H$ and therefore the chloride binding depends on the amount of $C-S-H$ in the sample. Justnes [31] also pointed out the fact that chloride sorption is dominated by the amount of $C-S-H$. Other authors considered

the electrical double layer theory in order to explain these observations [36,67,68]. This mechanism is based on the fact that the surface of the $C-S-H$ gel is negatively charged [64,73,74], and therefore it attracts cations (Ca^{2+}, Na^{+}) from the pore solution. This leads to the formation of a first ionic layer on the surface of gel hydration products, the Stern-layer [75]. These adsorbed cations attract negatively charged ions from the pore solution, forming a second ionic layer (the Gouy-Chapman layer). The adsorption capacity of the electrical double layer can be defined as a function of the specific surface of the $C-S-H$ gel, temperature, concentrations of various ions in the pore solution and their respective electrical charge. In order to consider all these opinions, further understanding of the structure and properties of $C-S-H$ is needed.

When a solid is in contact with a solution, the two media interact. In the case of a solid with a charged surface, immersed in an ionic solution, the phenomena at the level of the interface are quite complex. The electrical charge of the solid influences the state of the liquid at the interface level. This creates an interfacial region, the electrical double layer (EDL), which corresponds to a continuous transition between the solid surface and the initial state of the liquid.

The term "electrical double layer" is used to describe the arrangement of charges and orientated dipoles at the solid-liquid interface [76]. Helmholtz [77] proposed the first model for the EDL, consisting of two parallel planes of opposing charge. This is the simple case of a condenser, one side representing the charged surface of the solid, the other the ions that balance it. This model does not take into account the interactions between the charged surface and the ionic species in the solution, apart from the adsorbed ions. As a consequence, the concentration of ions in the solution does not influence this model. Gouy and Chapman [78] proposed a model that also takes into account the influence of the charged surface on the ions present in the immersing solution. They consider the EDL to be characterized by a potential difference and by the ionic concentrations. The different ions in the solution obey the distribution law defined by Boltzmann. In this model, the EDL is no longer just a compact layer on the surface of the solid, but an interfacial region in which ions can move to a certain degree. This region is termed "diffuse layer" and its thickness depends on the concentration of ions in the solution. While this model is more complex than the one of Helmholtz, it considers ions as punctual electrical charges, without taking into account the size of the ions in solution. This implies that the ions are to be found at a distance of x = 0 from the solid surface, which is impossible in reality, the minimum distance being set by the ionic radius of the ions present in the EDL. Stern [79] further elaborates the models of Helmholtz and Gouy-Chapman, describing a double layer made of a compact layer and a diffuse layer stretching into the solution. The ions in the diffuse layer are under the electrostatic influence of the charged surface, while the specific adsorption takes place in the compact layer. Grahame proposes a model of the compact layer made of two characteristic planes: one corresponding to the specifically adsorbed ions and the other one, further away from

the charged surface, corresponding to the adsorbed hydrated ions. Bockris et al. [76] consider the influence of the charged surface on the molecules of solvent, by adsorbing these onto the surface, at the level of the compact layer. In the case of dipolar solvents, like water, there is also an interaction between the solid surface and the solvent molecules, which have associated electrical dipoles.

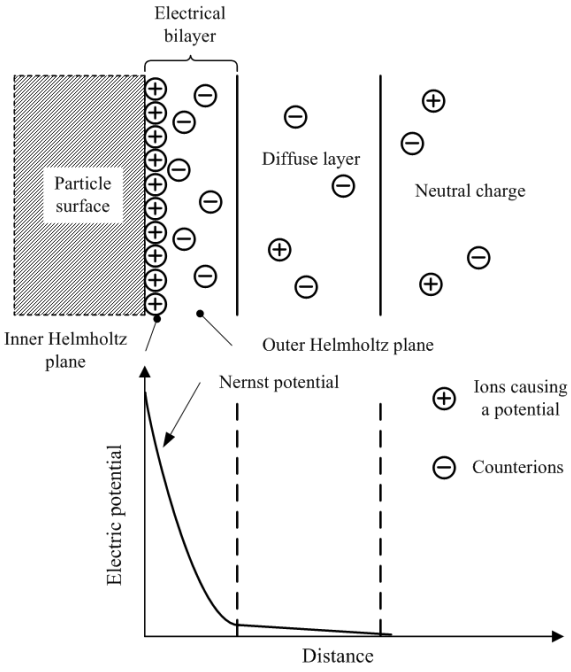

Figure 2.2. General scheme of the Electrical Double Layer (EDL) formation.

Other theories have been developed in order to take into consideration the interactions between ions, as well as their real size. The first theory was a Monte Carlo model, by Guldbrand et al. [80], followed by the AHNC theory by Kjellander and Marcelja [81]. The AHNC theory ("Anisotropic Hypernetted Chain Theory") can be used to calculate the interactions between charged particles, ions or surfaces. This theory also considers the different behaviour of ions in the proximity of the charged surface, depending on their ionic radius. These correlations are important in a concentrated solution or in the case of high surface charges, and were not taken into account by the theory of Boltzmann, except within a distance of half the ionic radius of the ions close to the charged surface.

Henocq [82] explains the adsorption of chloride ions on the surface of C−S−H by applying the model of the triple layer described by Stern [79] and Grahame [83] to the interface C−S−H/pore solution (Bockris et al. [76]). Based on the interpretation of electrokinetic potential curves, a structure made of a condensed layer of Na ions on the

surface (Stern internal layer), compensated partly by SiO^- groups and partly by an external layer (Stern external layer) made of hydroxyl (and chloride ions, in the presence of chlorides) was proposed. This external layer permits ionic exchanges with the solution. The adsorption of chloride ions can therefore be explained by an exchange mechanism between a chloride ion from the pore solution and a hydroxyl ion from the $C-S-H$ layers. The OH^- ion is loosely bound, permitting the Cl^- ion to be substituted in the interlayer space and ensure the electroneutrality of the system. Henocq [82] describes this mechanism by the following simplified equation:

$$[(C-S-H)\ldots Na\ldots OH]_s + Cl^- \leftrightarrow [(C-S-H)\ldots Na\ldots Cl]_s + OH^- \quad (2.4.8)$$

where s indicates the solid surface.
The EDL theory implies the influence of several factors over the chloride binding ability of the $C-S-H$ gel, the most important of which are the C/S ratio of the gel, the composition and pH of the pore solution and associated cation of the chloride ion.

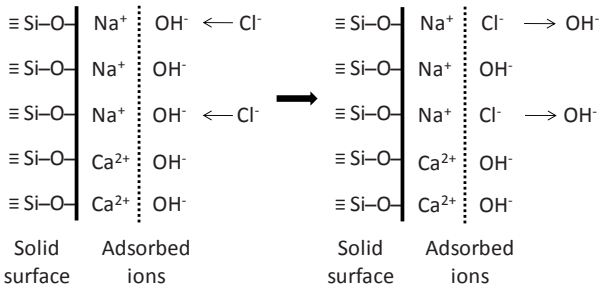

Figure 2.3. Simplified model of the ionic exchanges at the $C-S-H$ surface, from [84].

As explained in Section 2.1, the only source of chloride ions considered in this study is NaCl. A usual pH is assumed for the pore solution (12.5-13.4, according to [30] and a C/S ratio of 1.7 for the $C-S-H$ gel [62]). Moreover, the $C-S-H$ gel and the pore solution are considered to be homogenous in composition throughout a hardened paste in equilibrium with its surrounding solution. Therefore, all $C-S-H$ should have the same chloride binding ability, regardless of its source (C_3S or C_2S) and the pore solution is considered to have a constant pH throughout the sample.

2.5 Chloride binding isotherms related to binder composition and hydration products

All chloride binding isotherms in the following sections will be termed either for chloride binding capacities expressed in mg Cl/g hydration product conditioned to 11% r.h. [37,57,59], or for the chloride binding capacities expressed in mg Cl/g sample at 11% r.h.

(as calculated from [37,38,57]). The molar mass of each hydration product can be found in Table 2.3 and has already been incorporated in the following isotherm expressions where so needed. The term refers to the mass of the specified hydration product, in grams, calculated using Table 2.3. The mass of sample in grams at 11% r.h., m_{spl}, is always computed according to Eq. (2.2.6). Eq. (2.5.9) gives the general relation between $C^0_{b,hp}$ and $C_{b,hp}$:

$$C_{b,hp} = C^0_{b,hp} \cdot \frac{m_{hp}}{m_{spl}} \tag{2.5.9}$$

The chloride concentration of the external solution, c, is always expressed in mol Cl^-/l solution.

2.5.1 The chloride binding capacity of the AFm phase

Hirao et al. [57] studied the chloride binding of the pure AFm phase, as described in Section 2.4. They have found the following Freundlich-type isotherm which describes chloride binding by the monosulphate phase, in mg Cl/g monosulphate:

$$C^0_{b,SO_4-AFm} = 51.89\,c^{0.58} \tag{2.5.10}$$

As mentioned in Section 2.4, Birnin-Yauri and Glasser [58] consider that 100% of the quantity of $HO-AFm$ is completely transformed into Friedel's salt at a free chlorides concentration greater than 0.015 mol/l. Considering the fact that one mole of hydroxy-AFm binds two moles of chloride ions in order to form Friedel's salt, and using the molecular masses from Table 3, the amount of chloride which can be bound by C_4AH_{13}, in mg Cl/g $HO-AFm$ becomes:

$$C^0_{b,HO\text{-}AFm} = 126.5 \tag{2.5.11}$$

constant for external chloride concentrations over 0.015 mol/l.
The sum of Eqs. (2.5.10) and (2.5.11) will be used henceforth to compute the total binding capacity of the AFm phase.

2.5.2 The chloride binding capacity of the $C-S-H$ phase

Zibara [37] also determined the chloride binding ability of the hydration products of pure C_3S and C_2S in mg Cl/g $C-S-H$ gel formed, compensating for the amount of CH formed, because it is considered not to bind chlorides:

$$C^0_{b,C_3S} = 6.65\,c^{0.334} \tag{2.5.12}$$

$$C^0_{b,C_2S} = 7.89\,c^{0.136} \tag{2.5.13}$$

Even though their coefficients are quite different, the isotherms defined by Eqs. (2.5.12) and (2.5.13) show almost the same behaviour for the C_3S and C_2S phases when the amount of $C-S-H$ generated is taken into account. A combination of these isotherms that takes into account the C_3S/C_2S ratio of the cement will be used throughout this study. In order to combine these isotherms into one equation, the mass fraction of C_3S (δ_{C_3S}) and C_2S (δ_{C_2S}) reported to their sum will be used:

$$\delta_{C_3S} = \frac{m_{C_3S}}{m_{C_3S}+m_{C_2S}} \tag{2.5.14}$$

$$\delta_{C_2S} = \frac{m_{C_2S}}{m_{C_3S}+m_{C_2S}} = 1-\delta_{C_3S} \tag{2.5.15}$$

The chloride binding capacity of the $C-S-H$ phase in mg Cl/g $C-S-H$, as it will be computed in all following results and termed $C_{b,C-S-H,Z}$, reads:

$$C^0_{b,C\text{-}S\text{-}H,Z} = (6.65\,c^{0.334}\cdot\delta_{C_3S} + 7.89\,c^{0.136}\cdot\delta_{C_2S}) \tag{2.5.16}$$

Hirao et al. [57] experimentally determined a Langmuir-type isotherm for the chloride binding of the $C-S-H$ phase, in mg Cl/g $C-S-H$ gel conditioned at 11% r.h.:

$$C^0_{b,C\text{-}S\text{-}H,H} = 21.84\cdot\frac{2.65\,c}{1+2.65\,c} \tag{2.5.17}$$

Elakneswaran et al. [59] also proposed a chloride binding isotherm for the $C-S-H$ phase in mg Cl/g $C_{1.71}SH_{2.1}$, which has been fitted to the following Freundlich isotherm:

$$C^0_{b,C\text{-}S\text{-}H,E} = 12\,c^{0.63} \tag{2.5.18}$$

Figure 2.4 shows the isotherms (Eq. 2.5.10), (Eq. 2.5.11), (Eq. 2.5.16), (Eq. 2.5.17) and (Eq. 2.5.18), describing the chloride binding ability of monosulphate, hydroxy-AFm and respectively $C-S-H$ according to [37,57–59], in mg Cl/g hydrated phase.

Figure 2.5 shows the isotherms C_{b,SO_4-AFm}, $C_{b,HO\text{-}AFm}$, $C_{b,C\text{-}S\text{-}H,Z}$, $C_{b,C\text{-}S\text{-}H,H}$ and $C_{b,C\text{-}S\text{-}H,E}$ applied to HCP2 using Eq. (2.5.9), and so taking into consideration the relative amount of each hydrate in the cement paste. The large difference between the $C^0_{b,C\text{-}S\text{-}H,H}$, $C_{b,C\text{-}S\text{-}H,E}$ and $C^0_{b,C\text{-}S\text{-}H,Z}$ isotherms can have multiple explanations. The quantitative effects of a number of influencing factors cannot be precisely asserted. The first factor that needs to be considered is the very large w_0/b_0 (10:1) ratio employed in [57], which will not be

found in any real concrete structure, as opposed to the w_0/b_0 of 0.5 employed in [37]. Also, the fact that in [57] the solid and liquid fractions of the sample were separated by suction filtering and not by drying using acetone leads to the conclusion that the chloride amounts that can be bound by the gel water of the $C-S-H$, when fully rehydrated in chloride solution, were also included in the measurement.

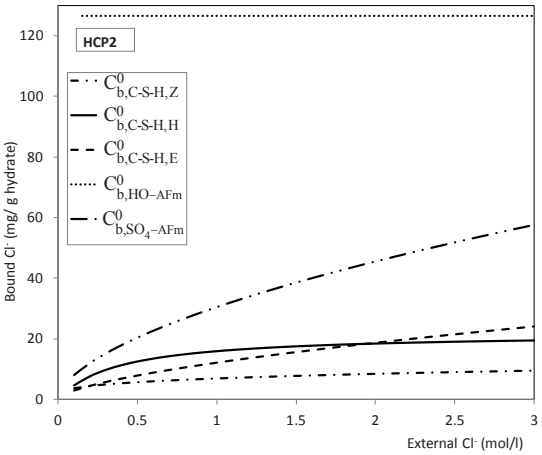

Figure 2.4. Isotherms (2.5.10), (2.5.11), (2.5.16), (2.5.17) and (2.5.18) describing the chloride binding ability of hydroxy-AFm, monosulphate and respectively $C-S-H$ at 11% r.h., according to [37,57–59]. The composition of paste HCP2 can be found in Table 2.9.

Furthermore, a small fraction (evaluated as ≤ 5%) of the free chlorides that entered the capillary space upon rehydration could still be present at the time of the chloride content measurement. In the case of the $C-S-H$ binding isotherm determined in [59], the results were deduced from the isotherms of HCP and portlandite. The phase assemblage was predicted using a speciation software, and corrected for the chemically bound chlorides determined through XRD measurements. The maximum external chloride concentration used in these experiments was 1 mol/l. However, at such low concentrations, the results given by XRD are not conclusive, as explained in Section 2.4.1. Conversely, Zibara [37] measured the chloride binding of hydrating C_3S and C_2S pastes with a w_0/b_0 of 0.5 with NaOH and KOH additions to mimic the control solution. The obtained values were corrected for the amount of CH formed, using the paste model detailed in Section 2.2.

In order to distinguish between the three mentioned isotherms for the chloride binding of $C-S-H$, the total bound chlorides will be calculated for all eight considered hardened cement pastes. The obtained values will be compared to the experimental data and the

best $C-S-H$ isotherm will be chosen based on relative error and standard deviation values.

Using the $C-S-H$ chloride binding isotherm (15) proposed by Hirao et al. [57], $C_{b,\,H}$ is computed as its sum with Eqs. (2.5.10) and (2.5.11).

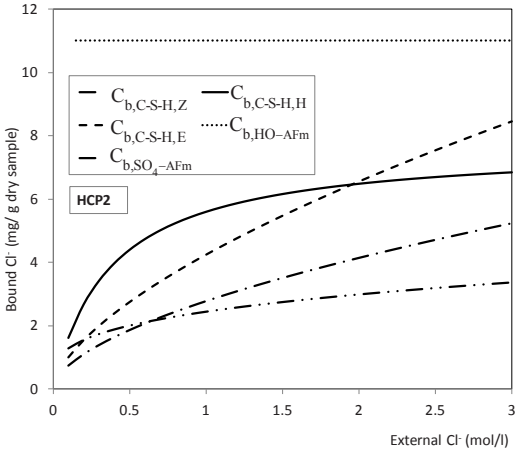

Figure 2.5. Isotherms (2.5.10), (2.5.11), (2.5.16), (2.5.17) and (2.5.18) applied to HCP2 (Table 2.9) using Eq. (2.5.9), and so taking into consideration the relative amount of each hydrate in the cement paste.

In the same way, $C_{b,\,Z}$, the sum of Eq. (2.5.16) with Eqs. (2.5.10) and (2.5.11) can be calculated. Last, using Eq. (2.5.18), Eqs. (2.5.10) and (2.5.11), the sum of the $C-S-H$ isotherm proposed by Elakneswaran et al. [59] and the isotherm of AFm, termed $C_{b,\,E}$, is computed. Figure 2.6 compares these three composed isotherms with the experimentally determined values for the composition of HCP6 as an example.

The $C_{b,\,E}$ isotherm is the poorest fit in terms of its shape when compared to the experimental data. Moreover, its relative error starts at 50% and increases with the increase of the external chlorides concentration. Therefore, this isotherm does not satisfactorily describe the chloride binding capacity of $C-S-H$. In terms of the shape of the curve, the $C_{b,\,H}$ isotherm is closest to the experimental data. However, it can be seen that, again, its predicted values are 50% higher than the experimentally obtained data.

The $C_{b,\,Z}$ isotherm has the lowest relative errors and standard deviations from experimental results, when compared to the $C_{b,\,H}$ and $C_{b,\,E}$ isotherms, even if the shape of the curve is not the best fit. The higher predicted values for the lower range of external chlorides can be attributed to the assumption that all $HO-AFm$ is already transformed into Friedel's salt, which might not be completely accurate for all cement pastes. Given these data, the $C_{b,\,Z}$ isotherm (Eq. 2.5.16) is chosen as the best to describe the chloride

binding capacity of the $C-S-H$ phase. Henceforth, the isotherm $C_{b,\,Z}$ will be referred to as "the basic model" henceforth. An "extended model" will now be presented, in order to include the chloride binding abilities of other hydrated phases in an OPC paste. The contributions of these phases are not as significant as the ones of AFm and $C-S-H$, but their addition shows a positive effect on the results of the new chloride binding model.

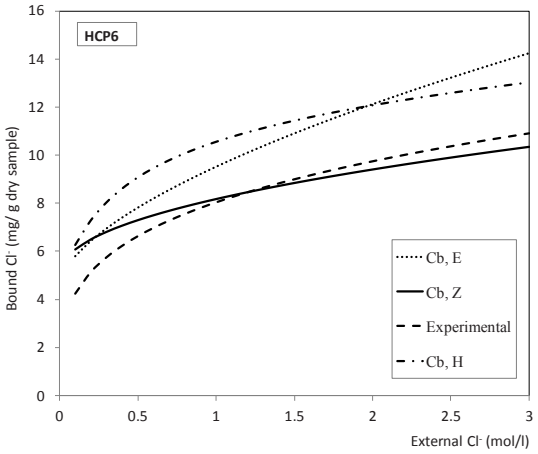

Figure 2.6. Comparison between $C_{b,\,Z}$, $C_{b,\,H}$ and $C_{b,\,E}$ and the experimental data from [37], for composition HCP6 (Table 2.9).

2.5.3 Chloride binding abilities of other OPC hydrates: the extended model

The other hydrated phases that are considered in literature to be able to bind chlorides are portlandite, Friedel's salt and ettringite, as discussed in Section 2.4.2. Elakneswaran et al. [59] have obtained chloride sorption isotherms of portlandite and Friedel's salt. Eqs. (2.5.19) and (2.5.20) describe the sorption capacity of portlandite and Friedel's salt, in mg Cl/g portlandite and mg Cl/g FS respectively, for free chloride concentrations under one mol/l:

$$C^{0}_{b,\,CH} = 0.087c^{0.62} \tag{2.5.19}$$

$$C^{0}_{b,\,FS} = 0.31c^{0.46} \tag{2.5.20}$$

The mass m_{FS} is computed for Friedel's salt at 11% r.h., $C_3A{\bullet}CaCl_2{\bullet}6H_2O$, with the molar mass of 489.27 g/mol:

$$m_{FS} = 6.9 \cdot (C_{b,\,C_4A\bar{S}H_{10}} + C_{b,\,C_4AH_{13}}) \tag{2.5.21}$$

Ettringite is also mentioned in [59], and believed to give a chloride sorption capacity lower than portlandite and Friedel's salt, but higher than tobermorite. The amount of AFt increases with the intrusion of chloride ions and the formation of Friedel's salt (see Section 2.4.2.), so this contribution needs to be taken into account (Eq. 2.5.22). In order to do this, the first assumption is that ettringite has the same chloride binding ability as tobermorite (which is estimated in Eq. 2.5.12), so that its minimum influence can be assessed. Then, the amount of newly formed ettringite needs to be estimated from the amount of Friedel's salt (Eq. 2.5.20), using the molecular mass of AFt from Table 2.3 and the initial ettringite amount formed before the intrusion of chlorides, from Table 2.5:

$$C_{b,AFt} = 6.65c^{0.334} \cdot \frac{m^{OPC}_{C_6A\bar{S}_3H_{12}} + 0.3m_{FS}}{m^{OPC}_{spl}} \tag{2.5.22}$$

Isotherms incorporating the contribution of portlandite, ettringite, Friedel's salt and all the possible combinations between them were constructed by adding the contribution of the respective phases to the $C_{b,\,Z}$ isotherm.

The influence of adding the binding capacity of portlandite or Friedel's salt alone is beneficial, even though very low, for all cases considered (compositions from Tables 2.8 and 2.9). Adding the contribution of the AFt phase does not improve the precision of the model, its influence being also very low, but either positive or negative for the considered hardened cement pastes. The combined effect of two of these phases, or all three together, is beneficial in most, but not in all cases. However, since these effects are extremely low (with contributions usually well under 1% of the total bound chlorides), they should only be taken into account for theoretical models with precise phase assemblages. For practical cases in which a high precision is not needed, the use of the basic model is recommended.

For the rest of this study, the total bound chlorides for all considered samples will be calculated using the isotherm $C_{b,\,Z,\,CH,\,FS}$, defined as the sum of Eqs. (2.5.10), (2.5.11), (2.5.16), (2.5.19) and (2.5.20) and termed from now on C_b. This extended model offers the best precision in predicting the chloride binding ability of hardened OPC pastes by incorporating the chloride binding abilities of both Friedel's salt and portlandite.

2.6 Comparison with other models from literature

Zibara [37] has proposed two expressions for the α_F coefficient of a Freundlich isotherm describing the chloride binding capacity of a hardened cement paste:

$$\alpha_F = 0.86\,x_{C_3A} + 0.44\,x_{C_4AF} + 0.16(x_{C_2S} + x_{C_3S}) - 12.44 \tag{2.6.23}$$

$$\alpha_F = 0.65\,x_{C_3A} + 0.24\,x_{C_4AF} - 0.35\,x_{SO_3} + 3.38 \tag{2.6.24}$$

and one expression for the β_F exponent of the same isotherm:

$$\beta_F = 0.003\, x_{C_3A} + 0.005\, x_{C_4AF} + 0.019\, x_{SO_3} + 0.23 \quad (2.6.25)$$

These coefficients depend on the composition of the considered cement (% mass of clinker minerals and % mass of SO_3). Equations (2.6.23)-(2.6.25) have been obtained by fitting experimental data to a number of cement compositions, without taking into account the water to binder ratio or age of the sample. Moreover, these fitted equations do not take into account the formed hydration products and have no physical or chemical basis for their predictions.

Based on Equations (2.5.10) and (2.5.17), Hirao et al. [57] estimated the total chloride binding capacity of cement paste as:

$$C_{b,H} = 0.62 \cdot \frac{2.65c}{1+2.65c} \cdot x_{CSH} + 1.38 c^{0.58} \cdot x_{AFm} \quad (2.6.26)$$

where $x_{C\text{-}S\text{-}H}$ and x_{AFM} should be calculated according to a method published by the Japan Concrete Institute. In this study, the $x_{C\text{-}S\text{-}H}$ and x_{AFM} quantities will be predicted using the paste model described in Section 2.2.

Figure 2.7 is an example applied on HCP6 and it shows the isotherms obtained using Eqs. (2.6.24) and (2.6.26), termed "Zibara" and Eq. (2.6.25), termed "Hirao", and compares them to the experimental results and to the chloride binding C_b predicted using the new extended model.

The use of either Eq. (2.6.23) or (2.6.24) when computing the "Zibara" isotherm will render almost identical results, so the choice is not influencing the presented values. Figure 2.8 compares the chloride binding capacity of each hydrated paste (compositions from Tables 2.8 and 2.9) with the experimental values at a free chloride concentration of 2 mol/l, as the regular value for the RCM test.

It can be seen from both Figures 2.7 and 2.8 that the proposed isotherm C_b is a very good fit for the considered experimental results.

The highest drawback of the Zibara model [37] is that it predicts the same amount of bound chlorides for OPC pastes obtained from the same cement but with different w_0/b_0 ratios and curing ages; in other words, that it is based only on a fit on cement composition and does not take into account other mixing and curing parameters.

Therefore, this model predicts the same chloride binding capacity for pastes HCP3÷HCP5, even though the authors have measured different values for each sample during the performed laboratory experiments.

Applying the hydration model described in Section 2.2 [61,62] to the model of Hirao et al. [57], the latter is found to perform well. In such conditions, the currently proposed model and the Hirao model [57] are compatible, and in good agreement with experiments. However, this hydration model assumes all AFm to consist of only one compound and does not make the distinction between the different chloride binding

capacities of the AFm members, as the newly proposed model does. The importance of this distinction will be further pointed out in the following section.

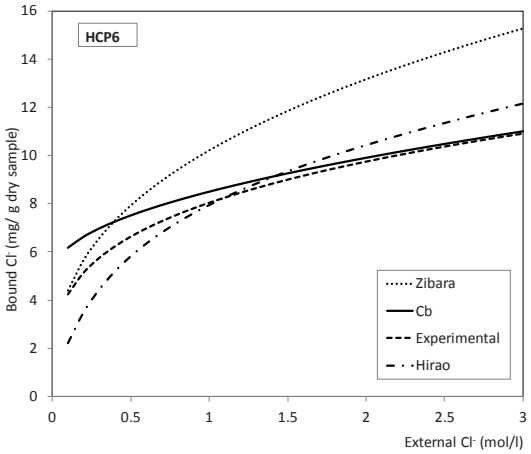

Figure 2.7. Comparison between the proposed model, the models of Hirao et al. [57] and Zibara [37], and the experimental data from [38], for composition HCP6 (see Table 2.9).

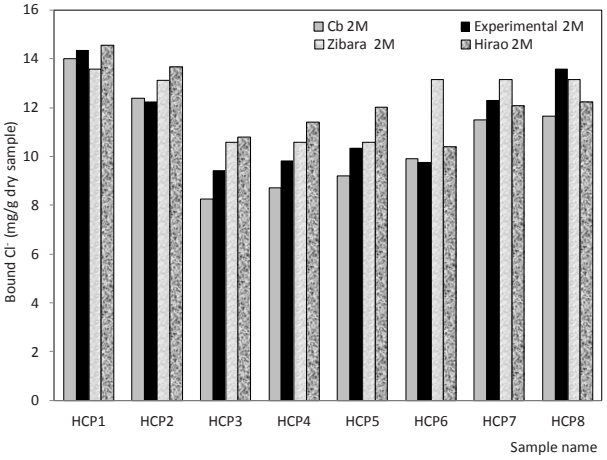

Figure 2.8. The chloride binding capacity of each hydrated paste (see Table 2.9) with the experimental values [38] at a free chloride concentration of 2 mol/l.

2.7 Summary and conclusions

New insights into the hydration products of OPC were used in this chapter. The quantities of hydration products were calculated for saturated state hydration and for samples that have been dried to 11% r.h. after hydration. The chloride binding of several hydrated phases ($C-S-H$, monosulphate, hydroxy-AFm, AFt, CH, and Friedel's salt) have been studied and estimated in relation to the chloride content of the pore solution.

Based on an extensive analysis of experimental data found in literature, a new chloride binding isotherm for the AFm phase is given. This formula takes into account the different chloride binding abilities of monosulphate and hydroxy-AFm. This difference between the chloride binding abilities of various members of the AFm family has not been taken into consideration in any other model, even though it is significant and its inclusion can change the results greatly. Using the new AFm isotherm and several sets of experimental chloride binding isotherms from literature, a new formula for estimating the chloride adsorption capacity of the $C-S-H$ phase is proposed (Eq. 2.5.16).

Combining the two new isotherms, for $C-S-H$ and AFm chloride binding in hardened cement paste, and the computed quantities of all hydration products, a new formula for the chloride binding capacity of OPC pastes has been deduced. This isotherm has been termed the "basic model". When compared to experimental data, the results obtained using this new chloride binding isotherm have proven to accurately describe the chloride binding capacity of OPC pastes, results being within 8% of the experimental values for the whole range of free chloride concentrations considered, of up to 3 mol/l. An "extended model" was also developed, which includes the contributions of portlandite, ettringite and the newly formed Friedel's salt. Adding the contributions of either of these phases has a positive influence on the precision of the model, but their estimation requires a clear understanding of the phase assemblage of a given paste. The addition of the contributions of both Friedel's salt and portlandite was found to be the most beneficial over the range of compositions of hardened cement pastes considered.

This new model is based on the chloride binding abilities of each hydrated phase, and therefore can distinguish between their contributions at different free chloride concentrations. The contribution of $HO-AFm$ is the greatest for all free chloride concentrations, but its importance decreases with the increase in free chlorides (from 60% at 0.3 mol/l external chlorides, to 30% at 3 mol/l), as all $HO-AFm$ is considered to be transformed to Friedel's salt external chloride concentrations of 0.015 mol/l. The contribution of monosulphate does not equal the one of $HO-AFm$ until high chloride concentrations, but it increases with the increase in free chlorides, from 13% at 0.3 mol/l external chlorides concentration, to over 33% of the total chloride binding capacity. The contribution of the AFm phases amounts to ~ 70% of the total chloride binding capacity of a cement paste, which is in line with the conclusions of [70], which state that Friedel's salt traps the most chlorides on a mass basis.

The contribution of $C-S-H$ is the one which remains fairly constant for the whole range of external chloride concentrations, between 25% and 28%. The lowest contributions are the ones of portlandite and Friedel's salt, whose sum amounts to only 2-5% of the total bound chlorides in an OPC paste. At an external chlorides concentration of 0.6 mol/l (usual for sea water), the total chloride binding capacity of an OPC paste can be divided between the hydrated products as: 49% to $HO-AFm$, 20% to SO_4-AFm, 28% to $C-S-H$ and 3% to portlandite and Friedel's salt. For higher concentrations this balance will change in favour of the monosulphate contribution. For example, at an external chlorides concentration of 2 mol/l, the following contributions of the hydrated phases were calculated: 37% to $HO-AFm$, 30% to SO_4-AFm, 28.5% to $C-S-H$ and 4.5% to portlandite and Friedel's salt. It can be concluded that, at lower concentrations, a high content in C_3A is beneficial for the ability of an OPC paste to bind chlorides, while at higher external chloride concentrations (for instance in salty lakes), the content in sulphates also becomes important.

Chapter 3

Chloride binding related to hydration products: slag-blended cements

3.1 Introduction

As discussed in the previous chapter, durability of concrete structures in marine environments is strongly related to their deterioration under chloride attack. In the Netherlands, the most used cement type is CEM III/B, which according to EN 197-1 [11] is a blend of OPC and 66-80% ground granulated blast furnace slag. Because of this preference, which is related to its increased durability in marine environments, among other factors, the chloride binding model will be extended to include slag-blended cements. This supplementary cementitious material has been briefly described in Section 1.5.1 and its hydration in the presence of portlandite and OPC will be detailed in this chapter.

A number of studies have considered the ability of slag-blended cements to resist chloride attack [32,37,53,54,85]. A consensus exists upon the increased capacity of slag blended cements to bind chlorides, compared to pure OPC. This phenomenon has been attributed to the higher alumina content of slag [85], or to the $[OH^-]/[Cl^-]$ ratio [54] and the negative role of sulphates has been highlighted [86]. In this study, only data obtained by the intrusion of external chloride ions into the sample [37] were employed, as opposed to internally-mixed chlorides [53,54]. Also of importance was the determination of complete chloride binding isotherms [37] as opposed to the chloride binding in one specific external chloride concentration point [53,54] and the availability of the compositional data regarding the OPC and slag employed [85]. All data employed in this study regarding chloride binding (selected from [37]) has been obtained using the "equilibrium method", in which the crushed hardened sample is kept in a NaCl solution of known concentration until equilibrium is reached.

In order to relate the amount of bound chlorides to the individual chloride binding capacity of each hydrated phase, a hydration model for slag-blended cements is needed. For this purpose, a combination of the OPC hydration model employed in Chapter 2 of this study, based on the work of Brouwers [61,62,65], the slag-blended cement hydration model by [87,88] and newer findings from literature [89–92] are used.

The binding ability of slag-blended cements comes from the interaction between the hydration of the cement and that of the slag. The two components react with different rates, and the slag hydration is activated by the portlandite formed during the OPC

hydration. The two separate hydration processes lead to the formation of hydration products, some of which can be traced back to the reaction of OPC components, some to the reaction of slag with water and portlandite, and some which are common to both processes. Here, the hydration of the OPC-component and the slag one will also be considered separately for the modelling point of view, even though the consumption of portlandite is not their only interaction in real OPC-slag systems (as detailed in Section 3.2).

3.2 The paste model

3.2.1 The hydration of the OPC component

As described in the previous chapter, the hydration of OPC is modelled based on a study of Brouwers [61,62,65] and takes into consideration the particular case of no carbonation. Table 2.1 reviews the chemical equations that describe the hydration of OPC under water-saturated conditions, while Table 2.2 details the molar equations used to compute the amounts of formed hydration products. The same notations used in [93] Chapter 2 were kept, with the exception of the superscript OPC, used to differentiate these hydration products from the ones of the slag component.

As this OPC hydration model is extensively described in [31,61,62,65] and Chapter 2, no further details will be given here. One observation should be made, however, on the composition of $C-S-H$, which will be relevant further. A number of studies [89,94,95] have reported a C/S ratio of 1.8-1.85 for pure $C-S-H$ in OPC pastes, together with a substitution of the Si by Al. The A/S ratio in OPC $C-S-H$ was found to be roughly 0.08 [89,94]. These values would lead to a C/(S+A) value of 1.7, which is consistent with the model presented in Chapter 2. However, the initial OPC hydration model does not take into account the Al substitution into $C-S-H$, but considers C/S to be 1.7. Hence, the $C-S-H$ structure $C_{1.7}SH_{3.2}$, used so far to describe composition of this hydration product, will be also considered in this chapter for the hydration of OPC. This choice will be described also from the chloride binding point of view in Section 3.4.2. In the case of slag-blended paste, the notation "$C-S-A-H$" will be used to describe the calcium aluminosilicate hydrate phase, which is known to be able to incorporate higher alumina amounts [89,92,94,95].

An important mention is the way the mass of sample will be calculated throughout this study. There are three types of samples which will be considered: pure OPC hydrated pastes, termed HCP1÷HCP3 for "hardened cement paste", OPC-slag blended hydrated pastes, termed S1÷S5 and theoretically computed "slag only" in which only the hydration products formed with the aid of CH (which is generated by hydrated OPC) are considered to constitute the sample (further details in Section 3.5). Moreover, the masses of all these samples will be computed at 11% r.h. The experimental data concerning the chloride binding capacity of hardened employed in this study [37] are also based on samples dried

at 11% r.h.. The water loss of certain hydration products upon drying has been estimated in [61,62,64,65]. This phenomenon leads to a decrease of molecular mass of the hydration products; however, the molar quantities are unaffected.
Using the molar amounts computed using the equations in Tables 2.2, 3.1 and 3.2, and the molecular masses of all considered hydration products at 100% r.h. and 11% r.h. (Table 2.3), the mass of each hydrated product at either of the two relative humidities considered can be computed: Table 2.2 lists the way all OPC hydration products molar amounts (Eqs. (2.2.2), (2.2.5) and (2.2.6)) that can be computed from the initial OPC composition.

Table 3.1. Molar relations between the amounts of hydration products and the oxide composition of slag in slag-blended cements [87,88], as described in Section 3.2.2.

$$n^{sl}_{C_4A\bar{S}H_{14}} = \gamma \cdot n^{sl}_{\bar{S}}$$

$$n^{sl}_{C_aSA_bH_{(a+1.5)}} = \gamma \cdot n^{sl}_{S}$$

$$n^{sl}_{M_5AH_{13}} = \gamma \cdot \frac{n^{sl}_{M}}{5}$$

$$n^{sl}_{C_6AFS_2H_8} = \gamma \cdot n^{sl}_{F}$$

$$n^{*}_{A} = \gamma \cdot n^{sl}_{A} - n^{sl}_{M_5AH_{13}} - n^{sl}_{C_6AFS_2H_8} - (\gamma \cdot n^{sl}_{\bar{S}} - n^{OPC}_{C_4AH_{22}})$$

$$n^{sl}_{C_4AH_{22}} = n^{*}_{A} - \gamma \cdot n^{sl}_{S} + b'$$

Table 3.2. Final molar amounts of hydration products in slag-blended cements after the hydration of both the OPC and the slag component, as described in Section 3.2.3.

$$n^{total}_{C_4A\bar{S}H_{14}} = n^{OPC}_{C_4A\bar{S}H_{14}} + n^{sl}_{C_4A\bar{S}H_{14}}$$

$$n^{total}_{C_4AH_{22}} = n^{sl}_{C_4AH_{22}}$$

$$n^{total}_{C_{\bar{a}}SA_{\bar{b}}H_{(\bar{a}+1.5)}} = n^{sl}_{S} + n^{OPC}_{C_{1.7}SH_{3.2}}$$

$$n^{final}_{CH} = n^{OPC}_{CH} - [(n^{sl}_{\bar{S}} - n^{OPC}_{C_4AH_{22}}) \cdot 4 + 6n^{sl}_{C_6AFS_2H_8} + a \cdot n^{sl}_{S} + 4 \cdot n^{sl}_{C_4AH_{22}} - n^{sl}_{C}]$$

Therefore, the total sample mass will be computed as follows:
In the case of OPC hydrated pastes (HCP1÷HCP3), m_{spl}^{OPC} will be computed using Eqs. (2.2.2)-(2.2.6).
The total mass of binder (OPC and slag) b_0 and thus the mass fractions of the two components, x^{OPC} and x^{sl}, respectively, can be considered as

$$b_0 = b_0^{OPC} + b_0^{sl} \tag{3.2.1}$$

$$x^{OPC} = \frac{b_0^{OPC}}{b_0},\ x^{sl} = \frac{b_0^{sl}}{b_0} \tag{3.2.2}$$

The degree of hydration of the OPC component will be the same as selected in Chapter 2, because all the samples are identical (in terms of composition, water/binder ratio, curing age and conditions etc.).

3.2.2 The hydration of the slag component

A general equation describing the hydration of the slag component in OPC-slag blended cements (in the presence of portlandite generated by the hydration of the OPC component) is formulated as

$$\begin{aligned} &C_{n_C^{sl}}S_{n_S^{sl}}A_{n_A^{sl}}M_{n_M^{sl}}\bar{S}_{n_{\bar{S}}^{sl}}F_{n_F^{sl}} + n_H H + n_{CH} CH \rightarrow n_{C-S-H}^{sl} C_{a'}SA_{b'}H_{(a'+1.5)} + n_{HT}^{sl} M_5AH_{13} + \\ &n_{HG}^{sl} C_6AFS_2H_8 + n_{AFt}^{sl} C_6A\bar{S}_3H_{32} + n_{HO-AFm}^{sl} C_4AH_{13} \end{aligned} \tag{3.2.3}$$

The hydration products considered in this model are a Mg-containing phase (M_5AH_{19} in saturated state), a Fe-containing phase ($C_6AFS_2H_{18}$, in order to maintain the saturated state considered in the OPC model), the same two AFm phases (SO_4-AFm, $C_4A\bar{S}H_{14}$ and $HO-AFm$, C_4AH_{10}) considered for OPC hydration and $C-S-H$ with a lower C/S ratio than the one formed by plain OPC and with a limited Al substitution. This model is based on the one presented by Chen and Brouwers [87,88], and modified in order to take into account newer findings from literature [89–92], which are detailed below. The fate of Mn in the slag hydration will not be considered in this chapter, for a number of reasons. Firstly, the model in [87,88] does not account for the contribution of manganese. Secondly, the oxidation state in which Mn is contained in the slag (Mn^{2+} as MnO or solid solutions (Fe,Mg,Mn)O [96] etc. or Mn^{3+} as Mn_2O_3 or a C_4AMn phase [97] or brownmillerite solid solutions [98]) is not known, so its hydration products cannot be predicted with any degree of accuracy.
An important observation to be made is that the formation of an AFt phase is not considered here. Recent studies [89–92] have shown that the amount of ettringite decreases with the increase of the amount of slag in the blended cement. Moreover, in

[90] and [91] no ettringite was found in the samples after 90 days of curing in samples containing 75% and 90% slag [91] or 60% slag [90]. Therefore, in this model all sulphates present in the slag are considered to react with the alumina in the slag to form monosulphate. This reaction, together with the formation of the Fe-containing hydrogarnet, is considered to take priority over the other reaction involving the aluminates (molar relations are presented in Table 2.2).

It has also been observed that the C/S ratio of the formed $C-S-H$ decreases as the proportion of slag in the mix increases [89,94,95] to a minimum of 1.2 in the case of pure slag. Based on the data presented in [89], the following relation was fitted between the C/S ratio of the slag $C-S-A-H$, referred to as a', and slag content (x^{sl}) in the mix:

$$a' = 1.7 - 0.5 \cdot x^{sl} \tag{3.2.4}$$

The alumina from slag still available for hydration after the formation of monosulphate and hydrogarnet (n_A^* in Table 3.1) can afterwards enter the composition of $C-S-H$ (eq. (3.2.5) below and $n^{sl}_{C_a{}'SA_{b'}H_{(a'+1.5)}}$ from Table 3.1) and, if a sufficient quantity still remains, form $HO-AFm$ ($n^{sl}_{C_4AH_{22}}$ in Table 3.1):

$$\begin{aligned} &n_A^* A + n^{total}_{C_a{}'SH_{(a'+1.5)}} C_a{}'SH_{(a'+1.5)} + 4(n_A^* - b'\cdot n^{total}_{C_a{}'SH_{(a'+1.5)}})CH + 18(n_A^* - b'\cdot n^{total}_{C_a{}'SH_{(a'+1.5)}})H \rightarrow \\ &n^{total}_{C_a{}'SA_{b'}H_{(a'+1.5)}} C_a{}'SA_{b'}H_{(a'+1.5)} + (n_A^* - b'\cdot n^{total}_{C_a{}'SH_{(a'+1.5)}})C_4AH_{22} \end{aligned} \tag{3.2.5}$$

Furthermore, it is known [87–89,95,99] that there is a relationship between the C/S and A/S ratios of slag generated. Therefore, the maximum A/S ratio of the final hydrated paste will be computed using a linear relationship [56,87,88] if the remaining alumina allows:

$$b' = \frac{1 - 0.4277 \cdot a'}{4.672} \tag{3.2.6}$$

A factor which largely influences the amounts of hydration products formed, as well as the C/S and A/S ratios, is the degree of hydration of the slag, γ. Lumley et al. [100] studied the hydration degree of various slag-OPC hardened cement pastes up to a year of curing, with w_0/b_0 ratios between 0.3 and 0.8 and x^{sl} ratios between 0 and 0.92. Taking the obtained values into consideration, as well as the age, slag content and w_0/b_0 ratio of each hydrated sample in this study, a degree of hydration was assigned to the slag component (Table 3.3).

In the case of these "slag only" samples (S1÷S5), their mass can be computed using the following relation:

$$m_{spl}^{sl} = m_{C_a SA_b H_{(a'+0.5)}}^{sl} + m_{C_4 A\bar{S}H_{10}}^{sl} + m_{C_6 AFS_2 H_8}^{sl} + m_{C_4 AH_{13}}^{sl} + m_{M_5 AH_7}^{sl} + (1-\gamma)(b_0^{sl} - m_{UO}^{sl}) + m_{UO}^{sl} \quad (3.2.7)$$

Table 3.1 lists the way all slag hydration products molar amounts ($n_{C_a SA_b H_{(a'+0.5)}}^{sl}$, $n_{C_4 A\bar{S}H_{10}}^{sl}$ etc.) that can be computed from the initial slag composition.

Table 3.3. Characteristics of all hydrated cement pastes (selected from [37]): initial water to binder ratio, w0/b0, curing age, slag ratio (x^{sl}), the estimated degree of hydration of the OPC (α) and the estimated degree of hydration of the slag (γ), the fitted Freundlich isotherm coefficients (αF and βF), the final C/S ratio of the $C-S-A-H$ phase ($\bar{a}$) and the mass of sample at 11% r.h. (mspl), computed using Eqs. (2.2.6), (3.2.7) and (3.2.10).

	w_0/b_0	Age (months)	x^{sl}	α	γ	α_F	β_F	$\bar{a}$	m_{spl} (g)
HCP1	0.3	2	0	0.75	-	6.92 7.42	0.359 0.372	1.70	113.49
HCP2	0.5	2	0	0.80	-	7.72 7.49 7.44	0.414 0.417 0.396	1.70	114.39
HCP3	0.5	9	0	0.85	-	7.28 7.29	0.443 0.409	1.70	115.28
S1	0.3	2	0.25	0.75	0.60	7.25 7.29	0.363 0.362	1.58	109.13
S2	0.5	2	0.25	0.80	0.70	10.23	0.411	1.58	109.43
S3	0.5	9	0.25	0.85	0.75	9.36	0.486	1.58	109.36
S4	0.3	2	0.40	0.75	0.55	7.83	0.396	1.50	109.88
S5	0.5	2	0.50	0.80	0.50	9.94	0.495	1.45	110.70

3.2.3 The hydration of slag-blended cements

The equilibrium of AFm phases

A first observation to be made is that, in the case of the hydration of the aluminate phases, there is no structural difference depending on whether the hydration product has been generated by the OPC or the slag component. However, as explained in Chapter 2, the $HO-AFm$ phase is readily transformed to monosulphate (SO_4-AFm) in the presence of sulphates [56]. In the hydration model of OPC, the $HO-AFm$ phase is formed only after depletion of sulphates. Therefore, when adding slag to the binder mix, the sulphate content of slag is considered to first transform the already existent $HO-AFm$ (because of the faster hydration of OPC) to SO_4-AFm. In this chapter, all Mg is considered to be bound into hydrotalcite, and therefore all Al needed for this reaction will be deducted from the Al available to form AFm phases (Table 3.1). The equilibrium between hydrotalcite and AFm formation is studied more in depth in [101,102].

The equilibrium of the $C-S-A-H$ phase

In the case of the $C-S-A-H$ phase, its composition will reach an equilibrium between the composition of the slag-generated $C-S-A-H$ and the OPC-generated one. Therefore, overall C/S and A/S ratios need to be computed. The value for the overall C/S ratio of $C-S-A-H$, formed by both the OPC and slag components of the blended cement can be computed as follows:

$$\bar{a} = \frac{1.7 \cdot n^{OPC}_{C_{1.7}SH_{3.2}} + a' \cdot n^{sl}_{s}}{n^{OPC}_{C_{1.7}SH_{3.2}} + n^{sl}_{s}} \tag{3.2.8}$$

while the A/S ratio, an average $\bar{b}$, can be computed by substituting Eq. (3.2.8) into Eq. (3.2.6).
In case of insufficient alumina, the A/S ratio will be computed using the following equation:

$$\bar{b} = \frac{n^{*}_{A}}{n^{OPC}_{C_{1.7}SH_{3.2}} + n^{sl}_{S}} \tag{3.2.9}$$

and the relations in Tables 3.1 and 3.2. Therefore, $C_{\bar{a}}SA_{\bar{b}}H_{(\bar{a}+1.5)}$ would describe the composition of the global $C-S-A-H$ phase.
In the case of these slag-blended hardened pastes (S1÷S5), the mass of sample can be computed as follows:

$$m_{spl} = m^{OPC}_{spl} \cdot x^{OPC} + m^{sl}_{spl} \cdot x^{sl} \tag{3.2.10}$$

3.3 Chloride binding of the slag-blended cement pastes

3.3.1 Binding isotherms

In the case of slag blended cements, the chloride binding ability will be due to the same hydration products as in the case of OPC. However, due to the differences in hydration, a number of changes will occur. The chloride binding of slag-blended hardened cement pastes will depend on three components: the chloride binding abilities of the OPC hydration products and of the slag hydration products, as well as the interaction between these two, which will result in a number of changes from the model presented in Chapter 2.

3.3.2 Chloride binding- experimental data used in this study

The experimental results have been selected from [37]. The oxide compositions of the OPC and the slag used can be found in Table 2.8 (termed "OPC 3" and "Slag", respectively).

In total 8 samples have been analysed- three hardened cement pastes (pure OPC) and five slag-blended cement hydrates pastes, with a slag content between 25% and 50%, and having various w_0/b_0 ratios and curing ages. The composition of these samples and their computed sample masses and the attributed degree of hydration (both for the OPC component, α and the slag component, γ) can be found in Tables 2.8 and Eqs. (2.5.10)-(2.5.16). Also in Table 3.3 the parameters of the fitted chloride binding Freundlich isotherms, α_F and β_F.

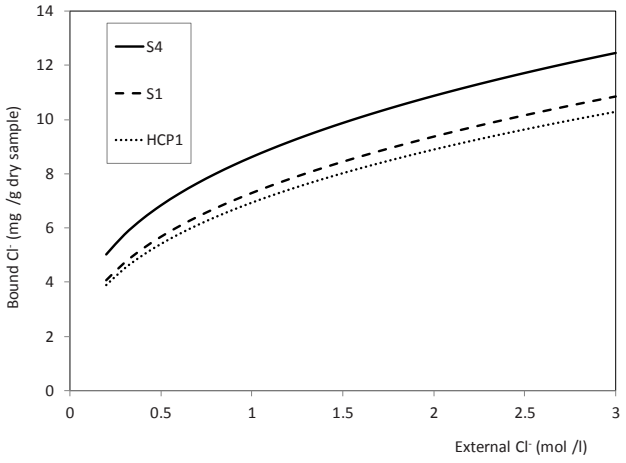

Figure 3.1. Experimental isotherms used in this study, selected for hydrated cement pastes with w_0/b_0 of 0.3 [37]. All details about the samples (HCP1 0% slag, S1 25% slag and S4 40% slag) can be found in Table 3.5.

Figures 3.1 and 3.2 show the experimentally obtained chloride binding isotherms for four slag-blended cement samples considered and two OPC pastes [37] are included, split based on their w_0/b_0 ratio. All the shown samples have the same curing age of 2 months before being exposed to the external chlorides.

Figure 3.1 shows three chloride binding isotherms of pastes with a w_0/b_0 of 0.3 and slag contents x^{sl} of 0% (HCP1), 25% (S1) and 40% (S4). As expected, the chloride binding capacity increases with the increase of the slag content (Section 3.1). The same trend can be seen in Figure 3.2, which presents three chloride binding isotherms of pastes with a w_0/b_0 of 0.5 and slag contents of 0% (HCP2), 25% (S2) and 50% (S5).

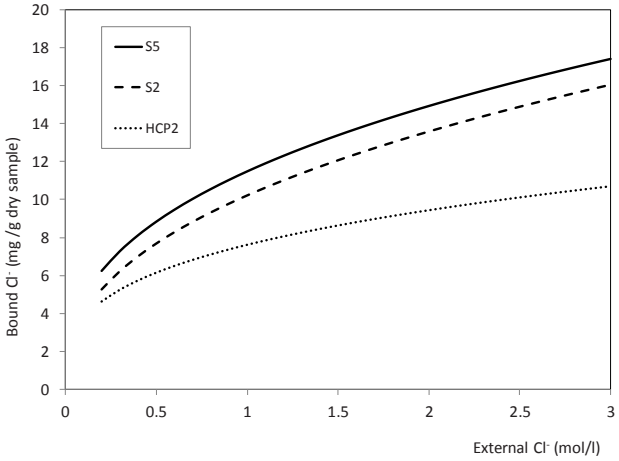

Figure 3.2. Experimental isotherms used in this study, selected for hydrated cement pastes with w_0/b_0 0.5 [37]. The composition of all samples (HCP2 0% slag, S2 25% slag and S5 50% slag) can be found in Table 3.5.

When comparing the two figures (for instance the S1 and S2 isotherms), it can be observed that the water/binder ratio, and implicitly the degree of hydration, has a large influence on the chloride binding capacity, which underlines the importance of taking into account such parameters as w_0/b_0 ratio, age of the sample, curing conditions etc. when evaluating chloride binding.

3.4 The chloride binding ability of slag-blended cement hydration products

The chloride binding isotherms in this study will be termed either $C^0_{b,hp}$ for chloride binding abilities expressed in mg Cl^-/g hydration product conditioned to 11% r.h., or $C_{b,hp}$ for the chloride binding capacities expressed in mg Cl^-/g sample at 11% r.h., m_{spl},

as also employed in Chapter 2. The term n_{hp} refers to the molar amount of the specified hydration product, in moles, calculated using Tables 3.2, 3.3 and 3.4. The mass of sample in grams at 11% r.h., m_{spl}, is computed as explained in Section 3.2.1. Equation (2.5.9) details the general relation between $C^0_{b,hp}$ and $C_{b,hp}$.
The three component chloride bindings (see Section 5) can be computed using the molar amounts in Tables 2.1, 3.1 and 3.2 and for C_b^{OPC}, C_b^{sl} and C_b^{total}, respectively, the molecular masses from Table 2.3 and the mass of sample m_{spl} from Table 3.3.
The chloride concentration of the external solution, c, is always expressed in mol Cl^-/l solution and considered to be in equilibrium with the pore solution. Therefore, the terms of "external", "free" or "equilibrium" chloride concentration will be used interchangeably throughout this chapter.

3.4.1 Chloride binding capacity of the aluminate phases in slag-blended cements

Firstly, the chloride binding of the aluminate phases will be considered to be described by the same equations detailed in Chapter 2. The "simplified version" of this model will be used, which does not take into consideration the contribution of CH and FS (Friedel's salt, $3CaO•Al_2O_3•CaCl_2•10H_2O$) to the physical bonding of chlorides. The reason for this choice is the low contribution of these two phases found in Chapter 2 (around 3% of the total bound chlorides), as well as ease of use. Moreover, the surface binding of chlorides by these two hydrates is controversial, and no data about their binding capacities in systems where hydrates with more negative surfaces ($C-S-A-H$ with various C/S ratios, see following section) coexist.
Another difference from the model presented in Chapter 2 is that the total amounts of $HO-AFm$ and SO_4-AFm (just as $C-S-A-H$) generated by both the hydration of OPC and the one of the slag (Table 3.3), will also be considered able to bind chlorides. The isotherms describing the chloride binding capacity of $HO-AFm$ and SO_4-AFm from OPC are given in Eqs. (2.5.10)-(2.5.16).

3.4.2 Chloride binding capacity of the phase in slag-blended cements

As explained in Section 3.2.2., the $C-S-A-H$ phase generated by slag-blended cements will have two main differences from the one formed by the hydration of pure OPC: the C/S ratio and the A/S ratio. However, as explained in Section 3.2.1, the value of 1.7 for the C/S ratio, considered for the $C-S-H$ formed through the hydration of OPC in Chapter 2, actually corresponds to the C/(S+A) ratio. Therefore, the C/(S+A) ratio will be taken into account also for the chloride binding capacity of the $C-S-A-H$ generated by the slag component.
A modification from the $C^0_{b,C-S-A-H,OPC}$ isotherm presented in Chapter 2, will be the use of a simplified relation which does not take into account the C_2S/C_3S ratio in OPC for the slag-generated $C-S-A-H$ chloride binding capacity. The $C-S-H$ isotherm

proposed in Chapter 2 was a combination of two isotherms proposed by Zibara [37] for $C-S-H$ formed by C_2S and C_3S, respectively. However (as explained in Chapter 2), there is no structural difference between the final products of hydration. In Chapter 2, a combination of the two isotherms was used for the sake of precision. The same isotherm will be used for the chloride binding of $C-S-A-H$ when referring to the individual hydration of OPC. However, the two isotherms proposed by Zibara [37] are almost identical. Therefore, the following relation was selected to further represent the chloride binding of a $C-S-A-H$ generated by slag:

$$C^0_{b,C_a{}'SA_b{}'H_{(a'+1.5)}} = \lambda \cdot 6.65\, c^{0.334} \tag{3.4.11}$$

As the selected chloride binding isotherm for $C-S-A-H$ is valid for a C/(S+A) ratio of 1.7, a correction needs to be done for lower values. Viallis [103] has studied the chloride binding ability of lyophilized $C-S-H$ gels with C/S ratios between 0.65 and 1.50, using a NaCl solution with the concentration of 0.5 mol/l. The results have shown that when the C/S ratio decreases from 1.55 to 1.2, the amount of bound chlorides increases. When the C/S ratio further decreases up to 0.8, the chloride binding capacity also slightly decreases, the trend accentuating (higher slope of the linear fit) for C/S ratios between 0.8 and 0.6. Because of using lyophilized $C-S-H$ gels, the measured amounts of bound chlorides were very different than when using alcohol for drying the gels. Therefore, just the ratio between the bound chlorides amounts is used here, since this is considered to be correct, as a ratio of results that follow the same experimental protocol.

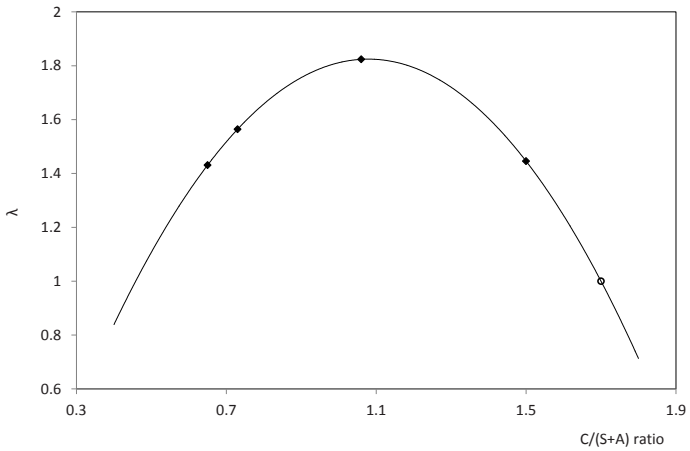

Figure 3.3. Correction for the binding capacity of $C-S-A-H$ as a function of the C/(S+A) ratio. Black diamonds represent data points from [103] and the hollow circles the points at C/(S+A)=1.7 and λ=1.

Figure 3.3 shows these ratios as a function of the C/S ratio in $C-S-H$ and the fitted parabolic equation, extrapolated to a C/S ratio of 1.7, which is considered to have a ratio of unity. The result of this equation will be considered as the coefficient λ by which the chloride binding of the $C-S-A-H$ phase needs to be multiplied in order to account for the differences in their C/S ratios. This coefficient will be calculated in the same way for both the OPC-slag blended cement samples, as well as the "slag only" samples:

$$\lambda = -2.1381\cdot\left(\frac{\bar{a}}{1+\bar{b}}\right)^2 + 4.6139\cdot\left(\frac{\bar{a}}{1+\bar{b}}\right) - 0.6646 \tag{3.4.12}$$

where $\bar{a}$ and $\bar{b}$ can be computed using Eqs. (3.2.8) and (3.2.9), respectively. The total amount of chlorides bound by a sample will be termed C_b and computed as the sum of the individual chloride binding abilities of $HO-AFm$, SO_4-AFm and $C-S-A-H$.

3.5 Chloride binding isotherms

Three types of chloride binding isotherms will be computed in this study- for the individual hydration of OPC (described in Table 3.1), C_b^{OPC}, the hydration of the slag component while only the role of CH produced by the OPC hydration is taken into account (molar amounts from Table 3.1), C_b^{sl}, and the total chloride binding of both components, C_b^{total}, using the amounts in Table 3.2, respectively. In all three cases, the general formula for the chloride binding capacity of the hydrated paste is expressed by:

$$C_b = C_{b,C-S-A-H} + C_{b,SO_4-AFm} + C_{b,HO-AFm} \tag{3.5.13}$$

where the three component chloride bindings can be computed using the molar amounts in Tables 2.1, 3.1 and 3.2 for C_b^{OPC}, C_b^{sl} and C_b^{total}, respectively.

3.5.1 Chloride binding of the slag-blended cement samples

In this section, the C_b^{total} isotherms will be computed for the S1-S5 samples (composition in Table 3.3) by computing the individual chloride binding isotherms of $C-S-A-H$, SO_4-AFm and $HO-AFm$ as described in Section 3.4 and using the molar amounts computed in Table 3.3. In other words, the total amounts of hydration products generated by the hydration of the slag-blended cements will be considered, including their interactions as described in Section 3.2.3.

Figure 3.4 shows how the computed C_b^{total} for S4 (composition from Table 3.3) compares to the experimental data, as well as the contribution of the SO_4-AFm and $C-S-A-H$ phases. In this case, the $C-S-A-H$ phase contributes about two thirds of the total bound chlorides. Furthermore, these two total contributions are split into their components in order to see the influence of the slag hydration products on the total chloride binding ability of the paste. Figures 3.5 and 3.6 show this breakdown for both

the SO_4-AFm and $C-S-A-H$ phases, respectively. From Figure 3.5 it can be seen that the contribution of the SO_4-AFm phase determined by the hydration of slag is slightly higher than the one of OPC. This can be explained by the fact that, as explained in Section 3.4.1 and Table 3.2, there are two mechanisms considered for the formation of SO_4-AFm through the hydration of slag, one involving the aluminate phase generated by the dissolving of the slag itself, and the second one coming from the conversion of $HO-AFm$ generated by the hydration of OPC into SO_4-AFm.

In the case of the $C-S-A-H$ phase (Figure 3.6), the trend is reversed: the contribution of the OPC-generated $C-S-A-H$ is slightly higher than the one generated by the slag. However, both these isotherms take into consideration the λ coefficient (see eq. (3.4.12)), which explains the increase of the $C-S-A-H$ chloride binding capacity. There is no structural difference between the two $C-S-A-H$ phases, only the computed amounts are dependent of the C and the S contents of the slag.

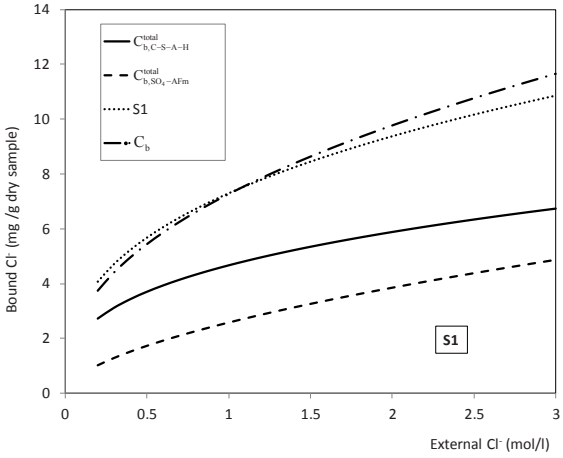

Figure 3.4. Chloride binding capacity of hydration products in hydrated slag-blended cement pastes, applied to sample S1 (see Table 3.3). Isotherms are described in Sections 3.4 and 3.5.

Figure 3.7 shows the breakdown of chloride binding capacity between the four mentioned phases as a function of the free chloride concentration. As it can be seen, the contribution of the $C-S-A-H$ phase slightly decreases from a total of 70% of the bound chlorides (39% the OPC-generated $C-S-A-H$ and 31% the slag-generated one) at 0.5 mol/l external chloride concentration to 63% at a free chloride concentration of 1.8 mol/l (divided as 35% the OPC- generated $C-S-A-H$ contribution and 28% the slag-generated amount). On the contrary, the contribution of the SO_4-AFm phase shows an increase from 30% of the bound chlorides (13.2% from the OPC-generated SO_4-AFm

and 16.8% from the slag hydration) at 0.5 mol/l external chloride concentration to 37% at a free chloride concentration of 1.8 mol/l (16.2% and 20.7% from the OPC-generated SO_4 – AFm and the slag-generated one, respectively).

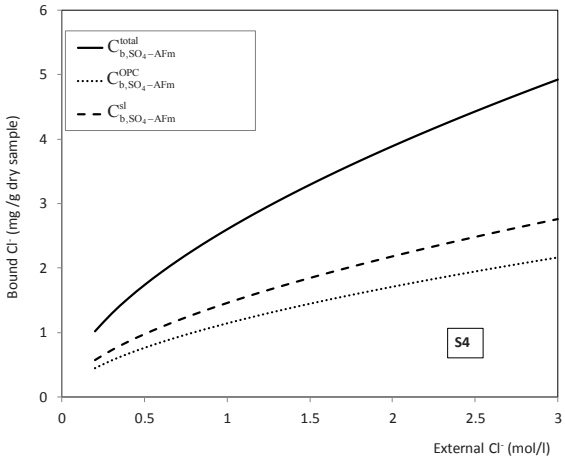

Figure 3.5. Chloride binding capacity of the phase in hydrated slag-blended cement pastes, applied to sample S4 (see Table 3.5). Isotherms are described in Section 3.4.1.

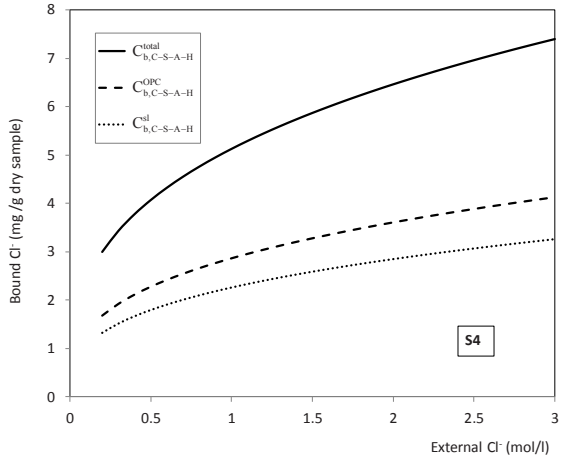

Figure 3.6. Chloride binding capacity of the phase in hydrated slag-blended cement pastes, applied to sample S4 (see Table 3.3). Isotherms are described in Section 3.4.2.

3.5.2 Evaluation of the contribution of the slag component to chloride binding

As explained in Section 3.2.3 and quantified in Table 3.2, C_b^{total} will not simply be a sum of C_b^{OPC} and C_b^{sl}, due to the fact that the hydration of the OPC-component and that of the slag component do not progress independently, as explained in Section 3.4. Therefore, it can be considered that the chloride binding capacity of slag-blended hydrated pastes consists of three components: one due to the hydration products of OPC remaining unmodified by the slag hydration (so just SO_4-AFm and $C-S-A-H$ when the λ coefficient set to unity), one due to the hydration products of the slag while only the role of CH produced by the OPC hydration is taken into account (actually C_b^{sl}), and one which represents the interaction of the two components of the binder.

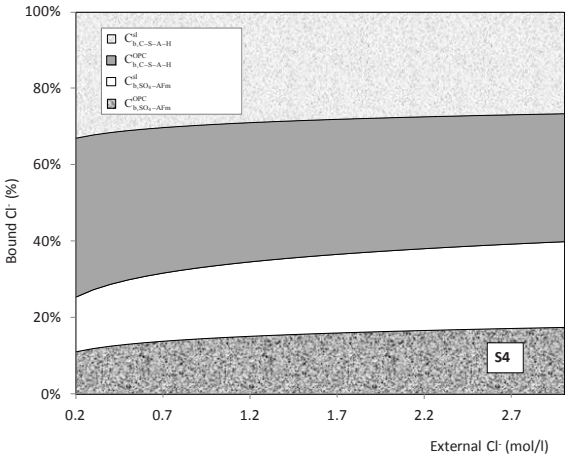

Figure 3.7. Breakdown of bound chlorides by hydration products as a function of equilibrium chloride concentration in the pore solution applied to sample S4 (Table 3.3). Isotherms are described in Sections 3.4 and 3.5.

In order to quantify this third component, three other equations will be used. The interaction between the OPC and the slag component of the binder can be described in terms relevant to their chloride binding abilities by two phenomena: the decrease of the C/(S+A) ratio of $C-S-A-H$ and the consumption of the $HO-AFm$ phase by the sulphate ions generated by slag. Therefore, the C_b^{sl} will be compared to the following three isotherms):

$$C_b^{diff} = C_b^{exp,total} - C_b^{exp,OPC} \cdot x^{OPC} \tag{3.5.14}$$

$$C_b^{corr1} = C_b^{diff} - C_{b,C-S-A-H}^{OPC} \cdot (\lambda - 1) \tag{3.5.15}$$

$$C_b^{corr2} = C_b^{corr1} + \frac{n_{C_4AH_{22}}^{OPC} \cdot M_{11\%r.h.,C_4AH_{22}}}{m_{spl}} \cdot (C^0_{b,SO_4-AFm} - C^0_{b,HO-AFm}) \quad (3.5.16)$$

The isotherm C_b^{diff} represents the difference between the total chloride binding ability of the slag-blended hydrated paste and the chloride binding of its OPC component, while taking into account the OPC proportion in the blended cement. If the interactions in Section 3.2.3 would not be taken into account (so the hydration would be described solely on the basis of Sections 3.2.1 and 3.2.2 as two separate processes- the hydration of the OPC-component and the one of the slag-component, respectively), the C_b^{diff} should be equal to C_b^{sl}.

Since it has been explained that this approach would be over-simplified, C_b^{corr1} is computed to account for the influence of the decreased C/S ratio of the $C-S-A-H$ produced by the OPC component (Section 3.2.3.2). This isotherm considers the fact that the $C-S-A-H$ generated from the OPC hydration has a higher C/S ratio and therefore a decreased chloride binding (see Section 3.4.2) compared to the $C-S-A-H$ of the slag-blended cement hydration. A correction is therefore applied to C_b^{diff} by subtracting this increase which is due to the λ coefficient (Eq. (3.4.11).

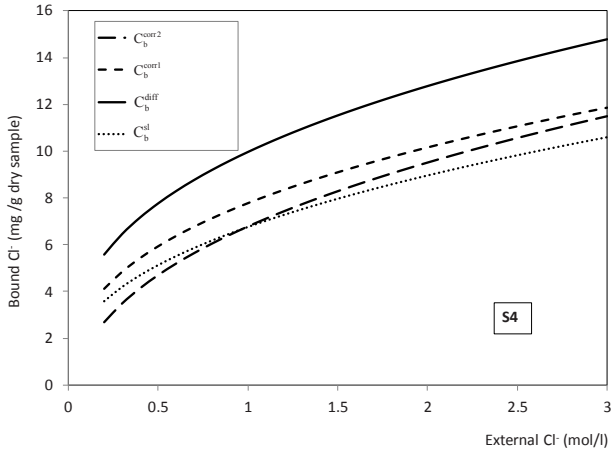

Figure 3.8. Chloride binding capacity of the slag component in hydrated slag-blended cement pastes applied to sample S4 (see Table 3.3). Isotherms are described in Section 3.5.2.

The third isotherm, C_b^{corr2}, further accounts for the transformation of $HO-AFm$ to SO_4-AFm, as described in Section 3.2.3.1. In order to achieve this, the contribution of OPC-generated $HO-AFm$ to the chloride binding is subtracted, and instead the influence of the newly-formed SO_4-AFm is added. The influence of this transformation on the

mass of the sample is considered to be negligible. In this way, both interactions considered in Section 3.2.3 are accounted for, and the contribution of the slag component of the blended cement can be validated by comparing the C_b^{corr2} and C_b^{sl} isotherms.

Figure 3.8 illustrates the C_b^{diff}, C_b^{corr1} and C_b^{corr2} isotherms for the sample S4, together with the C_b^{sl} isotherm for comparison. Initially, the difference between the C_b^{diff} and C_b^{sl} is quite significant.

When C_b^{corr1} is computed to account for the λ coefficient contribution, the difference to C_b^{sl} becomes lower. With the introduction of C_b^{corr2}, the match to C_b^{sl} becomes very good. Therefore, it can be concluded that, indeed, the interaction between the hydration of the OPC and that of the slag in terms of chloride binding ability can be estimated accurately by the decrease of the C/(S+A) ratio of $C-S-A-H$ and the consumption of the $HO-AFm$ phase by the sulphate ions generated by the slag dissolution. Moreover, this match proves that the model works independently for describing the chloride binding ability of the slag component, and also that the model used to quantify the hydration of the slag is valid.

3.6 Comparison with experimental data and other models from literature

The only non-kinetic chloride binding model which could be found in literature is the one of Dhir et al. [85]. While this model takes into account the slag percentage in the slag-blended cement and the concentration of free chlorides, it does not take into account other parameters such as w_0/b_0, curing age etc. Therefore, for the samples S1, S2 and S3, for instance, the model will yield the same predictions. The equation describing this model is:

$$C_b^{Dhir} = [-22.21 \cdot (x^{sl})^2 + 39.45 \cdot x^{sl} + 3.36] \cdot c + [6.84 \cdot (x^{sl})^2 - 6.40 \cdot x^{sl} + 3.64] \qquad (3.6.17)$$

and will be used for comparison purposes together with the C_b^{total} values and the experimental values (Freundlich isotherm parameters in Table 3.3) at two different free chloride concentrations. Here, the concentration of 0.5 mol/l was chosen as significant, being the usual chloride concentration of sea water. The second chosen concentration is 1.8 mol/l, as used in the Rapid Chloride Migration test [42]. Figure 3.9 shows the experimental isotherms, the C_b^{total} and C_b^{Dhir} at these two free chloride concentrations.

The results show that the proposed model estimates the chloride binding ability of slag-blended pastes with enough accuracy, the relative errors to experimental values being between 3.5% and 29%, with an average of ~ 17% over the whole interval of free chloride concentrations. These errors can have a number of possible sources, including the errors of the plain OPC chloride binding model of ~ 8% (as detailed in Chapter 2), the scatter of the experimental data used, the estimation of hydration degree based on age of

the sample and its composition and the role of slag-generated alumina during the hydration process.

The latter parameter was observed to have the highest impact on the estimation of chloride binding ability. The results presented in this study are based on the hydration of a slag with a low A/S ratio (as categorized by [89,94,95], A/S = 0.16 in the slag). For slags with a higher initial A/S ratio, the incorporation of A in the $C-S-A-H$ structure will also be increased. Moreover, if the alumina is sufficient, $HO-AFm$ could be formed after the complete reaction of the sulphates, and also contribute to the chloride binding. As explained in Chapter 2, the high chloride binding ability of $HO-AFm$ will have a significant influence on the total bound chlorides, even if this hydration product is formed only in small quantities. However, the complex relationship between the AFm phases in the hydrated cement matrix (as detailed in Chapter 2) can mostly account for the underestimation of the chloride binding capacity.

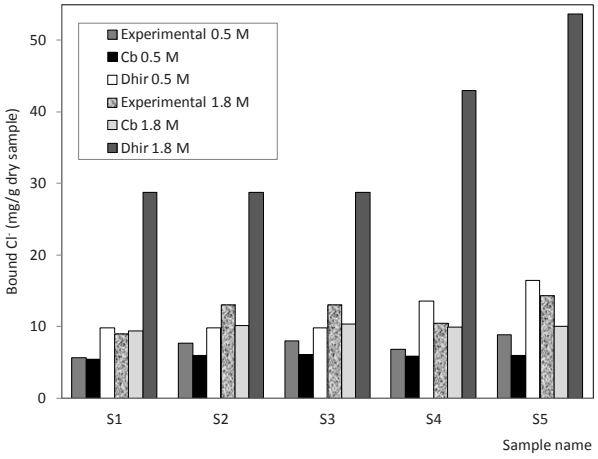

Figure 3.9. Chloride binding capacity of each hydrated paste (see Table 3.5) with experimental values [38] at free chloride concentrations of 0.5 mol/l and 1.8 mol/l (as explained in Section 3.6).

Also from Figure 3.9 it can be seen that the model proposed by Dhir et al. [85] overestimates the chloride binding capacity of the slag-blended cement pastes, with relative errors between 40 and 100% for a free chloride concentration of 0.5 mol/l. For larger free chloride concentrations, the model even predicts 3-3.5 times more bound chlorides than what is measured experimentally.

3.7 Summary and conclusions

Two hydration models [61,62,65,87,88] were combined in this study in order to describe the phase assemblage of a hydrated slag-blended cement paste. New insights into the hydration products of slag-blended cements [56,89–92,94,95] were employed to explain the interaction between the two components of the binder: the OPC and the slag. Separate hydration degrees were estimated for the two components [100] and the mass of each sample at 11% r.h. was computed accordingly. The considered phases able to bind chlorides are the AFm phases and the $C-S-A-H$ phase. The latter is considered to be able to incorporate alumina in its structure [88,89,94,95,104], and its C/S and A/S ratios are taken into account when estimating its chloride binding capacity [103].

The chloride binding capacity of slag-blended cement pastes is considered to be due to three processes: the hydration of the OPC component, the one of the slag component, which both generate chloride-binding hydrated phases, and the interaction of the two, which modifies the final phase assemblage. This third component can, in its turn, be attributed to a number of factors: the decrease of the C/S ratio of the $C-S-A-H$ phase, the incorporation of alumina in the $C-S-A-H$ structure, the transformation of $HO-AFm$ into SO_4-AFm in the presence of sulphates and the decreasing amount of ettringite formed with the increase of the slag content of the blend. All these factors are quantified in the present model, in order to ensure the accuracy of the chloride binding estimation.

When taking into consideration the breakdown of the bound chlorides by hydrated phase, it is observed that the $C-S-A-H$ phase is roughly responsible for two thirds of the bound chlorides, the rest being attributed to the AFm phases. These percentages vary slightly, the contribution of $C-S-A-H$ decreasing by ~ 10% points with the increase of the free chlorides concentration between 0.5 and 1.8 mol/l, while the contribution of SO_4-AFm increases by ~ 20% points. The contribution of the AFm phases could be much higher, if the considered slag had a higher initial A/S ratio. Its increase would determine multiple changes on the microstructure of the hydrated paste, the A/S ratio of $C-S-A-H$ and the amount of AFm phase being the most important.

Besides the A content, the C content of the slag is also important for the final C/S ratio of the $C-S-A-H$ phase, while its amount is influenced by the S content of the slag. Perhaps the most influential factor (together with the A content) on the chloride binding ability of the past is the $\bar{S}$ content of the slag. The sulphate content will determine the amount of $HO-AFm$ formed, which is the hydration product with the highest chloride binding capacity from all hydration products studied in this and previous chapters. Therefore, just like in the case of the OPC composition, but perhaps even more important, the composition of the slag is crucial to the maximum chloride binding capacity of the hydrated paste.

The presented model takes into account all these factors, together with the w_0/b_0 ratio and age of sample, through the two degrees of hydration estimated. By taking into consideration these compositional and curing factors, the accuracy of the model is highly improved from a previous model from literature, which only takes into account the slag content of the mix. This holds true for all free chloride concentrations considered, but the difference becomes more important at higher free chloride concentrations. The present chapter thus highlights the importance of the content of both aluminate phases and sulphates in the initial binder.

Chapter 4

Properties of various size fractions of crushed concrete related to process conditions*

4.1 Introduction

Recycling of construction and demolition waste (C&DW) is one of the important topics in concrete research nowadays. Oikonomou [10] gives an extensive comparative review of the C&DW recycling all over the world. For the EU, it is estimated that the annual generation of C&D waste is the largest single waste stream, apart from agricultural waste. The recycling goals of most European countries are ambitious- between 50% and 90% of their C&D waste production. In the Netherlands, Germany and Denmark landfilling has become more costly than recycling. In its report on "Recycled concrete", WBCSD [9] gives a breakdown of C&DW recycling on individual European countries. Among the total C&DW recovery, recycled aggregates account for 6% to 8% of aggregates use in Europe. The greatest users are the United Kingdom, the Netherlands, Belgium, Switzerland and Germany (data from 2005 and 2006 WBCSD [9]).
In order to turn C&DW into reusable RCA, it first needs to be sorted, crushed and in some case, decontaminated. Possible uses for the generated RCA include general bulk filler or filler in drainage projects, base or sub-base material in road construction, or replacement of new aggregates into concrete [105]. While the first three options are downcycling to low grade applications, the last one is the most favourable in terms of environmental protection, sustainable material use and economic benefits. In Europe, the most common application for RCAs is in road construction [106], while in part of the US and in Japan they are mostly used as replacement of new aggregates in concrete [107,108].
The main difference between natural aggregates for concrete and RCAs is the fact that the latter contain broken aggregate parts that have pieces of hardened cement paste attached to them. The amount of attached mortar or hardened cement paste has been related to the size fraction of RCA [109] and estimated to be between 20% and 40% by mass [109], increasing with the decrease of particle size. Higher values for the attached mortar content were reported in [105]: 60% for 4-8 mm RCA and 65% for the 0-0.3 mm RCA. Due to the presence of unreacted cement, the fine fraction of recycled concrete (RC) was observed to have self-cementing properties in [110]. It was shown that the density of RCA are lower than those of natural aggregates, which can also be explained by the existence of the attached hardened cement paste (hcp) [105,109–116].

* The content of this chapter was published in *Cement and Concrete Research* **52**, 11-21 (2013).

Fine RCA under 2 mm are not considered suitable for use in concrete because of their high attached cement paste content [105,117]. The workability of the mixes containing finer RCA was found to not be affected significantly even at high natural sand replacement levels and without the use of superplasticizer (SP) [118]; however, SP was deemed necessary in [113], while in [119] the workability was found to have an inverse relation to the replacement ratio.
The use of coarse RCA was found to be beneficial for the mechanical properties of concrete in [105], while the fine fraction was observed to have a detrimental effect and was not suitable for use in concrete mixes. Mortars using 100% RC sand were found to have a decrease of compressive strength of 33% [120] and concrete using RC particles under 5 mm as complete sand replacement was shown to have a very similar (30%) decrease [118]. The same study found a decrease of 15% of the compressive strength when just 25% of the natural sand was replaced by RC sand, while in [119] the same replacement level lead to higher compressive strength than the reference samples. The use of maximum replacement of 30% fine RC (0.074-1.19 mm) was found to not influence the compressive strength, but to reduce tensile strength [114].

4.2 Initial concrete

4.2.1 Recipe

A concrete recipe was designed in order to link the initial constituents of concrete to the composition of the recycled material and validate the results. Better quality can be thus ensured since no contaminating materials are mixed in the recycled materials. Moreover, an overall mass balance of ingoing and outgoing materials can be constructed.

Table 4.1. Designed recipe of the initial concrete mixture.

Material	Volume (dm^3)	Mass (kg)	Mass (%)
CEM I 42.5N	111.0	340.0	14.5
Limestone Powder	15.0	40.8	1.7
Sand N1	271.0	718.2	30.7
Gravel G1	248.8	659.3	28.2
Gravel G2	154.2	408.5	17.5
Water	170.0	170.0	7.3
Air	30.0	-	-
Total	1000.0	2336.9	100.0

The final objective is to be able to describe the composition of recycled concrete particles through simple physical analysis and establish some concepts that make knowing the initial composition less critical.
The design of the mix is based on the optimal packing density that can be obtained with the chosen materials. The mix design has been optimized by using the mix design optimization algorithm developed by Hüsken and Brouwers [121]. All granulometric information on the used materials has been included into the algorithm for this purpose. The optimal particle size distribution (PSD) for the mixture has been calculated using the modified Andreasen and Andersen equation. The recipe is shown in Table 4.1. A water/cement ratio of 0.5 was used, and the concrete was cast into plastic cups for hardening prior to crushing, besides cubes of 150 mm x 150 mm x 150 mm for strength determination.

4.2.2 Particle size distribution of the concrete constituents

The particle size distributions (PSDs) of the cement and limestone (Table 4.1) were determined using a Mastersizer 2000 Particle Analyser.

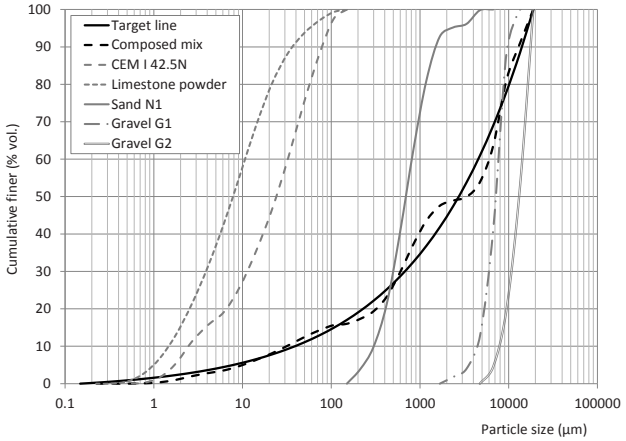

Figure 4.1. Particle size distributions of all the used materials (CEM I 42.5N, limestone powder, sand N1 and two gravel sizes, G1 and G2), the target function and the final mix of the designed initial concrete.

The PSDs of the three aggregate types (N1, G1 and G2, Table 4.1) were determined through dry sieving. The cumulative distributions of all the materials, the designed target line and the grading of the combined final mix [121] are shown in Figure 4.1.

4.2.3 Water content of aggregates

All aggregates were used as-received in the test program, in wet conditions as this is the case in practice. However, the water content was determined for each aggregate fraction, by drying at 105 ± 5ºC for 24 hours. These values were taken into account when designing the mixes for the test program. The water/binder ratio (w_0/b_0) of the mix was adjusted to take into account the water content of each aggregate type. Table 4.2 summarizes the water content of each of the considered aggregates.

Table 4.2. Water content of aggregates used for the initial concrete mix and their minimum and the maximum particle sizes.

Material	Water content (% of initial d.m.)	D_{min} (µm)	D_{max} (µm)
Sand N1	0.05	0.128	125
Gravel G1	0.10	0.275	5600
Gravel G2	0.10	710	8000

4.2.4 Concrete strength

After mixing, the concrete mixture was cast into cubes (150x150x150 mm, according to EN 12390-3 [122]), cured in water at a temperature of 20ºC and tested for compressive strength at the ages of 1, 3, 7, 28 and 91 days.

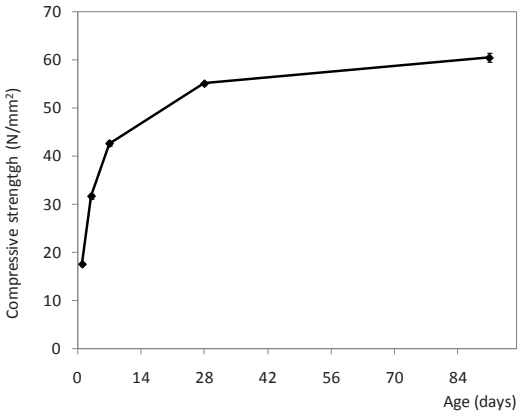

Figure 4.2. Compressive strength evolution in time of the initial concrete mixture (recipe in Table 4.1).

Average compressive strengths of three cubes were obtained at each testing age and are shown in Figure 4.2 together with their standard deviation, which is very low in all cases (between 0.07 and 1.86, corresponding to relative errors between 0.3 and 3%).

4.3 Crushing and fractioning the recycled concrete

The crushing of the concrete samples was performed after 91 days from the day of casting. A jaw crusher was used for this purpose. The material was crushed once and dry sieved in order to obtain its particle size distribution. This material will be termed RC-1 throughout this study. Through sieving the following fractions were obtained: < 150 μm (termed RC-1 0-150), 150-250 μm (termed RC-1 150-250), 250-300 μm (termed RC-1 250-300), 300-500 μm (termed RC-1 300-500), 500 μm - 1 mm (termed RC-1 500-1), 1-2 mm (termed RC-1 1-2), 2-4 mm (termed RC-1 2-4), 4-6 mm (termed RC-1 4-6), 6-8 mm (termed RC-1 6-8), 8-11.2 mm (termed RC-1 8-11.2), 11.2-16 mm (termed RC-1 11.2-16) and 16-32 mm (termed RC-1 16-32). After sieving, the material was brought back to the crusher 9 consecutive times, for a total of 10 crushing times, in order to obtain an optimal crushing. The obtained material, termed RC-2, was again sieved and divided into the same 12 fractions as the first time.

A third crushing method was used, and the generated particles termed RC-3 [123]. The crusher used for this purpose is a patented invention under a world patent number [124]. The particular crusher used in this research was built as a test model and is based on a commercial jaw crusher Fritsch pulverisette 1 model II. The purpose of this crusher is to separate concrete into its initial constituents- sand, gravel and cement paste, as opposed to ordinary crushers, which only reduce particle size by crushing the material randomly; in the case of concrete, this will include crushing through the aggregates as well as between them. This new type of crusher, termed "Smart Crusher" (SC), is intended to separate concrete into its constituents without damaging them, by adjusting the crushing force to an intermediate one between the average compressive strengths of the aggregates and the one of the hardened cement paste [124].

The concrete used for this crushing method was cast in plastic cups in the shape of a truncated cone (Φ_1 = 7.5 cm, Φ_2 = 5.5 cm, h = 10 cm) in order to better fit the inlet opening of the test crusher SC, as described in Section 4.2. The concrete samples were first pre-crushed using the jaw crusher in order to simulate industrial pre-crushing. After that, the obtained samples were crushed by the SC and particles bigger than 2 mm were re-fed to the crusher for one more crushing step. The obtained material was sieved according to [125], using the following sieve sizes: 63 μm, 125 μm, 200 μm, 300 μm, 500 μm, 1 mm, 2 mm, 4 mm, 5.6 mm, 8 mm, 11.2 mm, 16 mm and 22.4 mm, which generated 13 corresponding RC-3 fractions.

4.4 Characterization of the fractions

4.4.1 Particle size distributions

Table 4.3 shows the difference between the cumulative passings of the three obtained materials. The finest fractions (under 500 µm, which is the maximum particle size limit for which the measurement is considered reliable) were analysed using a Malvern Mastersizer 2000 and the Fraunhofer approximation.

Table 4.3. Characteristic particle size distribution parameters- D_{min}, D_{max}, d_{10}, d_{50} and d_{90} measured for the finest fractions of RC-1, RC-2 and RC-3.

	D_{min} [µm]	**D_{max} [µm]**	**d_{10} [µm]**	**d_{50} [µm]**	**d_{90} [µm]**
RC-1 0-150	0.96	208.9	10.9	68.5	169.2
RC-1 150-250	91.2	478.6	134.8	212.8	334.1
RC-1 250-300	138.0	630.9	212.7	310.5	450.3
RC-1 300-500	208.9	831.7	287.1	459.2	720.4
RC-2 0-150	0.96	208.9	6.0	49.7	127.4
RC-2 150-250	91.2	416.9	132.7	204.8	300.0
RC-2 250-300	158.5	549.5	217.8	306.5	417.9
RC-2 300-500	208.9	724.4	278.9	414.9	597.1
RC-3 0-150	0.48	275.4	4.36	45.7	158.5
RC-3 250-300	0.73	724.4	19.95	363.1	514.1
RC-3 300-500	0.95	954.9	316.2	478.6	696.4

The characteristic dimensions of d_{10}, d_{50} and d_{90} (corresponding to the mesh size for the passing of 10%, 50% and respectively 90% of the material), as well as the D_{min} and D_{max} of the finer fractions of all three materials are presented in Table 4.3. The analysis confirmed the smaller particle size of RC-2. Also, a larger scatter of the particle sizes could be seen, as $d_{0.9}$ is in almost all cases higher than the sieve size used for obtaining the fraction. Moreover, both D_{min} and D_{max} show a wider PSD than indicated by the sieving step. It can be seen that the D_{min} and D_{max} values of RC-1 and RC-2 fractions sieved between the same sizes are comparable. RC-2 has the same D_{min} as the corresponding RC-1 fractions or D_{min} is higher (in the case of RC-2 250-300). Conversely, D_{max} is consistently the same or lower in the case of RC-2, when compared to the corresponding RC-1 fraction. RC-3 fractions consistently have a much lower D_{min},

but higher D_{max} values, which suggests that the particles have an acicular shape in order to pass through the sieve openings. This suggests that the RC-2 fractions have a narrower range and are composed of finer particles, which is also seen from the of d_{10}, d_{50} and d_{90} values, while the RC-3 fractions have characteristic values intermediate between the RC-1 and RC-2 materials, excepting the finest range.

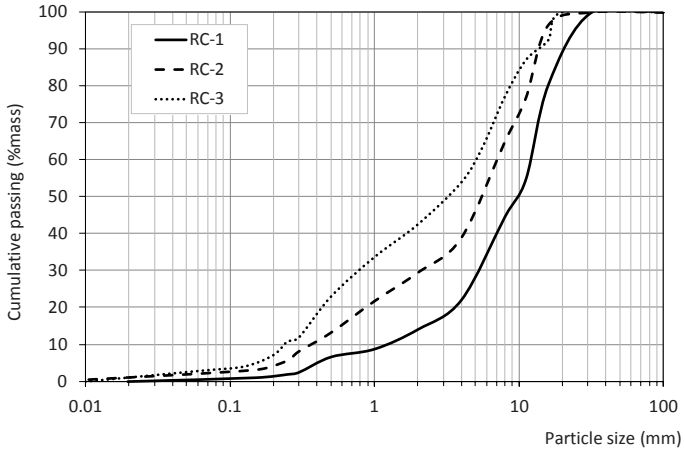

a.

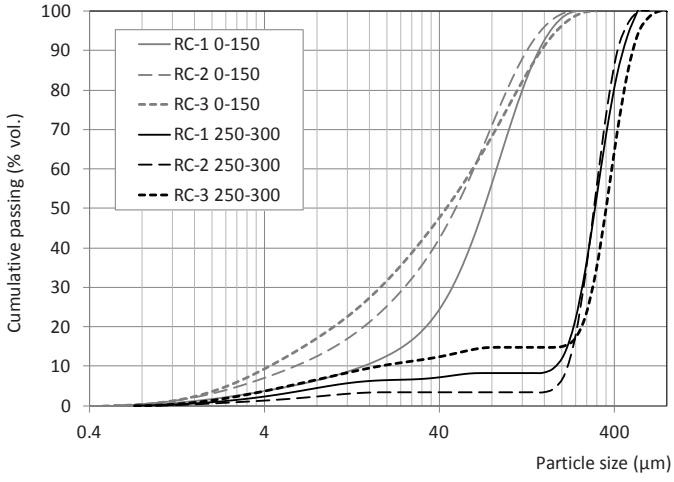

b.

Figure 4.3. a. Particle size distributions of the three crushed materials, RC-1 (crushed once) and RC-2 (after 10 crushing times) and RC-3 (from the Smart Crusher SC) on a logarithmic scale; **b.** Particle size distributions of RC-1, RC-2 and RC-3, fractions 0-150 and 250-300 µm.

Figure 4.3.a shows the particle size distributions of RC-1 and RC-2 and RC-3. It can be seen that the RC-3 particles are smaller than RC-2 and RC-1 ones: the SC generated 33.7% mass particles smaller than 1 mm, while RC-1 produced only 8.8% mass and the RC-2 21.7% mass particles smaller than 1 mm; this means that the SC produced 4 times more particles under 1 mm than RC-1.
In the case of particles under 0.5 mm, the SC (after the precrushing step) produced 23% mass of material, the RC-1 produced 6.7% mass of the total material and the RC-2 generated 13.2% mass; therefore, the SC produced about 3 times the RC-1 and about twice the RC-2 yield of particles under 0.5 mm. It should be kept in mind that the RC-2 sample concerns a treatment comprising 10 consecutive crushing steps.
Figure 4.3.b. shows all the cumulative PSDs of the finer fractions (0-150 and 250-300 μm) of both materials. While the RC-3 fractions are the finest of all three crushing methods, the RC-2 material is finer than the RC-1 for the smaller fraction but it has larger particles in the 250-300 μm range. The explanation is twofold: on one side by the increased percentage of fines under this dimension of RC-2 when compared to RC-1 and on the other side by the loss of fines during the consecutive crushing steps.

4.4.2 Densities of the recycled concrete

As explained in Section 4.1, the attached mortar on the RCA leads to a decrease in density; moreover, this decrease should be proportional to the attached mortar or hardened cement paste content. In order to verify this, the densities of all RC-3 fractions (Figure 4.4) were determined [123]. The samples were first milled to fine powder and then dried at 70°C before being measured using a He pycnometer (Micrometrics Accupyc 1340). The results were then used to compute the cement paste content of the samples (Table 4.4). The values for plain cement paste and plain quartz aggregates can be seen in Figure 4.9.
Particles under 63 μm have the lowest density among all the recycled materials, 2.45 g/cm^3 (Figure 4.4). Density has an increasing trend with particle size up to the size fraction 4-5.6 mm, after which it stays almost constant, around the value of 2.62 g/cm^3 up to particle sizes of 8 mm, after which it decreases. As previously explained, the maximum gravel dimension used for the initial concrete was 8 mm (Table 4.2); therefore, the size fractions above 8 mm have a larger amount of attached cement paste, which can explain the density increase of this size range of RCA.

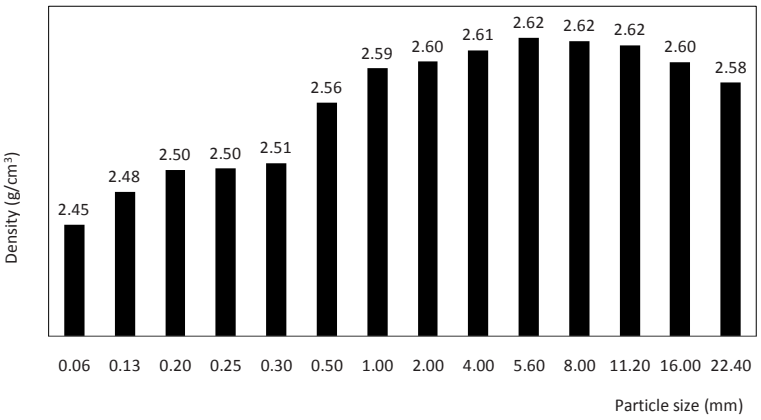

Figure 4.4. Densities of all RC-3 fractions obtained by the Smart Crusher; the D_{max} of each size class is indicated.

4.4.3 DSC-TG analysis of recycled concrete

For all fractions of all three materials (RC-1, RC-2 and RC-3), the thermal analysis was performed using a Netzsch STA F1 in inert atmosphere (N_2). Both thermogravimetric (TG) and differential scanning calorimetry (DSC) were performed on all samples.

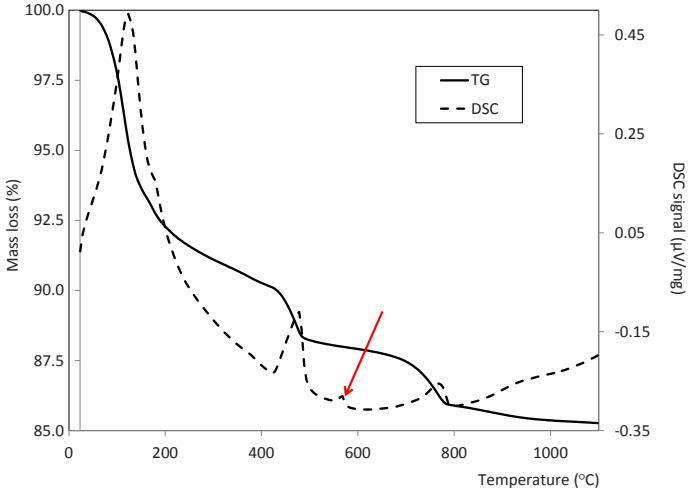

Figure 4.5. TG (continuous line) and DSC (dotted line) curves of RC-1 300-500 µm.

The thermal analysis was performed in alumina crucibles, up to a maximum temperature of 1100ºC, with heating and cooling speeds of 10ºC/min, and a temperature plateau at

1100ºC for one hour, to ensure steady state. The samples were milled beforehand to ensure homogeneity, and the experiments were reproduced with excellent accuracy. As an example, Figure 4.5 shows the TG-DSC analysis results of RC-1 300-500 μm. The DSC curve registers any thermal reaction (exo- or endothermic) which takes place within the sample. These are usually associated with a mass change which can be observed on the TG curve. However, there are reactions which take place without a mass change, but for which thermal effects can be observed. These are usually phase changes (like melting or solidifying of materials) or phase transitions (from one crystallographic form of a compound to another), which take place with the adsorption or release of energy. In Figure 4.5, such an effect can be observed at approx. 570ºC: the phase transition of α-SiO_2 to β-SiO_2 (marked with a red arrow in Figure 4.5). These effects are quantified using the area under the peak, which is proportional to the concentration of the respective compound within the sample.

Samples of hardened cement paste and milled quartz sand were made for the calibration of this measurement, using the same cement as for the initial concrete and a water/cement ratio of 0.7. These samples were cast in 40 mm × 40 mm × 160 mm prisms and cured under water for 8 months, after which they were crushed. In the case of these samples, the α-quartz can only be generated by the aggregates, which contain between 92 and 98% α-quartz (measurements by XRF and confirmed to be almost pure α-quartz by XRD, detailed in the next sections and Figure 5.5). The milled cement paste and sand were blended in ratios of 0%, 20%, 40%, 60%, 80% and 100% in order to obtain the calibration samples and dried at 105°C.

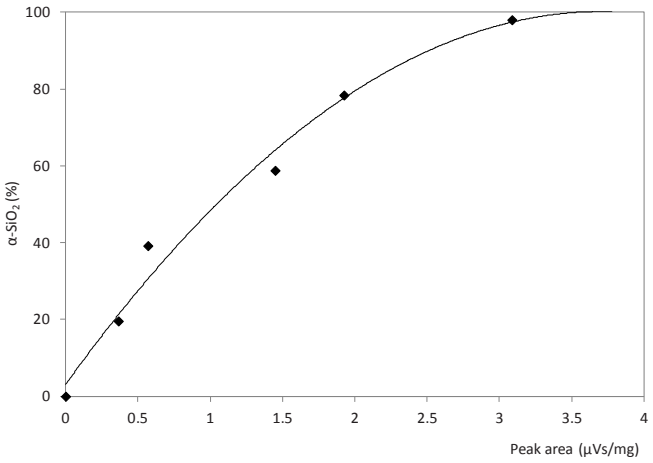

Figure 4.6. Calibration curve of α-quartz content against DCS measurements for sand-hardened cement paste mixtures.

All milled and dried RC-1, RC-2 and RC-3 samples were analysed by TG-DSC. A calibration curve was also obtained by analysing the calibration mixtures with known α-quartz contents. Figure 4.6 shows the calibration curve and the corresponding fitted line (Eq. 4.5.1, $R^2 = 0.982$) used to compute the α-quartz contents of all considered samples.

$$100 \cdot x_{\alpha-SiO_2}^{DSC} = -7.2367 \cdot (a_{\alpha\rightarrow\beta}^{DSC})^2 + 52.885 \cdot (a_{\alpha\rightarrow\beta}^{DSC}) + 2.9026 \quad (4.5.1)$$

where $x_{\alpha-SiO_2}^{DSC}$ is the mass fraction of α-quartz in the sample and $a_{\alpha\rightarrow\beta}^{DSC}$ is the area under the peak corresponding to the α →β-quartz transformation.

Figures 4.7a-c visually show the breakdown between cement paste and aggregates for all considered fractions. There are some differences to be observed between the three materials. In the case of RC-1 (Figure 4.7a), a constant increase of α-quartz content with particle size can be noticed. Particles above 8 mm have an α-quartz content over 80%, while the lowest α-quartz content registered is just above 40% (RC-1 0-150 μm). For RC-2 (Figure 4.7b), a similar increasing trend can be observed. However, the α-quartz content of particles above 1 mm becomes fairly constant at around 80%. The smallest RC-2 fraction (0-150 μm) has an α-quartz content of 33.4%, 20% lower than the corresponding RC-1 fraction. The RC-3 63 sample has the lowest α-quartz content, 26.4%, from all analysed samples (Figure 4.7c), the remaining 73.6% being hardened cement paste. The following RC-3 size fraction contains approximately 42% α-quartz and this percentage continues to increase with particle size up to the 5.6-8 mm sample, which has the highest α-quartz content, of 85.3%.

Figures 4.8a-c represent the cumulative distributions of the two components (aggregate and hardened cement paste), based on the crushing curves of RC-1, RC-2 and RC-3, respectively. For example, for RC-3 (Figure 4.8c), the values for the mass fractions, together with the content of aggregate and hardened cement paste can be found in Table 4.4.

The total of each component computed in this way correlates very well with the initial composition – 22.5% hardened cement paste (hcp) and 77.5% aggregates for RC-1 and 20.2% hcp and 79.8% aggregates for RC-2, compared to 22.4% hcp and 77.6% aggregates for the initial material. This overall mass balance confirms that the α-quartz method can indeed be used to assess the aggregate content of the recycled concrete fractions. The lower value of hcp for RC-2 is explained by the loss of very fine material during each crushing cycle. The cumulative totals for RC-3 are 76% aggregate and 24% hardened cement paste.

When comparing Figures 4.8a-c, a few observations can be made. In terms of the efficiency of recovering the hardened cement paste fraction, crushing just one time using a conventional jaw crusher (RC-1) is more advantageous than crushing the whole material 10 times (RC-2): for RC-1, a 50% recovery of total hcp can be achieved for particles under 2 mm, while the same value corresponds to material under 3 mm for RC-

2. Similarly, an 80% cumulative recovery of hcp is observed for material under 10 mm for RC-1 and under 11 mm for RC-2.

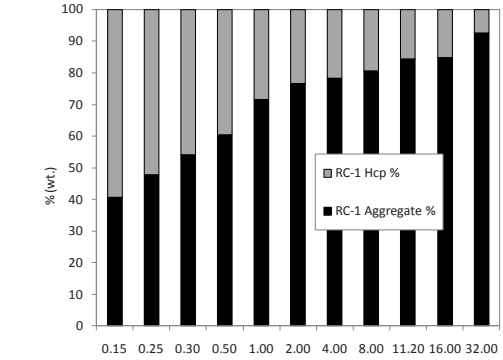

a.

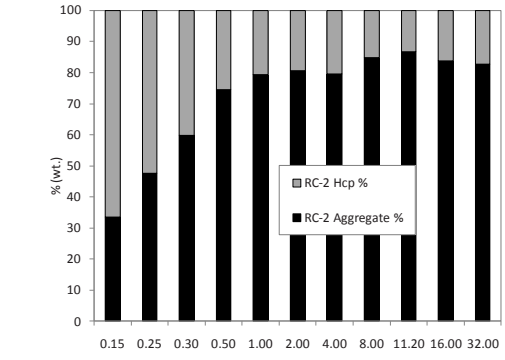

b.

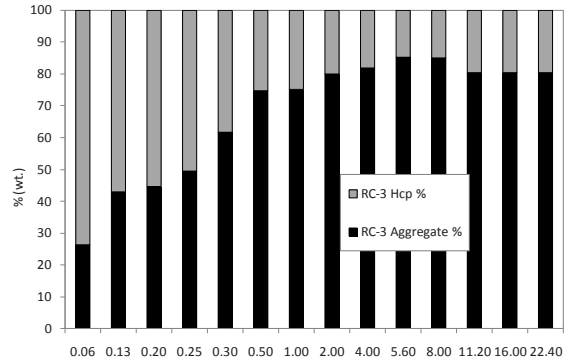

c.

Figure 4.7. Composition of all recycled concrete fractions divided into the aggregate (α-quartz) and hardened cement paste (hcp) components: **a.** RC-1; **b.** RC-2; **c.** RC-3.

Table 4.4. Mass fraction, breakdown into aggregate and hardened cement fractions obtained from DSC and the measured density of all RC-3 fractions, compared to the computed density and hardened cement paste content (Eq. 4.5.1).

	Mass fraction (% mass)	**Aggregates (% mass fraction)**	**Cement paste (% mass fraction) from DSC**	**Cement paste (% mass fraction) from density**	**Measured density (g/cm^3)**	**Computed density (g/cm^3)**
RC-3 0-63	2.93	26.37	73.63	62.18	2.45	2.42
RC-3 63-125	1.12	42.88	57.12	53.86	2.48	2.47
RC-3 125-200	3.11	44.68	55.32	48.17	2.50	2.48
RC-3 200-250	3.68	49.43	50.57	47.79	2.50	2.50
RC-3 250-300	1.05	61.60	38.40	46.39	2.51	2.54
RC-3 300-500	11.07	74.80	25.20	30.82	2.56	2.58
RC-3 500-1	10.7	75.11	24.89	22.05	2.59	2.58
RC-3 1-2	8.87	79.92	20.08	20.32	2.60	2.60
RC-3 2-4	11.38	81.88	18.12	17.38	2.61	2.61
RC-3 4-5.6	9.48	85.30	14.70	14.08	2.62	2.62
RC-3 5.6-8	18	85.12	14.88	15.05	2.62	2.62
RC-3 8-11.2	9.97	80.42	19.58	16.04	2.62	2.60
RC-3 11.2-16	5.37	80.32	19.68	20.47	2.60	2.60
RC-3 16-32	7.59	80.48	19.52	25.65	2.58	2.60

Another important observation is that the densities of the recycled concrete fractions have a correlation with the α-quartz contents. Figure 4.9.a shows the density of the samples (right y-axis) on the same graph with the α-SiO_2 contents (left y-axis).

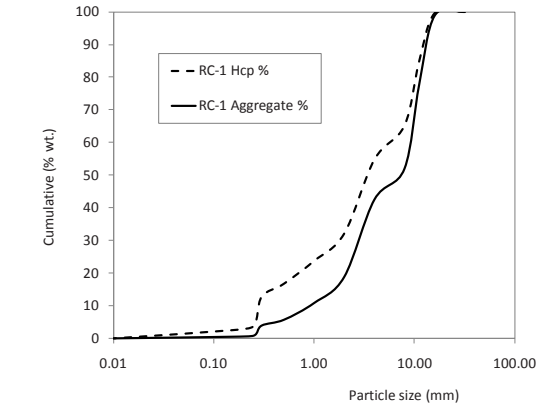

a.

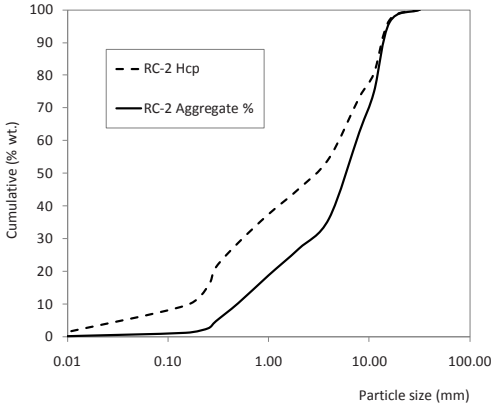

b.

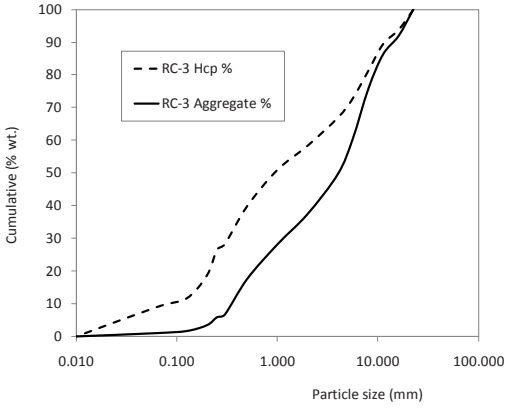

c.

Figure 4.8. Cumulative distribution of the hardened cement paste and aggregates in **a.** RC-1; **b.** RC-2; **c.** RC-3.

A good agreement between the density and α-quartz content of the recycled concrete aggregates can be observed. This suggests that density measurements can be used for the recycled concrete aggregates α-quartz content estimation.
From Figure 4.9b, a linear correlation can be observed between the measured density and α-quartz content obtained from DSC of each fraction, with an R^2 value of 0.974; this accuracy is of the same order as the quartz calibration (98%).

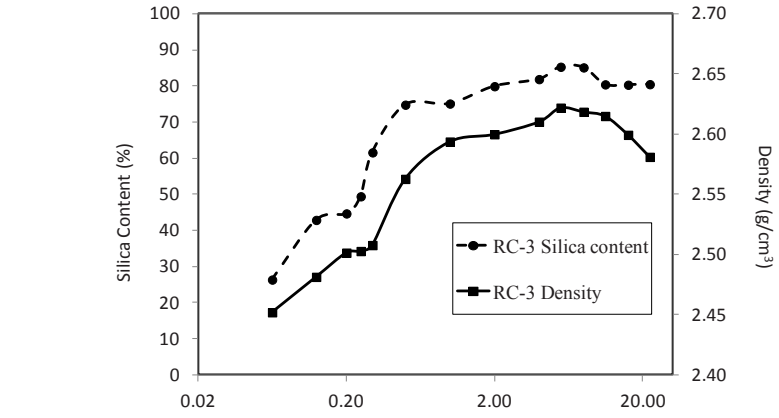

a.

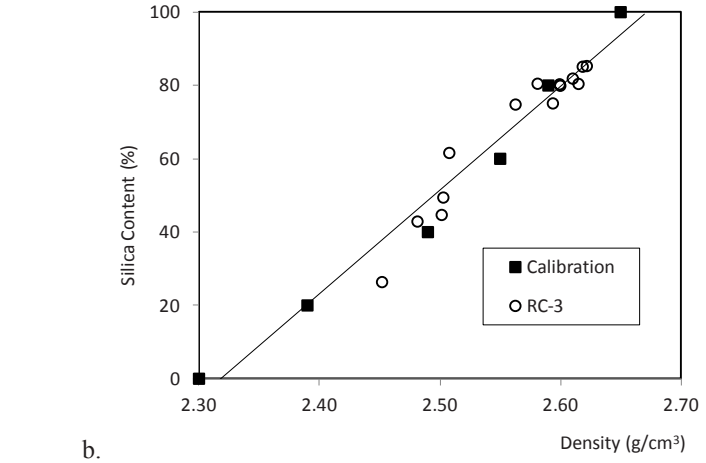

b.

Figure 4.9. a. Density (g/cm^3) and α-quartz content (%) of all fractions of RC-3, presented on a logarithmic scale; **b.** Relationship between the density and silica content of the calibration points and their corresponding linear fit and those of RC-3.

The density measurement results for the RC-3 series are shown in Figure 4.9 together with densities measured on the calibration mixes used for the TG/DSC measurement (Section 4.4.3) which contain between 0 and 100% hardened cement paste.
Therefore, the density computed using the linear fit, as well as the hardened cement paste content of each fraction estimated using the inverse equation are also shown in Table 4.4. From this data, it has been observed that the estimation of the hardened cement paste content using such a linear correlation is not very accurate (with average relative errors of ~ 11%, and a maximum relative error of 23%). This was to be expected, since the range of the hcp values is much larger (14-74%) than the one of the densities (2.45-2.62 g/cm^3). However, for the estimation of density from the hcp content, the relative errors are under 1.5% for the whole estimation range, which suggests that this correlation is an appropriate method for the verification of the DSC data.

4.4.4 XRF validations

The accuracy of the method described in Section 4.4.4 is validated by X-ray fluorescence analysis (Table 4.5). The mass fraction of SiO_2 measured by XRF ($x_{SiO_2}^{total}$) in the recycled concrete fractions is the sum of the aggregate-generated α-quartz and the SiO_2 contained in the hydration products. The latter can be computed from the chemical composition of the hardened cement paste fraction ($x_{SiO_2}^{hcp}$), which in turn is formed by cement and water (x_{cem+w_0/b_0}), correcting for the 1.7% of limestone which is also present in the mix. The mass fraction of α-quartz in each considered recycled concrete fraction is measured by DSC ($x_{\alpha-SiO_2}^{DSC}$) method.

$$x_{SiO_2}^{total} = x_{\alpha-SiO_2}^{DSC} + (1 - x_{\alpha-SiO_2}^{DSC}) \cdot x_{SiO_2}^{hcp} \tag{4.6.2}$$

where

$$x_{\alpha-SiO_2}^{DSC} + x_{hcp} = x_{\alpha-SiO_2}^{DSC} + (x_{cem+w_0/b_0}) = 1 \tag{4.6.3}$$

$$x_{SiO_2}^{hcp} = 0.2 \cdot x_{hcp} \cdot \frac{1}{1 + w_0 / b_0} \tag{4.6.4}$$

For instance, the SiO_2 content measured by XRF of RC-3 particles between 200 and 250 is 57.38%, while its α-quartz content determined by TG-DSC $x_{\alpha-SiO_2}^{DSC}$ is 49.43%. Therefore, the hydrated paste percentage x_{hcp} is 50.57%. Knowing that the cement used for the crushed samples contains 20% SiO_2 and the used w_0/b_0 ratio was 0.5, the SiO_2 fraction from hydration products $x_{SiO_2}^{hcp}$ becomes 6.74%. Therefore, the total SiO_2 content of the sample $x_{SiO_2}^{total}$ amounts to 56.17%, the error between the XRF result and the TG-DSC method being 2.1%.

Table 4.5. XRF-obtained SiO_2 content of the four finest RC-3 fractions, compared to the DSC results and the computed total silica (Eq. 4.6.3).

	$x^{DSC}_{\alpha-SiO_2}$ (%)	$x^{total}_{SiO_2}$ (%)	$x^{XRF}_{SiO_2}$ (%)
RC-3 0-63 μm	26.37	35.45	39.91
RC-3 63-125 μm	42.89	50.52	52.10
RC-3 125-200 μm	44.68	51.50	55.34
RC-3 200-250 μm	49.43	55.67	57.38

Table 4.5 shows this computation for all fractions of RC-3 under 250 μm. There is an additional expected error of the XRF measurement (besides the sample preparation errors which were minimized in terms of finely grinding and homogenizing), due to the computation of all elements in oxide form, since the TG analysis also shows the presence of carbonation to a larger extent than the one provided by the limestone. Therefore, the fit between the two analytical measurement techniques is considered to be a good indication of the accuracy of the results.

4.4.5 XRD and SEM/EDX

X-Ray diffraction analysis was performed on all previously described samples. Given their similarity, only a few selected fractions will be presented. Peaks belonging to SiO_2, $Ca(OH)_2$ and ettringite were identified in order to show the presence of hydrated cement paste and aggregates.

Additional tests were performed on the initial natural aggregates, which were confirmed by XRF to have between 92 and 98% equivalent quartz content. For the ease of calculation, all aggregates were considered to contain an average of 96% α-quartz. Figure 4.10 shows the RC-2 fractions with their complete diffraction patterns. It can be observed from the α-quartz peak that the aggregate content increases with increasing particle size, while the hcp content is higher for the smaller fractions, as it has also been observed using the DSC.

The microstructure of the finest recycled concrete fraction (RC-3 0-63) was investigated by scanning electron microscopy (SEM), with magnifications between 500x (Figure 4.11a) up to 5000x (Figure 4.11b). The energy dispersive X-Ray (EDX) detector was employed simultaneously for the elemental analysis of the recycled concrete fractions. In Figure 4.11c a sand grain can be seen with cement hydration products attached to its surface. The EDX map (Figure 4.11d) of silicon was taken for the exact same sample image, which verified that the "support" grain is indeed SiO_2.

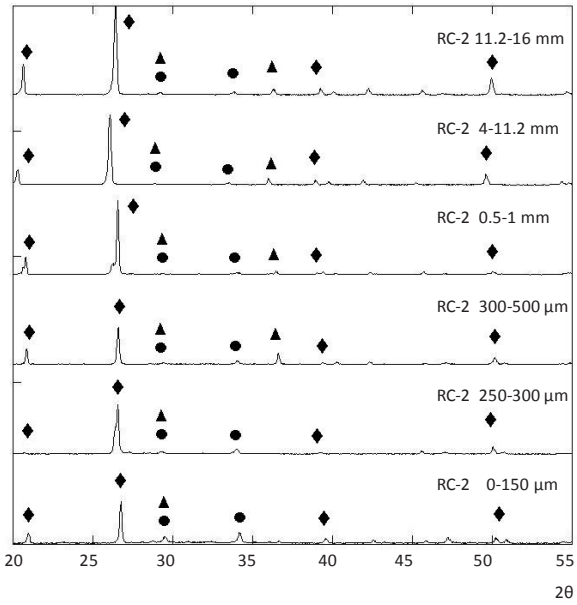

Figure 4.10. XRD analysis of RC-2 fractions, with relative peak intensities; ♦ = α-quartz, ● = portlandite, ▲ = ettringite.

Table 4.6. Particle size distributions of Norm sand NS (according to EN 196-1 [29]) and the corresponding composed mix of RC-3 sand (RCS).

Particle size (mm)	**NS (g)**	**RCS (g)**
< 0.075	2.9	3.0
0.075-0.15	120.8	121.0
0.15-0.50	316.2	318.0
0.50-1.0	428.3	430.0
1.0-1.4	250.9	251.0
1.4-2.0	225.9	227.0
Total (g)	1345.0	1350.0

The elemental map of Ca for instance shows an even distribution, which confirms the spread of the hydration products on the surface of the SiO_2 grain. These observations confirm the supposition that fine recycled concrete grains have irregular shapes, and that

acicular particles can be observed, which explain the increased D_{max} of each fraction (Table 4.3 and Section 4.3). Also, the fact that hydration products are sometimes stuck on a crushed aggregate grain explains the residual content of α-quartz even in fine recycled concrete fractions.

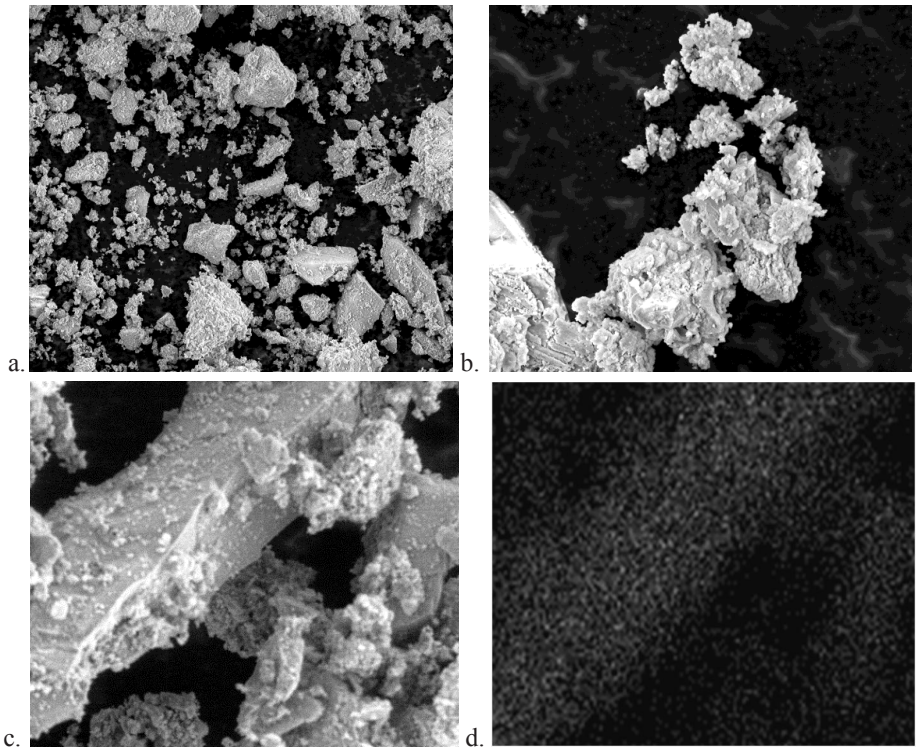

Figure 4.11. SEM image of RC-3 0-150 μm particles (**a.** 500x and **b.** 5000x) showing the hydration products, a silica fragment covered with hydration products (**c.** 4000x) and its silicon map from EDX (**d.**).

4.5 Recycled Concrete Sand replacement test

Recycled concrete sand (RCS) with a maximum particle size of 2 mm obtained from RC-3 was used to replace Norm sand (NS) in mortars using CEM I 42.5N, following EN 196-1 [29]. RCS, designed to have the same particle size distribution as Norm sand, was used to replace 100% of the NS. The PSDs of the employed NS and the generated RCS are presented in Table 4.6 [123].

4.5.1 Fresh mortar consistence

As computed in Section 4.4.3, RC-3 fractions under 2 mm contain between 73.6% and 20.1% hardened cement paste. Using the data from Table 4.4 and 4.6, the average hcp content of the RCS can be closely estimated to approximately 29.2%. Because of the porosity of the hardened cement paste, among other factors, the water demand of the RCS was expected to be higher than the one of the NS. In order to compensate for this, 1% mass of superplasticizer (SP) Glenium 51 BASF was used in the mortar mixture containing 100% RCS replacement of the norm sand. This addition permitted the sample to achieve flowability (otherwise it resembled earth-moist mixtures), even though it could reach a lower value of the spread, measured using a Hägermann cone (123 mm as opposed to 139 mm by the reference sample).

4.5.2 Strength results

The flexural and compressive strength of the 100% NS reference mortar and the 100% RCS mortar are shown in Figures 4.12a and 4.12b. The flexural strengths of the RCS mortar were higher than those of the NS-containing samples by 45.3%, 33.2% and 13.7% after 3, 7 and 28 days, respectively. This increase was expected and can be due to the more angular shape of the RCS aggregates (Figure 4.11c), which can partly interlock and thus lead to a higher flexural strength. The compressive strength of the RCS mortar increased even higher (65.6%) after 3 days, 40.3% after 7 days and just 1.1% after 28 days. This behaviour suggests that the RCS had an influence on the hydration of the cement, either accelerating it by providing additional nucleation sites, or bringing its own contribution. The hydration behaviour of RC fines will be studied more in depth in the next chapter.

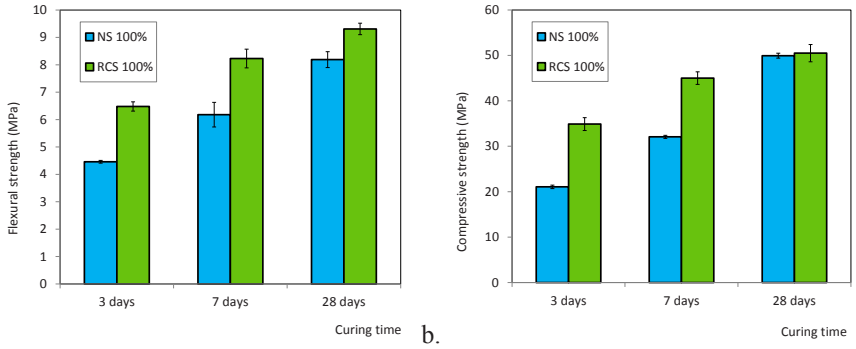

a. b.

Figure 4.12. a. Flexural and **b.** Compressive strength of sand replacement mortar, for standard mortars made according to EN 196-1 [29] using Norm sand (100% NS) and replacement of 100% of the sand with RCS (see also Table 4.6).

4.6 Real scale Smart Crusher

Following the experience with the lab-scale SC and its encouraging results, a real scale Smart Crusher has been built. Figure 4.13a represents a sketch of the Smart Crusher [124] and Figure 4.13b shows the real scale model. The capacity of the real-scale Smart Crusher is 40 t/h, and on an empty run has a nominal flow of charge of 0.9 A. Compared to the capacity of the lab-scale SC of 0.2 t/h, this value increases just over 2 times (from 0.4 A), even though the capacity increases 200 times.
The energy needed by the Smart Crusher to process one ton of concrete is 1 kWh, which is much lower than the 2.5 kWh/ton concrete needed by most commercial real scale crushers. Moreover, the real scale Smart Crusher weighs less than half compared to other commercial crushers of the same capacity and it is containable for ease of transport.

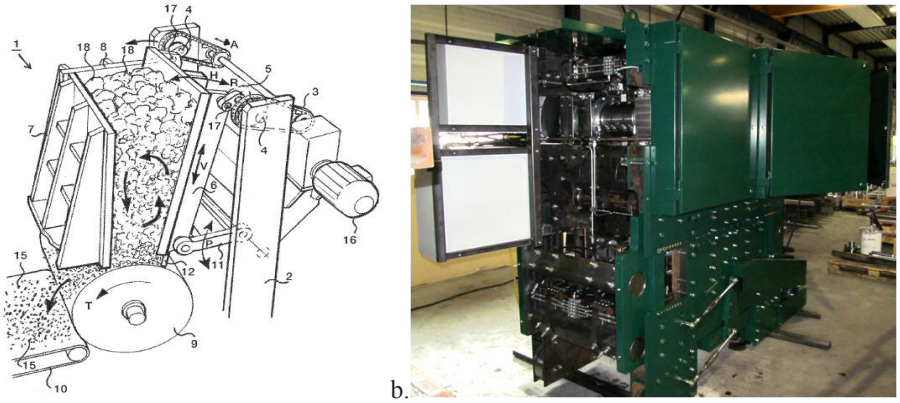

Figure 4.13. a. Sketch [124] and **b.** picture of the real scale Smart Crusher**.**

4.7 Conclusions and discussions

In this chapter, specially designed concrete was employed to mimic the concrete recycling process. Three crushing methods were used to study their influence on the properties of the obtained materials. A conventional jaw crusher was used for the first two crushing methods to obtain the RC-1 and RC-2 materials (one time crushing and 10 times returning through the crusher, respectively) and a Smart Crusher prototype was employed for the generation of the third material (RC-3). The resulting recycled concrete aggregates were sieved into fractions based on the particle sizes. All these fractions were then characterized by their density, thermal treatment reaction, XRD patterns, XRF composition and SEM-EDX images. It was found that the finer the RC fraction is, the less α–quartz they contain. Another observation is that the density of the RCs has a direct

correlation with its α–quartz content. The XRF and XRD tests confirmed the decrease of SiO_2 content with particle size.

A new method of quantifying the α-quartz content of the samples using the calibrated DSC signal was developed. The method was proven to be accurate by comparing with XRF results, and also following the trend indicated by XRD. The SEM-EDX technique provided further information on the morphology of the particles, which explains the particle size distributions of the finer fraction.

When comparing the α-quartz content of the materials obtained from all three crushing methods, some differences can be observed. The results have shown a much higher cement paste content in the fractions obtained from the Smart Crusher prototype SC (RC-3), as opposed to the conventional jaw crusher. The recovery of the cement paste, in the same particle size range, was improved by 50%, when comparing the RC-3 and RC-1 materials. This information becomes important when it is also correlated with the particle size distribution of the fractions obtained through the two methods. Sieving the two materials (RC-1 and RC-3) showed a much higher output of fines from the SC, up to five times in volume for the particles under 1 mm. Therefore, the crushed hardened cement paste particles recovery was 7.5 times the one from the conventional jaw crusher. Another conclusion was that the fines obtained from the SC contain much less α-SiO_2 than the ones from the RC-1 series. The RC-3 fines contained a maximum of 27% α-SiO_2 in the 0-63 μm fraction and under 42% in the 63-125 μm fraction, as opposed to approx. 40% in the finest fraction obtained from RC-1 and 34.4% for RC-2. An 80% cumulative recovery of the hardened cement paste can be achieved for particles under 10 and 11 mm for RC-1 and RC-2 respectively, while the same recovery rate is reached for RC-3 for particles under 8 mm, which is also an indication that the SC-produced aggregates are cleaner than the ones from a conventional jaw crusher, enabling a more sophisticated application for the former.

Recycled concrete sand was tested to replace 100% of the Norm sand in standard mortars. A significant decrease of flowability was observed; however, this was compensated with the addition of 1% superplasticizer by mass of cement. The mechanical properties of the RCS mortars proved to be promising, the samples achieving. higher strengths than the reference samples, especially for short curing times. The 3, 7 and 28 days flexural strengths increased with 45.3%, 33.2% and 13.7% respectively, compared to the reference mortar. The 3 and 7 days compressive strengths had even higher increases, of 65.6% and 40.3%, respectively. However, the 28 days compressive strength of the RCS mortar increased only by 1.1%, indicating that the positive effect of RCS is predominantly manifested at early ages.

All in all, it is shown that the crushing method has a large influence on the quality of the produced materials, and that an optimized crushing method can lead to streams enriched in either cement paste or aggregates. A difference in both composition and physical properties is observed for various sizes of crushed concrete. The use of recycled concrete

sand in mortar mixtures was proven to be beneficial in terms of mechanical properties, showing good promise for the use of such materials in concrete mixes.

Chapter 5

Activation of liberated concrete fines and application in mortars*

5.1 Introduction

The replacement of concrete ingredients- either cement or aggregates- can lead to a reduction in both generation of CO_2 and use of natural resources. An increasing source for both these types of replacement could be concrete and demolition waste, cleaned and treated in order to be used again in the building industry.

5.1.1 Construction and demolition waste

World Business Council for Sustainable Development has quantified [108] the C&D waste generation and recovery of some countries. The total C&D waste generated in 2011 ranged between 14 Mt in Australia to 201 Mt in Germany and 309 Mt in France. These large amounts of construction and demolition waste, if not treated properly, need to be landfilled as normal waste. The main reasons for the increase of the volume of C&D waste are old structures that have overcome their use expectancy and need to be demolished, new requirements and necessities leading to the demolition of otherwise still viable structures and destructive natural phenomena like earthquakes and storms [8].
The main re-use method for C&D waste is use as road-base material. However, an important application is also their use as aggregates in new concrete mixes. When comparing recycled aggregates to new aggregates or other building materials, a number of factors need to be taken into account [126]. A first factor is the land use impact – the use of recycled aggregates means that less waste goes to landfill, while also reducing the need of producing new aggregates. Another important factor is the transportation cost (including fuel use and CO_2 emissions), which can be much lower than in the case of new aggregates, if the C&D waste is located close to the construction site. New aggregates are usually transported from distant quarries to the construction site. Also to be mentioned are the useful life expectations- using recycled aggregates means that the concrete itself has a longer period of use than the structure it was initially part of.

5.1.2 The use of C&D waste as aggregates in new concrete

In the European Union, it is estimated that the construction and demolition rubble amounts to 500 kg per capita annually [5]. High recycling rates are achieved in countries

* The content of this chapter was published in *Construction and Building Materials* **50**, 1-12 (2014).

like the Netherlands, Japan, Belgium and Germany. The Netherlands had in 2011 a very high rate of C&D waste recovery, of approximately 95% of the generated 26 Mt [126]. In the US, the recycled aggregates can be divided by use in pavements (10-15%), other road construction and maintenance work (20–30%) and structural concrete (60–70%). Recycled aggregates are produced by natural aggregates producers (50%), contractors (36%) and debris recycling centres (14%) [127]. In Japan, the concrete recycling ratio reached 98% in 2003, from 65% in 1995, and it is mostly used as sub-base material in road construction [8]. Tam [8] analysed the situation of C&D waste recycling in Australia. It was found that concrete constitutes 81% of total C&D. The concrete recycling rate in Australia is about 40%, where it is mainly used for low-grade applications. The amount of C&D waste in China has reached 30–40% of the whole amount of municipal solid wastes, with waste concrete occupying a large percentage (around one third), according to Li [128]. The main identified sources for waste concrete in China are demolished concrete structures and elements, rejected structural precast members, laboratory-cast concrete specimens and airport pavements.

5.1.3 The use of C&D waste fine fractions in new concrete

The possibility of using recycled concrete fines to replace a part of the cement in the concrete recipes is investigated in the present chapter. Through a thermal treatment, hydrated cement paste can be dehydrated. Shui et al. [129] researched dehydrated cement paste (dcp) in depth, concluding that hardened cement paste treated at 500°C is mainly composed of dehydrated $C-S-H$, CaO, partially CH and non-crystalline dehydrated phases. Upon contact of the dehydrated paste with water, the initial hydration products such as the $C-S-H$ gel, ettringite and CH are recovered.

5.2 The dehydration and rehydration of hardened cement paste

5.2.1 The effects of thermal treatment on recycled concrete particles

During high temperature exposure of hardened cement paste (hcp), a sequence of physical and chemical processes takes place [129]. The main phenomenon is the evaporation of water from the hcp- both physically and chemically bound. Through this process, first the pore water, and then a part of the water retained by the hydration products is lost. Above 120°C, structural changes begin to take place, including the dehydration of $Ca(OH)_2$ around 450°C and decarbonation of $CaCO_3$ around 750°C. The dehydration process of hcp is completed at a temperature of about 800°C. Thus, a dehydrated cement paste (dcp) at a certain temperature will consist of partially or totally dehydrated products, hydration products that might not have been affected by the thermal treatment, and unhydrated cement. Castello et al. [130] report the decomposition of ettringite at a temperature as low as 90°C, even lower than the temperature at which the

free water is eliminated (105°C). Alonso et al. [131] concluded that ettringite became dehydrated abruptly after reaching the temperature of 100°C.
The $C-S-H$ gel is reported to start dehydration between the temperatures of 200°C and 400°C [130]. Handoo et al. [132] found by employing a scanning electron microscopy analysis that that the morphological changes of the $C-S-H$ gel take place mainly at a temperature higher than 600°C. Alonso et al. [131] concluded that the $C-S-H$ gel starts to dehydrate slightly as early as 100°C to 200°C, dehydrating gradually with the increase of temperature. They observed that from 600°C to 750°C, the solid phases contain mainly dehydrated $C-S-H$, CaO, anhydrous phases and dehydrated ettringite.
Tayyib [133] reported that portlandite decomposes at a relatively low temperature of about 400°C. However, Castello et al. [130] concluded that portlandite dehydrates between 530°C and 560°C. Table 5.1 gives an overview of the main transformations in a hcp with their respective temperatures.
All these decompositions take place with a mass loss, comprising usually of water or carbon dioxide. However, one of the processes is a phase transformation, which takes place without mass loss, but with a change in the structure. This is the transformation of crystalline silica from its α to the β form, which can be observed on a DSC curve, but does not give an effect on a TG one. Therefore, at around 580°C, the sand structure breaks down, but does not affect the mass of the sample (Table 5.1).

5.2.2 Rehydration of dehydrated cement pastes

Shui [129,134,135] found that dehydrated cement paste (dcp) can recover the original hydration products to a large extent after rehydration. Mechanical strength of the rehydrated dcp seems to depend on the initial dehydration temperature. Moreover, upon mixing with dcp an activation effect on fly ash was observed [135].

Table 5.1. Possible transformations of hardened cement paste samples during thermal treatment at different temperatures [129,134].

Temperature	Transformation
< 110ºC	Loss of physically bound water
~ 450ºC	Dissociation of portlandite
~ 570ºC	Transformation of quartz
~ 750ºC	Dissociation of carbonates
~ 1050ºC	Loss of chemically bound water

Upon contact with water, dehydrated phases recover their initial water content. CaO generated from the decomposition of $Ca(OH)_2$ and $CaCO_3$ will react with water to form $Ca(OH)_2$ again. The $C-S-H$ gel is also recovered. These rehydration processes are responsible for the build-up of strength, similar to the hydration of cement. Another cause is the hydration of initially unhydrated cement, that was part of the sample before the thermal treatment and that can now hydrate if in contact with water.
Shui et al. [129] reported the compressive strength results obtained from the rehydration of cement paste dehydrated at 500°C, noticing that the early hydration is very fast, the degree of rehydration after only one day reaching 0.7. The degree of rehydration progresses to 0.8, 0.85 and 0.9 in 3, 7 and 28 days respectively, which shows a slower rehydration rate after the initial first day. The explanations for the fast early hydration are the rehydration reactions of the dehydrated reaction products, the difference in the reactants, and the fact that the specific surface of dcp is much higher than the one of cement. As the rehydration progresses, the $C-S-H$ gel will recover its long chains, strengthening the structure.

5.2.3 Fresh properties of rehydrated concrete fines pastes

Shui et al. [134] compared the degree of rehydration of dcps obtained at different maximum temperatures; the evolution of rehydration is comparable for samples exposed to 400, 600 and 800°C respectively, and also the water needed to achieve standard consistency of a rehydrated dcp paste as a function of dehydration temperature. It was found that the required water of dcp linearly increases with the increase of the dehydration temperature from 300°C to 900°C. This is explained by the advancing of dehydration with temperature. Therefore, a sample dehydrated at a higher temperature has lost more water and needs a higher water amount in order to fully rehydrate. The results show that the water needed to achieve standard consistency of the rehydrated dcp increases from 32% for the dcp samples at room temperature up to 68% for the samples treated at 900°C. The initial and final setting time decreased with the increase of temperature. This would suggest that dcp can be suitable in earth-moist concrete mixes; if used in normal concrete, superplasticizer could be a solution for the higher water demand. The highest compressive strength of rehydrated dcp was achieved in the case of dcp treated at 800°C.

5.2.4 The use of dehydrated cement paste in new mortar recipes

Shui et al. [134] studied the compressive strength obtained by mortars containing recycled concrete fines (RCF) and the addition of pure cement and fly ash to the mixes. It was concluded that 20% fly ash addition doubles the compressive strength of the mortars. Adding a further 5% Portland cement, the final compressive strength was over four times the one of the mortar with just RCF. The beneficial effect of the fresh cement added can

be explained by the quick formation of $Ca(OH)_2$, which in its turn will aid the rehydration of the preheated RCF.
Shui et al. [134] compared the compressive strength obtained using dcp heated at temperatures between 300 and 900°C to unheated hcp and unhydrated cement. At three days curing, the untreated hcp does not develop any new compressive strength, while the dcp heated to 800°C shows the same strength development as plain cement. The compressive strength increases with the temperature of exposure, from 300 to 800°C. The sample heated at 900°C achieves lower strength than the one at 700°C at early curing times, but reaches almost the values of the sample heated at 800°C after 28 days.
In this chapter, real recycled concrete fines with a D_{max} of 150 μm are used instead of just cement paste. As seen in the previous chapter, smart crushing yield a hardened cement paste-enriched fraction. The main difference in this case is the presence of quartz particles (generated by crushing the concrete aggregates) in the recycled fines. Since this quartz fraction does not contribute to the strength development of the new mixtures, it is important to separate the recycled concrete fractions by silica content and make use of the most beneficial composition.

5.3 Materials and methods

5.3.1 The generation of the RCF

Recycled concrete fines generated from laboratory-made concrete were used in this research. This choice was made in order to be able to relate the composition of the concrete fines to the initial concrete one, while also optimizing the crushing method. The concrete recipe and properties can be found in Chapter 4 (Section 4.2).
The thermal treatment approach is intended to produce the material that can be used to replace cement. A novel patented crushing method [124] was used, employing a jaw crusher specially modified for concrete recycling. Details regarding this equipment can be found in Chapter 4 (Section 4.3). The concrete samples were first pre-crushed by the crusher only to reduce them to smaller pieces which can better fit the inlet. After that, the concretes were crushed by another two passes through the machine. Only particles bigger than 2 mm were re-fed to the crusher. The obtained material was sieved on the 150 μm sieve and the fines, termed RCF (for recycled concrete fines) further used in this study. This choice was made based on the silica content, the particle size and the amount of material that can be obtained from the source concrete (Chapter 4).
The PSD of the recycled material is very close to the one of the initial materials used to produce the concrete (Figure 5.1), especially in the aggregate size range (over 0.5 mm); this is an indication that the Smart Crusher 1 indeed separates the initial, clean aggregates from the hydrated cement fines. The deviation at lower particle sizes can be explained by the loss of fines during the consecutive crushing steps. The smart crushing method was found to produce much more recycled concrete fines and cleaner aggregates than a

conventional crusher. Moreover, the α-quartz amount of the recycled concrete fines was found to be significantly lower than the one obtained using a commercial jaw crusher. The recovery of the cement paste, in the same particle size range, was improved by ~ 50%, while the crushed cement paste particles recovery was 7.5 times the one from the conventional jaw crusher (Chapter 4).

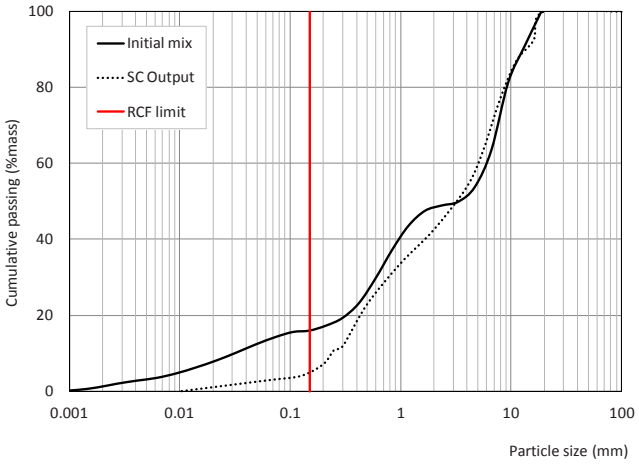

Figure 5.1. Particle size distributions of crushed material from the Smart Crusher (SC Output) on a logarithmic scale, compared to the initial concrete solids mix (Initial mix). The sieving size of 150 μm used for obtaining the RCF fraction is marked in red.

The hardened cement paste content of the RCF fraction below 150 μm is approximately 67.4%, the remaining 32.6% being α-quartz. The method for quantifying the α-quartz content of the sample based on DSC measurements is described in detail in the previous chapter.

5.3.2 Thermal treatment program

The TG analysis is used to determine the mass loss of a sample with the variation of temperature under inert atmosphere. The temperatures at which these mass loss effects occur are associated with the presence of certain compounds within the sample. These results complete the compositional information given by XRF, for instance being able to discern between CaO and $CaCO_3$. Unlike XRD, this technique can also be used to quantitatively, because the percentage of the mass loss can be correlated with the concentration of these components. The DSC curve registers any thermal reaction (exo- or endothermic) which takes place within the sample.

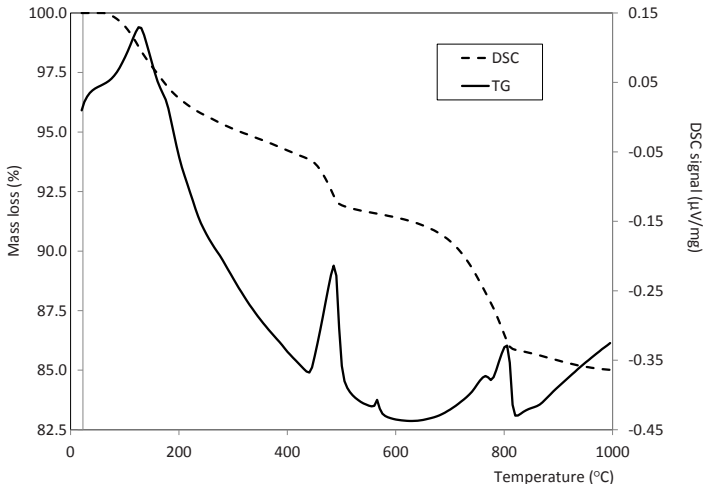

Figure 5.2. TG (% mass loss) and DTG (% mass loss/minute) curves of the RCF sample, together with its DSC signal curve (μV/mg) for a heating treatment up to 1000°C.

So, both thermogravimetric (TG) and differential scanning calorimetry (DSC) were performed, together with their first derivatives (DTG and DDSC) on the RCF sample using a Netzsch STA F1. The thermal analysis was performed up to a maximum temperature of 1100ºC, with heating and cooling speeds of 10ºC/min, and a temperature plateau at 1100ºC for one hour in Al_2O_3 crucibles, to ensure steady state. Figure 5.2 shows the TG-DTG analysis results of the recycled concrete fines

The first mass loss effect is visible between 100°C and 200°C (Table 5.1), due to the liberation of pore water and the liberation of physically bound water from certain hydration products, such as ettringite [130,136]. The second effect happens between 400°C and 500°C, due to the dehydration of portlandite [129,131]. The third effect appears at about 570°C, but only on the DSC curve. The reason is the transformation of quartz [129] which is a crystalline phase change process without mass loss. Around a temperature of 570°C, α-quartz undergoes a transformation into β-quartz, which comprises a swelling in volume and, therefore, a decrease in density. The densities of α-quartz and β-quartz are 2.65 g/cm^3 and 2.53 g/cm^3, respectively. This transformation is instantaneous and reversible. The quantification of α-quartz in the sample can be done by correlating the area of this peak with the content of α-quartz in known samples (Chapter 4). The fourth effect of the DSC curve appears between 700°C and 800°C: the decomposition of calcium carbonate with loss of CO_2 [129].

Based on the information above, the recycled concrete fines were thermally treated at 500°C, 800°C and 1100°C. These temperatures were chose to be slightly above the temperatures at which the major transformations take place, so that each of the latter can be considered complete. The following notations will be used throughout this chapter:

RCF-20 are RCF under 150 μm without thermal treatment (kept at room temperature); RCF-500, RCF-800 and RCF-1100 stand for RCF under 150 μm thermally treated at 500°C, 800°C and 1100°C, respectively.

5.4 Characterization of the recycled concrete fines

5.4.1 Chemical composition, PSD and density

The binders used in this research are CEM I 42.5N (ENCI B.V., the Netherlands) and the recycled concrete fines (RCF), as obtained from the crushing (Section 5.3.1) or thermally treated (Section 5.3.2). Two commercially available secondary binders were also used: a powder coal fly ash and a ground granulated blast furnace slag. The oxide compositions of all above-mentioned materials are shown in Table 5.2.
The chemical composition of the RCF can be found in Table 5.2. It has the estimated CaO content of 33% and the SiO_2 content of 44%, 32% by mass of sample being α-quartz (so the sample consists of approximately 1/3 aggregate and 2/3 hardened cement paste). The loss on ignition is due to the water and CO_2 which can be released through thermal treatment, and its value is in line with the one provided by the TG analysis. The fly ash is a low-lime commercially available fly ash. In the Netherlands, slag-blended cement represents over half of the cement market share [104]. Therefore, a ground granulated blast furnace slag is being employed in this study and its activation by RCF is considered.

Table 5.2. Chemical composition of the binder materials used in this research: the reference cement (CEM I 42.5N), the recycled concrete fines with particle sizes under 150 μm (RCF) and the two secondary binders used for comparison (a powder coal fly ash and a ground granulated blast furnace slag commercially available in the Netherlands); N/A= not available.

Oxide	**CEM I 42.5N**	**RCF**	**Fly ash**	**Slag**
Al_2O_3	5.0	2.3	22.3	12.6
SiO_2	20.0	44.6	55.0	35.0
SO_3	2.2	1.0	1.4	0.1
CaO	63.0	32.8	4.4	39.2
Fe_2O_3	3.0	1.4	8.4	0.4
MgO	1.6	0.7	1.9	8.9
LOI	1.1	17.1	N/A	1.3

In order to verify that a thermal treatment will not affect the PSD of the recycled concrete fines significantly, a grinding test was employed. This step also had the role to decide whether the thermal treatment would be more efficient before the last crushing step (so on 2 mm particles), or on the final RCF-20.
The interest was higher for the hardened paste component of the recycled concrete, rather than on the quartz, whose structure after the end of the thermal treatment would not be different. Therefore, samples of hardened cement paste (HCP) with a high water/cement ratio and long mixing time were made, in order to ensure a degree of hydration close to unity. The samples were moulded into prisms and kept under water for 6 months and then crushed and sieved. The fraction 2-4 mm was selected for the grinding experiments. The samples were then dried in an oven at 110, 400, 600 and 800°C (and termed HCP-110, HCP-400, HCP-600 and HCP-800, respectively). All these samples, together with a room temperature one (so untreated, termed HCP-20) were ground under the same conditions (grinding time, number of runs, scraping etc.) and the result analysed using a Mastersizer 2000 laser diffractometer. The results (cumulative PSD) are shown in Figure 5.3.

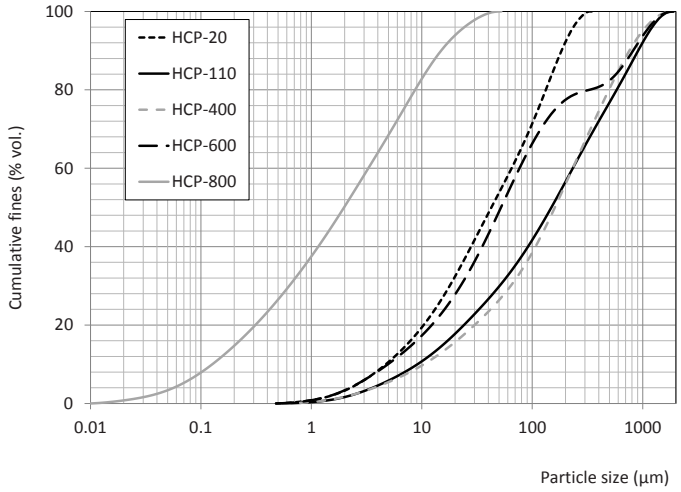

Figure 5.3. Particle size distributions of thermally treated (110-800°C) hardened cement paste samples, undergone the same grinding procedure.

It can be observed that the room temperature sample possesses the finest PSD. However, no significant difference was found between the samples, except a low tendency to agglomerate for the RCF treated at 110 and 400°C. The samples treated at higher temperatures (600 and 800°C) benefited from the volume expansion due to the transformation between α- and β-quartz, and therefore show a PSD which is finer than the original one. Given the fact that the thermally treated cement paste proved harder to grind than the untreated one (even by a small margin), the thermal treatment was performed on

the particles under 150 µm directly, rather than on the 2 mm ones (which would have meant treating also a much larger fraction of the recycled aggregates).

Table 5.3. d_{10}, d_{50} and d_{90} PSD characteristic parameters and the density measured for the untreated (RCF-20) and thermally treated recycled concrete fines at different temperatures between 500 and 1100°C. The cement, fly ash and slag employed in the study are included for comparison.

	d_{10} (µm)	**d_{50} (µm)**	**d_{90} (µm)**	**Density (g/cm^3)**
RCF-20	3.7	38.2	133.8	2.52
RCF-500	5.0	33.9	117.2	2.65
RCF-800	9.1	42.5	118.0	2.92
RCF-1100	9.8	49.1	139.6	2.89
CEM I 42.5N	4.1	23.4	72.6	3.15
Fly ash	3.4	19.2	94.3	2.36
Slag	2.3	13.4	37.1	2.88

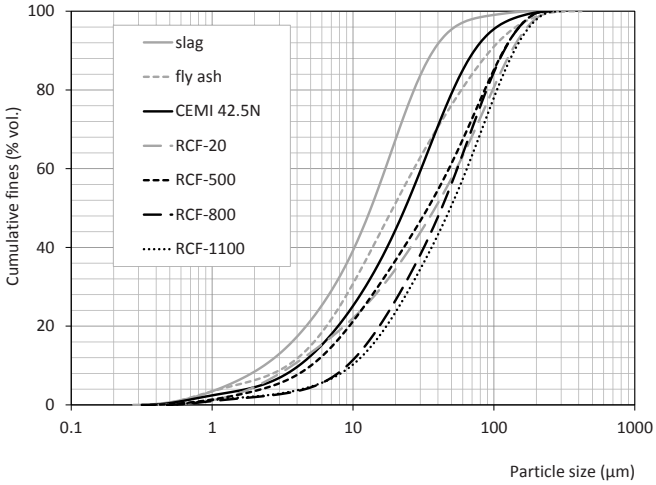

Figure 5.4. Particle size distributions of all binder materials used in this research: untreated (RCF-20) and thermally treated recycled concrete fines at different temperatures between 500 and 1100°C. The cement, fly ash and slag employed in the study are included for comparison.

The PSDs of the binders were also measured by laser granulometry (Mastersizer 2000); the particle size distributions are presented in Figure 5.4. The equivalent particle size corresponding to 10%, 50% and 90% passing of all investigated materials (d_{10}, d_{50} and d_{90}) are presented in Table 5.3.
It can be seen from Figure 5.4 and Table 5.3 that the slag has the finest particle sizes among all the binders, while the fly ash and the cement have similar particle sizes which are larger than the slag. RCF-20 is made up of even larger particles, which tend to clump together during the thermal treatment (an effect more visible for the RCF-800 and RCF-1100 samples).
Another physical property which was measured before and after each thermal treatment is density. The densities of all RCF samples were measured by an AccuPyc II 1340 He pycnometer. The results are also presented in Table 5.3. As it was expected, the densities of the RCF increase with the elevated thermal treatment temperature, until 800°C. This is due to the loss of physically and chemically bound water during the thermal treatment procedure.

5.4.2 XRD and SEM

X-ray Diffraction was employed before and after the thermal treatment of the RCF samples. The samples were analysed using a Rigaku-Geigerflex spectrometer. The obtained diffractograms of the reference RCF-20, RCF treated at 500°C (RCF-500) and 800°C (RCF-800) are illustrated in Figure 5.5, where the main crystalline phases are identified and marked. The diffractograms of the gravel used in the initial concrete mix is also added in order to show that the only main phase of this material is α-quartz, and also to serve as comparison for the recycled concrete samples above. The diffractograms of the sand and two types of gravel used in the initial mix are almost identical, which confirms their composition of 92-98% SiO_2 obtained through XRF.
In Figure 5.5, the typical reflections associated to α-quartz, C_2S, portlandite, calcite and lime are shown for each of the samples. In the 500°C-treated sample, the significant differences from the reference RCF-20 are the significant reduction of the peaks of portlandite, which correlates with the TG-DSC analysis. Between the temperature of 500°C and 800°C, the peaks corresponding to calcite also decrease almost completely. This phenomenon was to be expected, due to the dissociation of calcite at around 750°C. In the RCF-800 diffractogram, the peaks corresponding to lime are more intense than for RCF-500. The corresponding transformations were listed in Table 5.1. Portlandite is still present in the 800°C-treated sample, even though in even lower amount than in the RCF-500, which can be explained by the rehydration of small amounts of the increased CaO content due to atmospheric moisture.

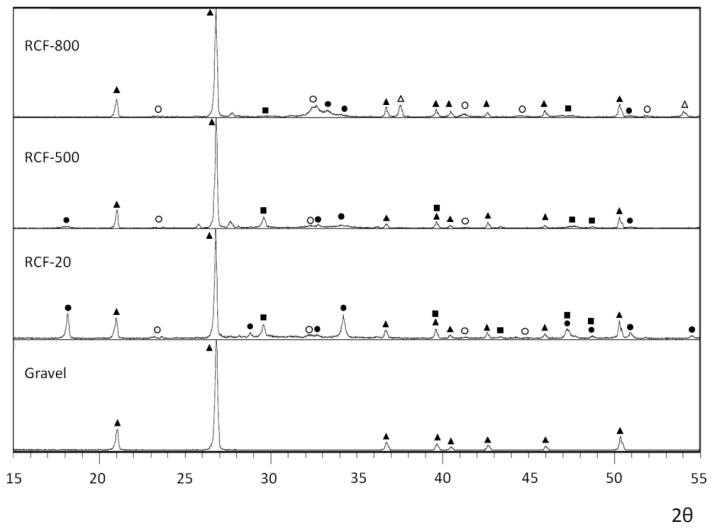

Figure 5.5. XRD of reference RCF-20 and thermally treated RCF at 500°C and 800°C. A gravel sample used in the initial concrete mix which was recycled and measured by XRF to contain 98% SiO_2 is included for comparison. α-Quartz (▲); C_2S (○); Portlandite (●); Calcite (■); Lime (Δ).

The mineral which is present in all samples and has the highest peak intensities is α–quartz. This can be explained by the presence of crushed silica aggregates in the RCF samples. As explained in Section 5.2, the transformation from α-quartz to β-quartz takes place around 570°C and it is reversible. Therefore, no β-quartz can be detected in the RCF-800, since the XRD is performed after the sample has been cooled down to room temperature.

An interesting observation can be made regarding the detection of a C_2S/C_3S phase in all three RCF diffractograms. This can be attributed to the content of unhydrated cement in the RCF sample, which was to be expected, given the age of the samples is less than one year at the time of analysis. A more valuable piece of information is the increase of the C_2S/C_3S peaks intensities in the RCF-800 sample, which suggests that the thermal treatment of recycled concrete fines determines the formation of a calcium-rich silicate phase similar to the one found in unhydrated cement. Snellings et al. [137] have observed such belite formation at temperatures around 890°C.

In order to further observe these transformations visible on the diffractograms, all three RCF samples were also investigated by scanning electron microscopy (SEM). The images are presented in Figure 5.6. The samples were analysed using a high resolution scanning electron microscope (FEI Quanta 600 FEG-SEM) with a Schottky field emitter gun (at a voltage of 2 – 10 keV) in high vacuum mode. All pictures shown were taken at

a magnification of 5000x. Figures 5.6a-b show the RCF-20 sample, Figures 5.6c-d the RCF-500 sample and Figures 5.6e-f the RCF-800 samples.
Hydration products can be seen in Figure 5.6a of the recycled concrete fines. Some plate-like formations (portlandite and AFm phases) can be observed. An ettringite needle can be identified, but generally these were not observed in these samples, or observed on the XRD spectra. This can be due to the crushing process, which probably destroyed the fragile ettringite needles. In Figure 5.6b, plate-shaped hydration products can be observed more clearly, together with a fragment of fractured gypsum, which could not be identified in the XRD analysis, probably due to its low amount in the samples.
Figure 5.6c shows a RCF-500 sample, in which the dehydrated cement paste still shows clear plate-like formations. Dehydration cracks are visible in this image, and a fragment of broken calcite can be identified. Figure 5.6d further shows plate-shaped hydration products (possibly calcite, which is not yet decomposed at 500°C) and a piece of fractured quartz (top left corner), generated by the crushing of the aggregates during the pre-crushing stage. This formation is similar to the ones identified in Chapter 4 and hydration products can be seen on its surface.
Figure 5.6e shows cracks on a RCF-800 sample, which can be due to either the dehydration process or to the $\alpha \rightarrow \beta$ quartz transformation, which occurs with a swell in volume. Molten spots can be observed in this image, together with new formations - small needles which could be C_2S, as indicated by the diffractograms taken of these samples. Figure 5.6f also shows local melting, as well as newly formed plates, which can be portlandite, according to the XRD pattern. A feathery structure of decomposed hydration products is visible in the centre of the image.

5.4.3 Calorimetry study of the recycled concrete fines

All RCF samples were mixed with water and placed in a TAM Air isothermal calorimeter in order to observe and measure their rehydration behaviour, which is presented in Figure 5.7. Initial tests have shown that there is no significant change recorded between 72 and 168 hours (7 days), so all heat generation curves are shown up to 72 hours for clarity.
The total heat released per gram of binder is presented in Table 5.4, for a hydration duration of 24 and 72 hours. For each sample, the percentage of the cumulative heat relative to the one of the reference is shown in brackets.
These values can be compared to the cement content of each sample, also included in Table 5.4. If they are higher than the cement content, it means that the replacement material contributes to the heat generation or it accelerates the hydration of cement. If the two values were the same, the replacement material can be considered inert. A heat ratio lower than the cement content indicates a detrimental effect of the replacement material up to the duration of the rest, 24 or 72 hours.
The reference for most of the samples (excluding slag-blended ones as explained below) was a CEM I 42.5N paste with a w_0/b_0 ratio of 0.5, obtained as an average of 3

measurements. 10% of the cement was replaced by RCF-20, RCF-500 and RCF-800 respectively, in order to assess the influence of the recycled concrete fines on the cement hydration. Furthermore, samples containing just RCF and water were also analysed, to see if there is any hydraulic activity present.

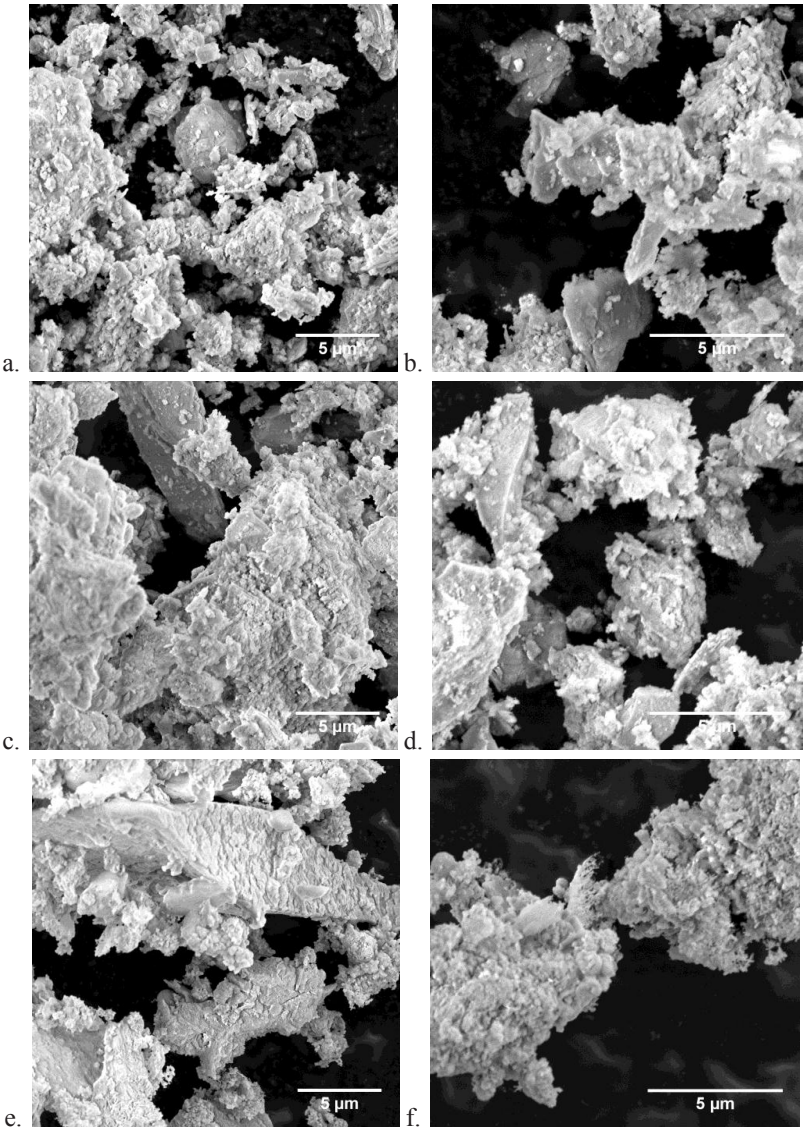

Figure 5.6. SEM images of untreated RCF-20 (**a.** and **b.**), RCF-500 (**c.** and **d.**) and RCF-800 (**e.** and **f.**) at the magnification of 5000x.

Due to the large water demand of the recycled concrete fines, the RCF-20 and RCF-500 pastes were mixed with a w_0/b_0 ratio of 0.7, while RCF-800 needed a w_0/b_0 of 0.9 to achieve similar flowability before being placed in the calorimeter.

Blended samples containing either fly ash or slag were also tested, in order to test the possibility of using RCF as an activator for pozzolanic binders. Three samples containing 80% CEM I 42.5N, 10% commercial fly ash and 10% RCF-20, RCF-500 or RCF-800 were measured and the heat release of the fly ash-RCF blends compared to the same cement paste reference. Besides these, four slag-containing samples were also evaluated, using a sample containing 70% slag and 30% CEM I 42.5N with a w_0/b_0 ratio of 0.7 as reference. Afterwards, 33% of the cement was in turn replaced by RCF-20, RCF-500 and RCF-800 (for final blends containing 70% slag, 20% CEM I and 10% RCF), while keeping the same water/binder (w_0/b_0) ratio.

All samples were mixed externally and then inserted into the measurement slots within minutes of adding the water to the powders. For this reason, the first peak observed on heat flow plots cannot be taken into account. While this peak is partly due to the initial hydration of cement and rehydration of thermally treated RCF, it also includes the disturbance of the system at the introduction of the samples, together with other factors pertaining to the sample preparation. Therefore, this initial high peak will not be included in the computation of the cumulative heat generated by each sample, for which the integration will begin at the inflexion point when the heat flow starts to rise again after the initial drop.

Figure 5.7a shows the cumulative heat generated by the RCF-20, RCF-500 and RCF-800, compared to CEM I. For RCF-20, almost no hydration can be detected, this being the lowest of the registered curves. The small heat generation can be attributed to the unhydrated cement that can be contained in the recycled concrete fraction. The RCF-500 sample shows a significantly higher heat generation, due to the rehydration of the thermally treated hydration products (Table 5.1). Even though, using the same line of reasoning, the RCF-800 should have the highest heat generation, it has proven to give only slightly higher results than RCF-20. This effect can be attributed to the high water demand of the RCF-800, even though a w_0/b_0 ratio of 0.9 was used, compared to a 0.7 ratio for the other two RCF samples. In order to check this hypothesis, Figure 5.7b shows only the first 6 hours of hydration of the same samples, in terms of heat flow. It can be seen that RCF-800 has a much higher first peak of hydration than RCF-20, RCF-500 or even the pure cement paste. This peak, however, as explained above, cannot be taken into account when computing the cumulative generated heat.

Figure 5.7c shows the calorimetric behaviour of samples in which 10% of the cement was replaced by thermally treated RCF. RCF-500 and RCF-800 behave in a promising way: their heat generation after 72 h showing that they do not hinder the hydration of cement significantly after that curing time (Table 5.4).

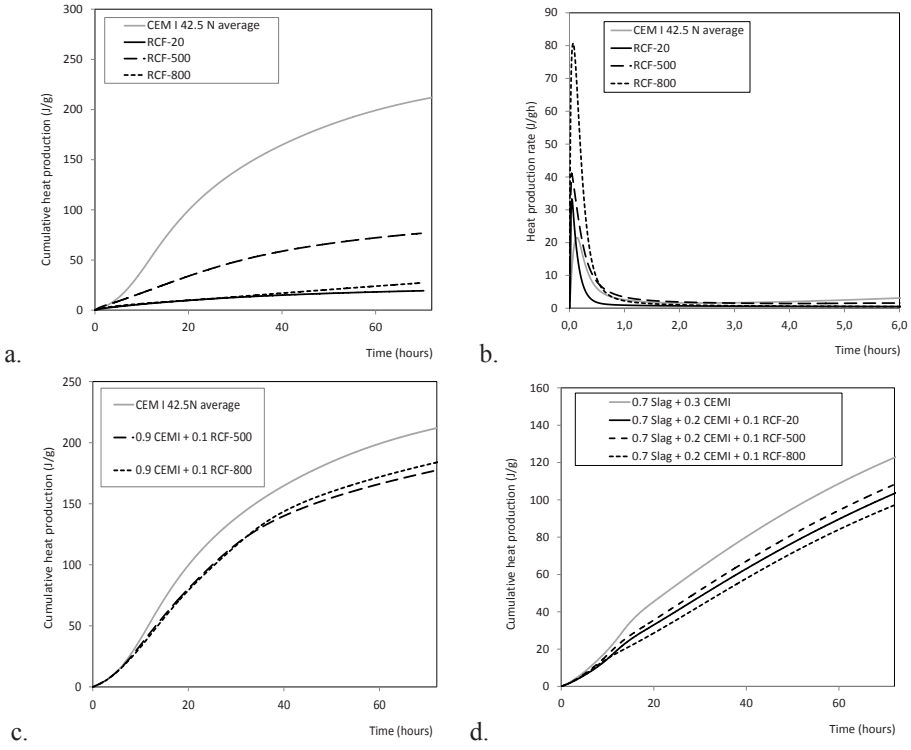

Figure 5.7. Calorimetric curves of RCF-20, 500°C-treated RCF (RCF-500) and 800°C-treated RCF (RCF-800) in a mix with water (**a.** and **b.**), as 10% cement replacement (**c.**) and as cement replacement in a slag-cement mix (**d.**). Measurements up to 72 hours.

The RCF-800-containing sample has a better effect than RCF-500, which supports the hypothesis of insufficient water for the hydration of this sample. Three more samples where 20% of the cement was replaced by a mixture of commercial fly ash and the three RCF types in a 1:1 ratio were also studied. The results are shown only in Table 5.4, as the behaviour of all three samples was almost identical. The binding efficiency of all fly-ash-RCF mixes was higher than the replacement level (highest one being 94%, compared to a cement content level of 80%, see Table 5.4), which suggests that they are suitable mixtures for the replacement of cement. This is further studied in Section 5.5 through mechanical strength tests.

Figure 5.7d shows the results obtained by the 4 slag-containing samples. In this case, the mixture containing RCF-500 has proven to be the best one. The poorer performance of the RCF-800 sample can again be explained by the increased water demand of this material. When comparing the results in Table 5.4, these samples show the most

promising effect for the replacement of cement, achieving up to 87% of the heat generated by the cement at a 67% cement content.

Table 5.4. Total heat released per gram of binder mix for the first 24 and 72 (*70) hours of hydration, ratios of cement/powder and water/powder and the percentage represented by each sample generated heat of the one of the reference. Mixes shown in **bold** are used as reference for all following samples.

Binder	CEM I in sample/ CEM I in reference ratio	Water/ powder ratio	Cumulative heat after 24h (J/g binder) (ratio of reference)	Cumulative heat after 72h (J/g binder) (ratio of reference)
100% CEM I average	**1**	**0.7**	**107.99 (100%)**	**209.94 (100%)**
100% RCF-20	0	0.7	10.91 (10%)	19.39* (9%)
100% RCF-500	0	0.7	38.85 (36%)	76.63*(37%)
100% RCF-800	0	0.9	10.89 (10%)	27.07* (13%)
90% CEM I + 10% RCF-500	0.9	0.7	84.71 (78%)	174.79 (83%)
90% CEM I + 10% RCF-800	0.9	0.7	84.95 (79%)	181.53 (86%)
80% CEM I + 10% fly ash + 10% RCF-20	0.8	0.7	93.20 (86%)	195.79 (93%)
80% CEM I + 10% fly ash + 10% RCF-500	0.8	0.7	97.16 (90%)	196.81 (94%)
80% CEM I + 10% fly ash + 10% RCF-800	0.8	0.7	90.89 (84%)	170.46 (81%)
70% slag + 30% CEM I	**1**	**0.7**	**47.73 (100%)**	**119.64 (100%)**
70% slag + 20% CEM I + 10% RCF-20	0.67	0.7	33.78 (71%)	99.61 (83%)
70% slag + 20% CEM I + 10% RCF-500	0.67	0.7	36.75 (77%)	104.63 (87%)
70% slag + 20% CEM I + 10% RCF-800	0.67	0.7	28.98 (61%)	93.28 (78%)

5.5 RCF replacement tests in mortars

5.5.1 OPC replacement test

Untreated RCF-20, 500°C-treated RCF (RCF-500) and 800°C-treated RCF (RCF-800) were used to replace 10%, 20% and 30% by mass of cement in the standard mortar recipe.

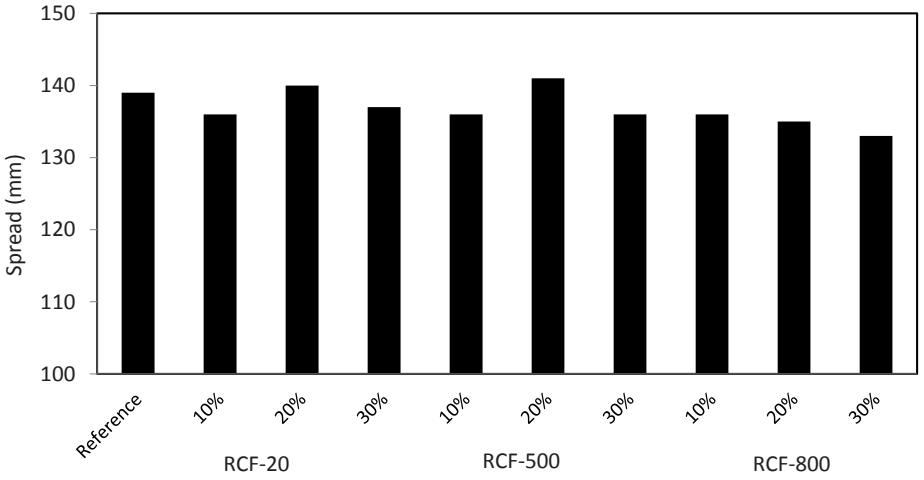

Figure 5.8. Final spread of standard fresh mortars (after application of SP for certain samples, as explained in the text): reference (where the binder is CEM I 42.5N) and 10%, 20% and 30% replacement of the cement by RCF-20, RCF-500 and RCF-800 by mass of binder.

Standard mortar (following EN 196-1 [29]) was made as the reference, using CEM I 45.2 N as only binder (1350 g Norm sand, 450 g binder, 225 g water). Coal combustion fly ash was used as reference cement replacement. The 7 and 28 days flexural and compressive strengths were measured in order to quantify the mechanical strength development.

The flowability of the fresh mortar samples was measured following [28]. Both the original and the thermally treated RCFs have a higher water demand than cement. In order to obtain a similar spread as the reference mortar, superplasticizer (Glenium 51, BASF) was applied to the samples in which 20% and 30% of the OPC was replaced by RCF. The 10% replacement samples achieved sufficient flowability without the use of superplasticizer (SP).

Figure 5.8 shows the spread achieved by the SP-containing mortar samples related to their RCF content. It was expected that the use of RCF would increase the water demand of the mortar samples, decreasing the fresh mortar spread. It was found that additions of 0.12% and 0.24% (by mass of binder) of superplasticizer were needed for the 20% RCF

and the 30% RCF replacement mortar samples respectively. RCF-800 displayed the highest water demand, which was to be expected due to its larger free lime content. Moreover, all dehydrated RCF samples will rehydrate very fast upon contact with water, which leads to a higher water demand. The flexural and compressive strength attained by all mortar samples are presented in Figures 5.9 a-d.

It is observed from Figure 5.9a that the 10% RCF-500 containing mortar achieves the lowest flexural strength of its replacement ratio class; fly ash, untreated RCF-20 and RCF-800 obtained very good flexural strength compared to the reference mortar. At a 20% replacement ratio, the highest flexural strength was obtained by the RCF-800 containing mix. Furthermore, for both 10% and 20% replacement ratios, the use of RCF-800 lead to a very similar flexural strength of the sample. Finally, increasing the replacement level to 30% by mass of cement leads to a significant decrease of flexural strength for all investigated mortars mixes; this can be explained by the low flowability achieved by the sample, and therefore the low water availability for the hydration process.

As can be seen from Figure 5.9b, RCF-500 continues to have the highest detrimental impact also on the 7 days compressive strength of the mortars. At 10% and 20% replacements, RCF-800 has a higher strength than the rest of the replacement materials, but still lower than the reference. It can be seen that the compressive strengths decrease less than the replacement level, indicating that the RCF brings its own contribution to the strength development. All materials used to substitute 30% of the OPC by mass cause a decrease of the 7 days compressive strength higher than 30%, the coal combustion fly ash leading to the lowest decrease (of 30.8%) compared to the OPC reference. As can be seen from Figure 5.9c, at 28 days the increased replacement ratio no longer decreases the 28 days flexural strength of the mortar samples. For instance, a 30% replacement of OPC by RCF-500 leads to a higher flexural strength (5.84 MPa) than a 20% replacement (5.64 MPa). The same can be observed in the case of 10% and 30% replacement of OPC by RCF-800, which lead to flexural strengths of 6.93 MPa and 7.18 MPa respectively. A 20% replacement of OPC by mass by either coal combustion fly ash or RCF-800 lead to a decrease of less than 20% of the reference sample strength. This indicates that fly ash and RCF-800 can contribute to the 28 days strength development of the mortar samples, which is in line with Shui [134].

At a 10% replacement ratio, fly ash, untreated RCF-20 and RCF-800 showed good mechanical performances; the decrease of compressive strength was less than 10% of the reference sample one in all cases and all samples would still qualify as strength class 42.5 following [26]. At a 20% replacement ratio, fly ash and RCF-800 performed better than 80% of the strength of the reference mortar, indicating that RCF-800 plays a role in the strength development. Moreover, the samples containing RCF-800 behave very similarly to the ones where coal combustion fly ash was used as secondary binder, for all

replacement levels. RCF-500, on the other hand, has the poorest behaviour at the 10% and 20% replacement ratios; however, is the best for the 30% replacement ratio.

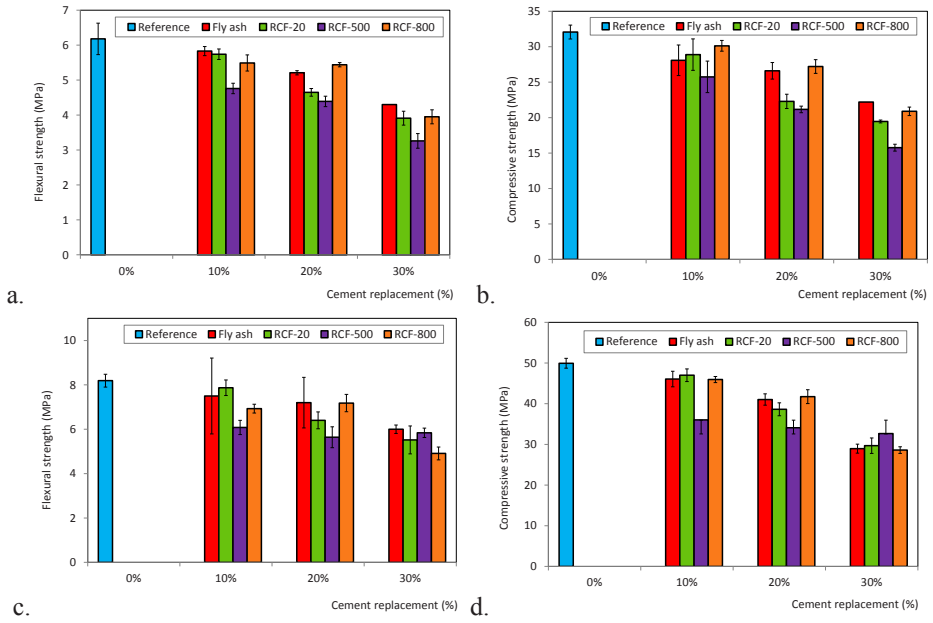

Figure 5.9 Mechanical properties of standard mortars : reference (CEM I 42.5N) and 10%, 20% and 30% replacement of the cement by fly ash, RCF-20, RCF-500 and RCF-800 by mass of binder. **a.**7 days flexural strength. **b.** 7 days compressive strength. **c.** 28 days flexural strength. **d.** 28 days compressive strength.

There are a number of factors which contribute to the obtained results. RCF, either untreated or thermally treated, has a higher water demand than cement. When replacing 10% of OPC by mass, RCF-20 acts mainly as a filler, which can provide nucleation sites for the cement hydration products; at a 20% replacement level, its higher water demand becomes significant, affecting the strength development. RCF-500, which contains dehydrated cement paste including the CaO generated during the thermal treatment, has an even more increased its water demand, which will have a greater effect than the rehydration reactions can compensate for.

For comparison purposes, 1100°C-treated RCF was also used to replace 10% of the cement; however, the attained 28 days compressive strength of this sample proved to be only 36.86 MPa, even lower than the RCF-500. Due to this result (which is in line with [134]), further experiments using RCF-1100 were not performed. An explanation for the poor compressive strength is that at the temperature of 1100°C, the structures of the

hydration products are radically affected by the loss of chemically bound water, so that the initial hydration products can not be recovered through rehydration.

5.5.2 Combining thermally treated RCFs with fly ash

So far, it has been shown that recycled concrete fines have a binder efficiency comparable to that of powder coal fly ash up to the measured 28 days of hydration. Also, Shui [135] has shown that dehydrated cement paste can act as an activator for fly ash. In this research, RCF-800 was combined with coal combustion fly ash as a secondary binder to replace OPC in mortar mixes. It was found that RCF-800 could decrease the fresh mortar flowability. When RCF was used to replace 20% of cement, superplasticizer was needed in order to achieve a good flowability. Fly ash, on the contrary, has the property of increasing the flowability when used in concrete [138]. Moreover, the free lime generated in RCF-800 is believed to activate the pozzolanic properties of fly ash. RCF-800 and fly ash in a 1:1 ratio were used to replace 20% by mass of OPC in standard mortar mixes, thus resulting in the following recipe: 1350 g Norm sand, 360 g CEM I 42.5N, 45 g fly ash, 45 g RCF-800, 225 g water.
The fresh mortar flowability was tested according to EN 1015-3 [139], the 10% RCF-800 + 10% fly ash mortar sample having a spread of 141 mm (compared to the 139 mm achieved by the reference sample). Therefore, it can be considered that the use of 10% of fly ash can fully compensate the fresh mortar flowability loss caused by 10% of RCF-800. So, by using RCF-800 along with fly ash, the flowability of the mix can be maintained while the cement replacement ratio increases.
Mortar recipes made by replacing cement by 20% of RCF-800 and by 20% of fly ash by mass of cement in the standard mortar recipe are also used for comparison; the obtained 7 and 28 days flexural and compressive strengths are shown in Figure 5.10a and b together with the computed standard deviations based on 3 samples for flexural strength and 6 samples for compressive strength. As it can be seen in Figure 10a, the sample in which both RCF and fly ash are used reaches the lowest 7 days flexural strength of the group (reduced by 36.7% from the reference). However, same sample attained a 28 days flexural strength of 7.19 MPa, which is only 12.2% lower than the reference, which suggests that the strength development of the combination of fly ash and RCF-800 continues over longer curing periods.
It is illustrated in Figure 5.10b that all three 20% cement replacement samples achieve very close 28 days compressive strengths. The sample containing both fly ash and RCF-800 has a compressive strength development which mirrors its slow flexural strength development.

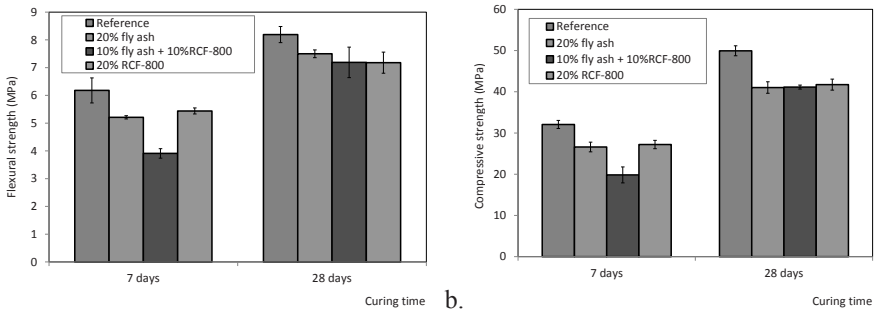

Figure 5.10. a. 7 days and 28 days flexural strength of the reference, 10% RCF-800 + 10% fly ash, 20% RCF-800 and 20% fly ash replacement mortars. **b.** 7 days and 28 days compressive strength of the reference, 10% RCF-800+ 10% fly ash, 20% RCF-800 and 20% fly ash replacement mortars.

The following conclusions can be drawn based on the experimental results: fly ash is able to compensate the fresh mortar flowability loss caused by RCF-800. Using both RCF-800 and coal combustion fly ash in a 1:1 ratio leads to slow strength development, but its 28 days mechanical properties are encouraging.

5.5.3 Slag cement replacement test

In the Netherlands, CEM III/B (which contains 66-80% ground granulated blast furnace slag (EN 197-1 [11]) represents over half of the binder market [104]. In order to quantify the influence of RCF on the hydration of slag-blended cement, mortar samples containing 70% of slag mixed with 30% of CEM I 42.5N as binder were made as reference. RCF, both untreated and thermally treated, were used to replace 33% of the cement in the slag-cement blend, thus the recipes using a binder combination of 70% slag, 20% CEM I and 10% RCF. The water/binder ratio was kept at 0.5. Figure 5.11 presents the 7 and 28 days compressive strength of these mortars; it can be seen that the untreated RCF-20 containing mix achieves the lowest compressive strength after both 7 and 28 days of curing. Both RCF-500 and RCF-800 increase the 7 and 28 days compressive strengths by 7.5% and 14.7% and respectively 8.8% and 20.1%, probably due to their increased free lime content, as well as the rehydration of their initial hydration products.

5.5.4 Comparison between expected and achieved binding ability of RCFs

Table 5.5 compares the 7 and 28-days compressive strengths of all the mortars detailed in Section 5.5 to the ones of the reference mortars. Just as in the case of the calorimetry results (Table 5.4), a ratio between the compressive strength of each sample containing RCF and its reference mortar compressive strength is computed, in order to be related to the cement ratio in the sample.

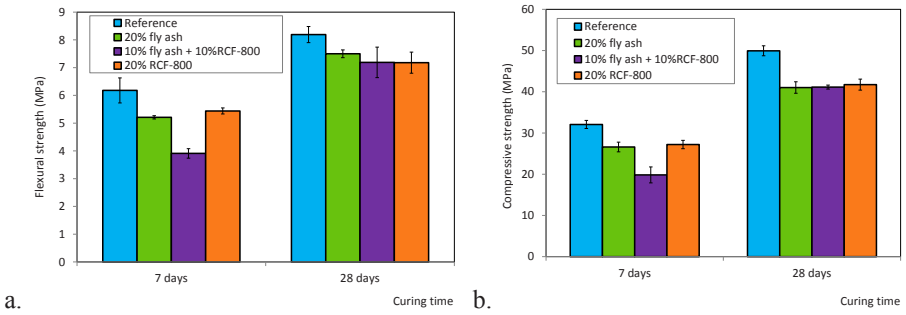

Figure 5.10. a. 7 days and 28 days flexural strength of the reference, 10% RCF-800 + 10% fly ash, 20% RCF-800 and 20% fly ash replacement mortars. **b.** 7 days and 28 days compressive strength of the reference, 10% RCF-800+ 10% fly ash, 20% RCF-800 and 20% fly ash replacement mortars.

The following conclusions can be drawn based on the experimental results: fly ash is able to compensate the fresh mortar flowability loss caused by RCF-800. Using both RCF-800 and coal combustion fly ash in a 1:1 ratio leads to slow strength development, but its 28 days mechanical properties are encouraging.

5.5.3 Slag cement replacement test

In the Netherlands, CEM III/B (which contains 66-80% ground granulated blast furnace slag (EN 197-1 [11]) represents over half of the binder market [104]. In order to quantify the influence of RCF on the hydration of slag-blended cement, mortar samples containing 70% of slag mixed with 30% of CEM I 42.5N as binder were made as reference. RCF, both untreated and thermally treated, were used to replace 33% of the cement in the slag-cement blend, thus the recipes using a binder combination of 70% slag, 20% CEM I and 10% RCF. The water/binder ratio was kept at 0.5. Figure 5.11 presents the 7 and 28 days compressive strength of these mortars; it can be seen that the untreated RCF-20 containing mix achieves the lowest compressive strength after both 7 and 28 days of curing. Both RCF-500 and RCF-800 increase the 7 and 28 days compressive strengths by 7.5% and 14.7% and respectively 8.8% and 20.1%, probably due to their increased free lime content, as well as the rehydration of their initial hydration products.

5.5.4 Comparison between expected and achieved binding ability of RCFs

Table 5.5 compares the 7 and 28-days compressive strengths of all the mortars detailed in Section 5.5 to the ones of the reference mortars. Just as in the case of the calorimetry results (Table 5.4), a ratio between the compressive strength of each sample containing RCF and its reference mortar compressive strength is computed, in order to be related to the cement ratio in the sample.

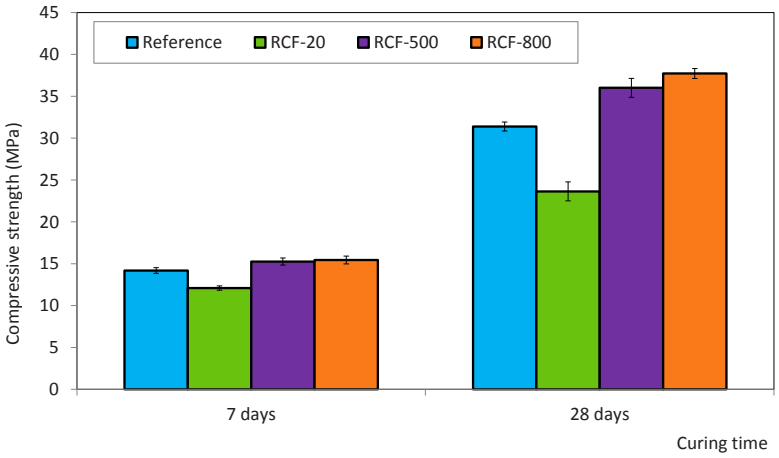

Figure 5.11. 7 days and 28 days compressive strength of slag-blended cement mortars, containing 70% slag + 20% CEM I 42.5N + 10% RCF as binder. The reference is 70% slag + 30% CEM I 42.5N.

It can be observed that the use of 10% RCF-20, 10% RCF-800, 20% RCF-800 and 10% RCF-800 + 10% fly ash lead to a higher compressive strength than if an inert material would have been used as replacement. An interesting observation is that the compressive strength ratio after 28 days is in some cases lower than the ratio after 7 days, especially in the case of the thermally-treated fines, as well as for the higher cement replacement level of 30%. This suggests that the beneficial effect of the additions manifests itself in the early hydration stages. The only samples that achieve a higher compressive strength than the reference are those containing slag and thermally treated recycled concrete fines. Both RCF-500 and RCF-800 prove to be able to activate the slag in the mixture to a certain degree, which can be explained by their higher content of CaO which will regenerate portlandite for the slag hydration upon contact with water.

Moreover, in the case of RCF-800, this effect is even more pronounced after 28 days than after 7 days, which is consistent with the slower hydration of the slag. This effect can also be observed for the sample containing 10% RCF-800 + 10% fly ash, for which a similar explanation can be envisaged. These 4 samples containing either fly ash or slag and RCF, as well as the ones containing 90% CEM I and 10% RCF were also analysed using isothermal calorimetry (Table 5.4). It can be said almost unanimously for these samples that the compressive strength achieved was higher than indicated by the calorimetric results.

This suggests that the recycled concrete fines have not only a role in generating compressive strength by their rehydration or hydration of residual unhydrated cement, but also by providing a filler effect in mortar mixes, as well as probably acting as nucleation sites for the further hydration of the cement component.
Both these effects cannot be indicated by calorimetry, but are probably due to the increased compressive strength achieved, especially for the 90% CEM I + 10% RCF containing samples, for which it was shown that the main beneficial effect of RCF is manifested in the first hours of hydration. For the slag- and fly-ash- containing samples, it would be interesting to also follow the strength development over longer curing times. This will be done in a future study, together with optimizing the mix parameters in order to maximize the beneficial effect of RCF. At longer curing times, also the possible contribution of the newly formed calcium silicate phase indicated on the XRD pattern of RCF-800 needs attention.

5.6 Conclusions and discussions

The main objective of this research was to use recycled concrete fines (RCF) to replace part of the cement in new concrete production. A thermal treatment method was employed to test its activation effect on the recycled fines. The characterization of the thermally-treated RCF suggested that calcium silicate phase similar to the ones in cement is formed during the treatment at 800°C. It was found that the rehydration of the thermally treated concrete fines is a rapid process, occurring in the first hour after contact with water. Also, the RCF-800 required a higher water/binder ratio to achieve full rehydration. The calorimetric measurements indicate that the mix of RCF and fly ash or slag is the most promising way of reuse for both the untreated and thermally treated concrete fines.
It was demonstrated that untreated RCF-20 and RCF-800 can be used to replace up to 20% of the cement in standard mortar samples without a significant loss of strength. The samples with 10% of the CEM I 42.5N cement replaced by untreated RCF-20 or RCF800 still meet the criteria of strength class 42.5 as described in EN 197-1 [11]. The mechanical strength of RCF-800 –containing mortars was also compared to a class F fly ash-containing mortar (ASTM C618 [26]). It was found that RCF-800 had mechanical performances equivalent to fly ash. RCF-500 –containing mortars showed a more significant strength loss at a 20% cement replacement level; the same effect was observed when the replacement of 30% of cement was attempted by all considered secondary binders.
RCF samples treated at both 500°C and 800°C showed a pronounced activation effect on ground granulated blast furnace slag. It was found that the replacement of CEM I by 10% of RCF-500 and RCF-800 can increase the 28 days compressive strength of the slag-cement blend by 14.7% and 20.1%, respectively, which can be attributed to the higher lime content of these samples.

Most of the mortar samples containing RCFs were found to have a higher compressive strength than their cement content, which suggests that the addition of recycled concrete fines also contributes to the development of mechanical properties. This can be due to the rehydration of the thermally treated fines, but also to the filler effect of all RCFs, as well as their contribution by providing nucleation sites for the hydration of cement.

Chapter 6

Characterization of bio-energy fly ashes as building materials

6.1 Introduction

Worldwide increased concern of the CO_2 emissions and dependency from fossil fuels leads to an increasing use of renewable energy sources in order to decrease the greenhouse emissions. One of the possible renewable energy sources is biomass that can be used as a replacement of coal in power plants. These so-called bio-power plants use waste wood as fuel to produce heat. The thermal energy is then consumed in steam turbines to generate electricity for the plant's own need or to supply the electricity grid. This central method of electricity generation was already applied during the industrial revolution. During that time, pulverized coal was used as fossil fuel and there was no awareness of the by-products released in the environment by the exhaust gases. However, those by-products (CO_2 emissions and air-polluting fly ashes) increased health problems near the factories. When these hazards were recognized, better installations were constructed to collect fly ashes using cyclone separators, electrostatic precipitators or bag houses to filter the exhaust gases. Also the combustion chamber processes were improved, resulting in the generation of lower amounts of by-products. The collected coal combustion fly ashes were disposed at landfill sites. However, those responsible for the disposal of fly ash are constantly seeking potential ash utilization options because of high costs and increasing production. Nowadays, fly ash can be used for ground stabilization under roads or applied in concrete mixtures due to its physical and chemical properties. Fly ash is a fine material that can be used as a filler in concrete mixtures. Also, due to its pozzolanic activity, it can be used as a binder to partly replace cement and therefore reduce the use of natural resources. As already mentioned in Section 1.5.1, in the Netherlands the majority of coal combustion fly ash is applied [24]. Also in the previous chapters, coal combustion fly ash has been extensively employed.

The increasing use of biomass for electricity generation in power plants leads to the production of fly ashes different from these "conventional" coal combustion fly ash. These fly ashes created from burning biomass have different characteristics and properties in comparison to coal combustion fly ash. It has become important to find new ways for the reuse of bio-energy fly ashes in concrete mixtures. So far the reuse of this type of fly ashes has not started because of the following reasons:

1. Bio-energy fly ash is a chemically and physically variable product, which makes its combination with cement more challenging. Its particle size distribution, loss on ignition, density, specific surface area, leaching, as well as pozzolanic/cementitious properties need to be tested to confirm its suitability;
2. Bio-energy fly ash contains contaminants like lead, zinc and chromium and large amounts of chlorides that may have negative influences on the hydration of cement;
3. As replacement of cement, its slow pozzolanic activity influences the hydration process, consequently lowering the properties of concrete at early ages;
4. So far there is no treatment method to remove the contaminants and increase the activity of contaminated fly ash, which could make its utilization more cost-efficient and sustainable.

The aim of this research is to use bio fly ashes from bio-energy power plants in cement-based mixtures. The role of this type of fly ash in a concrete mixture as a binder (partly replacing cement) or filler will be investigated. The aim is to develop a more sustainable and cost-efficient concrete that gives by-products a second life and with that, reduces the CO_2 content of cement and concrete. In order to do so, bio-energy fly ashes need to be treated to remove unwanted particles so that they can be used in the concrete industry. The results of this chapter and also Chapter 7 were also presented in [143]. The following objectives can be defined in accordance with the problem definition:
1. Determine the physical and chemical properties of the different fly ashes;
2. Remove unwanted contaminants in the bio-energy fly ashes by treatment to increase their applicability in concrete mixtures.
3. Test the performance of the optimized bio fly ashes in mortar mixtures.

6.2 Fly ash origin and types

In this chapter as well as in Chapter 7, different types of fly ashes from two power plants are investigated [143]. Each power plant has its own technology of bio-energy fly ash generation. However, one thing they have in common is that the generated bio-energy fly ashes cannot be reused as they are because of their concentration of unburnt components and harmful substances (metals and salts). To get more insight about these fly ashes in general, background information about the origin of the material and production is very important. In this section the background information of the fly ashes is provided.

6.2.1 Bio-power plant installations

The bio-energy fly ashes used in this study were collected from the cyclone and electrostatic precipitators of two different power plants in the Netherlands. The reason for this approach is that fly ashes generated in power plants are inherently variable materials, because of several factors. Among these are the type and mineralogical composition of

the fuel, degree of pulverization, type of furnace and oxidation conditions including fuel ratio and the manner in which fly ash is collected, handled and stored before use.
Since no two installations or plants have all of these factors in common, fly ash from various power plants is likely to be different. The following types of bio-power plant fly ash are examined: boiler fly ash (BF1) and cyclone fly ash (BF2) from the Twence-Hengelo plant and cyclone fly ash (BF3) and filter fly ash (BF4) from the HVC-Alkmaar plant. Using several types of fly ash, a more general approach of treatment and application can be sought.
In the HVC-Alkmaar plant, 170000 t of waste wood (dry biomass) are incinerated every year, compared to 140000 t of waste wood incinerated by the Twence-Hengelo plant. The bio-power plant of HVC-Alkmaar delivers 25 MW electricity, which is equal to the electricity use of 60000 households and the produced heat can be used for 48000 houses [140]. An overview of the fuel incineration and by-products (bottom ash, fly ash and air pollution control (ACP) residues) for the years 2008 and 2009 is provided in Table 6.1.

Table 6.1: Fuel incineration and by-products [141].

Year	Installation	Incinerated fuel (ton)	Unburnt residue	Bottom ash (%)	Fly ash (%)	APC-salts (%)
2008	HVC-Alkmaar	171829	8624	54	25	21
2008	Twence-Hengelo	137440	12587	66	20	14
2009	HVC-Alkmaar	176000	6485	29	50	22
2009	Twence-Hengelo	147894	15766	66	22	11

The bio-power plants described in this study are built recently. The Twence-Hengelo plant is in operation since 2007 and one year later the HVC-Alkmaar plant started to operate. The fuel used in the bio-power plants of HVC-Alkmaar and Twence-Hengelo is a waste mainly consisting of wood. The wooden waste can be divided into three different classes, namely A-wood, B- wood and C-wood. A description and examples for each class of wood are provided in Table 6.2. Not all these types of timber are suitable as fuel for the bio-power plants because of their components. Usually the wood waste used in the bio-power plants consists mainly of B-wood. Other compositions, such as beam grass, cocoa husks and residual products, nuts, shells and kernels are also used as fuel.

Table 6.2: Classification of wooden waste and their description [142].

Class	Description	Example
A-wood	Unpainted and untreated wood	Beams Stair components Rafters Battens Pruning wood Pallet wood
B-wood	Wood products not mentioned in classes A and C, including painted, varnished and glued wood.	Hard-board Soft-board Chipboard Wood fibreboard Pressed wood Furniture (except rattan) Painted wood Doors and frames (without glass and aluminium) Demolition wood Plywood
C-wood	Impregnated wood and preserved wood (CC and CCA-wood); CCA wood also contains copper, chromium and arsenic, CC Wood contains copper and chromium, but not arsenic. Timber with other agents (fungicides, insecticides, boron-containing compounds, quaternary ammonium compounds).	Garden fencing / fence parts Meadow poles Green wood (wood used in playgrounds)

According to the National Waste Management Plan (NWMP) [142] "the minimum standard for manufacturing and processing of A- and B-wood is useful application". To be useful, the application of the wooden waste should satisfy certain requirements:

1. By combustion, energy is generated and recovered and then used in the combustion process; a portion of the generated energy must actually be used, either immediately in the form of heat, or after conversion in the form of electricity;
2. Most of the waste must be consumed during the operation and most of the energy generated must be recovered and used. Because most of the waste must be incinerated, the waste has to consist of at least 50% organic matter;

3. The installation that is using the fuel should not have the function/status of waste incineration.

The bio-power plant system meets all three requirements, because more energy is recovered than what is used for production. Recovery takes place in the form of partly electricity and partly heat. In addition, the used biomass consists of more than 50% organic material. The system runs on A-wood when wood biomass in the form of wood chips is no longer available. This means that the power plant is not primarily designed for the incineration of waste, but to produce electricity and heat. This is very important because otherwise the class A and B wood could not be used according to the requirements described in [142]. Since no fossil fuel is involved, the electricity that is generated from the bio-power plants obtains the label of 100% green energy.

6.2.2 Incineration processes

This section presents the processes of wooden waste treatment for the HVC-Alkmaar and Twence-Hengelo power plants. Because these bio-power plants can have different process stages, an explanation is provided for the insight into the process of bio-energy fly ash extraction from waste products. The overall process can vary for every power plant, but in general the principle works as follows: waste wood is delivered by ship, train or truck and goes to the warehouse. Sometimes, the wood waste supplied by trains and ships first needs to be unpacked before it goes to the waste bunker. This can be performed automatically by special unpacking machinery. In the warehouse, fully automatic cranes mix the supplied waste in the bunker. This is an important step because the supply comes from different factories that process different products and mixing is crucial for minimizing this effect. Afterwards, the wood is delivered from the bunker to the funnels, where the waste slides (due to gravity) into the combustion chamber.
There are different types of combustion chambers available for the incineration of waste. The two mainly used types are the grill oven (furnace) and the fluidized bed incinerator.

The grill oven
The grill oven consists of the following devices: moving tiles for the transport of waste materials; combustion zones; a water basin and an air suction system. The transport tiles can shift and tumble under an angle over each other and thus move the waste coming from the funnels over the surface of the grill. The waste then undergoes various stages of the combustion process, like drying, degassing, and finally burning under temperatures around 850°C. After a combustion time of around one hour, the solid combustion residues left on the grate (bottom ash) fall in a basin filled with water. The liquid level in the basin is regulated. Evaporated water is removed with the suction system for the combustion air. Besides cooling down the bottom ash, the basin is used to maintain the pressure in the combustion chamber (water seal). At the same time, extra air is coming

through the air supply below the grills to cool them down and to provide oxygen for combustion. The amount of air, waste dosage and grill control device are controlled by an automatic process control system (automatic firing). The rest of the air is used as combustion air, which is functioning as recirculation air blown over the grill in order to achieve proper turbulence and hence a better post-combustion, improving the efficiency of the system. In some designs, the first part of these grills is cooled by water, which improves the durability of the system and facilitates the combustion (because the supplied air now only fulfils the role of supplying oxygen) and reduces the NO_x emissions.
In general, a sufficiently high temperature (above 850°C), the presence of oxygen (residual content of at least 6% in the flue gases), sufficient stand time (at least two seconds) and thorough mixing of the flue gases should provide a complete burning of the wood.

The fluidized bed incinerator
In this type of incinerator, the biomass is fed to the fluidized bed, which contains a large amount of sand (an inert, non-combustible material). From the bottom combustion air is blown through the fluidized bed at high speed. The high volume of air passing the fluidized bed creates turbulence that ensures the complete combustion of the fuel particles. Also, by providing primary and secondary combustion air for a staged combustion and recirculation, the formation of NO_x is reduced. Therefore, the combustion in the furnace can be characterized as a "low NO_x" process. A cyclone removes the solid and unburnt particles from the flue gases and carries it back to the bed.
There are two main types of fluidized beds. In the first one, the velocity is chosen so that the sand and the fuel just perform a bubbling motion. This can be called a stationary fluidized bed or a bubbling fluidized bed (BFB). In the second type, the speed of the airflow is further increased creating flows that are carrying sand and fuel. Such an installation is called a circulating fluidized bed (CFB); this is the system used at the HVC-Alkmaar plant. Compared to a BFB, the CFB has the advantage that by the greater turbulence the heat transfer will be higher, which means a lower flue stream resulting in a highly efficient system. The disadvantages of the CFB are the higher use of electric power due to the need for an increased airflow and the higher dust concentration in the flue gas. Most of the dust, however, is simply separated from the flue gas in the cyclone. Unburnt particles from the flue gases are going back to the combustion chamber. That process is controlled by the cyclone. After this, there is another cyclone that captures red-hot ash particles and ash particles greater than 10 μm. The fly ash that is removed by the cyclone is stored in closed fly ash silos.
After the combustion chamber the flue gases pass first through three sections (the radiant section) and then the fourth section (the convection part of the boiler), where the existing heat is recovered. In the first three sections, the gases release heat through radiation to the water tubes resulting in a steam production. The cooling of the gases occurs without

direct contact between the gas stream and the heated surfaces of the boiler, in order to prevent corrosion. During the passage of flue gas through the boiler the radiation decreases and more convective transfer takes place. During this process direct contact between flue gases and pipes is required. During all these processes the temperature is reducing and part of the ash in the gas is falling down. This so-called bottom ash is then collected and stored in storage tanks.
From the process described above hot water and steam are produced. The steam can flow through a turbine to produce electricity. The hot water can be used for district heating, in which case the transfer takes place through a heat exchanger. Also, the hot water can go to an evaporator to be converted in to steam. This steam can then be transported to the turbine.
For the separation of fly ash from the boiler outlet, an electrostatic filter is installed. This filter and the combination of the two-way ash handling system of the boiler make it possible to clean fly ash that can be reused. For the removal of dust a fine fibre filter is used. A dry powder (CaO or $NaHCO_3$) is injected on the cloth filter to absorb fine particles and powdered limestone is added to prevent fire and explosions. The next cleaning step is to remove the acidic components and ammonia from the flue gases. This is done by a wet cleaning process with water.
So, in general, fly ashes in the grill oven are collected in the following way: coarser particles in the boiler, finer particles in the electrostatic filter and in the cloth filter. In the fluidized bed incinerator, fly ash is collected as follows: coarser particles in the cyclone and finer particles in the electrostatic filter.

6.3 Bio-energy fly ash

The increase of using biomass for electricity generation in power plants leads to fly ashes different from the "conventional" coal combustion fly ash. The bio-energy fly ash created from burning biomass has different characteristics and properties in comparison to coal combustion fly ashes because of the different combustion input and therefore, additional research is needed to prove its applicability in concrete mixtures. Their characteristics and properties will be further described in this section.
Fly ash can be used in concrete as a filler or partial replacement of cement due to its particle-size distribution and pozzolanic properties, as it will be described in Section 6.3.4. The mineralogical composition, crystalline and non-crystalline phases, particle morphology as well as their physical characteristics define largely the pozzolanic reactivity of fly ash. The physical characteristics of fly ash which affect concrete performance are loss on ignition, fineness, moisture content, specific gravity, and pozzolanic activity.
Fly ash consists of glassy and crystalline phases. Portland cement can interact with the alumino-silicates present in fly ash with the creation of cementitious compounds possessing adhesive properties. In contrast to pozzolanic fly ashes (Class F according to

ASTM C618 [26]), self cementitious fly ashes (Class C according to ASTM C618 [26]) are able to hydrate in a similar way to Portland cement. The degree of self-hardening generally varies with the calcium oxide content of the fly ash.
In this chapter, five fly ashes will be used: two fly ashes provided by Twence-Hengelo (a boiler ash termed BF1 and a cyclone ash termed BF2), two fly ashes provided by HVC-Alkmaar (a cyclone ash termed BF3 and a filter ash termed BF4) and a commercial powder coal fly ash simply termed "fly ash" (Class F according to ASTM C618 [26]), which will be used as reference. Details regarding its oxide composition and its particle size distribution can be found in Tables 5.2 and 5.3, respectively.

Table 6.3. Terminology of all fly ashes used in Chapters 6, 7 and 8 of this thesis.

Fly ash name	Fly ash type	Type of incineration bed
BF1	Boiler ash	Grill oven
BF2	Cyclone ash	Grill oven
BF3	Cyclone ash	Fluidized bed
BF4	Filter ash	Fluidized bed
Fly ash	Pulverised coal combustion fly ash	

6.3.1 Colour

Bio-energy fly ash can be classified by colour; this quality is important for aesthetic reasons but can also be used to distinguish particles that contain a large amount of iron oxide and unburnt coal. These particles are dark, blackish in colour and changes in their concentration can affect the overall colour of the fly ash. Figure 1 presents the four different bio-energy fly ashes investigated in this research. The BF1 and BF2 fly ashes are much darker than the BF3 and BF4 ones, which indicates a higher carbon content. The BF3 and BF4 fly ashes are stickier and consist of clumped particles.
The BF2 cyclone fly ash has a consistency more like fine powder (particle size under 0.125 mm) and the BF1 boiler fly ash – like a mix of fine powder and coal dust. From an aesthetic point of view, the amount of fly ash that is used can have an influence on the colour of the final concrete. In Figure 6.1 only unburnt coal particles (black) can be distinguished from the other particles in the samples; other unburnt particles have a similar colour as the rest of the sample and are therefore hard to detect visually.

6.3.2 Particle Morphology

While examining coal combustion fly ash using an optical microscope, it can be seen that it consists of small particles that are typically spherical and fused together. These spherical particles can be very useful in concrete because they can function as a lubricant between the irregularly shaped cement particles [23]. There are however different types of spherical particles; the most common are described below:

1. Cenospheres, small spherical particles that are hollow, owing to an entrapment of gases by the molten phase during the burning process; these represent about 20% of the total fly ash particles;
2. Plerospheres, the spherical hollow particles that contain entrapment of particles instead of gases; due to the low density of cenospheres, they are valuable for low density concrete production.

Figure 6.1: Pictures of the four different fly ashes from both bio-energy power plants [143].

Figure 6.2 presents the reference fly ash under an Olympus SZX9 microscope with a magnification of 150x and software package AnalisySIS 3.2. For the separation of cenospheres and plerospheres from the fly ash, drops of water are used. Figure 6.2a illustrates the reference fly ash under water and Figure 6.2b the same fly ash on the surface of the water, where a large amount of cenospheres and plerospheres can be clearly seen.

Comparing Figures 6.2c-d, which present the BF2 fly ash, Figures 6.2a-b indicate that the bio-energy fly ash is much coarser and has almost no floating spheres but instead floating carbon particles. Also the particle size distribution is far greater than that of the reference fly ash, which can indicate a lower pozzolanic activity.

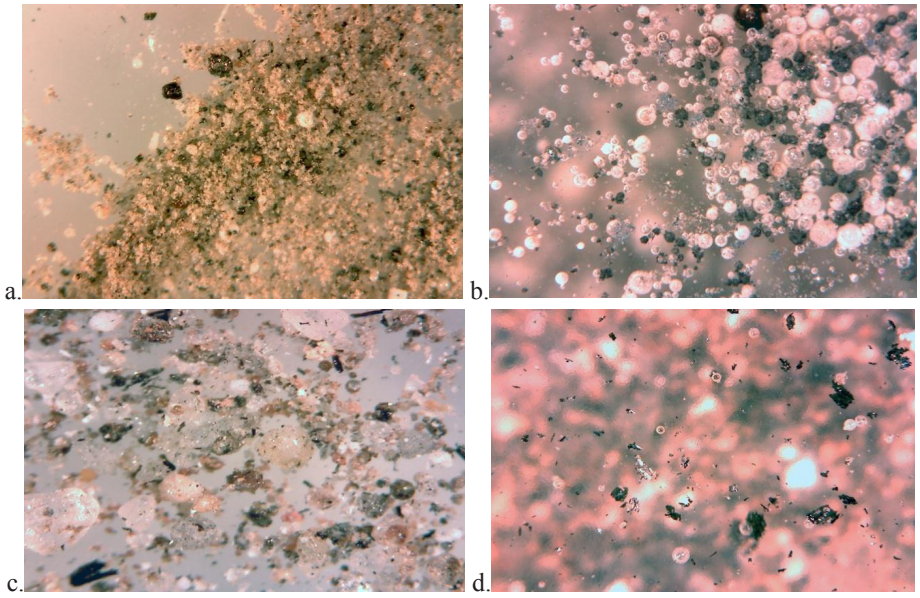

Figure 6.2. a. Reference fly ash under water indicating small spheres and minerals. **b.** Reference fly ash floating on water indicating low density spheres; **c.** BF2 cyclone fly ash under water, indicating coarse materials. **d.** BF2 cyclone fly ash floating on water indicating low density spheres and carbon particles [143].

6.3.3 Scanning Electron Microscopy

To have a closer view of the particles in the studied fly ashes than provided by an optical microscope, scanning electron microscopy (SEM) is performed. In this research a Philips XL 30 ESEM- FEG equipped with GSE, SE, BSE and EDX detectors is used to observe the external morphology of the fly ashes.

Figures 6.3a and 6.3b show the BF1 boiler fly ash at two levels of magnification, while Figures 6.3c and 6.3d present the BF4 filter fly ash, also in a general view, as well as in detail. From Figures 6.3a and 6.3c it can be concluded that BF4 has smaller particles (well under 100 μm) compared to BF1. As already observed in Figure 6.1, the BF1 and BF2 samples seem coarser than BF3 and BF4.

Moreover, in Figure 6.2 it can be seen that BF2 has coarser particles than the reference coal combustion fly ash. Therefore, it can be expected that the BF3 and BF4 fly ashes

will have a particle size distribution close to that of the coal combustion fly ash, which will be confirmed by laser granulometry in Section 6.3.4.
According to the CUR [23] regarding coal-combustion fly ash, an increase of particles smaller than 10 μm would indicate a higher amount of spherical particles. However, the bio-energy fly ashes do not present spherical particles even in their fine fraction, indicating again that bio-energy fly ash is of an entirely different nature. This hypothesis is supported by the picture of BF4 (Figure 6.3d) illustrating irregularly-shaped particles even for particles smaller than 20 μm.

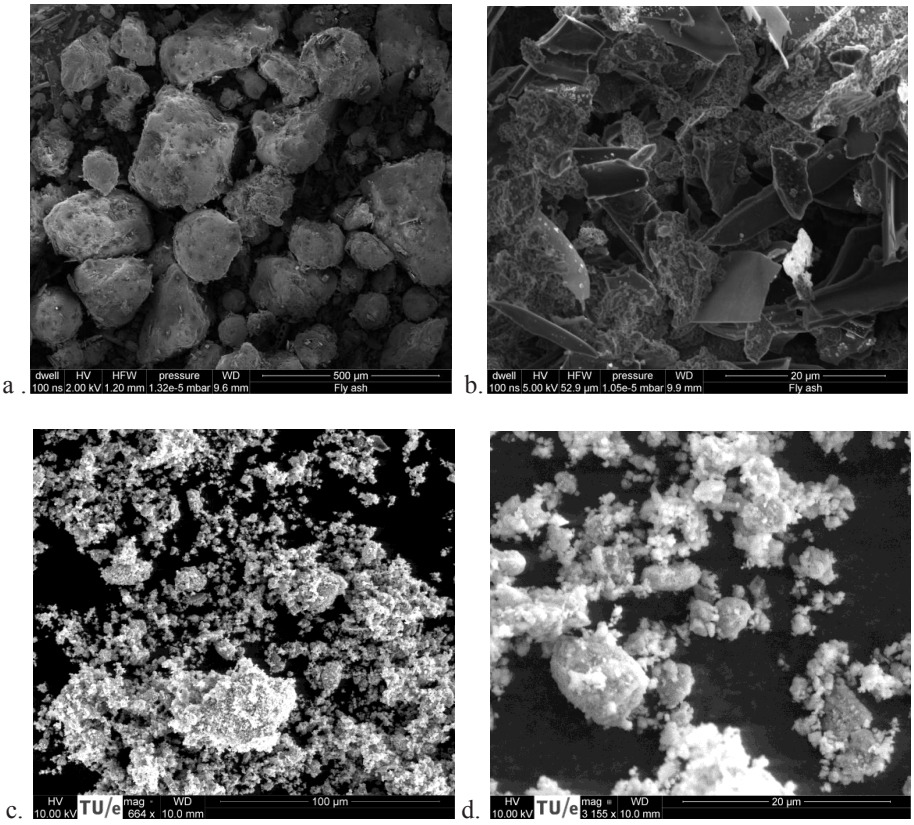

Figure 6.3: SEM images. **a.** BF1 boiler fly ash (lower magnification), **b.** BF1 boiler fly ash (higher magnification), **c.** BF4 filter fly ash (lower magnification), **d.** BF4 filter fly ash (higher magnification).

Moreover, when comparing Figures 6.3b and 6.3d, it seems that the BF1 fly ash contains crystalline phases, while BF4 contains a higher amount of amorphous particles. This suggests a higher reactivity of the BF4 fly ash, which will be further investigated in the

next chapter. XRD can also be employed to study the mineral composition of the bio fly ashes in comparison to coal combustion fly ash.

6.3.4 Fineness

Fineness is one of the primary physical characteristics of fly ash that relates to its pozzolanic activity [144]. When examining fly ash for its particle size distribution (PSD) the EN 450 [25] sets the limit of 40% for the maximum amount of fly ash retained on the 45 μm mesh sieve on wet sieving, as a quality control measure. Figure 6.4 illustrates the particle size distributions (PSDs) for five different types of fly ash measured with a Mastersizer 2000 using the laser diffraction method. This data is summarized in Table 6.4. The fly ashes BF1 and BF2 examined with the Mastersizer are sieved to a maximum particle size of 250 μm. However, from the results presented in Figure 6.4, about 10% of the particles still have a larger size. This is due to the fact that some particles are needle-shaped, so if they are lying horizontally on the sieve they will be stopped, but falling vertically they will slip through the sieve mesh openings.
As Figure 6.4 illustrates, the BF3 and BF4 ashes are finer than the fly ashes BF1 and BF2. This can be related to the burning process through which the HVC-Alkmaar plant reduces the waste for the combustion chamber into small fragments. As expected, the BF4 filter fly ash has a larger amount of fine particles than BF3 cyclone ash. This can be explained by the fact that gasses with fly ashes coming from the combustion chamber are first collected with the cyclone (BF3) or boiler (BF1) which collect the coarser particles, and after that the bag filter (BF4) or cyclone (BF2) collect the remaining fly ashes. However, the boiler ash BF1 has finer particles than the BF3 which in general was not expected; this could be mainly carbon dust. Comparing the result with the reference fly ash, BF3 is slightly coarser while BF4 is slightly finer.
For using fly ash as a filler, fly ash should contain fine spherical particles instead of the fused forms, as mentioned in Section 6.3.2. So far BF4 fulfils this requirement and the requirements of EN 450 [25] for maximum retained fly ash on the 45 μm sieve.
The fineness of fly ash is also defined by its specific surface area (SSA) per unit of mass. If the surface area is very large, a considerable amount of small particles forming a large active area are available. However, the effect of an increase in specific surface area beyond 6000 cm^2/g is reported to be insignificant [145]. Table 6.4 presents the specific surface area of the fly ashes estimated with the Mastersizer 2000. This method, however, provides only an estimation, since it does not account for the surface associated with the shape of the particles. According to this method the specific surface area of BF1 and BF2 is much smaller compared to the reference or BF3 and BF4 fly ashes.

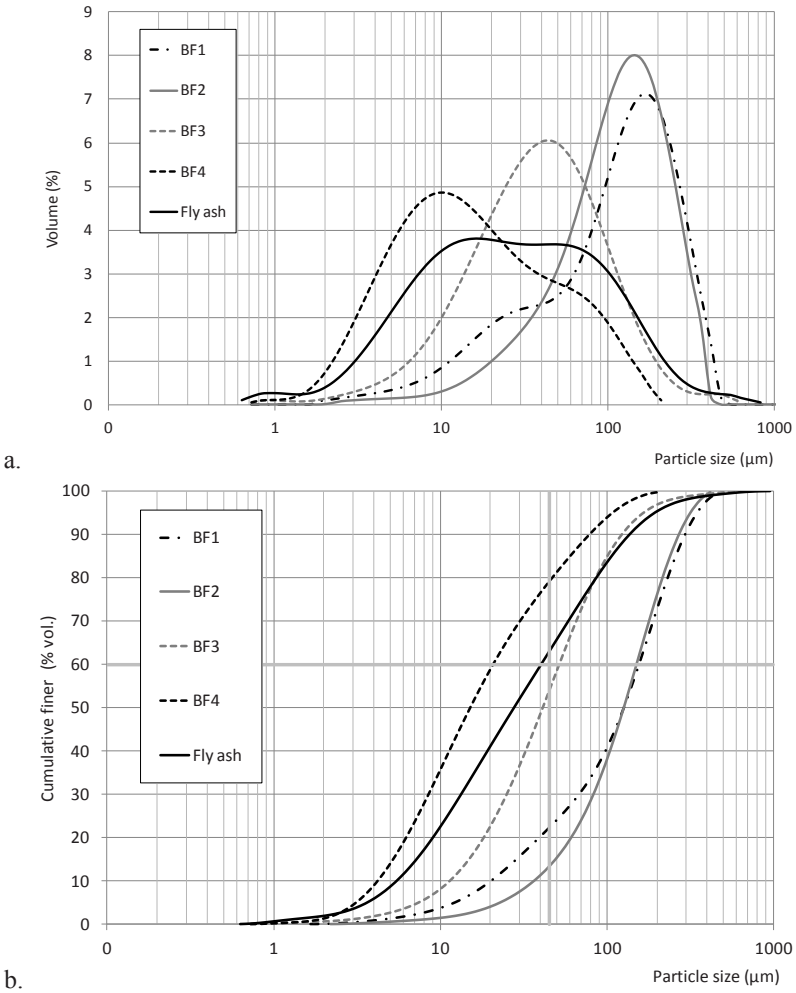

Figure 6.4. a. Particle size distribution (PSD) of the five fly ashes, **b.** Cumulative finer volume of the fly ashes. The lines at size of 45 µm and volume of 60% indicate the break point between good and less positive quality of fly ash as described by EN 450 [25].

6.3.5 Density

Fly ashes can be distinguished by their density. To measure the density, the fly ash is first dried in the oven at a temperature of 105°C according to EN-12880 [146] for 14 hours in order to remove adsorbed water. Table 6.4 presents the different densities of fly ash measured with a Micromeritics AccuPyc II 1340 gas pycnometer. The obtained densities are quite high compared to coal combustion fly ashes which have densities around 2.1-2.4

g/cm^3, but still lower than cement (± 3.1 g/cm^3). The lower density of the reference fly ash is probably due to the cenospheres and plerospheres as described in Section 6.3.2.

6.3.6 Composition

X-Ray Fluorescence

Table 6.5 lists the mass percentages of the most important oxides present in the fly ashes; this is used for oxide engineering later on. In this method the oxides of different fly ashes are compared with a reference, which can be found in Table 5.2. This may help to predict how the material will react when mixed with cement; the smaller the difference, the better the chances of a successful replacement.

Table 6.4. PSD characteristics, specific surface area (SSA) and density of all four bio fly ashes and the reference powder coal fly ash.

	Boiler fly ash (BF1)	**Cyclone fly ash (BF2)**	**Cyclone fly ash (BF3)**	**Filter fly ash (BF4)**	**Reference fly ash**
D_{min} (µm)	1.7	2.2	0.7	0.7	0.6
d_{10} (µm)	18	8.7	10	3.8	5.0
d_{50} (µm)	110	110	38	13	25
d_{60} (µm)	138	130	47	19	30
d_{80} (µm)	202	187	75	40	106
d_{90} (µm)	255	235	110	69	120
D_{max} (µm)	479	417	631	209	832
SSA (cm^2/g)	382	559	1160	2690	2090
Density (g/cm^3)	2.65	2.68	2.73	2.59	2.36

On one hand, the calcium oxide amount is lower in bio-energy fly ash than in cement but higher than in the reference fly ash. On the other hand, the amount of silicate is much higher in most of the bio-energy fly ashes compared to cement but lower than in the reference fly ash.

This combination will result in a low C/S ratio which can have both negative and positive effects on the final hydration products, depending on the ratio. In general the bio-energy fly ashes have more similarities from the point of view of oxide composition with cement than with the reference fly ash. Table 6.6 presents the maximum and minimum values of the concentrations of the main contaminants for the four different bio-energy power plant fly ashes, also obtained by X-ray fluorescence (XRF).

Table 6.5. Oxide composition obtained by XRF and loss on ignition up to 950°C of the four fly ash types.

Oxide	Boiler fly ash (BF1) (% mass)	Cyclone fly ash (BF2) (% mass)	Cyclone fly ash (BF3) (% mass)	Filter fly ash (BF4) (% mass)
CaO	32.9	28.5	29.4	43.5
SiO_2	22.1	33.3	18.2	5.7
Al_2O_3	3.7	4.8	6.8	2.4
Fe_2O_3	6.6	5.7	4.2	2.3
SO_3	7.6	6.5	10.0	10.2
Remaining oxides	21.9	16.4	20.8	17.2
LOI	5.4	5.0	11.8	22.9

Table 6.6: Elemental composition range of the four bio fly ashes obtained by XRF (provided by the producers).

Element (symbol)	Boiler fly ash (BF1) (mg/kg d.m.)	Cyclone fly ash (BF2) (mg/kg d.m.)	Cyclone fly ash (BF3) (mg/kg d.m.)	Filter fly ash (BF4) (mg/kg d.m.)
Antimony (Sb)	28-49	65-300	67	110
Bromide (Br^-)	15-59	15-150	130	420
Chloride (Cl^-)	990-5600	5300-27000	23000	83000
Fluoride (F^-)	2-6.8	6.9-100	5	2.1
Copper (Cu)	210-380	210-620	830	890
Molybdenum (Mo)	4.6-5.8	7.1-13	8.8	11
Selenium (Se)	< 4	4-9.4	4	4
Sulphate (SO_4^{2-})	9800-15000	11000-16000	7200	6100
Vanadium (V)	23-27	39-45	39	30
Zinc (Zn)	1100-3300	2700-10000	4600	3000

These values are based on leaching tests, which will be further discussed in the following chapters. The samples for the concentration measurements are collected twice per year at the corresponding power plant. It can be seen that for each plant the concentration of the components is varying. This is due to the different fuel types, the combustion process and

the collecting point of each plant, as mentioned in Section 6.2. The content of all elements is reported in milligrams of element per kilogram of dry sample (mg/kg ds).

X-Ray Diffraction

An in-depth analysis using X-ray diffraction (XRD) provides knowledge about the mineral composition of the fly ashes.

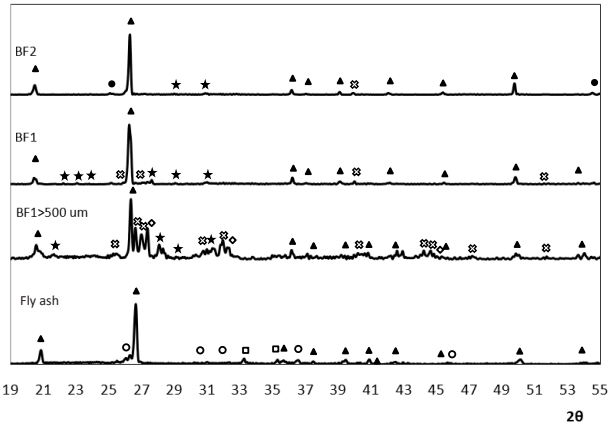

a.

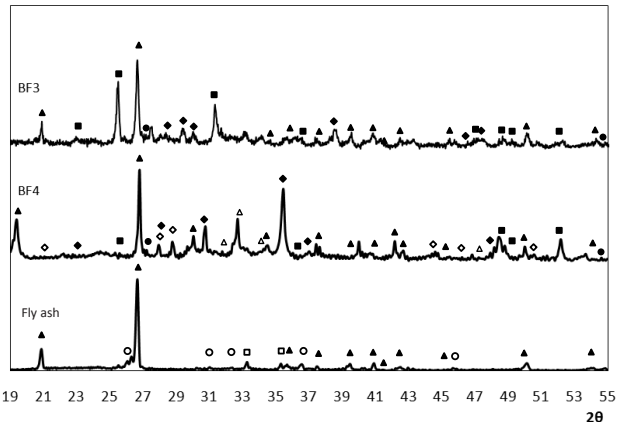

b.

Figure 6.5. a. X-Ray diffractograms of the fly ash (reference) and BF1, BF1> 500μm and BF2 bio fly ashes, **b.** X-Ray diffractograms of the fly ash (reference), BF3 and BF4 bio fly ashes. $CaSO_4$ (▲); $2Al_2O_3 \cdot SiO_2$ (○); TiO_2 (●); SiO_2 (■); $Ca(OH)_2$ (△) ; $CaCO_3$ (◆); Fe_2O_3 (□); NaCl (◇); CaO (★) ; K-containing phase (of the type $K_2Pb_2(CrO_4)_3$ or $K_2Ca_2(SO_4)_3$, **x**).

The reference coal combustion fly ash is mainly constituted of quartz (SiO_2), hematite (Fe_2O_3) and mullite ($2Al_2O_3 \cdot SiO_2$). Quartz is also the main constituent of all the four investigated fly ashes, followed by Ca-containing compounds ($CaSO_4$, $CaCO_3$, CaO or $Ca(OH)_2$) and TiO_2 in various crystalline phases. Chlorides were hard to detect by XRD, being in too low quantity to be clearly visible (phases under 10% by mass are expected to be hard to identify). Still, the BF4 fly ash diffractograms permitted the identification of halite (NaCl). This is in line with the XRF composition which shows that BF4 contains the largest amount of chlorides from all the investigated fly ashes. The largest fraction of BF1 (particles larger than 500 μm) were also expected to contain a high amount of chlorides and indeed, NaCl could also be observed by XRD as present in its mineralogical composition.

6.3.7 Carbon content/loss on ignition test

Loss on ignition (LOI) is defined as the mass loss that takes place when heating up materials to a temperature of 950°C, according to EN-196-2 [147]. In the first phase, water is evaporated and organic matter is combusted to ash and carbon dioxide at a temperature between 500 and 550°C. This LOI can be calculated using:

$$LOI_{550} = \frac{DW_{105} - DW_{550}}{DW_{105}} \cdot 100 \tag{6.3.1}$$

where LOI_{550} represents the LOI at 550°C (as a percentage), DW_{105} represents the dry weight of the sample after drying (usually 12–24 h at ca. 105°C) and before combustion, and DW_{550} is the dry weight of the sample after heating to 550°C (both in g). In a second phase, calcium carbonate decomposes with the release of CO_2, leaving calcium oxide; in this case, the LOI is calculated as:

$$LOI_{950} = \frac{DW_{105} - DW_{950}}{DW_{105}} \cdot 100 \tag{6.3.2}$$

where LOI_{950} is the LOI at 950°C (as a percentage) and DW_{950} represents the dry weight of the sample after heating to 950°C [148]. To calculate the LOI for fly ash the total mass loss of the dry weight up to 950°C needs to be considered.

Because the LOI has a high relation with the carbon content of bio-energy fly ash, a low LOI practically in most cases means low carbon content. A low carbon content of bio-energy fly ash is important because high carbon contents may lead to the following negative effects when the fly ash is applied in concrete mixtures [149]:

a.

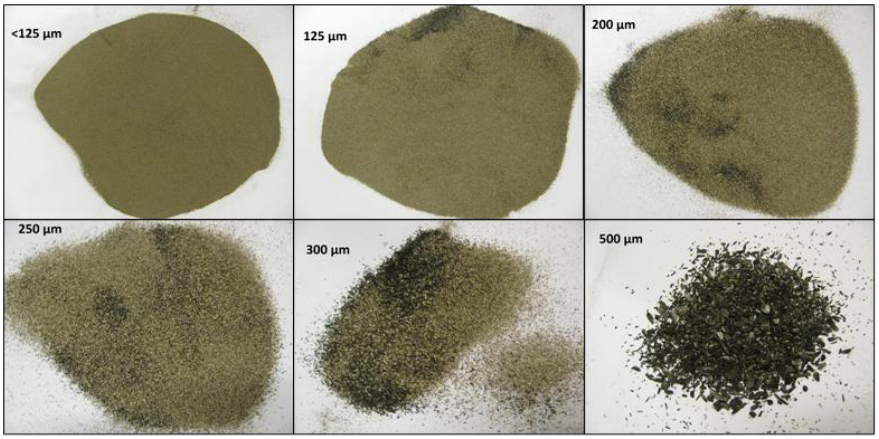

b.

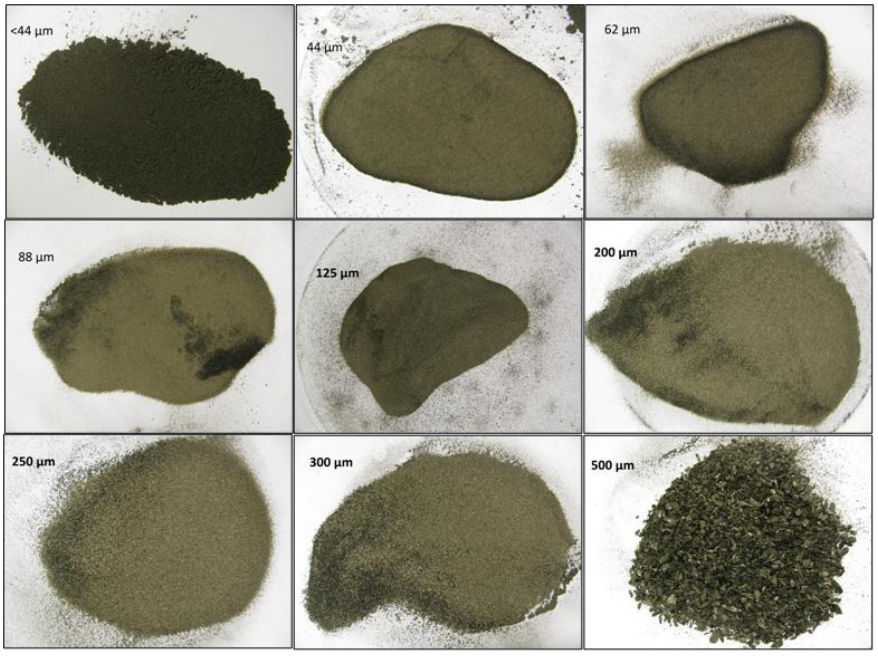

Figure 6.6. a. Sieved Twence cyclone fly ash (BF2) from 500 to < 125 µm, **b.** Sieved Twence boiler fly ash (BF1) ash from 500 to < 44 µm [143].

1. Coarse coal particles can form galvanic elements with pre-stressed steel products. As a result, small electric circuits are created, which can cause the corrosion of the reinforcement (pitting). Therefore, it is not often used in combination with pre-loaded and pre-tensioned steel. For that reason, high carbon fly ash can only be used in combination

with CEM I, because it consists of less/no coal particles, while in CEM II a part of the clinker is replaced by fly ash or blast furnace slag which contain coal particles, 60% of which are smaller than 45 μm.
In addition there is a requirement that the amount of fly ash particles larger than 212 μm should be less or equal to 3% by mass (NEN 5950 [150]);
2. The absorption of the cellulating agent by the carbon particles can prevent the formation of air bubbles, which can decrease the resistance of concrete to frost and de-icing salts and thus have a negative effect on the durability of concrete,
3. Carbon particles absorb water and thus reduce the available water for concrete to flow and for the cement to hydrate.

The LOI presented in Table 6.4 was measured while creating fused beads for the XRF elemental analysis, and is therefore the loss on ignition of the fly ashes at a temperature higher than 1000 °C, which should be very similar to LOI_{950}.
The BF1 boiler fly ash has a large amount of unburnt coal as also illustrated in Figure 6.6 and Table 6.4. This can be due to the combustion installation of the grill oven instead of a fluidized bed oven, where a less efficient combustion takes place. The fact that the BF2 cyclone fly ash and BF3 and BF4 ashes have a comparable amount of loss on ignition (LOI) is probably due to the fact that the LOI of the BF1 and BF2 ashes is mostly carbon, while in the BF3 and BF4 ashes consist of other elements. According to EN 450 [25] a LOI lower than 5% is allowed for coal combustion fly ash.
As illustrated in Figure 6.6, the BF1 and BF2 fly ashes contain black coal particles which be visually observed. Firstly, fly ashes are sieved from 500 to 125 μm to remove the large unburnt coal particles and to investigate their amount.
It is found that BF1 boiler fly ash consists of 13.1% coarse carbon particles and that the carbon particles also remain in the lower sieve diameters as illustrated in Figure 6.6 (visual analysis) and presented in Figure 6.4 (measured). However, the BF2 cyclone fly ash has only 0.7% coarse carbon particles larger than 500 μm and the carbon particles are almost entirely filtered out using the 125 μm sieve diameter as illustrated in Figures 6.4 and 6.6. The remaining fly ash < 125 μm constitutes 41.5% of the total amount of fly ash, which means that it is much more suitable for application in concrete than the BF1, based on its finer particles that are reacting faster and have less/non carbon content.

6.4 Fly ash properties and legislation

Fly ashes from different power plants have variable amounts of each constituent element due to the applied combustion process and fuel type. As described in Section 6.2.1, the fuel used in the bio-energy power plants mainly consists of B-wood and can be composed of many different products (e.g. window frames made from timber). However, these products all have their own manufacturing process and finishing (e.g. paint or impregnation). This has an influence on the quantities of different elements in wood and

eventually in fly ash. The fly ash is seen as a waste and should not be hazardous in order to be landfilled; the best option when possible is to use it in a building material production.

6.4.1 Leaching value

In order to evaluate the fly ash in terms of its environmental impact, a leaching test is performed. The leaching values for elements are determined by EN 12457 [27] using a column test. In this test the liquid flows through the solid sample. The amount of that liquid should be at least two times, but less than ten times the volume of the solid sample. The emission values stated in the Landfill Ban Decree [5] are defined by a relative amount of liquid to solid (L/S) equal to ten. However, this amount is hard to obtain for powder samples. In that case a L/S equal to two can be applied and finally extrapolated to ten [28]:

$$E_{L/S=10} = E_{L/S=y} \cdot \frac{1-e^{-K\cdot 10}}{1-e^{-K\cdot y}} \tag{6.4.3}$$

where $E_{L/S} = 10$ is the cumulative leaching of a building material, soil or sludge at a ratio of liquid to solid (L/S) of ten, $E_{L/S} = y$ is the cumulative leaching of a building material, soil or sludge with a L/S value equal to y, which is equal or higher than two, but lower or equal to ten and K is material-dependent constant representing a measure of the rate of leaching. The values are given in Table 6.7 [28].

Table 6.7. K-unit per element [28].

Element	K	Element	K
Antimony (Sb)	0.04	Nickel (Ni)	0.25
Arsenic (As)	0.01	Selenium (Se)	0.16
Barium (Ba)	0.17	Tin (Sn)	0.10
Cadmium (Cd)	0.32	Vanadium (V)	0.04
Chromium (Cr)	0.25	Zinc (Zn)	0.28
Cobalt (Co)	0.13	Bromide (Br^-)	0.51
Copper (Cu)	0.27	Chloride (Cl^-)	0.65
Lead (Pb)	0.18	Fluoride (F^-)	0.26
Molybdenum (Mo)	0.38	Sulphate (SO_4^{2-})	0.33

6.4.2 Landfill

The fly ash can be seen as a waste or as building material; both products need to fulfil certain requirements. The Landfill Ban Decree [5] contains requirements that classify waste streams into inert, non-hazardous and hazardous.

Table 6.8. Classification of Inert, Non-hazardous, Hazardous and No-landfill elements [5] in the fly ashes (L/S = 10), in mg contaminant/kg d.m.

	Inert	**Non-hazardous**	**Hazardous**	**No landfill**	**BF1**	**BF2**	**BF3**	**BF4**
Sb	< 0.06	*0.06-0.7*	**0.7-5**	< 5	*0.33*	*0.33*	*0.33*	*0.33*
As	< 0.5	*0.5-2*	**2-25**	< 25	*0.48*	*0.48*	*0.96*	*0.96*
Ba	< 20	*20-100*	**100-300**	< 300	1.30	2.07	16.73	*88.88*
Cd	< 0.04	*0.04-1*	**1-5**	< 5	0.02	0.02	*0.04*	*0.04*
Cl^-	< 800	*800-15000*	**15000-25000**	< 25000	*5764*	*12628*	**21000**	80000
Cr	< 0.5	*0.5-10*	**10-70**	< 70	*3.27*	0.23	0.41	0.41
F^-	< 10	*10-150*	**150-500**	< 500	4.57	*17.35*	9.30	8.09
Cu	< 2	*2-50*	**50-100**	< 100	0.22	0.22	0.55	1.7
Hg	< 0.01	*0.01-0.2*	**0.2-2**	< 2	0.00	0.00	*0.01*	*0.02*
Pb	< 0.5	*0.5-10*	**10-50**	< 50	0.28	**30.37**	*0.86*	*1.52*
Mo	< 0.5	*0.5-10*	**10-30**	< 30	*3.67*	*1.84*	*1.18*	*0.87*
Ni	< 0.4	*0.4-10*	**10-40**	< 40	0.23	*3.03*	*0.41*	0.1
Se	< 0.1	*0.1-0.5*	**0.5-7**	< 7	*0.23*	**1.22**	*0.43*	*0.21*
SO_4^{2-}	< 1000	*1000-20000*	**20000-50000**	< 50000	**25915**	*16545*	*15000*	*15000*
Zn	< 4	*4-50*	**50-200**	< 200	3.94	*11.39*	*13.84*	*11*

If the sample does not fulfil these requirements, it cannot be used even for landfill, before it undergoes a certain treatment. The leaching values of the different fly ashes from the bio-power plant compared to the classifying values according to the Landfill Ban Decree are presented in Table 6.8. The values in *italics* represent the "non-hazardous" category, the ones in **bold** belong to the "hazardous" class and the underlined ones to the "no landfill" one.

It can be seen that almost all the leached quantities of elements in the fly ash would qualify it as non-hazardous. Only the chloride, lead and sulphate contents are far above the limit, which means that the fly ashes cannot go to landfill before having a pre-treatment to remove unwanted elements. The cleaning process can be a chemical treatment, immobilization using binders or washing techniques, as will be described in Chapter 7.

6.4.3 Building material

If the fly ash is intended for application in building production it should also fulfil other requirements stated in the Soil Quality Regulation [28]. This decree divides the building materials into different categories:

1. Shaped building materials;
2. Non-shaped building materials without insulation - management - control (Dutch: IBC -measures);
3. Non-shaped building materials that need IBC-measures, termed an IBC-building material.

To distinguish if a building material belongs in the "shaped" group, the following requirements should be satisfied:

1. The smallest element in the material should have a volume of at least 50 cm^3;
2. The material needs to be in a solid shape.

In other words, the building materials should consist of large shaped volumes and should not show abrasion (wearing). This category does not apply to bulk materials like fly ashes, but to final products like bricks or precast concrete elements.
The materials that do not fulfil these requirements are automatically referred to the "non-shaped" group, like ashes and granulates. If the materials cannot be applied without isolation measures, they belong to the non-shaped IBC building materials. Fly ash is a non-shaped building material because it is in powder form. When fly ash is applied into concrete blocks it will become a shaped building material. This concrete block will need to fulfil the requirements that are associated with shaped building materials.
The requirements of the Soil Quality Regulation [28] encompass maximum leaching values. The considered elements are those which are mainly available in building materials and can influence the soil quality.
In Table 6.9 the considered fly ashes are compared with the requirements for a non-shaped building material determined for L/S = 2 [28]. All these materials need to undergo treatment to remove the detrimental substances. However, if it is impossible to fulfil all the non-shaped building material requirements it can be used in a shaped building

material; part of the elements will then be immobilized and therefore not hazardous substances anymore [151]. In general there are three sorts of materials:

Table 6.8. Leaching of building materials requirements compared with the fly ash values (L/S = 2) according to the Soil Quality Regulation [28].

Contaminant	Shaped building materials (mg/m^2)	Non-shaped building materials (mg/kg)	IBC materials (mg/kg)	BF1 (mg/kg)	BF2 (mg/kg)	BF3 (mg/kg)	BF4 (mg/kg)
Sb	8.7	0.32	0.7	0.078	0.1	0.17	0.17
As	260	0.9	2	0.1	0.73	0.48	0.48
Ba	1500	22	100	0.46	0.01	48.21	9.07
Cd	3.8	0.04	0.06	0.01	0.1	0.02	0.02
Cr	120	0.63	7	1.4	0.1	0.23	0.23
Co	60	0.54	2.4	0.1	0.1	0.32	0.32
Cu	98	0.9	10	0.1	0.001	0.96	0.31
Hg	1.5	0.02	0.08	0.001	11	0.01	0.00
Pb	81	2.3	2.1	0.1	1	0.83	0.47
Mo	144	1	15	2	1.3	0.51	0.70
Ni	400	0.44	8.3	0.1	0.42	0.23	0.23
Se	4.8	0.15	3	0.078	0.2	0.11	0.23
Sn	50	0.4	2.3	0.2	0.1	0.35	0.35
V	320	1.8	20	0.1	5.2	0.43	0.43
Zn	800	4.5	14	1.8	80	0.99	7.89
Br^-	670	20	34	0.46	9200	559.59	310.88
Cl^-	110000	616	8800	4200	7.6	108432.5	28823.84
F^-	2500	55	1500	2	8300	4.57	5.25
SO_4^{2-}	165000	1.730	20000	13000	0.1	1993.42	2990.13

1. The ones that fulfil all the requirements and can be used without any treatment;
2. The ones that do not fulfil all this requirements and need to be treated;

3. The ones that do not fulfil all these requirements but can be put in a shaped building material where the elements will be immobilized and fulfil the requirements for shaped materials.

6.4.4 Further regulation for coal combustion fly ash

The EN 450 [25] describes legislations for coal combustion fly ash concerning properties like particle size distribution and chemical composition. It is stated that the pozzolanic activity of fly ash is determined by the content of SiO_2 and Al_2O_3, and that the reactive form of SiO_2 should be at least 25% (mass). Additional requirements are:

1. Loss on ignition ≤ 5% (mass);
2. Chloride content ≤ 0.10% (mass) = 1000 mg/kg d.m.
3. Sulphate content ≤ 3.0% (mass) = 30000 mg/kg d.m.
4. Free calcium oxide ≤ 1.0% (mass) = 10000 mg/kg d.m.

Besides these, physical requirements are assessed as follows: at first, the maximum sieved residue on the 45 μm sieve is ≤ 40% (mass). Secondly, the compressive strength loss by replacing 25% of the cement by fly ash in concrete mixtures should be less than 25% after 28 days and 15% after 90 days.

Chlorides, especially $CaCl_2$, were added in the past to concrete to increase its hydration rate. Later a negative effect was found-the corrosion of steel reinforcement. Chlorides reduce the durability of reinforced concrete. Steel reinforcement in concrete is protected against corrosion by the "passive layer" on the steel surface. This passive layer is created due to oxidation of the steel combined with a high alkaline environment. However, when a sufficient amount of chlorides reaches the steel reinforcement, corrosion starts reducing the quality and function of the steel reinforcement. All these aspects were discussed in detail in Chapter 2.
The bio-energy fly ashes contain large amounts of chlorides which makes them unsuitable to use in reinforced concrete (Table 6.9). Most chlorides however are soluble and can be removed using water treatments. This approach will be further discussed in Chapter 7.
From different studies including a complete review of Yudovich & Ketris [152] it is known that coal ash can contain large amounts (more than 1000 ppm) of Cl^- containing phases. The species of Cl occurring in coal ash are surprisingly varied. Among them are found:

1. Inorganic salts like NaCl and other chlorides, Cl^- bearing silicates, carbonates, sulphides, as well as dissolved chlorides in pore water; these compounds are dealt with in Chapters 2 and 3.

2. Organic-associated Cl seems to predominate in coal. It may consist of two types: firstly, minor site ("true" Cl_{org}) water-insoluble Cl^- organic compounds, where Cl is covalently bound with coal organic matter [152]; secondly, "semi-organic" Cl, as anionic species Cl^-, which is partly or fully water-soluble Cl sorbed on the pore surface of coal organic matter. Such a Cl form does not enter the coal organic macromolecule and may be exchangeable Yudovich & Ketris [152].

Furthermore it needs to be noted that small-sized coal particles can contain more Cl than large size coal particles [152]. All this information indicates that coal particles in fly ashes can contain large amounts of chlorine that can be represented by chlorides. In Chapter 7, further research is done on this phenomena and possible occurring problems when trying to wash out these chlorides.

6.5 Summary and discussion

During this research [143], working with different types of fly ash, it can be stated that the well-known coal-combustion fly ash that has been used for decades is completely different than bio-energy fly ash described in this chapter. The benefits of coal combustion fly ash like a small particle size distribution, and the presence of cenospheres and plerospheres, increasing the workability and creating a denser structure do not naturally apply to bio-energy fly ash. Studying the physical and chemical properties, bio-energy fly ash has larger particle sizes with very few cenospheres and plerospheres. The larger particle size distribution would negatively affect the reactivity of bio-energy fly ash and would make it less suitable in concrete mixtures. Less cenospheres and plerospheres are leading to a material with higher density and less glassy phases.
Most of the bio-energy fly ashes consist of fused particles with unburnt coal particles that negatively affect the workability. These fused particles as well as coal particles can be related to the incomplete burning process, a process where the focal point is feeding the combustion chamber, keeping the fire and temperatures constant, resulting in waste streams that contain incompletely burned particles. These particles negatively affect the use of the fly ash in concrete mixtures, resulting in a need for different treatment methods and making this material already more expensive than coal combustion fly ash. However, when not using the material in concrete mixtures it will be landfilled, which is also not desirable because of increasing costs.
The use of the EN 450 [25], which is designed for coal combustion fly ash, as a quality measure for bio-energy fly ash is debatable. Still the requirements regarding developed strength and chloride content can be applied because these are safety measures to ensure quality.
The next chapter will deal with possible treatment steps for all four bio fly ashes, and the results of such measures in terms of chloride content, carbon content and finess. The optimized treatment for each of the fly ashes will be used to produce larger amounts for

mortar testing. The flexural and compressive strength of bio fly ash-containing mortars will be measured for various cement replacement levels.

Chapter 7

The treatment and application of bio-energy fly ashes

The treatment of bio-energy fly ashes is divided into five different steps [143]. These include the removal of coarse and fine carbon particles, chlorides, metallic aluminium and fulfilling the requirements like particle size distribution according to EN 450 [25]. The removal of heavy metals will not be tested after these steps. However, after the water treatment almost all leachable metals should be removed. The remaining metals can be enclosed into the cement matrix as described by van Eijk [151]. The final scope is to ensure that the fly ash can be classified as non-hazardous or even inert [5].

7.1 Treatment methods

The treatments steps used in this research depend on the bio-energy fly ash and moreover the compounds which it consist of. In general the following treatment methodology (Figure 7.1) will be used:
Firstly, carbon particles are removed, because of the negative effect on the chloride removal. Secondly, the fly ash is washed to reduce the soluble chlorides and aluminium content and in the end grinding can be performed to decrease the PSD and possibly increase the reactivity of the bio-energy fly ashes.

7.1.1 Sieving

This treatment is needed for bio-energy fly ashes with a high content of carbon. Using a sieve of 500 μm, coarse carbon particles will be removed. In this way the LOI will be reduced, as well as the chloride content of the fly ash. The relation between removing carbon and chlorides has already been discussed in Chapter 6.

7.1.2 Thermal treatment and air-filtering

This treatment is needed for bio-energy fly ashes with a high content of fine carbon particles (< 40 μm). These fly ashes can be recognized by their black appearance, even after Treatment 1. For this treatment, two options (2a and 2b) are available: treatment 2a is a thermal treatment and treatment 2b is a separation by electrostatic filters (both for industrial use). However, in the laboratory the thermal treatment is performed by using an oven and electrostatic filters are replaced by a shaking device with air suction. These measures should give similar end results as the above described industrial processes. The

choice of which method to use depends on whether there are phases present that can change when a thermal treatment is used.

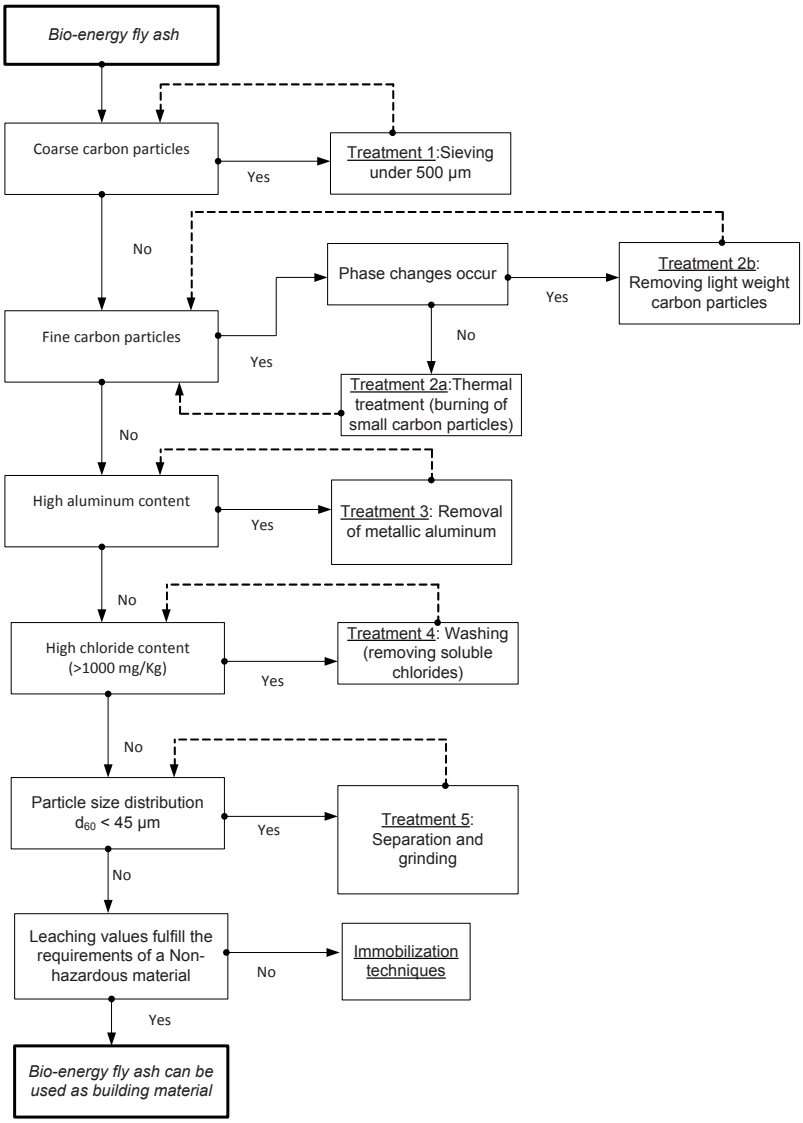

Figure 7.1. Treatment method for the bio fly-ashes [143].

A phase change can result in crystallization which negatively affects the pozzolanic reactivity of the fly ashes, and should therefore be avoided. Phase changes depend on the

content of the fly ash, but can for example consist of: formation of mullite or hematite, crystallization of melilite or oxidation of magnetite. In general the reduction of the glass phase and increase of crystalline phase occur at temperatures above 700°C, resulting in a decrease of the pozzolanic activity [153].
If there is a possibility of phase change, Treatment 2a is not an option and Treatment 2b can be applied. Treatment 2b uses a shaking mechanism with air exhaust. By shaking, the light coal particles are lifted and removed using the air exhaust.
When well calibrated, the removal of fine light particles that are not coal should be limited. In Section 7.3.1, the difference between these two methods and the removal of fine particles is further discussed.

7.1.3 Metallic aluminium removal

This treatment is only required when large amounts of metallic aluminium are present, which in contact with water in an alkaline environment will form hydrogen:

$$2Al + 2HO^- + 6H_2O \rightarrow 2Al(OH)_4^- + 3H_2 \uparrow \quad (7.1.1)$$

If this happens in the mortars, an increase in volume will take place, resulting in an increase of porosity and decrease of compressive and flexural strengths. To remove the unwanted aluminium for industrial purposes, an eddy current separator can be used. In this way a powerful varying magnetic field separates the non-ferrous metals from the rest of the material. However, this technique cannot be used for fine particles, so it is a treatment step that should be thoroughly applied on the unincinerated material. For laboratory use, the fly ash is stirred in water for 72 hours with a L/S of four.

7.1.4 Washing

Water treatment is used to remove water soluble compounds (mostly chlorides). For this, four steps are performed:

1. Fly ash in combination with demineralised water is shaken in bottles using a “Stuart reciprocating shaker SSL2” to remove soluble chlorides and metal ions;
2. The water is separated from the fly ash using 15-30 μm filters;
3. The fly ash retained on the filter is flushed with demineralised water to remove remaining water with soluble minerals;
4. The remaining fly ash is dried to remove the available water content.

The efficiency of the water treatment technique depends on several factors: temperature of water, pH of water, water/solid ratio, oscillation speed, treatment duration, amount of flushing water, filter size; their influence will be evaluated for obtaining the optimal treatment parameters.

A chemical method is used to determine the chloride content of the solid or liquid samples. Both these methods are based on the precipitation reaction of chlorides with silver ions (in this case, silver nitrate being the source):

$$Cl^- + AgNO_3 \rightarrow AgCl + NO_3^- \tag{7.1.2}$$

For measuring the chloride content of solid materials, two grams solid material (bio-energy fly ash), together with 37 ml of demineralised water and 3 ml of nitric acid is combined in a bottle. The mix is then stirred using a magnetic stirrer on a heating plate of 45°C for 15 minutes. Afterwards, the solution is filtered and flushed with demineralised water until a volume of filtrate of 100 ml is obtained. From this, 2-10 ml, depending on the chloride content, can be measured using Metrohm 785 DMP Titrino with a 0.01 mol/l solution of silver nitrate. The chloride content can be computed as:

$$C_t = \frac{B_{100} \cdot V \cdot 35.5 \cdot Z_{0.01}}{1000 \cdot G \cdot P_{10}} \tag{7.1.3}$$

where P_{10} is the amount in the pipette in ml (used for determination of the concentration of chloride), B_{100} is the total volume of the solution (in ml), V is the titrated silver nitrate solution in ml and $Z_{0.01}$ the concentration of silver nitrate in moles per litre (M) and G is the used solid (bio-energy fly ash) in grams filtered for the procedure.

7.1.5 Separation/Grinding

This last treatment method is used to reduce the size of the particles using a ball mill (only for laboratory use), at the same time increasing the reactivity of the particles. This results in an increase of pozzolanic activity at early curing ages, creating compacter concrete with a higher density and higher flexural and compressive strength.

7.2 Optimizing the washing treatment step

7.2.1 BF1 boiler fly ash

In order to investigate the quantity of chloride which is removed from solid boiler fly ash BF1 by distilled water, the chloride content of (BF1) is determined as explained above. This is done for two pairs of measurements. The first one is a pure BF1 without any changes. The second one is a ground BF1. Samples A1 to A4 present the pure BF1 and samples A5 to A8 – the ground BF1. Sample A9 is sieved, ground and represents everything below 500 μm (87% of mass), while sample A10 is sieved, ground and represents everything above 500 μm (13% by mass). The results are presented in Table 7.1, where samples 9 and 10 together are assumed to constitute 100% by mass.

It can be seen that samples A1-A4 contain less chlorides than samples A5-A8, probably because not all chloride ions from these samples were dissolved (some chloride ions contained in coal particles were not dissolved in water). This is in contrast to the samples A5-A8 which are ground, and therefore chloride particles were released and could be dissolved in water. Sample A10 is coarse carbon that was retained on the 500 µm sieve and represents 13% by mass. Even this low content by mass contains almost 50% of the chlorides. This explains why samples A5-A8 have more chlorides than sample A9, because a small part of carbon with chlorides was still present. Nevertheless, because of the small amount of two grams that is investigated, samples A5-A8 are not necessarily representative of the chloride content in BF1. However, it is believed that sample A9 together with sample A10 give a good representation, giving a total chloride content of 5225 mg/kg. Moreover, this value is close to the results from the XRF analysis (5600 mg/kg, Table 6.6). These results show that coal particles have a large influence on the chloride content of a fly ash, as chlorides attach and combine with coal particles as described in Chapter 6. These facts can explain the observed differences between the samples tested for repeatability.

Table 7.1. Chloride content of solid BF1 boiler fly ash in mg Cl/kg fly ash.

Sample	**A1**	**A2**	**A3**	**A4**	**A5**	**A6**	**A7**	**A8**	**A9**	**A10**
mg Cl/ kg BF1	2680	2545	3554	2751	3714	3634	3738	3772	3282	18236

In this first experiment with boiler fly ash (BF1), different treatment parameters and their influence on fly ash properties are investigated. In this case the fly ash is shaken for one hour with different water of different temperatures (20 and 60°C), two different shaking speeds (120 and 240 rpm) and two different liquid to solid ratios (L/S = 2, L/S = 4). The remaining chlorides are measured by taking three ml of the leachate and measuring the chloride content by titration. The results are given in Table 7.2 and present an improvement by increasing the shaking speed compared to the original, especially for a L/S ratio of two. The larger quantity of chlorides which are removable with an L/S = 2 can be explained by different theories. Firstly, because of gravity, particles are more attached to the bottom surface and the water pressure downwards reduces the movement of the particles, the so-called “damping effect”. Secondly, when waves are close to the bottom surface, a higher turbulent flow is realized, the “mixing effect”. When the flow is further away from the bottom surface the waves have almost no influence on the particles and reduce the efficiency of dissolving chlorides. The increase of temperature for L/S = 4 has a bit more advantage than for L/S = 2. It is believed that this is due to the more rapid decrease in temperature of L/S = 2 and therefore has a shorter effect, even though the

samples were thermally insulated before the treatment. A combination of increased temperature and L/S ratio works well for removing chloride ions, because the positive effects cumulate.

In order to monitor the behaviour of the bio-energy fly ash in time, the chloride content of BF1 is measured during one hour with a shaking speed of 120 rpm, extracting every 15 min 3 ml and adding 3 ml demineralised-water to keep the L/S ratio constant. For each step the calculation is corrected for the removed content of chlorides in each three ml. In order to observe differences between 2 samples, the bottles with a L/S ratio equal to 2 and 4 are measured twice to check reliability (group A and B). Results are presented in Figure 7.1.

Table 7.2. Removed chlorides from boiler fly ash BF1with different parameters (percentage removed is calculated from the original 5226 mg/kg).

	20°C, 120 rpm (mg/kg)	**20°C, 240 rpm (mg/kg)**	**60°C, 120 rpm (mg/kg)**	**60°C, 240 rpm (mg/kg)**
L/S = 2	1957	2575	2091	2867
%Cl removed	37.4%	49.3%	40.0%	54.9%
L/S = 4	2043	2320	2320	2702
%Cl removed	39.1%	44.4%	44.4%	51.7%

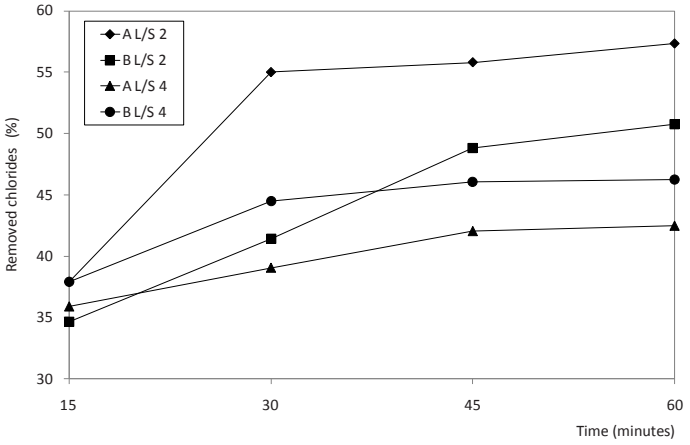

Figure 7.1. Chlorides removed from boiler fly ash (BF1) during 60 minutes with different L/S ratios; 2 samples (A and B) were measured to check reproducibility.

From Figure 7.1 it can be concluded that in time more chlorides are removed. However, the measurements are hardly repeatable. To evaluate the reliability of the previous results, a second test is performed. In this case, five bottles of boiler fly ash (BF1) are washed (BF1-W). The used fly ash is coming from the same batch of 15 kg. From this bucket five samples of 100 grams are taken while mixing. The 100 gram is then put into bottles (A-E) which are shaken for one hour at a speed of 120 rpm and with L/S = 4 to test the repeatability. Furthermore, the chloride content in the used distilled water is measured three times to see if there is a large variability. The results are presented in Table 7.3.
The results in Table 7.3 show that in every sample there is a deviation of results. Sample D has the largest variation of 1.1%; the lowest difference is sample A with a variation of 0.3%. Comparing the samples and taking the lowest value of sample D and the highest value of sample E results in the worst case scenario with a difference between the samples of 6.7%, which is still considered acceptable.

Table 7.3. Investigation of five washed BF1-W boiler fly ash samples (A-E), to determine the chloride removal repeatability (percentage removed is calculated from the original 5226 mg/kg).

L/S = 4	**Sample BF1-W (A) (mg/kg)**	**Sample BF1-W (B) (mg/kg)**	**Sample BF1-W (C) (mg/kg)**	**Sample BF1-W (D) (mg/kg)**	**Sample BF-/W (E) (mg/kg)**
Removed Cl^-	1980-1993	2153-2172	1997-2026	1852-1905	2149-2200
Reduction*	37.9-38.1%	41.2-41.6%	38.2-38.8%	35.4-36.5%	41.1-42.1%

7.2.2 BF2 cyclone fly ash

To investigate the quantity of removed chlorides from the cyclone fly ash BF2, first the initial chloride content of plain BF2 is determined. This is done for two pairs of measurements. The first one is plain BF2 without any changes. The second one is ground BF2. Samples B1-B3 present the plain BF2 and samples B4-B6 the ground BF2. Sample B7 represents the average of samples B4-B6 and is taken as 100% chloride content because of the small differences between samples B4-B6. The results are presented in Table 7.4.
From Table 7.4 it can be stated that the difference between the original sample and ground sample is very small. This is probably due to smaller content of carbon particles. The results are in contrast to BF1, where a large difference was observed. The initial chloride content will be from now on considered to be 4131 mg Cl/kg BF2 fly ash. In order to monitor the behaviour of the bio-energy fly ash in time upon washing with water,

the chloride content of four samples BF2 are measured and presented in Figure 7.2. The four samples are divided into two groups, A and B, both measured every 15 minutes for one hour, with a shaking speed of 120 rpm and two different liquid to solid ratios (L/S), namely 2 and 4.

Table 7.4: Chloride content of solid BF2 cyclone fly ash in mg Cl/kg fly ash; the B7 sample represents the average of the B4-B6 samples.

Sample	**B1**	**B2**	**B3**	**B4**	**B5**	**B6**	**B7**
Chloride content mg Cl/kg BF1	3887	4276	4020	4158	4090	4143	4131

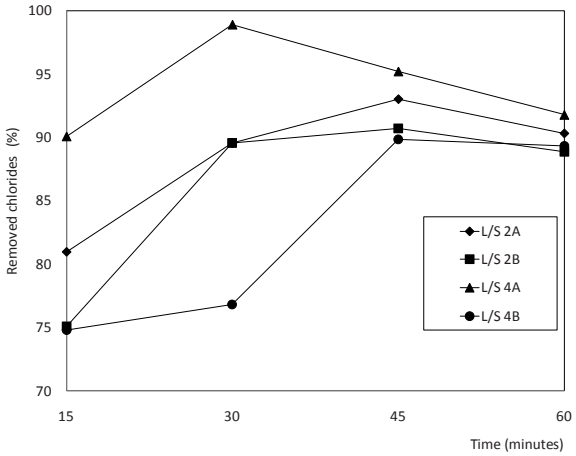

Figure 7.2. Chloride remove in the BF2 cyclone fly ash during 60 minutes with different L/S ratios; 2 samples (A and B) were measured to check reproducibility.

It was expected that with increasing time more and more chlorides would be removed. However, Figure 7.3 illustrates that there are still differences inside the sample pairs, although this is already considerably reduced compared to BF1. The reduced but still present inaccuracy can have different reasons. One of the first reasons would be that the chloride content in fly ash is not homogenously distributed, resulting in a difference in chloride removal. However, perhaps the 3 ml analysed from every sample are not representative for the total 400 ml used. This would explain why at 60 minutes all the results are in close agreement, because at this time the washing stopped and 50 ml of

water was extracted for measuring the chloride content, so this value is probably the most representative.
The next measurement is performed using a L/S ratio of 2 and taking 25 ml samples instead of the three ml used to confirm this statement. Also the shaking speed is increased to 240 rpm because this would reduce the time to solve the chlorides in water. The results (illustrated in Figure 7.3) look more promising. Not only the discrepancy between the samples decreased, but close to 30 minutes more than 95% of chlorides are removed. The fact that there is still a slight shift in the results during time could be explained by small measurement errors.

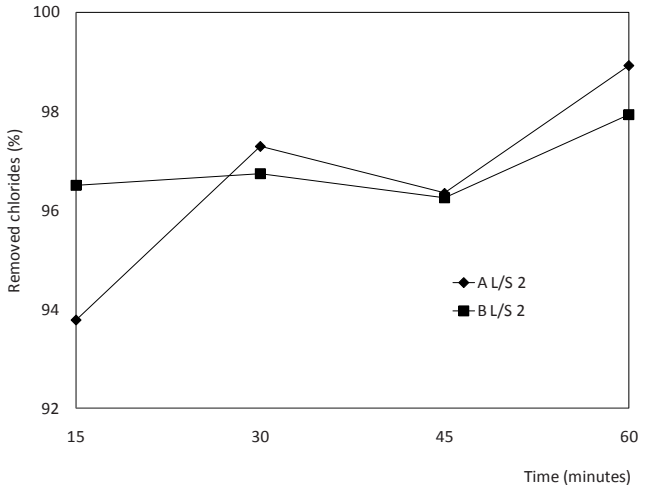

Figure 7.3. Chloride ions removed in the BF2 cyclone fly ash during 60 minutes with a L/S = 2 and a shaking speed of 240 rpm for samples A and B.

The difference between these results is however less than 5%. Therefore, further investigations for the other fly ashes are made using the knowledge that a large sample size of 25 ml of water is needed and that carbon particles have a large influence on the outcome of the washing technique because of possible chloride content.

7.3 Evaluation of the chloride removal efficiency of all treatment steps

7.3.1 BF1 boiler fly ash

To ensure that the maximum chloride content will not exceed 1000 mg/kg as mentioned in Chapter 6 (according to EN 450 [25]), the following treatment steps are carried out:

1. The bio-energy fly ash is sieved on a 500 µm sieve, to remove large coal particles (S);
2. The bio-energy fly ash is:
    a. air filtered removing fine coal particles (AF);
    b. thermally treated at 750°C, to incinerate fine coal particles (H).
3. Each of the samples described under step two are then washed using the water treatment (W).

The results are illustrated in Figure 7.4. The first step already reduced the available chloride content with 45%. This is due to absorbed chloride and chlorine in the carbon structure. Washing this fly ash will result in a total decrease of 51%. This is 6% lower than not washing, from which it can be concluded that washing has almost no effect as long as fine carbon particles are still present. The soluble chlorides are probably attached to the surface of the carbon particles and thus prevented their dissolution in water. Removing the fine carbon particles using Treatment 2a or 2b results in a reduction of 75% and 70%, respectively, compared to the original fly ash. Washing these fly ashes results in a total reduction of 93% and 82%. This indicates that first removing the coal particles increases the removal of chlorides. Secondly, air filtering removes chlorides that are less soluble and with this decreases the remaining chloride content.

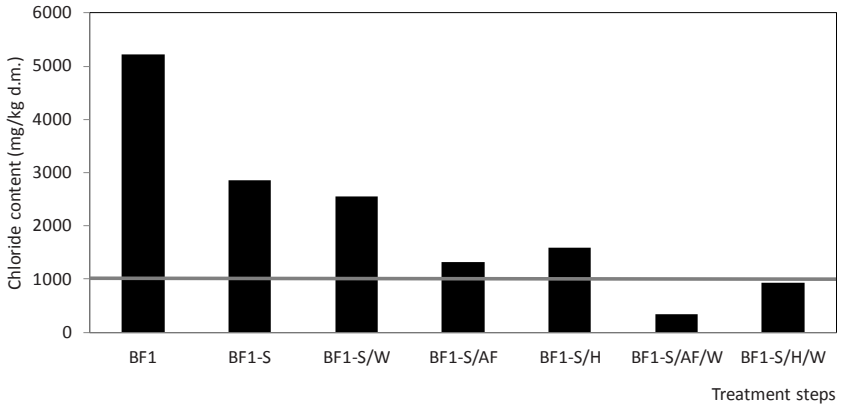

Figure 7.4. Chloride ions in BF1 boiler fly ash before and after different treatment steps (notations from Section 7.3.5 and Table 7.5).

7.3.2 BF2 cyclone fly ash

Since this fly ash only has large carbon particles the following steps are performed:

1. The bio-energy fly ash is sieved on a 500 µm sieve, to remove large coal particles;
2. The bio-energy fly ash is washed using the water treatment.

The results are illustrated in Figure 7.5. The chlorides in BF2 ash are readily soluble and after just the washing treatment the fly ash almost fulfils the maximum limit of 1000 mg/kg. When sieved on a 500 μm sieve, the chloride content is reduced by 12%. After sieving on a 500 μm sieve and water treatment only 9% of the chloride content remains, compared to 29% when washed without sieving. This means that by removing carbon the efficiency of the treatment increases by 8%, and as a result the chloride content fulfils the stated requirements.

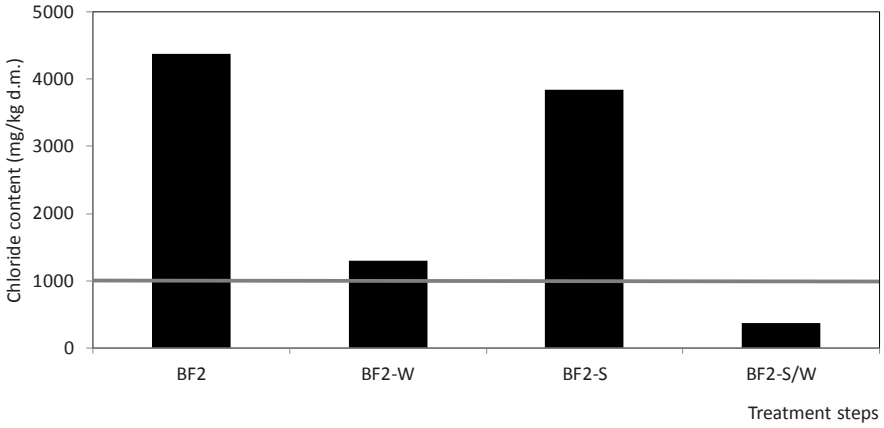

Figure 7.5. Chloride ions in the BF2 cyclone fly ash before and after different treatment steps.

7.3.3 BF3 cyclone fly ash

This fly ash has no carbon content issues and therefore the water treatment could immediately be applied to fulfil the chloride requirements (Figure 7.6a). However, before treatment almost all the metal aluminium is removed. This is done by shaking the fly ash in a bottle with water using a L/S = 4, for 72 hours. The alkalis leached out of the fly ash during this time ensure a high enough pH for the reaction described by (Eq. 7.1.1) to take place. After washing the chloride content is reduced by 96% and fulfils the stated requirements.

7.3.4 BF4 filter fly ash

This fly ash does not contain any carbon particles (like BF3) and therefore can immediately be water treated. It also contains metallic aluminium, but because the water treatment was not successful further research has not been performed. As it can be seen from Figure 7.6b, the chloride content of this fly ash is 86 times more than allowed. After

treatment this amount is reduced by 80% but still it is too high to be used as cement replacement in concrete structures.

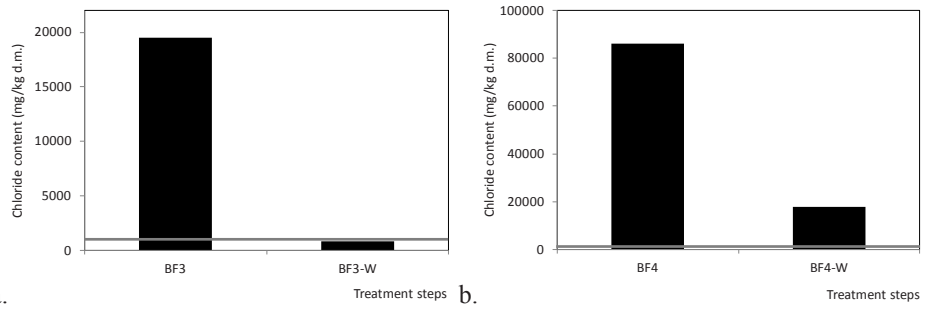

Figure 7.6. Chloride ions in the **a.** BF3 cyclone fly ash and **b.** BF4 filter fly ash before and after treatment.

7.3.5 Final treated samples

After investigating the chloride content decrease of all the treatment options on all four bio fly-ashes, the final treatment method for each of these was selected. In the case of BF1, two treatment routes were chosen, both through air-filtering (AF) and heating (H); therefore, two treated samples will be investigated further, and termed BF1-T1 and BF1-T2. The BF2 and BF3 fly ashes each undergo only one treatment route (see Sections 7.3.2 and 7.3.3) and therefore the final treated samples will from here onwards be termed BF2-T and BF3-T. The BF4 sample will not be investigated further, as explained in Section 7.3.4.

Table 7.5. Treatment steps undergone by the BF1, BF2 and BF3 samples before being used as cement replacement.

Treatment	BF1-T1	BF1-T2	BF2-T	BF3-T
Sieving < 500 μm (S)	X	X	X	
Air-filtering (AF)	X			
Heating (H)		X		
Washing (W)	X	X	X	X
Grinding (G)	X	X	X	

Table 7.5 summarizes the treatment steps undergone by the BF1, BF2 and BF3 samples before being considered useable as non-shaped materials in concrete. Incompletely-treated samples (ones that underwent only some, but not all, of the treatment steps) will

still be referred to using the abbreviation for the used treatments, as also mentioned in Table 7.5. For instance, a BF1 sample which has only been sieved will be termed BF1-S, while a BF1 sample which underwent sieving (S), heating (H) and washing (W), but not grinding (G), will be termed BF1-S/H/W.

7.4 Evaluation of the influence of treatment steps on the PSD of the bio fly ashes

The effect of removing fine coal particles by thermal treatment or air filtering on the particle size distribution (PSD) will be discussed in this section, as well as the effect of the water treatment. Furthermore, the bio-energy fly ash samples will be ground in order to fulfil the EN 450 [25] and NEN 5950 [150] requirements concerning finess.

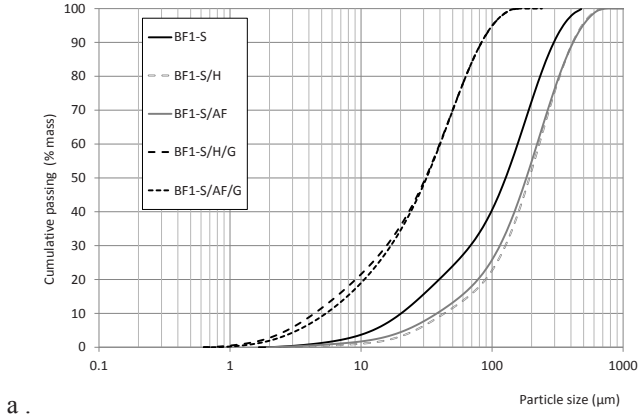

a .

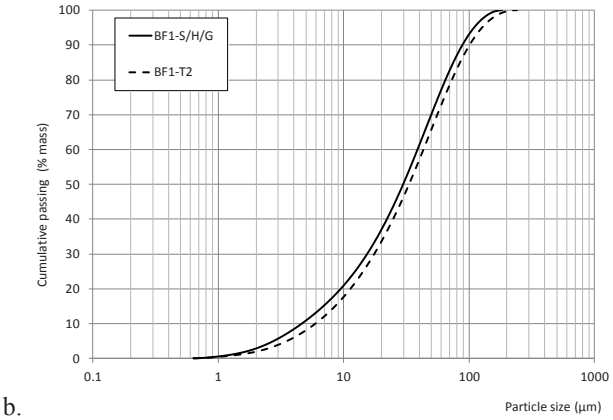

b.

Figure 7.7. PSD of **a.** BF1 and **b.** of BF1-H boiler thermally treated before and after different treatment steps (notations from Section 7.3.5 and Table 7.5).

7.4.1 BF1 boiler fly ash

In Figure 7.7a the effect of both thermal treatment (BF1-S/H) and air filtering (BF1-S/AF) on the PSD of the fly ashes are illustrated, together with the original PSD of the BF1 boiler fly ash which was sieved to under 500 µm, BF1-S. Also ground BF1 (BF1-S/AF/G and BF1-S/H/G) which fulfil the EN 450 [25] are presented and will be used for strength development in the following sections.

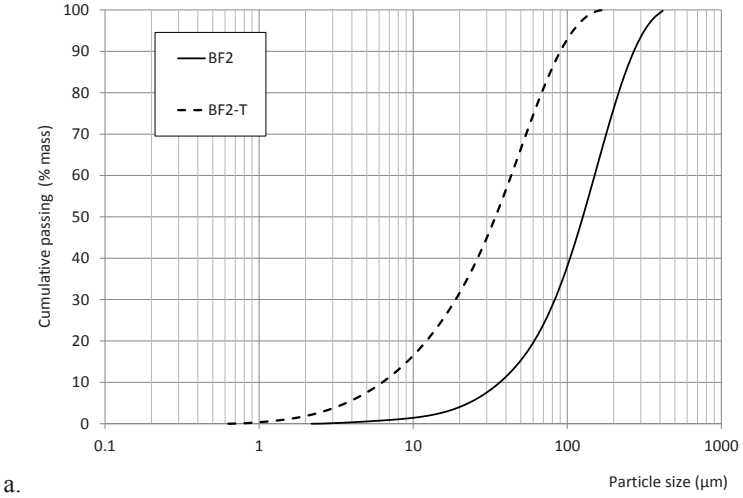

a.

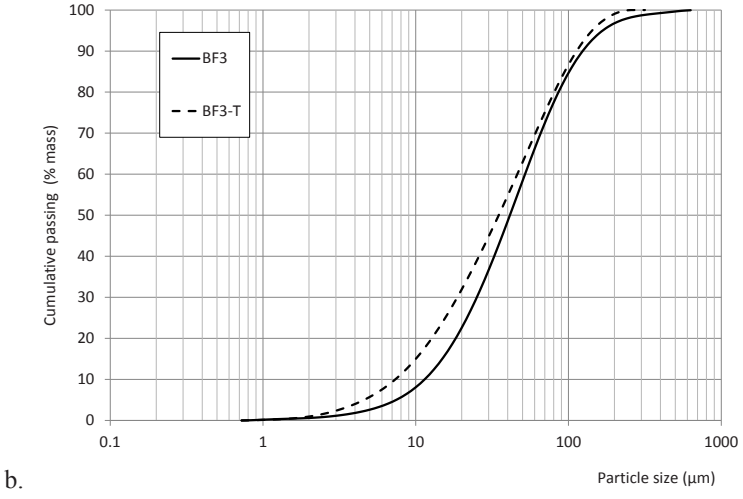

b.

Figure 7.8. PSD of **a.** BF2 cyclone fly ash before and after the sieving, washing and grinding treatments and **b.** BF3 fly ash before and after the washing treatment.

It can be seen that the thermal and the air filtering treatment yield almost the same PSD. Both PSDs are shifted to the right, indicating coarser particles due to the removal of the fine coal particles. Looking at the ground fly ash, 65% is smaller than 45 μm and 0.1% is larger than 212 μm, fulfilling the stated requirements concerning finess.
The effect of the water treatment on the PSD of this fly ash is illustrated in Figure 7.7b. To obtain these results, the fly ash is first heated and ground (BF1-S/H/G) and afterwards separated into two groups where one is water treated for comparison (BF1-S/H/G/W). The effect of the water treatment is negligible and only the soluble materials that are removed provide a small change in the PSD.

7.4.2 BF2 and BF3

Both BF2 and BF3 are water treated and ground. The results are presented in Figure 7.8. Also these two bio-energy fly ashes are fulfilling the stated requirements after successfully being water treated and ground.

7.4.3 Comparison between the PSD of the original and treated bio-energy fly ash

The data described in Table 7.6 indicates that even after grinding of the bio-energy fly ashes, the reference fly ash still has a smaller PSD and a larger SSA. However, there is a large improvement after treatment (all d_{10}, d_{50} and d_{90} decrease when compared to the vales in Table 6.4).

Table 7.6: PSD, SSA and LOI up to 950°C of the treated bio-energy fly ashes (notations from Table 7.5) which can be compared to the properties of commercial fly ash (from Table 6.4) and the initial properties (Tables 6.4 and 6.5).

	BF1-T2	**BF1-T1**	**BF2-T**	**BF3-T**
D_{min}(μm)	0.7	0.8	0.7	0.7
d_{10} (μm)	4	5	6	7
d_{50} (μm)	31	31	34	34
d_{60} (μm)	40	40	42	46
d_{80} (μm)	63	63	68	80
d_{90} (μm)	83	82	90	113
D_{max}(μm)	158	158	182	275
SSA (cm^2/g)	1980	1720	1590	1370
LOI	3.9	1.4	3.3	9.4

7.5 Scanning electron microscopy (SEM)

In order to investigate the possible pozzolanic properties (activated by the leaching of alkalis from the fly ash during treatment) of the BF3 and BF4 fly ashes and the effect of the water treatment, 1 hour water-treated, 24 hours and 72 hours water treated BF3 are investigated and compared with water treated BF4. The results are presented in Figure 7.9.

After water treatment of one hour, almost no cementitious properties are found in both BF3 and BF1. However, after 72 hours of water treatment there seem to be hydration products formed that completely cover the surface of the bio-energy fly ash particles. It seems that the three days of BF3 water treatment to remove metallic aluminium had an additional effect than expected, indicating that the BF3 fly ash has self-cementing properties. This result is not observed when the BF1 is washed.

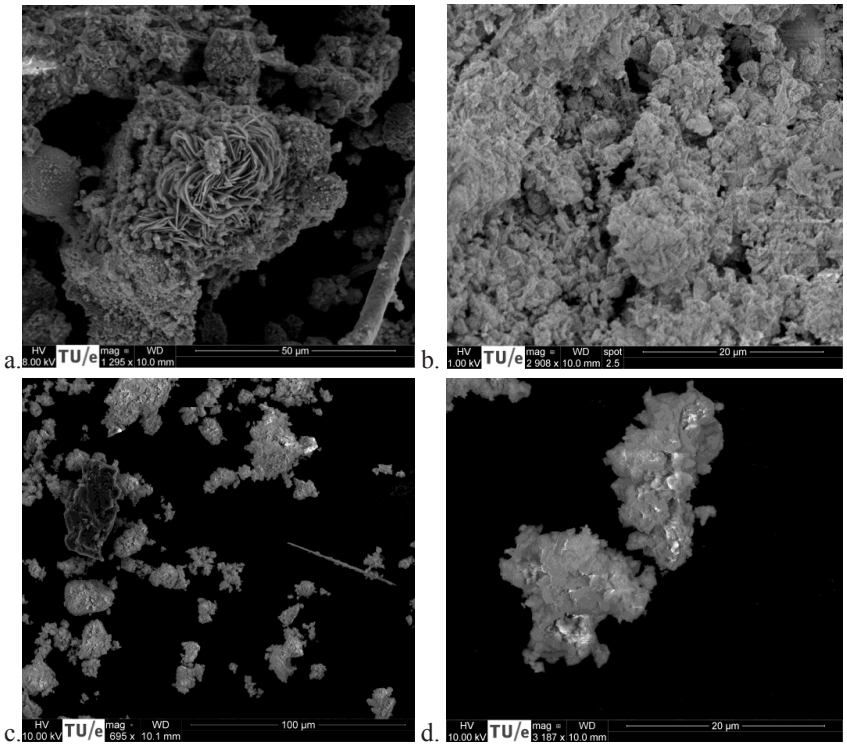

Figure 7.9. Samples BF3 (**a.** and **b.)** and BF4 (**c.** and **d.)** after the washing treatment at two levels of magnification.

7.6 X-ray diffraction pattern (XRD)

X-ray diffraction was used to try to identify the Cl-containing phases which can be removed through the washing process. For this purpose, the BF4 diffractograms of the original fly ash and the washed one (BF4-W) were subtracted, in order to highlight only certain changes. The results of BF4 are presented in Figure 7.10. The BF4 sample was chosen for containing the largest amounts of chlorides both before and after washing (as shown in Figure 7.6), therefore increasing the chance of observing the changes on a diffractogram more clearly.

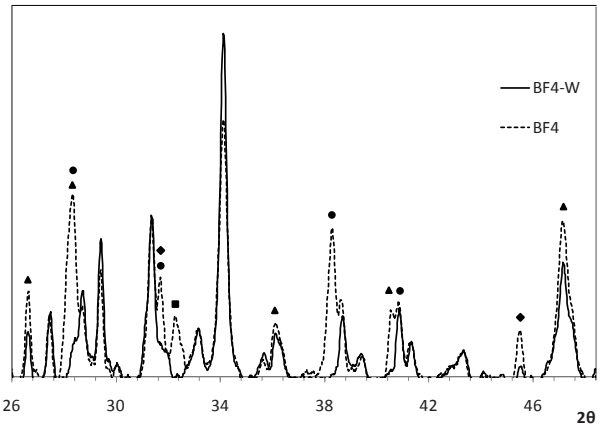

Figure 7.10. XRD pattern of original BF-4 and water treated BF4-W highlighting just the chloride peaks: $MgCl_2$ (■), KCl (▲), NaCl (◆) and $CaCl_2$ (●).

BF4 contains phases like anhydrite ($CaSO_4$), portlandite ($Ca(OH)_2$), quartz (SiO_2), chlorides ($CaCl_2$ and NaCl) and calcite ($CaCO_3$), which were detailed in Chapter 6. After the water treatment the structure is similar and there is a visible increase of $Ca(OH)_2$ and a decrease of all the four investigated chlorides (NaCl, KCl, $CaCl_2$ and $MgCl_2$).

7.7 Final leaching estimation of the treated bio fly ashes

The treated samples, BF1-T1, BF1-T2, BF2-T and BF3-T were tested for the leaching of contaminants, before attempting their use as cement replacement. However, because the official leaching test [28]) is time-consuming, an accelerated test was performed. The four treated samples were washed for 24 hours with water, with an L/S ratio of 10 and a shaking speed of 240 rpm. The leachate was then analysed and the results are presented in Table 7.7.

The results of this leaching test are expected to be much higher than the usual column leaching test, due to the shaking of the samples for 24 hours at high rotational speed.

Therefore, the values are not directly comparable to the ones presented in Tables 6.8 or 6.9. However, these values will be compared with the non-shaped building materials requirements [28] presented in Table 6.9, trusting that these values will be lower than the column test ones. It can be observed from Table 7.7 that only the antimony, chromium and sulphate levels are still over the legal limit (values in **bold**). In all cases, the leached chlorides are well under the legal limit.

Table 7.7. Results of the 24-hours leaching test on the finally treated bio fly ashes.

Element/Ion	**BF1-T1 (mg/kg d.m.)**	**BF1-T2 (mg/kg d.m.)**	**BF2-T (mg/kg d.m.)**	**BF3-T (mg/kg d.m.)**
Antimony (Sb)	**0.94**	0.044	**1**	**0.46**
Arsenic (As)	0.1	0.1	0.45	0.1
Barium (Ba)	2.7	1.2	2.7	2.3
Cadmium (Cd)	0.01	0.01	0.01	0.01
Chromium (Cr)	**3.3**	**3.5**	**1.9**	**7.5**
Cobalt (Co)	0.1	0.1	0.1	0.1
Copper (Cu)	0.1	0.1	0.1	0.1
Mercury (Hg)	0.005	0.005	0.005	0.005
Lead (Pb)	0.1	0.1	0.1	0.1
Molybdenum (Mo)	0.2	0.7	0.22	0.36
Nickel (Ni)	0.1	0.1	0.1	0.1
Selenium (Se)	0.039	0.04	0.039	0.08
Tin (Sn)	0.1	0.1	0.1	0.1
Vanadium (V)	0.36	0.12	0.29	0.18
Zinc (Zn)	0.2	0.2	0.2	0.2
Bromide (Br^-)	2	2	2	2.1
Chloride (Cl^-)	38	84	56	180
Fluoride (F^-)	3.2	2	12	4.6
Sulphate (SO_4^{2-})	**4200**	**5900**	**5700**	**14000**

In the case of both antimony and chromium, the leaching values were under or very close to the legal limits even before the treatment steps (see Table 6.9), so it is assumed that this will continue to be the case with the final treated samples. In the case of sulphates, the BF2 and BF3 samples were originally under or just over the legal limit, so the very much increased leaching values presented in Table 7.7 are not trustworthy- especially in the case of BF3, which originally did not leached almost any sulphates at all.
Moreover, the values in Table 7.7 for sulphates for BF3-T exceed even the compositional ones determined by XRF (Table 6.6). However, in the case of BF1-T1 and BF1-T2 the values for sulphates are under the compositional determination, but still much higher than the data in Table 6.9. Therefore, the sulphate leaching test will be repeated and also the complete column leaching test should be performed on all samples. However, the very much decreased chloride leaching levels achieved using the above-described method prove promising that all the rest of the maximum contaminant leaching values will also be met.

7.8 Conclusions regarding the treatment steps

7.8.1 Carbon removal

Because of the high LOI of the BF1 and BF2 bio-energy fly ashes (Table 6.5), mainly due to the high carbon content and the negative influence of carbon on the chloride removal of bio-energy fly ash, the carbon content needed to be reduced [143]. After the thermal or air filtering treatment the carbon content is significantly reduced and fulfils the LOI requirements. The reduction of the carbon content (Table 7.6) caused the removal of chlorides present in the carbon structure. Furthermore, it increased the efficiency of the water treatment to remove chlorides. When carbon was still present, the soluble chlorides where attached to the surface of the carbon particles and prevented from dissolving in water. Due to the reduction of carbon, the chlorides could now dissolve in water.

7.8.2 Water treatment

The impact of shaking speed and time and temperature on the efficiency of the washing treatment has been evaluated [143]. Until 30-60 minutes the removal of chloride ions was stable. For this research this was sufficient because when applied in an industrial environment, hours of water-treatments are increasing the costs and decreasing the possible utilization. However, longer duration could remove chlorides with low solubility which would make the method more beneficial. During the treatment also other soluble elements are dissolved in the water, but this quantity has not been fully investigated, and perhaps increasing the time will have a positive effect on removing these elements too. The same principle applies to the shaking speed or the increase of temperature. However, it also needs to be considered that the water treatment is not always beneficial, even if it is needed to reduce the chloride content.

Among the used bio-energy fly ashes, there are bio-energy fly ashes with cementitious properties, mainly due to the available free lime and anhydrite. Available free lime will, in contact with water, form portlandite that will ensure a high pH, activating the fly ash. Reducing the amount of free lime by washing will decrease the activation of fly ash and will result in a strength decrease. The available anhydrite will increase long term strength, but after a long water treatment the anhydrite is also consumed.
All in all, this research shows that the method of water treating bio-energy fly ash to remove soluble elements is effective, but still there is a need for further optimization to increase the removal of soluble elements and to ensure the reliability and efficiency of the method.
So far, the water treatment used for non-cementitious fly ashes indicates a positive effect on the strength development by decreasing the concentration of contaminants that otherwise would have disturbed the cement matrix.

7.8.3 Grinding

When grinding the materials, they fulfil not only the requirements described in EN 450 [25] regarding particle size distribution (PSD), but also the requirements that the maximum percentage larger than 212 μm should not exceed 3% mass (NEN 5950 [150]), and the expected pozzolanic activity and workability. As described earlier, decreasing the PSD and increasing the specific surface area increases the reactivity of fly ashes and has a positive effect on the strength development during the first 28 days. However, in this research there was no investigation why the initial bio-energy fly ashes from the two factories (Twence Hengelo and HVC Alkmaar) have different particle size distributions. Firstly, HVC Alkmaar crushes its waste wood before incineration and the supplied fly ashes have a cumulative particle size distribution of 85% below 100 μm. If this would be the reason of a decrease in particle size distribution it could be preferable to first decrease the size of the waste that is incinerated in a more efficient way and thereby decreasing the size of the bio-energy fly ashes; also hard coal is pulverised prior to incineration, hence the term “pulverised coal fly ash”.
Secondly, the two factories have a different incineration process, and because of the high carbon content of Twence Hengelo it can be concluded that the burning process of this factory is less complete, and probably also the reason of coarser particles.

7.9 Strength development

The bio-energy fly ashes are used as 5%, 10% and 20% cement replacement. Mortars are produced using the standard method described in EN 196-1 [29] and are cured under water for 28 days. The 7 day strength is not measured because of the slow reactivity of fly ash in general.

Figures 7.11-13 illustrate the 5%, 10% and 20% replacement of cement by the different bio-energy fly ashes. The results are separated in original bio-energy fly ash, treated bio-energy fly ash (fulfilling the carbon and chloride requirements) and the afterwards ground bio-energy fly ash that also fulfils the requirements for particle size distribution. In all cases, the figures display the 28 days flexural and compressive strength achieved by the samples.

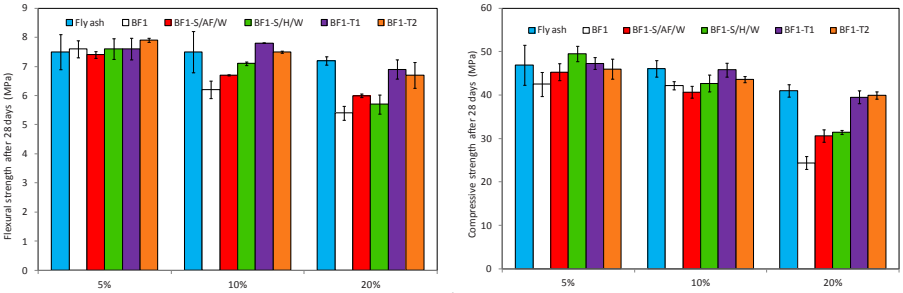

a. b

Figure 7.11. The 28 days flexural (**a.**) and compressive (**b.**) strength of the original and four treated BF1 samples.

When considering the 28 days results, for both flexural (Figure 7.11a) and compressive (Figure 7.11b) strength, the two fully treated fly ashes, BF1-T1 and BF1-T2 show similar behaviour. Moreover, their results are also at the same level with the cement replacement by coal combustion fly ash, even at 20% replacement. At a 5% replacement of cement by mass, all the investigated samples perform very well, equalling or surpassing the reference sample. Especially at 10% replacement, the unground samples start showing a poorer performance than the ground ones. At 20% replacement, this behaviour becomes obvious.

The two samples which were cleaned but not ground, BF1-S/AF/W and BF1-S/H/W, show a clear improvement from the original BF1, but much lower performance than the final treated samples BF1 and BF2. The same behaviour is observed for both flexural and compressive strength, but is more clearly visible for the latter. While the other treated samples, BF1-S/AF/W, BF1-S/H/W and BF1-T2 show very similar results (which are also comparable to the original BF1 strength, tested only in the case of 10% replacement), BF1-T1 shows an achieved compressive strength higher with 20% for both 10% and 20% cement replacement, which indicated that this sample displays cementitious properties. The same trends as for the BF1 samples can be observed in the case of the BF2-containing mortars.

In the case of the 28 days compressive strength, for 5% and 10% cement replacement, there is no visible loss of mechanical properties for either the original or treated BF2 samples. However, when considering the 20% cement replacement samples, the

detrimental effect of the untreated BF2 can clearly be seen, while at the same time the beneficial effect of the grinding step becomes obvious.

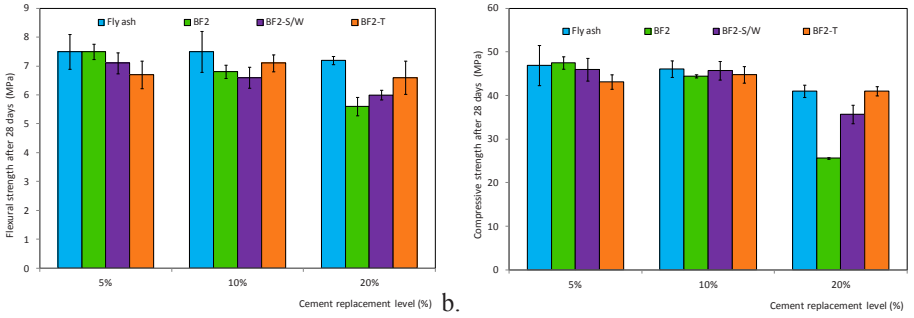

Figure 7.12. The 28 days flexural (**a.**) and compressive (**b.**) strength of the original and two treated BF2 samples.

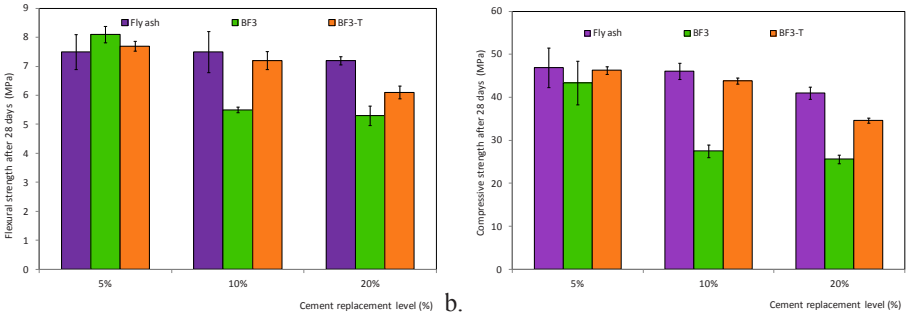

Figure 7.13. The 28 days flexural (**a.**) and compressive (**b.**) strength of the original and treated BF3 samples.

In the case of the BF3 samples, the difference between the original and treated fly ash is even more obvious. The loss of compressive strength at 10% and 20% replacement of cement by mass in standard mortars is remarkable; on the contrary, the treated BF3-T sample performs much better, with almost no loss of compressive strength for 5% and 10% cement replacement.

7.10 Discussions and conclusions

The aim of this research was to combine four different bio-energy fly ashes from bio-energy power plants in mortar mixtures. The roles of this type of fly ash in a concrete mixture as a binder (partly replacing cement) or filler were investigated. First, physical and chemical properties of the different fly ashes were determined followed by the determination of unwanted contaminants and needed treatment methods. Second, tests were performed to indicate any improvement and if the use of bio-energy fly ash is promising. To draw conclusions, the obtained data is compared with reference pulverised coal combustion fly ash.

The bio-energy fly ashes delivered by HVC-Alkmaar have self cementitious and pozzolanic properties and the one from Twence-Hengelo has pozzolanic properties. Physical and chemical properties like particle size distribution and oxide composition of the fly ashes vary enormous among each other and are also not really comparable with the reference fly ash. The same applies for the amount of unwanted contaminants like chlorides and carbon. This all can however be related to the used fuel for the incineration plants and the used burning processes.

By using different treatment techniques like grinding, thermally and water treating bio-energy fly ash, it is tried to upgrade bio-energy fly ash to a material comparable with the reference fly ash.

From the results in can be concluded that the thermal treatment and water treatment method reduce unwanted contaminants and not only render the material not hazardous, but they also increase the potential of the material as cement replacement. After treatment and grinding the bio-energy fly ash performs similarly as coal combustion fly ash.

It was expected that the strength results of ground bio-energy fly ash would indicate higher strength results than plain bio-energy fly ash. However, from the obtained strength results the decrease in particle size distribution only has a significant effect when a high percentage of bio-energy fly ash is used. Upon 5% and 10% replacement the effect is barely visible and may indicate that bio-energy fly ash is not as sensitive to a decrease of particle sizes as the normal reference fly ash. Moreover, the grinding in order to reduce the particle sizes is an expensive method.

Replacing cement with fly ash will in most cases result in a lower strength during the first 28 days. The more cement is replaced the less strength is developed. Comparing the replacement of cement with original not treated fly ash and washed fly ash indicates an increase of strength for most of the bio-energy fly ashes. Only BF2 has lower strength results at 5% replacement, and cementitious bio energy fly ashes such as BF4 show a negative effect on the strength development after washing.

In general BF3 is less promising at high replacement levels compared to the BF1 and BF2 fly ashes. There are several reasons that can lead to lower strength results. In the original BF3 there was a high amount of metallic aluminium and chlorides present. It is believed that the chlorides have no effect on the 28 days strength development and only

affect the durability of the concrete when used with reinforcement. However, the available metallic aluminium, which in contact with an alkaline solution generates hydrogen, will increase the volume of the sample, resulting in an increase of porosity and decrease of compressive and flexural strengths. From preliminary trials it was concluded that the removal of metallic aluminium by using water will take longer than 24 hours. From experiments it took 72 hours to remove the available metallic aluminium. The removed quantity was only visually observed, showing the formation of hydrogen up to the 72 hours. After this period of time no formation of hydrogen was observed. This is later confirmed when no deformation of the prisms was detected when measuring strength results. The effect of 72 hours of water treatment is further investigated using SEM and XRD.

SEM images of the 72 hours treated BF3 illustrate the formation of hydration products on the surface of the particles. Because of these hydration products, the washing treatment of BF3 affects the strength results and is the reason that BF3 for 20% replacement has a lower strength compared to the BF1 and BF2 fly ashes. If metallic aluminium could be removed by an eddy current separator and one hour of water treatment does not affect the fly ash (as is believed due to previous results), BF3 can still have a potential as filler or as a partly replacement of cement, with the same properties as the BF1 and BF2 fly ashes.

Comparing thermally treated BF1 with air filtered BF1, comparable results are found for 20% replacement. Also the strength results of the ground samples with different replacement percentages of 5% and 10% are similar.

It is believed that the obtained strength results can be improved because of two effects during the mixing of the samples. First, the water demand is kept the same for different replacement factors because it was uncertain whether the bio-energy fly ash behaves the same as the reference fly ash. From the strength results and the delayed strength increase in time, it seems that bio-energy fly ash indeed possesses pozzolanic properties and that the water demand therefore could be decreased. Second, the used jolting method described in EN 196-1 [29] is believed to be insufficient. After grinding, a high porosity was found by insufficient removal of air bubbles. It is therefore preferred to use a vibration table.

Finally, normally the spherical shape of the fly ash particles produces a rolling effect at the point of aggregate contact, reducing friction and improving the fluidity of the cement paste. It was found that for treated bio-energy fly ash the spread of the ground and not ground bio-energy fly ash was good at all replacement factors, despite the coarse particles. This is an improvement because the spread of the original bio-energy fly ash was poor (probably due to trace elements and contaminants on the surface of the particles). This would indicate the need for plasticizers. Because of the good flow ability of the treated bio-energy fly ashes, the use of plasticizers was not necessary.

Chapter 8

Paper sludge fly ash applied in cementitious mixes

8.1 Introduction

Paper sludge is a residue from the paper recycling process. In the past it consisted of unusable ingredients that needed landfilling or be sent to incineration plants. Nowadays, using an adjusted burning process with low emissions, fly ashes with good pozzolanic properties and without any hazardous contaminants are generated. Application options are already in place, such as a 10% replacement of cement or substitute in soil stabilization, although on a larger scale there is still no application available. There is therefore the need to increase the knowledge about the utilization of paper-sludge fly ashes because of increasing landfill costs. So far the reuse of these materials in the concrete industry is limited because of the increased water demand and content of free lime, which can reduce the properties of concrete.
The aim of this research is to find new utilization applications for paper sludge fly ash from paper-residue burning factories. The role of these materials in a concrete mixture as a binder (partly replacing cement) or filler will be investigated. The scope is to develop a more sustainable and cost-efficient concrete that gives by-products a second life and with that, reduces the CO_2 emissions of the cement production industry. In order to do so, paper-sludge fly ash needs to be chemically optimized to increase its utilization in the concrete industry. The findings in this chapter include results already described in [143].

8.2 The production of paper sludge fly ash

Paper sludge fly ash is currently used as replacement for cement/lime and as substitute in soil stabilization. The challenges however with paper sludge fly ash are the moderate rheological properties of its water-based mixture and its low density. To gain more insight about paper sludge fly ash, background information about the origin of the material and production is very important. In this section the background information of paper sludge ashes is provided.
The paper recycling industry produces wastes, out of which 10% paper sludge that cannot be reused anymore for the production of new paper because of its too short fibres (paper cannot bind anymore) or the high content of inorganic materials and ink. However, given the land scarcity in the densely populated Netherlands, and the risk of long term soil and groundwater contamination, the Dutch Government introduced new legislation and landfill taxes in order to promote finding an alternative to landfill. While conventional

industrial incineration offered a possible solution, concern about dioxin emissions, together with protests from local communities made this option unacceptable [20].
Paper sludge is the residue of the paper recycling process. It mainly consists of 50% water, 25% short fibres providing strength to paper and 25% other minerals like calcium oxide (which gives paper a white colour) and clay to make paper smooth. Before being transported to the combustion plant, large amounts of water are removed in order to lower the transport costs.
In the early nineties, four large Dutch paper producers entered a partnership to solve the paper residue problem. Using a newly developed incineration process, it was found that minerals can be recovered and paper recycling waste streams can be used to manufacture paper sludge fly ash. This requires a combustion process under strict conditions to activate the kaolin clay [20].
The installation of the combustion of paper sludge is comparable with the fluidized bed installation (described in Section 6.2.2 of this thesis). The small changes in the installation will be shortly described per stage. The complete process is illustrated in Figure 8.1.

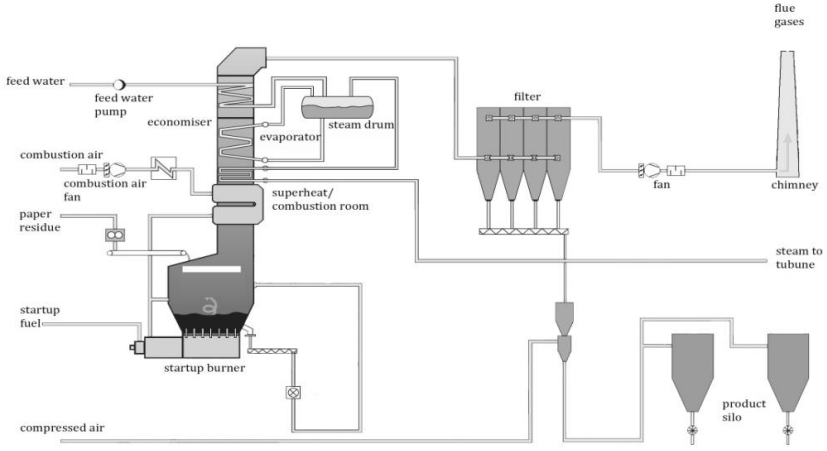

Figure 8.1. Schematic overview of the paper sludge production process [154].

Paper sludge coming from paper recycling factories is firstly stored in a big bunker. The storage capacity of this bunker is 500 t. This is necessary because the pulp supply rate varies, since it depends on 20 different sources. In the bunker the different paper sludges are mixed to get a more homogeneous mixture. From that point, paper sludge is transported with cranes to different inlets of pelletizers. Around 3800 t of paper sludge is incinerated every week in a 24 hours, 7 days per week process; ~ 24% is transformed into paper sludge fly ash, depending on the pulp supply. The maximum incineration capacity is 25 t of paper sludge per hour.

The pelletizers make pellets from the paper sludge; this method increases the efficiency in the combustion chamber by providing a higher contact surface, which leads to low emissions and better final product.
The combustion chamber consists of two sections; the lower part is the fluidized bed and the upper part is the freeboard which is insulated to decrease the emission. From the pelletizers the pellets are dropped from a certain height into the fluidized bed. Instead of burning at a high temperature, the temperature of the bed is kept around 780°C. In this way, the pellets are not completely burned and useful materials like metakaolin and calcium carbonate will be kept. Partly the pulp is incinerated at the top of the freeboard; the remaining part is incinerated inside the bed. There, calcium oxide (CaO) present in the paper sludge sticks on the sand particles, creating balls of burned paper sludge which will grow with more sticking CaO particles (the "snowball effect"). For that reason, compared to other fluidized beds, the bed in the paper sludge factory increases in size. There are two options to control the growth of the bed; one is by reducing the pellet amount entering the combustion chamber; the second, by removing fluidized balls between one and three mm and crushing them into a maximum size of two mm to keep the bed into shape.
After the combustion chamber the remaining product is guided to the bag house filter by a primary air flow to remove the coarse and fine particles from the gas flow. The system is completely cooled by water, which is turned into steam and is used in a steam turbine to generate electricity. Weekly around 500 MWh of electricity can be generated. However, this value depends on the pulp supply. Because the burning residue is sticking on the wall surface of the combustion chamber, big air horns which produce vibrations and remove the burned paper residue from the walls are used. In the end of the process all materials are stored in two silos with a capacity of 300 t each.
The complete process from bunker to silos is monitored and registered in the control room. At full capacity, the plant can produce 50000 t of paper-sludge fly ash per year, which, by comparison, constitutes only 1% of the total Dutch cement production per year [154].

8.3 Paper sludge fly ash properties

Paper sludge fly ash possesses pozzolanic activity due to the fact that it contains metakaolin. Metakaolin is obtained from kaolin clay. This fine white clay mineral is an aluminium disilicate $Al_2O_3 \cdot 2SiO_2$ (AS_2). Its hydration products in the presence of portlandite depend on the AS_2/CH ratio and reaction temperature [155–157].
When kaolin is heated at a temperature between 500 and 800°C, the dehydroxylization of kaolin takes place, forming metakaolin:

$$Al_2Si_2O_5(OH)_4 \rightarrow AS_2 + 4H \qquad (8.3.1)$$

When higher temperatures are used, mullite is formed:

$$2AS_2 \rightarrow A_2S_3 + S \tag{8.3.2}$$

Mullite is an unwanted crystalline material because it is not reactive. Metakaolin is a silica-based product that, upon reaction with portlandite ($Ca(OH)_2$) and water produces $C-S-H$ gel at ambient temperature. Metakaolin also contains alumina that reacts with CH to produce additional alumina-containing phases, including C_4AH_{13}, C_2ASH_8, and C_3AH_6 [158,159].
In this study, two fly ashes will be used as follows:
1. Paper sludge fly ash, termed PsFA;
2. Commercial coal combustion fly ash known as: PKVA SMZ (Class F according to ASTM C618 [26]) and has been described in terms of its oxide composition and particle size distribution in Tables 5.2 and 5.3, respectively.

8.3.1 Oxide composition

Table 8.1 presents the most important oxides in paper sludge fly ash (PsFA), coal combustion fly ash and CEM I 42.5N. The data is used for oxide engineering. In this method the oxides of different fly ashes are compared with a reference. In this way, an expectation can be made of how the material will react; the smaller the difference, the better the performance that can be expected. The calcium and silica oxide amount is similar to that of cement (Table 8.1). The oxide compositions of the CEM I 42.5N and coal combustion fly ash can be found in Table 6.5.

Table 8.1. Oxide composition of PsFA paper sludge fly ash, obtained by XRF.

Oxide	MgO	Al_2O_3	SiO_2	SO_3	CaO	Fe_2O_3
(%)	2.0	15.0	22.0	1.0	57.0	0.7

It can be seen that the composition of PsFA is closer to the one of cement than to the one of the reference fly ash. The main difference is the high alumina content; otherwise, both CaO and SiO_2 contents are very close to the ones of CEM I 42.5N. This is encouraging for the pozzolanic properties of the PsFA; however, the mineral phases which actually make up the paper sludge fly ash will define its binding properties.

8.3.2 Fineness

Generally speaking, in a concrete mix, a larger amount of particles smaller than 45 μm can result in a better flowability and more pozzolanic activity. The higher pozzolanic activity is due to reaction kinetics: finer particles react faster. Also the workability of the

concrete mix will be higher because smaller particles result in a higher flowability [23]. For other fly ash types, a large percentage of particles larger than the 45 μm has been reported to have a negative effect on the 28 days strengths of normally cured Portland cement fly ash mortars [160,161].

Fineness is one of the primary physical characteristics of fly ash that relates to its pozzolanic activity [144]. When examining coal combustion fly ash for its particle size distribution the EN 450 [25] sets the limit of 40% for the maximum amount of fly ash retained on the 45 μm mesh sieve on wet sieving, as a quality control measure. Figure 8.2a illustrates the particle size distribution (PSD) of the three considered materials measured with a Mastersizer 2000 using the laser diffraction method, while Figure 8.2b presents the cumulative particle size distribution (PSD) of the same powders.

Compared to coal combustion fly ash, paper sludge fly ash (PsFA) has more small particles below 10 μm and more than 50% of the particles are smaller than that of coal combustion fly ash. Probably the reason is that metakaolin is 99.9% finer than 16 μm with a mean particle size of 3 μm, which is mainly responsible for the pozzolanic activity of the fly ash.

Table 8.2. Physical properties of paper sludge fly ash, compared to the reference coal combustion fly ash and a CEM I 42.5N.

	Paper sludge fly ash (PsFA)	**Reference Fly ash**	**CEM I 42.5N**
D_{min} (μm)	0.19	0.6	0.36
d_{10} (μm)	1.8	5.0	4.37
d_{50} (μm)	20	25	23
d_{60} (μm)	32	30	30
d_{80} (μm)	70	106	51
d_{90} (μm)	93	120	72
D_{max} (μm)	590	832	240
Specific surface area (cm^2/g)	12000	2090	2940

So far, both coal combustion fly ash and paper sludge fly ash (PsFA) fulfil the requirements of EN 450 [11] for maximum retained fly ash on the 45 μm sieve. The fineness of fly ash is also defined by a specific surface area per unit of mass. If the surface area is very large a considerable amount of small particles forming a large active area are available. However, the effect of the increase in specific surface area beyond 6000 cm^2/g is reported to be insignificant [145].

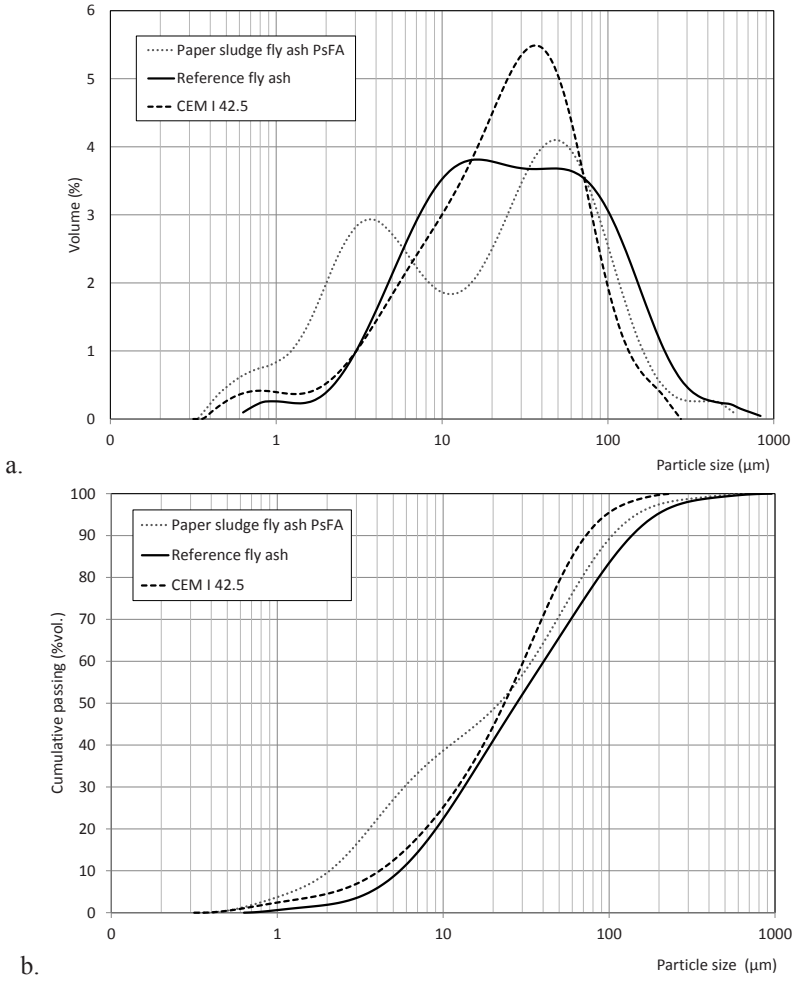

Figure 8.2. a. Particle size distribution and **b.** Cumulative finer volume of the paper sludge fly ash (PsFA) compared to the reference pulverised coal combustion fly ash and CEM I 42.5N (Table 8.1).

Table 8.2 presents the specific surface area of the fly ashes estimated with the Mastersizer 2000 (by assuming all particles to be spherical). This method, however, does not account for the surface area changes associated with the shape of the particles. According to this method, the specific surface area of paper sludge fly ash is much higher in comparison with coal combustion fly ash. However, as the specific surface area is higher than 6000 cm^2/g, it will probably increase the water demand.

8.3.3 Effect of paper sludge fly ash on cement hydration

Generally, paper-sludge fly ash contains 23% CaO (calcium oxide as free lime, quicklime), 41% $CaCO_3$ (calcium carbonate) and 29% Al_2O_3•$2SiO_2$ metakaolin as the main constituents [154]. However, these can slightly vary because of the varying input from different factories. In concrete, these compounds have the following function: metakaolin is a reactive addition with pozzolanic properties. $CaCO_3$ can be involved in the hydration of the aluminate phases, leading to the formation of mono- and hemicarboaluminate hydrates [162–164]. CaO will react with water and therefore has a negative effect on the concrete because less water is available for cement hydration. At the same time it also has a positive effect, creating portlandite, needed for the pozzolanic reaction of fly ash. Although $Ca(OH)_2$ is produced by the combination of calcium oxide and water, in normal cement mixtures the negative effect of reducing available water for the cement hydration makes its application as cement replacement only suitable up to an amount of 10% with a small increase of the water cement ratio [154].

8.4 Treatment of paper sludge fly ash

Two treatment routes are investigated in order to chemically upgrade paper sludge fly ash. The first one is to treat paper sludge fly ash with water to reduce the amount of free lime and at the same time increase the amount of portlandite that could be used to activate the pozzolanic reaction of metakaolin, or at least reduce the water demand of paper sludge fly ash [143]. The second one is to thermally treat paper sludge fly ash to remove calcite by releasing carbon dioxide and therefore increase the concentration of free lime that later will be treated with water to increase the amount of portlandite.

8.4.1 Water addition

To calculate the amount of water that is needed to form portlandite, a study is performed to investigate the water demand by using XRF data, to see how much quicklime could be turned into portlandite. Table 8.1 presents the XRF-data that illustrates that 46% of the total composition is in the form of CaO. The molar mass of CaO, M_C, is 56 g/mol and the molar mass of water, M_W, is 18 g/mol. To transfer all the CaO into portlandite the following amount of water is needed :

$$\frac{m_H}{m_C} = \frac{M_H}{M_C} \cdot x_C \tag{8.4.3}$$

where x_c is the percentage CaO in the fly ash, resulting in:

$$\frac{m_H}{m_C} = 0.18 \tag{8.4.4}$$

This water demand would be needed if all quicklime would be free lime and would react with water. However, XRF identifies elements not compounds, and the result of the analysis is exposed in % of oxides. In the case of paper sludge fly ash, all Ca is considered by XRF to be CaO, but actually it will be a mixture of CaO, $CaCO_3$, $Ca(OH)_2$ and other minor Ca-containing phases.
In order to sufficiently distribute the water that is needed to treat paper sludge fly ash, a special sprayer is used to distribute fine water droplets. The quantity of water added to the paper sludge fly ash is measured using a balance. The final water-treated sample will be termed PsFA-W throughout this chapter.

8.4.2 Thermal treatment

Thermogravimetric analysis (TGA) is performed on the original and treated samples in order to make a prediction of available percentages of quicklime, portlandite and calcite by measuring the mass loss when increasing temperature. There were three main mass loss intervals expected: the loss of physical water under 120°C, the decomposition of portlandite between 400 and 600°C and the decomposition of calcite between 700 and 800 °C. In order to minimize inaccuracies due to the superimposing of thermal effects, larger intervals will be used for comparison, after taking care that no other effect can be seen on the TG curve. Besides the original PsFA sample and the water-treated one, PsFA-W (described above), two more samples are now introduced: one thermally treated at 750°C termed PSFA-H (heated) and one which is again water treated after heating, termed PsFA-H/W. The results are presented in Table 8.3 and Figure 8.3.
Table 8.3 also presents the stoichiometrically calculated amounts of $Ca(OH)_2$ and $CaCO_3$ based on the mass loss in the mentioned intervals, assuming only water and only CO_2 have been removed between 350-600°C and 600-900°C respectively. These amounts are then subtracted from the estimated CaO content obtained from the XRF measurement (Section 8.3.1), assuming that CaO, $Ca(OH)_2$ and $CaCO_3$ are the only Ca-containing phases within the PsFA samples.
The low amount of water still present after the thermal treatment at 750°C which can be evaporated under 150°C represents the rehydration of PsFA-H using atmospheric water. The remaining very low content of $CaCO_3$ estimated even after the thermal treatment can be due to atmospheric recarbonation or to the incomplete decarbonation during the treatment; however, the percentage is negligible.
In the case of both water-treated samples, the effect of the added water is not as high as was expected. In the case of the PsFA-W sample, water-treating the original fly ash only converted a small part of the estimated free lime to portlandite. This suggests that there are other Ca-containing phases within the PsFA which do not readily react with water. In the case of the sample heated before the water treatment, PsFA-H/W, around half of the CaO has been transformed to portlandite.

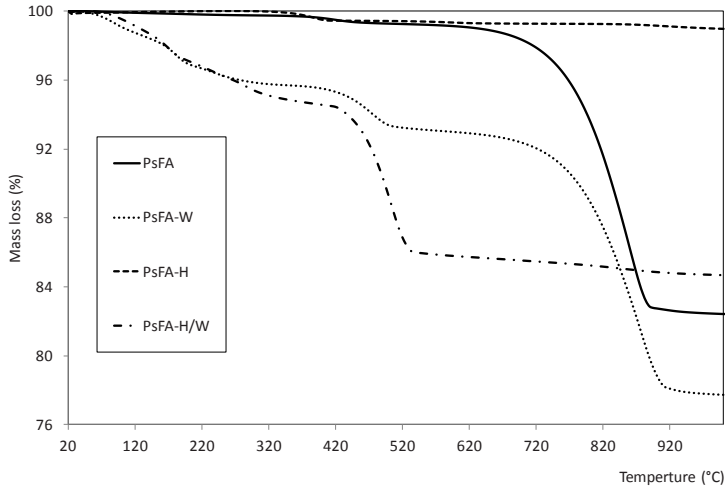

Figure 8.3. Mass loss of original and treated paper sludge fly ash.

Table 8.3. Mass loss of original and treated paper sludge fly ash and predicted % of Ca-containing compounds.

	PsFA	**PsFA-H**	**PsFA-W**	**PsFA-H/W**
20-150°C	-0.14	-0.05	-1.72	-1.53
350-600°C	-0.6	-0.56	-2.71	-9.08
600-900°C	-16.35	-0.17	-14.07	-0.93
$Ca(OH)_2$ (% mass)	1.87	1.74	8.43	28.25
$CaCO_3$ (% mass)	20.81	0.22	17.91	1.18
CaO (% mass)	34.32	55.04	30.66	27.56

The amount is consistent with the CaO formed through decarbonation through heating, which suggests that all $CaCO_3$ has been transformed to $Ca(OH)_2$ through the combined treatment. However, there is still half of the Ca determined by XRF which probably forms other Ca-containing phases which were not affected by the employed treatment methods.

8.4.3 XRD

X-ray diffraction is performed in order to check the effect of the treatments and to make sure no side effects occur. Analyses are performed using α-Cu radiation with a step size of 0.02 degrees and 1-second count time. Pattern processing was done using EVA software and the ICCDD pattern database. The results are presented in Figure 8.4.
By looking at the X-ray diffraction patterns illustrated in Figure 8.4, it can be seen that the original paper sludge fly ash consists of a high content of calcite and some small peaks of quicklime and quartz. One hour after the water treatment, the quicklime is reduced but not completely consumed. At that time no formation of portlandite was detected. However, after twelve hours the formation of portlandite could be detected.

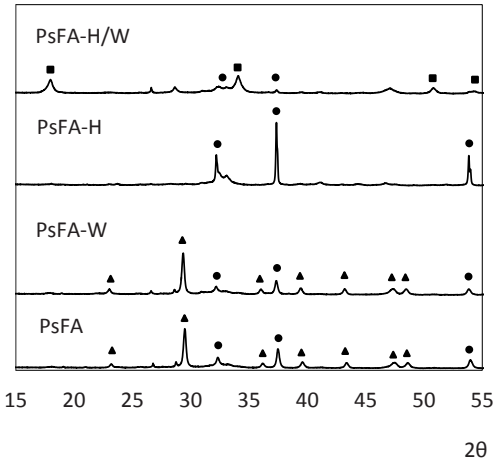

Figure 8.4. XRD-pattern of original and treated paper sludge fly ash highlighting the Ca-containing phases: CaO (●), $Ca(OH)_2$ (■), $CaCO_3$ (▲).

The effect of thermal treating paper sludge fly ash for one hour at 750°C is also investigated. After the thermal treatment no calcite or portlandite could be detected anymore and only free lime was detected. Finally a thermally treated and water treated paper sludge fly ash is investigated after 12 hours. As expected all calcite is turned into lime and later into portlandite. Still not all lime is transformed into portlandite, which confirms the thermo gravimetric analysis (TGA).
From the XRD results and Table 8.3 it can be clearly seen that there is a decrease of calcite after thermal treatment, which is almost completely turned into quicklime. Furthermore, after thermal and water treatments there is a large increase of portlandite. It can however be concluded that not all the free lime is used for the formation of portlandite. When only water-treated, the amount of portlandite is increased but the

amount of quicklime is not significantly reduced. Observing the results of TGA and XRD there is still 50% of quicklime available after treatments. It is possible that the calcium oxide content obtained from XRF could include other Ca- containing compounds than calcite, portlandite and quicklime, which were not identifiable through this method.

8.5 The binder potential of paper sludge fly ash

While examining the physical and chemical properties of paper sludge fly ash as described in Section 8.3, two possible options to increase the utilization of paper sludge fly ash can be suggested:
1. Reduce the high water demand by lowering the free lime content of paper sludge fly ash;
2. Use paper sludge fly ash as activator for coal combustion or other types of fly ashes or secondary building materials.
The first option has been addressed so far in this chapter. The second one will now be investigated through isothermal calorimetry and the influence of the PsFA on the mechanical properties of standard mortars [29].

8.5.1 Isothermal calorimetry

In order to test the pozzolanic properties of PsFA, isothermal calorimetry tests were performed using a TAM Air calorimeter. A mix of PsFA and reference fly ash was used to test if any self-cementitious properties can be identified for paper sludge fly ash, either treated or not. For this purpose, mixes containing 80% reference fly ash and 20% of respectively PsFA, PsFA-W, PsFA-H and PsFA-H/W with a water/powder ratio of 0.7 were measured. The results can be seen in Table 8.4, where the cumulative released heat after 24 and 72 hours is presented.
As expected, the poorest performance is exhibited by the water-treated samples, PsFA-W and PsFA-H/W, in which the free lime has already been converted to portlandite. The thermally treated sample, PsFA-H, shows a more exothermic behaviour; however, the highest heat release has been achieved in the case of original, untreated PsFA-reference fly ash mix.
A second series of samples was tested, in which Portland cement is combined with the reference fly ash and the PsFA samples in a ratio of 8:1:1. The resulting samples therefore contain 80% CEM I 42.5N, 10% reference fly ash and 10% of respectively PsFA, PsFA-W, PsFA-H and PsFA-H/W.
A plain CEM I result (average of three measurements) is also included in Table 8.4 for comparison. After 24 hours of hydration (water/powder ratio of 0.7), the mix containing the water-treated PsFA-W releases the highest amount of heat, almost equalling the one of pure cement, while the other samples display a lower heat release.

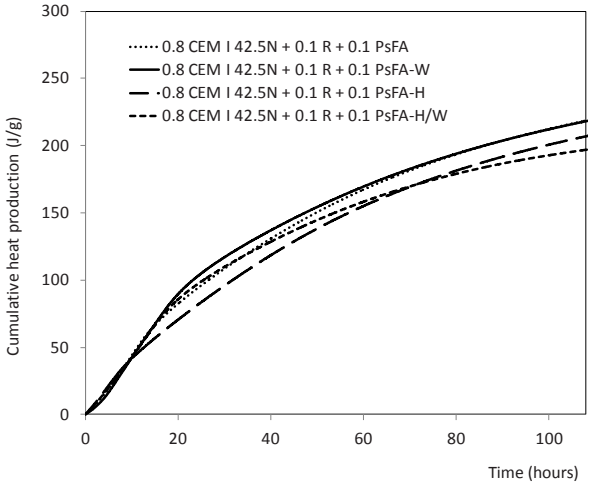

Figure 8.5. Cumulative heat production of the original and treated paper sludge fly ashes.

Table 8.4. Cumulative heat production after 24 and 72 hours of the produced pastes with a water/powder ratio of 0.7.

Sample	Cumulative heat after 24 h (J/g)	Cumulative heat after 72 h (J/g)
PsFA 20% + fly ash 80%	31.34	39.50
PsFA-H 20% + fly ash 80%	24.55	24.48
PsFA-W 20% + fly ash 80%	9.36	10.43
PsFA-H/W 20% + fly ash 80%	12.12	15.22
CEM I 42.5N 80% + PsFA 10% + fly ash 10%	93.32	183.95
CEM I 42.5N 80% + PsFA-H 10% + fly ash 10%	81.02	172.08
CEM I 42.5N 80% + PsFA-W 10% + fly ash 10%	102.37	185.28
CEM I 42.5N 80% + PsFA-H/W 10% + fly ash 10%	92.29	171.39
CEM I 42.5N 100%	107.99	209.94

However, after 72 hours, while the PsFA-W sample still has the most promising behaviour, the original PsFA almost equals it. Figure 6 illustrates these four CEM I-reference fly ash R- PsFA mixes, up to a hydration time of 108 hours. It can be seen that the sample containing PsFA-W has the highest heat release throughout the whole analysis

time; however, after around 72 hours, the original PsFA-containing sample reaches the same heat release. The two thermally treated samples clearly have a lower heat release, indicating they will contribute less to the early strength development.

8.5.2 Mechanical properties

To investigate if after different treatment steps the flexural and compressive strength results of paper sludge fly ash are improved, standard mortars incorporating the original and the treated PsFA are made according to EN 196-1 [29]. Furthermore, the effect of paper sludge fly ash on coal combustion fly ash is investigated to see if the activation can be accelerated by the formation of portlandite [143]. The results (Table 8.5) can be divided into two groups.

The first group consist of 10% replacement of cement with:

1. Original paper sludge fly ash termed PsFA 10%;
2. Thermally treated paper sludge fly ash termed PsFA-H 10%;
3. Thermal and water treated paper sludge fly ash termed PsFA-H/W 10%;
4. Water treated paper sludge fly ash termed PsFA-W 10%.

The second group consist of 10% coal combustion fly ash with:

1. 10% thermally treated paper sludge fly ash termed, PsFA-H 10% + fly ash 10%;
2. 10% thermal water treated paper sludge fly ash termed, PsFA-H/W 10% + fly ash 10%;
3. 10% water treated paper sludge fly ash termed, PsFA-W 10% + fly ash 10%.

Additionally mortars are made with 10% (fly ash 10%) and 20% coal combustion fly ash (fly ash 20%) and an additional 20% original paper sludge fly ash (PsFA 20%), and samples are containing recycled concrete fines (RCF described in Chapter 5) and bio-energy fly ash (BFA2-T described in Chapter 7).
Before the samples are cured, fresh mortars are investigated on the workability and where needed Glenium 51 (BASF, with a concentration of 35%) superplasticizer (SP) is added to achieve a spread of 140 mm. The recipes are presented in Table 8.5. After one day the samples are demolded and cured under water for 7 and 28 days.

Table 8.5. PsFA mixtures tested for 7 and 28 days flexural and compressive strength.

Recipes	CEM I (g)	PsFA (g)	Fly ash (g)	SP (ml)
CEM I 42.5N 90% + fly ash 10%	405	-	45	-
CEM I 42.5N 80% + fly ash 20%	360	-	90	-
CEM I 42.5N 90% + PsFA 10%	405	45	-	2
CEM I 42.5N 80% + PsFA 20%	360	90	-	2
CEM I 42.5N 90% + PsFA-H 10%	405	45	-	2
CEM I 42.5N 90% + PsFA-H/W 10%	405	45	-	0.5
CEM I 42.5N 90% + PsFA-W 10%	405	45	-	0.5
CEM I 42.5N 80% + PsFA-H 10% + fly ash 10%	360	45	45	0.5
CEM I 42.5N 80% + PsFA-H/W 10% + fly ash 10%	360	45	45	0.5
CEM I 42.5N 80% + PsFA-W 10% + fly ash 10%	360	45	45	0.5

Figures 8.6-10 show the flexural and compressive strength development of all considered samples. Figure 8.6 illustrates the samples with a 10% cement replacement. The reference is the sample with 10% of cement replaced by the reference fly ash. It can be seen that the sample performing the best is the one using the original PsFA, after both 7 and 28 days, achieving higher flexural and compressive strengths than the reference sample. All the PsFA-containing mortars display a higher 7 days compressive strength than the reference fly ash, but this effect is no longer observed after 28 days of hydration.

Figure 8.7 shows the mortar samples using the same replacement materials, but this time as 20% replacement of cement by mass. The same trend as in the case of the 10% samples can be observed, with the mention that in this case all the PsFA samples perform slightly better than the reference one in terms of 28 days compressive strengths, regardless of the applied treatment method.

Three mortar recipes were designed using a combination of fly ash and recycled concrete fines (RCF); the results are illustrated in Figure 8.8. The RCF material has been thoroughly investigated in Chapter 5 and [123]; the thermally treated sample RCF-800 has been chosen for the following experimental program. The reference sample this time is the one containing 10% reference fly ash and 10% RCF-800. A sample in which 20% of cement by mass is replaced by RCF-800 is also shown for comparison.

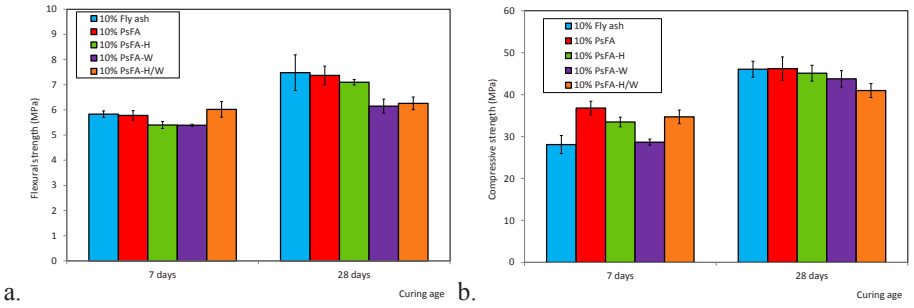

Figure 8.6. The flexural **(a.)** and compressive **(b.)** strength of PsFA-containing mortars after 7 and 28 days of curing; cement replacement of 10% by mass.

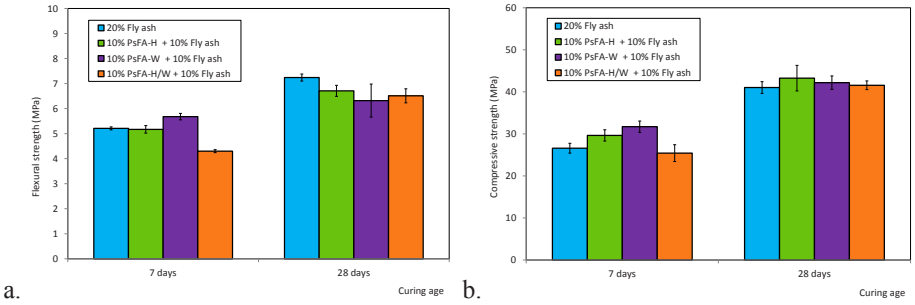

Figure 8.7. The flexural **(a.)** and compressive **(b.)** strength of PsFA-containing mortars after 7 and 28 days of curing; cement replacement of 20% by mass.

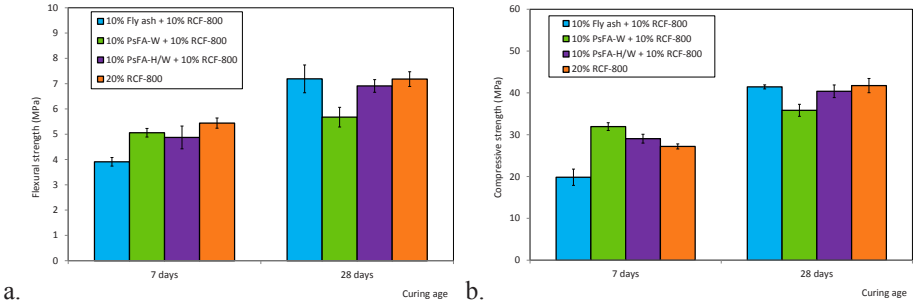

Figure 8.8. The flexural **(a.)** and compressive **(b.)** strength of PsFA and RCF-containing mortars after 7 and 28 days of curing; cement replacement of 20% by mass.

Both the flexural and the compressive strengths after 7 days are highly improved by the replacement of the reference fly ash by PsFA-H/W and especially PsFA-W, which

reaches a 7-days compressive strength of almost double the one of the reference. After 28 days, however, this is no longer the case, but the achieved mechanical properties are still high enough, the sample containing PsFA-W reaching almost the same strength as the reference one.

Samples containing a higher cement replacement were also designed: two samples in which 30% of the cement is replaced by 20% reference fly ash and 10% PsFA and respectively10% reference fly ash and 20% PsFA and a recipe in which 40% of the CEM I is replaced by 20% reference fly ash and 20% PsFA. Besides these, a sample in which 20% of the CEM I is replaced by 10% PsFA and 10% bio-energy fly ash is also tested. The employed bio fly ash, termed BFA2-T, has been characterized in Chapter 6 and [143]. These samples were cured for 28 and 90 days and their flexural and compressive strengths are shown in Figure 8.9.

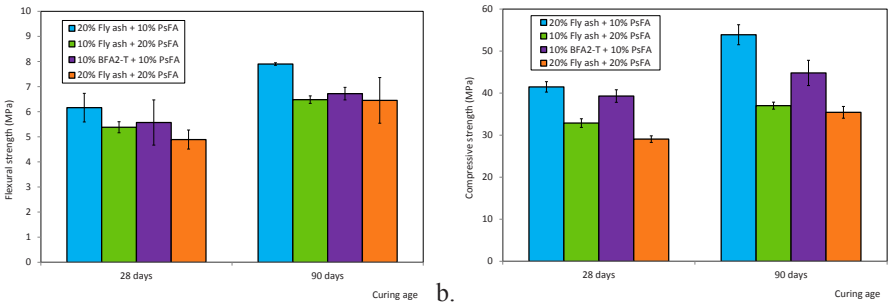

Figure 8.9. The flexural **(a.)** and compressive **(b.)** strength of PsFA and RCF-containing mortars after 28 and 90 days of curing, using a higher cement replacement level between of 20 and 40% by mass; BFA2-T is described in Table 7.5.

As it was also observed in the previous samples, the main beneficial effect of the addition of paper sludge fly ash is observed at early ages. The strength development of these samples after 90 days of curing is much lower than the one of coal combustion fly ash-containing mortars, which underlines this behaviour.

8.6 Discussion and conclusions

In this study, utilization options are investigated for paper-sludge fly ash. The main challenges are the increased water demand and content of free lime, which may reduce the properties of mortars. First, the physical and chemical properties of paper sludge fly ash are investigated [143], leading to the suggestion of two possible options to increase the utilization of paper sludge fly ash - decreasing the high water demand by lowering the free lime content of paper sludge fly ash, and the use of paper sludge fly ash as activator for coal combustion or other types of fly ashes.

After investigation, several attempts to decrease the free lime content or to use it sufficiently did not have positive effects on the strength results compared to untreated paper sludge fly ash. However, it is found that untreated paper sludge fly ash has a positive effect on coal combustion fly ash and can by this increase its utilization. Combining paper sludge fly ash with coal combustion fly ash increases the strength results for all obtained treatment methods, indicating that the paper sludge fly ash is a good alternative to replace 50% of coal combustion fly ash, increasing strength at 28 and even at 7 days by its activation properties. Further research could examine the potential of larger replacement or even increase the use of coal combustion fly ash.

So far, from the obtained strength results the following conclusions can be drawn. Firstly, samples containing 10% treated paper sludge fly ash (thermal and/or water treatment) give lower strength results than the original paper sludge fly ash, indicating that the treatment of this fly ash is not increasing its potential. However, combining paper sludge fly ash with coal combustion fly ash indeed increased the strength results for all obtained treatment methods, indicating that paper sludge fly ash is able to activate coal combustion fly ash.

From the results it can be seen that thermally treated paper sludge fly ash (PsFA-H 10%) performs acceptably at both 7 and 28 days, but not better than the original untreated paper sludge fly ash (PsFA 10%). The reason could be that quicklime absorbed too much water, and less water was available for the cement hydration, resulting in a lower strength. However, the strength decrease is < 1% (could be considered as measurement error) in comparison with the original, indicating that the water demand was estimated correctly. The combination of PsFA-H 10% with coal combustion fly ash performed better than the same replacement factor only than with 20% coal combustion fly ash. When comparing PsFA-H 10% with water treated paper sludge fly ash (PsFA-W 10%), higher strength results are found for PsFA-H 10%. It seems that the high lime content of PsFA-H 10% is used more efficiently during hydration (increasing the strength), while PsFA-W 10% has only available portlandite that will leach out when not bound.

At an early age, PsFA-W 10% exhibits a decrease of flexural and compressive strength, suggesting that metakaolin is activated by the water treatment before the paper sludge fly ash is used in mortars. This was expected because the calculated water demand of 10% was increased to a water demand of 20% as the lower water demand seemed to have no effect. However, TGA and XRF tests, through mass balances, show that there is still available quicklime that has not yet reacted with water. After 28 days the compressive strength of PsFA-W 10% is only 1.5 MPa lower than that of PsFA-H 10%, meaning that the effect on metakaolin is not high or may even not occur. Furthermore, expansion was not observed for any of the samples. It seems that not all quicklime reacts with water. However, there might be other compounds in paper sludge fly ash that absorb/react with water.

The effect of the water treatment is clearly seen by the results obtained by thermally and water treated paper sludge fly ash (PsFA-H/W 10%) and the one with added 10% coal combustion fly ash (PsFA-H/W 10% + fly ash 10%). Coal combustion fly ash decreased the water demand, making more water available for cement and paper sludge fly ash to hydrate. In this way, the strength results of PsFA-H/W 10% + fly ash 10% are higher than without coal combustion fly ash, even though the cement content is 10% lower. Furthermore the strength results with coal combustion fly ash are for each treatment higher than strength results obtained from PsFA 20% or 20% coal combustion fly ash (fly ash 20%).

Finally, the 7 days strength results when combining paper sludge fly ash (either thermal, water-or combined treatment) and coal combustion fly ash are lower than that without coal combustion fly ash. This is due to the low early strength contribution of coal combustion fly ash and the high early strength contribution of paper sludge fly ash. However, comparing it with 20% fly ash, a strength increase is found because of the early strength development of paper sludge fly ash.

Chapter 9

The use of MSWI bottom ash in concrete mixtures

9.1 Introduction

Municipal solid waste incineration (MSWI) plants generate several types of solid residual materials. Typical residues of MSWI by grate combustion are bottom ash, boiler ash, fly ash and air pollution control (APC) residues, among others. Boiler ash represents the coarse fraction of the particles carried over by the flue gases from the combustion chamber, while fly ashes are made up of the fine particles in the flue gases downstream of the heat recovery units. APC residues include the fine material captured prior to effluent gas discharge into the atmosphere.

Bottom ash contains elevated concentrations of Br^-, Cu, Mo, Sb, Cl^- and SO_4^{2-}, among others. Certain waste particles contain large concentrations of contaminants, which can lead to higher emissions. Experimental research has shown that the largest part of the contaminants (heavy metals) is absorbed by the smaller size bottom ash particles (sludge). Chimenos [165] quantified the metal content of bottom ash by particle size, concluding that the concentrations of Pb, Zn, Cu, Mn, Sn, Cr, Ni and Cd all peak in the 0-2 mm fraction and continue to decrease steeply in bottom ash particles in the 2-6 mm fraction; larger particles have much lower metal concentrations. Mueller et al. [166] also studied the distribution of certain contaminants in the bottom ash. Acid and water soluble chlorides and sulphates, as well as aluminium were found to decrease in concentration with the increase of particle size. The leaching of chlorides and sulphates, as well as of ionic species of Cu and Sb are evaluated in [167].

In the Netherlands, bottom ash is mainly used as road base material. However, this type of material can also be treated and upgraded into a granulate fraction for use in concrete mixes. Upgrading this type of waste to a new building material is a sustainable approach which leads to lower landfilled quantities of the material as well as reducing the demand for natural aggregates in concrete. In order to obtain a suitable building material from the bottom ash, a complex sequence of treatment steps is necessary. These treatment steps include fractionation, metal recovery (both ferrous and non-ferrous), screening and wet cleaning of the bottom ash into a clean granulate fraction. The use of bottom ash particles as aggregates in mortars and concretes have been studied in literature. Al-Rawas et al. [168] used bottom ash as sand replacement in mortars, up to 40% of natural sand; all samples achieved a higher compressive strength than the reference after 28 days. However, the slump of the samples decreased significantly with the increase of bottom ash use.

The use of bottom ash as concrete aggregate is also investigated by Müller and Rübner [166]. Two mechanisms are identified as the cause of durability issues in concrete containing bottom ash- the reaction of metallic aluminium in bottom ash with the alkali environment, and the possibility of ASR. Pera et al. [169] used 4-20 mm bottom ash as aggregate in concrete. The study found that bottom ash has a lower density, a higher water demand and lower strength than natural gravel. Moreover, the main detrimental factor was the content of metallic aluminium. It is concluded that, if the bottom ash is alkali-treated to remove the metallic aluminium, it can be used as 50% replacement of aggregates in concrete without affecting the durability. The review in [170] concluded that concrete incorporating bottom ash as 50% replacement of aggregates can achieve a 28 days compressive strength of 25 MPa. Courard et al. [171] proposed the use of bottom ash as aggregate in concrete pavement tiles; the conclusion is that a sufficiently aged bottom ash (minimum six weeks) that has undergone post-incineration treatment (removal of ferrous parts and sieving) can be successfully used for this purpose. Moreover, sufficient compaction was deemed necessary, to compensate the higher water demand of the bottom ash.
This study investigates the suitability of bottom ash granulates as natural aggregate replacement in concrete mixes. Bottom ash is a heterogeneous material, consisting of glass particles, synthetic ceramics fragments, minerals (quartz, calcite, lime, feldspars), paramagnetic and diamagnetic metals and unburnt organic matter. The proportion of these constituents can vary with the particle size and will affect the properties of the final concrete mix. The separation and washing techniques also influence both the particle size and constituent proportions of the MSWI bottom ash. Therefore, different size fractions of bottom ash granulates were studied, with various dimension ranging between 0 and 40 mm. These were further separated into smaller particle ranges, and their chemical and mineralogical composition studied. Leaching tests were performed on different size fractions, along with quantifying the aluminium content. The water content and density of all materials was measured. Based on this information, new concrete recipes were designed and tested for compressive strength. The results show that this type of material can be used successfully as aggregate in concrete recipes.

9.2 Treatment methods of MSWI bottom ash granulates

Sabbas et al. [172] summarize the possible treatments for bottom ash. The main classes of such operations are physical and chemical separation, stabilization/solidification techniques and thermal treatment. The first category comprises a larger number of possible treatment steps, which are commonly used in combination to treat bottom ashes: size separation, magnetic separation, eddy current separation, washing, chemical extraction/precipitation etc. The second category comprises weathering (aging) of the bottom ash, as well as the use of binders for immobilizing contaminants. Santos et al. [173] concluded from a literature review that a weathering step reduces the leaching of

Pb, Mo and Zn from bottom ash, but it is not useful in the case of Cr, Cu and Sb. Mangialardi [174] found that a washing step is capable of removing the contaminants (Al, Cd, Pb, Zn) through two different mechanisms: precipitation of aluminium hydroxide and adsorption of cadmium, lead and zinc ions onto flock particles of $Al(OH)_3$. Three treatment sequences were used to generate the materials investigated in this chapter, which were provided, treated and partly analysed by Van Gansewinkel Minerals, the Netherlands. In this study, all final treated bottom ash fractions are termed FORZ composite granulates, or FCG, and referred to by their particle sizes. A first material, termed FCG 0-8, was selected from bottom ash treated in 2009 following a 3-steps process (Sections 9.2.1 and 9.5). The second treatment line was used in 2010 and follows similar steps, but is upgraded and optimized for cleaner aggregate production. From this stage, a fraction 2-40 mm termed FCG 2-40 was obtained (Sections 9.2.2 and 9.6). In 2012, an improved line of treatment was used to generate a 2-20 mm fraction, referred to as FCG 2-20 (Sections 9.2.3 and 9.7). The differences between the treatment stages and the obtained granulates will be described in detail in the following section.

9.2.1 Phase 1a of bottom ash treatment

The first cleaning treatment of bottom ash comprised five steps, which include both physical and chemical separation steps, as classified in [172]:

Step 1. Weathering fresh MSWI bottom ash
The fresh material is weathered for around 6 months. Weathering reduces the quantitative leaching of heavy metals (e.g. copper) and further reduces the reactivity of the material.

Step 2. Dry separation MSWI bottom ash
Bottom ash from the depot is first treated by extracting the large fraction of ferrous metals < 400 mm (overhead magnet). The generated bottom ash fraction is crushed to obtain a 0-40 mm fraction.

Step 3. Dry separation and metals recovery
The fraction 0-40 mm is treated with overhead magnets and separated in many smaller fractions. The fractions are treated with overhead magnets and with 3 eddy current magnet systems for optimal recovery of non-ferrous metals. Organics and plastics are largely recovered. All mineral fractions are mixed together generating one mineral granulate fraction 0-40 mm. A 0-8 fraction of the bottom ash is separated after this stage, which will be investigated further under the name of “FCG 0-8” in order to show the relevance of the washing step on the whole treatment phase.

Step 4. Wet separation and washing treatment
The mineral bottom ash fraction 0-40 mm is treated in a mobile washing plant. The input fraction is firstly separated from ferrous parts with overhead magnet and then split into four fractions: an organic floating fraction, a 0-63 µm sludge, a fine granulate 63 µm-2 mm fraction and a coarse granulate fraction 2-40 mm. The organic fraction is reused in the incineration process. The sludge fraction contains the largest amount of heavy metals and salts. The wet cleaning technique is based on concentrating the potential contaminants from the input fraction into the sludge fraction. The fine granulate fraction is more or less a sandy fraction and the coarse fraction is a stony/glassy granulate fraction. The washing water from the washing plant is treated and filtered and reused within the process. No process water discharge is needed. The washed granulate fraction 2-40 mm is further treated with the mobile ferrous and non-ferrous unit.

Step 5. Final treatment of the bottom ash granulate
The total washed fraction 2-40 mm is treated with overhead magnet reducing the total of small ferrous particles. In addition, extra non-ferrous metals are recovered with an eddy current system.
This final material is then separated in three fractions: a 0-8 mm, an 8-16 mm and a 16-40 mm.

9.2.2 Phase 1b of bottom ash treatment

The treatment steps used to produce the FCG 2-40 mm fraction are similar to the ones already described above for the bottom ash generated in 2009; therefore, just the differences between the two processes will be summarized in this paragraph.
Step 1 is the weathering step, but this material is weathered for a shorter interval, between 3 and 6 months. Step 2, besides ferrous separation, includes a separation using a ballistic separation technique, which generates two bottom ash fractions, 0-2 mm and 2-40 mm. This is the main difference between the treatment of the bottom ash from 2009 and this treatment line used in 2010; after this step, the three remaining Steps (3, 4 and 5 as termed above) are the same, only applied for the 2-40 mm fraction instead of a 0-40 mm fraction. The final treated fraction which has undergone all five steps of treatment will be further referred to as FCG 2-40.

9.2.3 Phase 2 of bottom ash treatment

Freshly produced MSWI bottom ash from the incinerator AVR-Van Gansewinkel Duiven, the Netherlands, is treated on site to produce a new building material. The initial fresh bottom ash consists of 80% mineral material (sintered ash, stone, glass and ceramics), 5-13% ferrous metals, 2-5% non-ferrous metals (Cu, Al, Zn, Pb) and 1-3% unburnt organic material (paper, textiles, plastic). The final fraction is a 2-20 mm

heterogeneous aggregate, which is called FORZ composite granulate (FCG). The treatment process is a combination of dry and wet separation techniques [175–177], which can be divided into five separate steps. Since these five steps present multiple differences from the two treatment lines presented above, they will be described again in detail.

Step 1. Weathering of fresh MSWI bottom ash
Freshly produced bottom ash (a batch of 1000 t) is transported from the MSWI incineration towards a depot. The fresh material is weathered for around 3 months. Longer weathering can strongly influence the further oxidation of ferrous and non-ferrous metals.

Step 2. Dry separation MSWI bottom ash
The weathered bottom ash is first treated by extracting the large fraction of ferrous metals < 400 mm using an overhead magnet. The generated bottom ash fraction is separated with a drum sieve (60 mm mesh) in two fractions, particles under 31.5 mm and above 31.5 mm. Both fractions are again treated by extracting the large fraction of ferrous metals using 2 overhead magnets. The fraction 0-31.5 mm is the input material for the 3rd step and is further treated, extracting large non-ferrous metals, large minerals e.g. stones and slag and the large unburnt organic fraction.

Step 3. Wet separation and washing treatment
The mineral bottom ash fraction 0-31.5 mm is treated with a mobile wet separation-washing plant; this step is similar to Step 4 presented in the two previous cases of FCG 0-8 and FCG 2-40, with the difference that in this process the maximum particle size is 31.5 mm instead of 40 mm.

Step 4. Dry separation and metals recovery washed granulate
The washed granulate fraction 2-31.5 mm is treated with an overhead magnet for the separation of ferrous metals and separated in two fractions: 2-16 mm and 16-31.5 mm. Both fractions are treated with an overhead magnet and additionally with a cascade double sequenced eddy current magnet system for optimal recovery of non-ferrous metals. A separation into two divided partial fractions is needed, creating more favourable particle size fractions and particle densities, which is needed for an optimal non-ferrous recovery. The fraction 16-31.5 mm is additionally treated (handpicked) for the recovery of stainless steel. Both fractions are mixed together generating one mineral granulate fraction. Step 4 is the final treatment step for introducing the granulate (non-shaped) building material as base material for the road and construction industries. However, an additional step is necessary for generating a material which is usable as concrete constituent.

Step 5. Final treatment of the bottom ash granulate (for application in concrete)
The final fraction of Step 4 can be additionally treated for application in concrete. The total fraction is treated with a drum magnet, reducing the amount of small ferrous particles, which would interact with the cementitious matrix when applied in concrete and thus lead to a change in colour of the product.. In addition, extra non-ferrous metals are recovered with a double sequenced eddy current system. The total fraction is finally sieved (mesh 22 mm) into a final granulate fraction 2-20 mm. The final FCG fraction contains 55-60% SiO_2, ~ 10% CaO and ~ 6% Al_2O_3, which is close to other secondary building materials used in concrete. This fraction will be investigated further in this study, and referred to as FCG 2-20.

9.3 Leaching behaviour of the MSWI bottom ash granulates

An important analysis for secondary building materials which needs to be performed in order to establish their possibility of use as building materials is the leaching of contaminants. In the Netherlands, the legislative document that regulates the use of building materials is the Soil Quality Decree [28], which has been described in Section 6.4 of this thesis.
The leaching results, determined following the requirements of the NEN 7375 standard [178] for the three considered fractions, FCG 0-8, FCG 2-40 and FCG 2-20 mm (Table 9.1) were provided by Van Gansewinkel Minerals. The aim of the treatment of the bottom ash was to achieve either the acceptable emissions of non-shaped building materials for FCG, or the requirements of shaped materials for prefab concrete containing FCG.
The FCG 0-8 was expected to be the most contaminated step, due to its least sophisticated treatment method, as well as to its smallest particle size. Its leaching of contaminants is within the norm of the SQR [28], except for antimony, chlorides and sulphates (5 times higher than the accepted limit). The leaching values of FCG 2-40 are well within the limits set for non-shaped materials, with the exception of the value of antimony. This indicated that a more complete treatment method needs to be considered. Therefore, the leaching of the FCG 2-20 was studied after various treatment steps; these results can also be found in Table 9.1. The leaching of the FCG 2-20 was expected to be higher than the one of FCG 2-40, because it is known that the contaminants are concentrated in the smaller particle sizes (Section 9.1); the large fraction, between 20 and 40 mm, which is missing from the FCG 2-20, could be considered as fairly clean, and therefore the leaching of contaminants by mass of bottom ash will be increased in the case of the lower particle sized FCG 2-20.
Three separate leaching tests were done on the FCG 2-20. The leaching of the material after Step 4 and after Step 5 is presented in Table 9.1, to show the efficiency of Step 5. Beside these, the leaching of FCG 2-20 which followed Steps 1, 2 and 4 (not going

through the washing step- Step 3) is also shown for illustrating the role of Step 3. Most of the contaminants were under the SQR limit from the first treatment onwards, but still continued to decrease as treatment steps were added. Some contaminants show a slight increase in leaching, which can be just a consequence of changing the redox conditions or composition of the granulates by removing unwanted components.

Table 9.1 Leaching data of the FCG 0-8, 2-40 and 2-20 fractions, which can be compared to the maximum levels for non-shaped and IBC materials, as demanded by the Soil Quality Decree [28] (Table 6.9).

Contaminant	**FCG 0-8**	**FCG 2-40**	**Steps 1+2+4 (mg/kg) FCG 2-20**	**Steps 1÷4 (mg/kg) FCG 2-20**	**Steps 1÷5 (mg/kg) FCG 2-20**
Antimony (Sb)	0.34	0.32	0.86	0.3	0.41
Arsenic (As)	< 0.050	< 0.2	0.1	0.2	0.1
Barium (Ba)	< 0.60	< 0.6	0.37	0.6	0.28
Cadmium (Cd)	< 0.0010	< 0.007	0.007	0.007	0.01
Chromium (Cr)	0.052	< 0.1	0.05	0.07	0.1
Cobalt (Co)	< 0.030	< 0.07	0.05	0.1	0.1
Copper (Cu)	0.2	0.29	0.76	0.163	0.13
Mercury (Hg)	0.0005	< 0.005	0.002	0.005	0.005
Nickel (Ni)	< 0.050	< 0.2	0.1	0.3	0.1
Molybdenum (Mo)	0.61	0.81	0.3	0.309	0.36
Lead (Pb)	< 0.10	< 0.3	0.1	0.2	0.1
Selenium (Se)	0.029	< 0.009	0.0094	0.009	0.039
Tin (Sn)	< 0.030	< 0.02	0.02	0.02	0.1
Vanadium (V)	< 0.20	< 0.3	0.1	0.3	0.1
Zinc (Zn)	< 0.30	< 0.7	0.2	0.7	0.2
Bromide (Br^-)	< 0.50	2.45	15	5.35	4.1
Chloride (Cl^-)	3000	518	2000	910	690
Fluoride (F^-)	5.5	0.33	7	5.85	72
Sulphate (SO_4^{2-})	6400	98	3800	2400	2300

The elements that had leaching values close to the limit (mainly Cu and Br) have shown a clear decrease after both Step 3 and Step 5 of the treatment. Chlorides and sulphates, as well as Sb, have decreased by a considerable percentage, but are still above the legal limit. The leaching of these elements makes the use of FCG 2-20 only possible as concrete aggregates when used in prefab concrete elements, because the contaminants will be bound by the cementitious matrix and the “shaped materials” limits will apply.

The leaching of an untreated 0-2 fraction, sieved from the 0-40 was also analysed. The main differences were found in leaching of Ba (5-12 times higher) and Mo (2-3 times higher), which is in line with the findings of [165], that the smaller fractions are more contaminated.

9.4 Materials used in concrete mixtures

9.4.1 Powders

The particle size distributions (PSDs) of the employed powders were analysed using the Mastersizer 2000 laser granulometer available in the TU/e laboratories. The obtained PSDs, were used in the mix design process, as detailed in Section 5.1. Three binders, a CEM I 52.5N, a fly ash and a CEM III/B 42.5N were used in testing the FCG 0-8 and FCG 2-40. A fourth binder, a CEM II/A-LL 42.5, was used for the FCG 2-20 mix. These PSDs can be found in Figures 9.1, 9.4-9.6 and 9.9.

9.4.2 Aggregates

All aggregates were used as-received in the test program, in wet conditions as this is the case in practice. However, the water content was determined for each aggregate fraction, by drying at 105 ± 5ºC for 24 hours. These values were taken into account when designing the mixes for the test program. The water/cement ratio of the mix was adjusted to take into account the water content of each aggregate type. Table 9.2 summarizes the water content of each of the considered aggregates. Three of these (the N1 sand and the G1 and G2 gravels) were described in more detail in Chapter 4.

Table 9.2. Physical properties of all aggregates used (*estimated value).

Material	Water content (% initial mass)	Water content (% d. m.)	D_{min} (µm)	D_{max} (µm)	Density (g/cm^3)
Sand N1	0.05	0.05	128	125	2.65
Gravel G1	0.10	0.10	275	5600	2.65
Gravel G2	0.10	0.10	710	8000	2.65
FCG 0-8	12.65	14.48	60.3	8000	2.45*
FCG 2-40	5.81	6.19	150	37650	2.41
FCG 2-20	1.69	1.72	63	22400	2.41
Sand R1 0-4	7.76	8.48	74.1	6693.3	2.28
Sand N2 0-4	2.68	2.8	74.1	6693.3	2.53
Sand S1	3.40	3.52	125	8000	2.64
Gravel G3	3.38	3.50	125	16000	2.57
Gravel G4	0.89	0.91	2000	22400	2.57

Commercially available natural aggregates were used as reference for the test program. A 0-2 sand (Sand N1), a 2-8 gravel (Gravel G1) and an 8-16 gravel (Gravel G2) were selected. The PSD of these aggregates were determined through dry sieving (see Figure 9.1), and the results used in the mix design algorithm (described in Chapter 4). In a further step, certain percentages of these aggregates were replaced by FCG with the same PSD range, as detailed in Section 9.5.
The specific density of the dry aggregates was also determined; the FCG 2-40 has a lower (2.408 g/cm^3) density than the one of natural aggregates (2.65 g/cm3 for the first three mentioned and 2.53 g/cm^3 for N2 0-4), but higher than the one of the recycled sand R1 0-4 (2.28 g/cm^3). The difference in the content of SiO_2 of natural aggregates (between 92 and 98% as explained in Chapter 4) and R1 0-4 (expected to be below 60%) will also have an impact on the strength of the recipes.
A third test program is centred on the use of FCG 2-20 as prefab concrete constituent; the recipe designed using this material is compared with a reference one, which contains three types of aggregates: a natural sand termed N3 and two gravel types termed G3 and G4. The properties of these aggregates are also included in Table 9.2.

9.5 Phase 1a FCG 0-8- laboratory tests

The FCG fraction 0-8 generated through the treatment phase 1a was used in the first part of the test program on laboratory scale. Figure 9.1 presents the cumulative particle size distributions of all materials used in the first part of the tests, together with the computed target PSD and the actual mix PSD. These last two curves were obtained using an optimization algorithm [126], which has already been introduced in Chapter 4. Using this algorithm, the deviation between the optimal distribution and the actual one can be calculated. The ideal case would be reached when the value of the deviation equals zero. The purpose of the optimization is to lower the value of the deviation as much as possible. The R^2 value, which is another measure of how well the composed mix matches the target line, is included for each composed mix in its description (Table 9.3).

9.5.1 Composition of the designed mixtures

In order to assess the suitability of the FORZ composite granulates (FCG) as aggregates replacement, 9 different concrete mixes were prepared, which follow two optimized recipes. For each mix, four batches were prepared, each batch for 3 test specimens. Table 9.3 presents the composition of all these mixes, with regard to the replacement levels of FCG 0-8. The replacement levels used were 0, 10, 15 and 25% FCG 0-8 on Recipe 1 (with Mix 1 as reference) and 0, 10, 15, 25 and 35% FCG 0-8 on Recipe 2 (with Mix 8 as reference). FCG 0-8 has a PSD between the ones of the Sand N1 and the Gravel G1. Because of this, the replacement using FCG 0-8 will be done by replacing 65% of the sand and 35% of the gravel, as FCG 0-8 has 65% of its particles under 2 mm.

Table 9.3. Proportion of the FCG 0-8 as aggregate replacement for the 9 mixes, and the deviation of each mix from the target PSD.

	% FCG 0-8	**Deviation**	**R^2**
Recipe 1			
Mix 1	**0**	**1658.5**	**0.908**
Mix 2	10	1500.4	0.933
Mix 3	15	1438.2	0.935
Mix 4	25	1428.6	0.935
Recipe 2			
Mix 5	**0**	**968.7**	**0.946**
Mix 6	10	917.1	0.959
Mix 7	15	892.4	0.960
Mix 8	25	859.4	0.961
Mix 9	35	825.8	0.962

The two columns "Deviation" (integrated area between the target line and the actual PSD curve of the chosen mix) and "R^2" (the coefficient of determination) included in Table 9.3 are methods of measuring the fit between the target line computed using the optimization algorithm and the actual recipe grading curve. The lower the deviation or the higher R^2 is, the better the packing of the mix. Because the difference between the qualities of the mixes is easier to compare on the deviation value, rather than on R^2 which can have very similar values (see Table 9.3), the deviation will be used from now on as a measure of the particle packing quality. Figure 9.1 shows an example of the output of the optimization algorithm, in which the difference between the two designed mixes (Recipe 1-Mix 1 and Recipe 2-Mix 5) can be observed.

According to the deviation values of the mixes, the replacement of natural aggregates by FCG 0-8 should be beneficial for the mix, as the packing density improves. Therefore, mixes 2-4 and 6-9 are expected to perform slightly better than the initial mixes (1 and 5). However, the packing density is not the only influencing factor for the final strength of the samples, as the properties of the FCG also can play an important role.

It was observed during the preparation of the samples that the mixes became increasingly stiffer as the proportion of FCG 0-8 was increased. The standard compaction method did not produce optimum results, as in the case of the reference recipes. The water addition should be therefore adjusted to the higher water demand of the FCG aggregates. In the

current test, the same water to cement ratio was used for all samples, in order to ease the comparison between the results. The distribution modulus q was chosen to be 0.3.

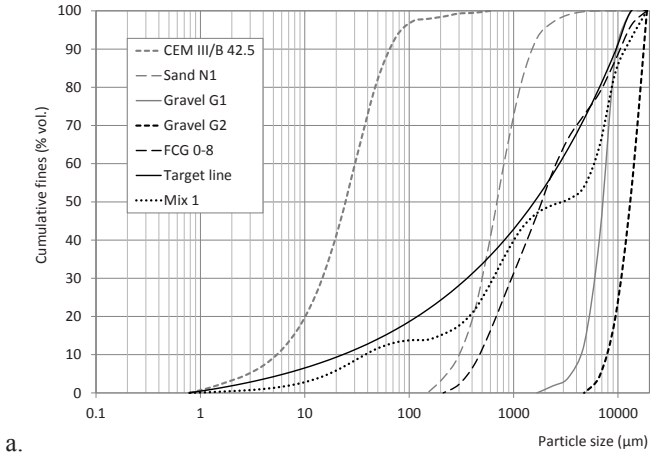

a.

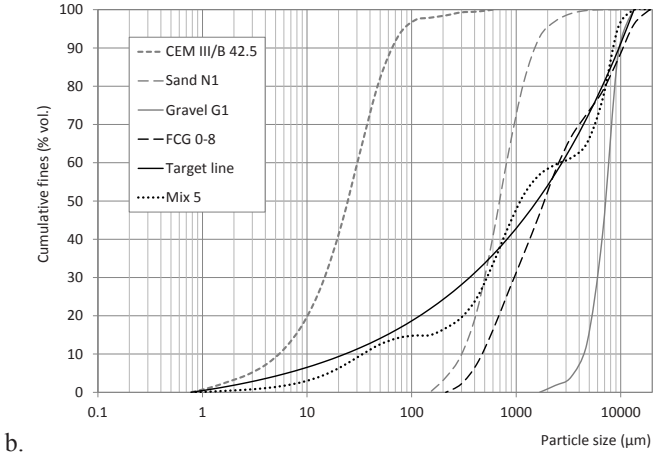

b.

Figure 9.1. Example of target line determined using the optimization algorithm, for the reference mixes of **a.** Recipe 1 and **b.** Recipe 2.

Table 9.4 summarizes the amount of each component for a batch of concrete for Recipes 1 and 2. The amount of water is already corrected for the water content of the aggregates. All samples were mixed, mould and cured according to the EN 196-1 standard [29].

9.5.2 Mechanical strength results

In this section, graphs comparing the compressive and flexural strength of all composed mixes (Table 9.3) will be shown and discussed. Figures 9.2 and 9.3 correlate the

compressive and flexural strengths of Mixes 1-4 and Mixes 5-9 respectively with the level of FCG 0-8 replacement in the mix.

Table 9.4. Proportion of each component in kg/m^3 of concrete for Recipe 1 and Recipe 2 reference mixtures.

	CEM III/B 42.5	**Sand N1**	**Gravel G1**	**Gravel G2**	**Water**
Recipe 1	263	668	669	283	131
Recipe 2	281	842	749	-	170

In the case of the compressive strength (Figure 9.2a), an addition of 10% FCG is beneficial, the results being slightly better than for the reference mix at all 3 test dates: 3, 7 and 28 days. For a replacement of 15% FCG 0-8, a decrease of approximately 10% in compressive strength can be observed. This is still encouraging since the strength decrease is slightly lower than the aggregate replacement level. For the 25% FCG 0-8 however, the decrease in compressive strength is more significant.

Similar results can be seen from Figure 9.2b, which depicts the average flexural strength of Mixes 1-4 for the test dates of 3, 7 and 28 days. The increase in strength for the 10% FCG 0-8 replacement is even more pronounced than in the case of compressive strength, but also the decreases at 15% and 25% FCG 0-8 are higher. These results indicate that a 10% replacement of natural aggregates with FCG 0-8 is beneficial for the mix, and a 15% replacement can still be accepted. However, a higher replacement level (in this case 25%) is detrimental to the mechanical properties of the concrete mix.

Figure 9.3 shows the strength development of the mixes based on Recipe 2 (Table 9.3), which is optimized for the replacement of FCG 0-8. It needs to be mentioned that, as it can be seen in Table 9.4, Recipe 2 has a 6.8% higher cement content, and also a higher water/cement ratio than Recipe 1. These factors influence the final mechanical properties, but the following comparison between the latter will highlight differences which are much higher than what can be expected through just the increased cement content and therefore must also be due to the type of aggregates employed.

In the case of compressive strength (Figure 9.3a), the replacement of up to 25% of the natural aggregates did not affect the results obtained after 3 days of curing. For the 7 and 28 days tests, a decrease is observed for the 10 and 15% FCG 0-8, but the strength stays the same for the mixes with 25% and 35% FCG 0-8. For the mix with 35% FCG 0-8 the results for 3 and 7 days are slightly below the ones obtained from Mixes 2-4 (Figure 9.2a), but the strength attained after 28 days is with approximately 70% higher in the case of Mix 8 (Recipe 2, 25% FCG 0-8), as can be seen in Figure 9.3a.

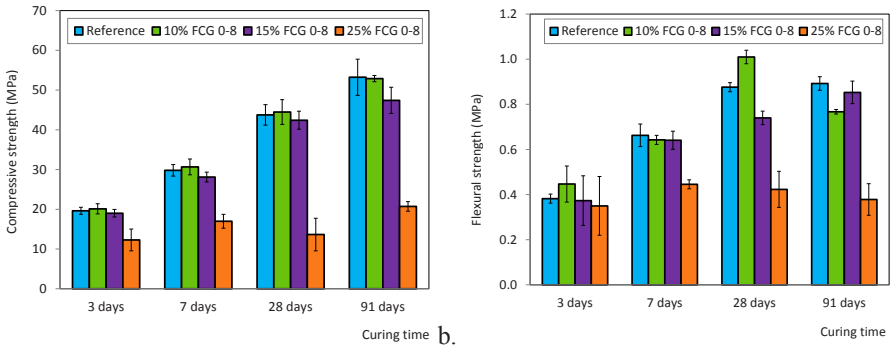

Figure 9.2. a. Compressive and **b.** flexural strength for 0-25% FCG 0-8 replacement by mass in Recipe 1 (Table 9.3).

The compressive strength of Mix 4 (Recipe 1, 25% FCG 0-8) is similar to the one of Mix 9 (Recipe 2, 35% FCG 0-8) after 28 days. This shows that Recipe 2 is better suited for the replacement of FCG 0-8 aggregates, and also that this can be further improved.

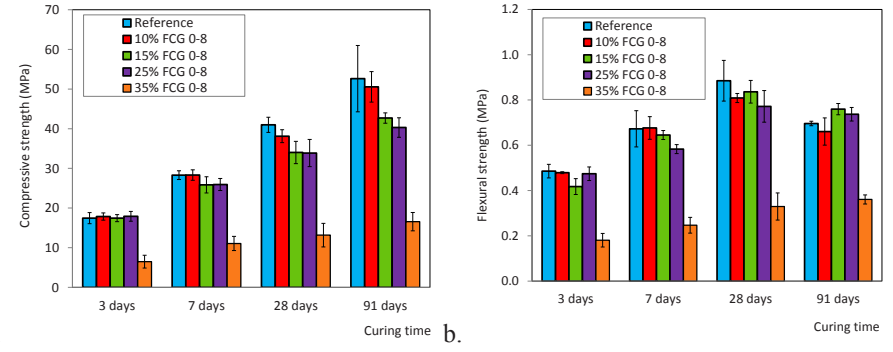

Figure 9.3. a. Compressive and **b.** flexural strength for 0-35% FCG 0-8 replacement by mass in Recipe 2 (Table 9.3).

In Figure 9.3b, a comparable trend can be observed in the case of flexural strength for the 3 days tests- a replacement of up to 25% FCG 0-8 does not influence the results significantly. The decrease after 7 and 28 days is more visible, but still it is not greater than 10%. Again, for the mix with 35% FCG 0-8 there is a sudden decrease in strength. When comparing to the results obtained for Mixes 2-4 (Recipe 1, Table 9.4), the same trend as in the case of compressive strength can be observed. Also here, the 35% replacing of natural aggregates with FCG 0-8 gives the same strength as Mix 4 (25%

FCG 0-8, Recipe 1) after 28 days, and much higher values for the replacement level of 25%.
As explained in Section 9.5.1, the water demand of the mixes increases with the FCG replacement level. For this reason, the mixes, designed with the same water to cement ratio for comparison purposes, will get drier with increasing FCG 0-8 content. The decrease of strength that can be observed can be in a large part explained by this phenomenon, as drier mixes are harder to compact, and a lower degree of compaction will lead to decreased compressive strength. Adjusting the water to cement ratio with the replacement level of natural aggregates by FCG can solve this issue.

9.6 Phase 1b FCG 2-40- use in ready-mix concrete

The PSDs of the FCG 2-40 and the two types of sand used in the second part of the tests can be found in Figures 9.4-9.6. The R1 sand is a recycled concrete sand, while the N2 is a natural 0-4 sand. The PSD of FCG 2-40 was provided by Van Gansewinkel Minerals, with the mention that, while still fairly stable, this distribution can vary to a certain degree from one batch to another.

9.6.1 Concrete recipes design and optimization

The second part of the test program involved the testing of the replacement of 100% of the aggregates in a concrete mix by the FCG 2-40.

Table 9.5. Proportion of each component for the pilot test using the FCG 2-40.

Material	Recipe I (kg/m^3)	Recipe II (kg/m^3)	Recipe III (kg/m^3)	Recipe IV (kg/m^3)	Recipe A (kg/m^3)	Recipe B (kg/m^3)
Sand R1 0-4	673	679	688		790	
Sand N2 0-4				809		817
FCG 2-40	902	881	893*	902*	678	977
CEM I 52.5N	290		290	290	210	210
Fly Ash	80		80	80	205	99
CEM III/B 42.5N		370				
Glenium Sky 523	2.22	2.22	2.22	-	2.49	-
Water/cement	0.527	0.527	0.527	0.473	0.53	0.57
Deviation	1509.2	7885	1300.5	311.33	1059.2	113.04

Four mixes (termed Recipes I, II, III and IV) were designed and tested. These included the use of recycled concrete sand (termed R1 0-4) or natural sand (N2 0-4) and the 2-40 FCG fraction. The difference between Recipes I and II is the binder used, in the first case

CEM I 52.5N and fly ash and in the case of Recipe II, CEM III /B 42.5. The use of CEM III/B 42.5 will minimize the risk of alkali-silica reactions (ASR).

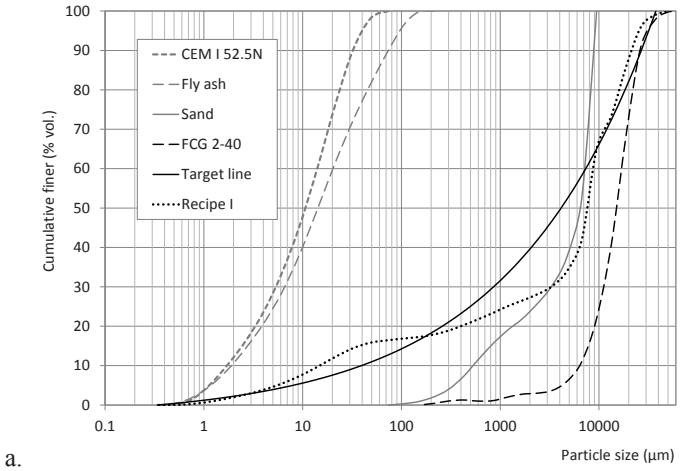

a.

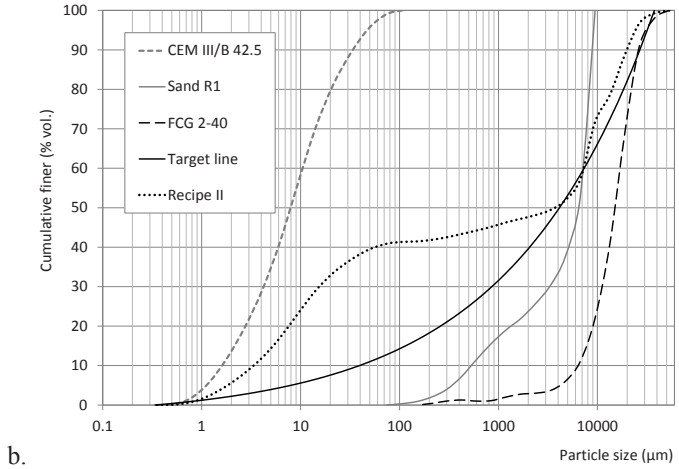

b.

Figure 9.4. a. Recipe I and **b.** Recipe II PSD of constituents and target lines.

Because it has a high content of slag (above 66%) it is assumed that practically no alkalis are contributed by the cement. Therefore, CEM III/B is generally recommended for use with aggregates that might be reactive, as well as with recycled aggregates. Also, when compared to CEM I, CEM III/B N has higher sulphate and chloride attack resistance, being able to bind more of the harmful ions when they would be released by the aggregates. Another property of CEM III/B is that it has a lower water demand than CEM

I, so it can balance to a certain extent the increased water demand of the recycled aggregates.

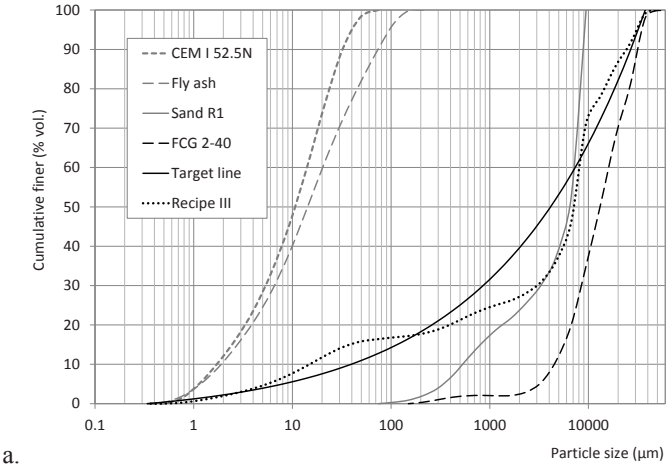

a.

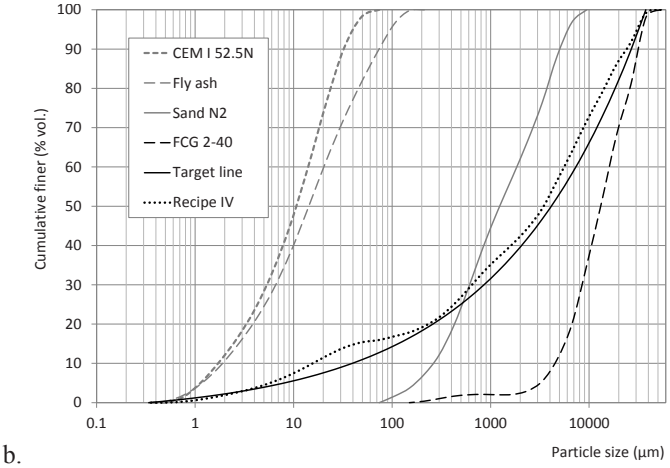

b.

Figure 9.5. a. Recipe III and **b.** Recipe IV PSD of constituents and target lines.

Based on the high deviation value (Table 9.5), which suggested a poorer packing density, a lower compressive strength would be expected for Recipe II. However, since the use of CEM III/B decreases the water demand and the risk of ASR, these effects might counteract the poorer packing density. Comparing Recipes III and IV, which are the same (and also using the case CEM I 52.5N and fly ash as Recipe I), except that III uses recycled R1 0-4 sand and IV uses natural N2 0-4 sand. Also, when using natural sand, the water demand was lower and there was no need to add plasticizer to the mix.

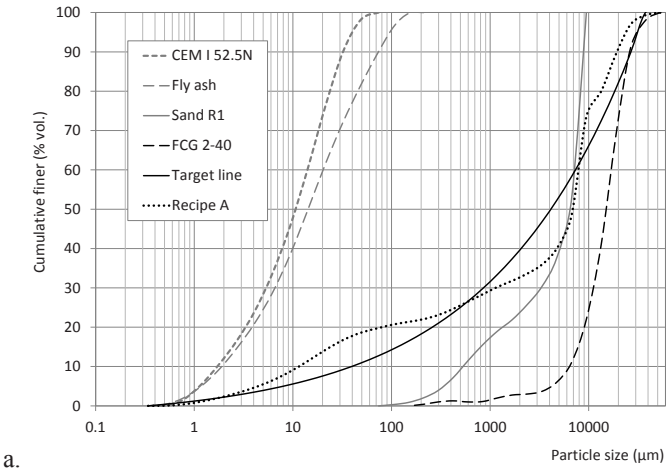

a.

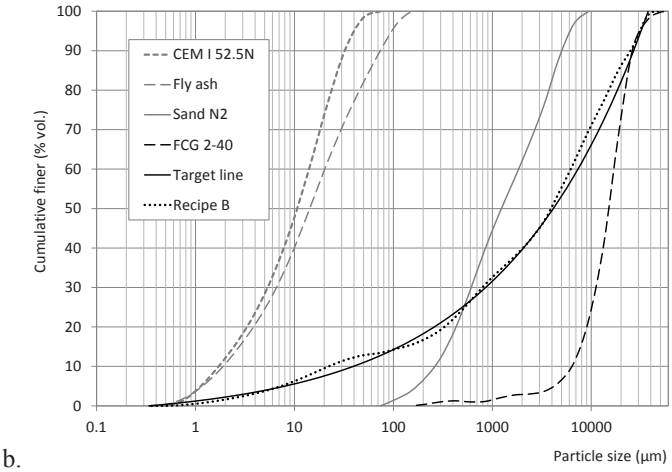

b.

Figure 9.6. a. Recipe A and **b.** Recipe B PSD of constituents and target lines.

The deviation of Recipe III was also comparable to the one of Recipe I (Table 9.5); however, Recipe IV showed a much lower deviation. Based on the results of these four recipes, two more were suggested in order to reduce the cement content, while still aiming for a C20/25 class. Recipes A and B (Table 9.5) were designed, again in order to show the influence of the R1 0-4 sand on the mechanical properties of the mixes. The deviation of Recipe B was extremely low, which indicates a very dense packing of the mix.

Recipes A and B were designed to keep the water to fines ratio constant to 0.52, so the water to cement ratio has been adjusted according to the content of particles under 125 µm. An increase in the quantity of FCG 2-40 used will also lead to a higher water

demand. The same is valid also for the use of the R1 0-4 recycled sand. For all six designed Recipes, a distribution modulus q of 0.3 is used. Table 9.5 shows the composition of all six recipes and their deviation from the target PSD curve.
Figures 9.4-9.6 show how the designed mixes compare to the target line computed based on the PSD of all materials in the mix. Figure 9.4 shows the gap in PSD caused by the use of only CEM III/B, without the contribution of the fly ash to the integral PSD. The deviation from the target line (mentioned also in Table 9.5) is clearly extremely low for Recipe B (Figure 9.6), the difference from Recipe A being explained by the use of recycled sand in the latter. The same difference can be seen in Figure 9.5.
Even from Figure 9.4 it is clear that the packing of the particles in mix II is much poorer than the one in Recipe I, where the fly ash provided particles between 1 and 100 microns needed to complete the particle grading curve.

9.6.2 Mechanical strength results

When considering the FCG 2-40 test program, only compressive strength was measured, since for this part of the study 150 mm cubes were cast instead of prisms.

Table 9.6. Compressive strength attained by the mixes detailed in Table 9.5.

Recipe name	Compressive strength after 3 days (N/mm^2)	Compressive strength after 7 days (N/mm^2)	Compressive strength after 14 days (N/mm^2)	Compressive strength after 28 days (N/mm^2)
Recipe I	-	16. 6 ± 1.1	19.5 ± 2.3	24.0 ± 1.8
Recipe II	-	16.6 ± 4.2	22.1 ± 4.9	27.3 ± 4.6
Recipe III	-	16.8 ± 1.7	19.5 ± 3.3	23.4 ± 2.9
Recipe IV	-	29.6	35.5	38.5
Recipe A	12.4	16.9 ± 0.4	-	26.0
Recipe B	13.0	18.8 ± 0.2	-	29.3

Table 9.6 shows the compressive strength attained by all mixes presented in Table 9.5 after 3, 7, 14 and 28 days. The difference in strength between Recipes I and II comes (among other factors) from the type of cement used- CEM III/B instead of CEM I and fly ash (details in Section 9.6.1). The fact that CEM III/B decreases the water demand of the mix can account for the increased strength of these samples.
As already mentioned in Section 9.6.1, the only difference between the Recipes III and IV is the type of sand used. For Recipe III, the recycled R1 0-4 sand was used, which increases the water demand of the mix. For Recipe IV, natural sand was used instead of

the recycled sand, in order to show only the influence of the FCG 2-40 aggregates on the mix, rather than the combined influence of the recycled sand and recycled FCG. Using just the FCG 2-40 in combination with natural sand greatly increased the obtained compressive strength, which shows that the FCG 2-40 are suitable for use in concrete mixes.

The results for Recipe B at 7 and 14 days are similar to the ones obtained with Recipes I and III, but with a cement content lowered from a 290 kg/m^3 to 210 kg/m^3 (so a decrease of 27.5%). Fly ash was still used, but the total amount of binder needed in Recipe B still decreased from 370 to 310 kg/m^3. Results at 28 days are better for Recipe B than Recipe A, which is explained by the influence of the used sand. The aim of these last two recipes was to produce a concrete with a minimum 20 N/mm^2 compressive strength at 28 days, which has been even surpassed.

9.6.3 Chemical analysis and metallic Al content

During the FCG 2-40 part of the testing program, cracking and swelling of the samples were observed. However, these were not present in the samples prepared during the FCG 0-8 of the testing program. The explanation is the much higher level of replacement in the FCG 2-40 part, from a maximum of 35% to 100%. The higher addition of FCG caused the swelling and cracking of the concrete specimens, which can be due to a number of reasons.

The cracking was also observed using a Scanning Electron Microscope with a coupled EDAX sensor to detect the present chemical elements. Figure 9.7b shows a magnified crack, clearly originating from one of the burst gas bubbles. The investigation of the sulphur distribution on the same area of the sample did not show a higher concentration in or around the crack, which rules out late ettringite formation as a reason for the crack generation.

Aubert et al. [179] studied the effects of metallic aluminium contained in MSWI fly ashes on cement-based materials. Results showed that the studied ash contains an appreciable amount of metallic aluminium. Swellings were observed on cement pastes and mortars containing ash during the first 24 h of hydration. The causes of this phenomenon were analysed and it was concluded that ettringite formation occurs after the end of the expansion reaction, so metallic aluminium is the sole responsible for the observed swelling. The consequences of swelling were analysed by measuring the compressive strength of mortars, induced cracking leading to a significant decrease of mechanical properties.

The FCG 2-40 bottom ash was split into 4 fractions (0-4 mm, 4-11.2 mm, 11.2-16 mm and 16-32 mm, over 32 mm the volume being very small) and the content of metallic Al analysed. Table 9.7 shows the values found, in mass percentages of Al in dry bottom ash and the water content of each fraction. The determination was made by measuring the generated volume of H_2 (Eq. 7.1.1).

a.  b. 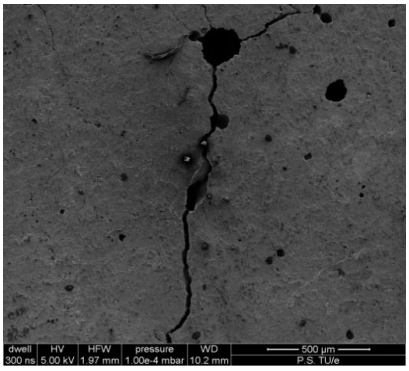

Figure 9.7. a. Macroscopic cracking in the concrete blocks and **b.** the crack propagation observed by SEM.

Table 9.7. Metallic Al content of the FCG 2-40, divided by size fractions.

Fraction (mm)	Al content (% mass)	Water content (% mass)
0-4	0.73±0.03	6.40
4-11.2	0.18±0.07	6.99
11.2-16	0.12±0.03	6.27
16-32	0.03±0.02	5.79

The method was based on the Dutch concept CUR "Bewerkte Avi-Bodemas Als Toeslagmateriaal Voor Beton", and is very similar to the one employed by Aubert et al. [179], who had observed swelling at a content of approximately 0.2% Al. This is a similar value to the one obtained for the 4-11.2 fraction, while the content in Al of the 0-4 fraction exceeds almost 4 times that value.

9.6.4 Leaching results

The leaching of contaminants was measured for the Recipe III (composition from Table 9.5). Table 9.8 shows the results, compared to the maximum accepted values, given by the Dutch Soil Quality Decree (SQR) [28] and mentioned in Table 6.9. For concrete blocks, meeting the "Shaped materials" values is required. The shaped concrete sample with FCG 2-40 mm meets the needed leaching requirement of the Dutch degree. When compared to the non-shaped material requirements (crushed material), leaching results fall almost completely within the norm. The only problem components are barium which is above the limit and copper which is close to the upper limit. Copper can be related to the FCG 2-40 and barium to the 0-4 recycled granulates.

Table 9.8. Leaching data of Recipe III (composition in Table 9.5) which can be compared to the requirements of the SQR [28] from Table 6.9.

Contaminant	**Crushed sample Recipe III (mg/kg d.m.)**	**Shaped sample Recipe III (mg/m^2)**
Antimony (Sb)	0.012	0.84
Arsenic (As)	< 0.05	1.00
Barium (Ba)	42	38.14
Cadmium (Cd)	< 0.001	0.02
Chromium (Cr)	< 0.05	1.00
Cobalt (Co)	0.071	0.60
Copper (Cu)	0.89	1.18
Mercury (Hg)	< 0.0004	0.01
Nickel (Ni)	0.066	1.00
Molybdenum (Mo)	0.27	0.36
Lead (Pb)	0.82	2.01
Selenium (Se)	< 0.007	0.14
Tin (Sn)	< 0.02	0.40
Vanadium (V)	< 0.1	2.01
Zinc (Zn)	< 0.2	4.01
Bromide (Br^-)	3.6	12.45
Chloride (Cl^-)	220	521.93
Fluoride (F^-)	3	24.09
Sulphate (SO_4^{2-})	20	321.19

9.7 Phase 2 FCG 2-20 – pilot test

9.7.1 Concrete design

The bottom ash granulates FCG 2-20 obtained at the end of the treatment (Section 9.2.3) were used in a concrete mix designed for kerb stones to replace 20% of the aggregates.

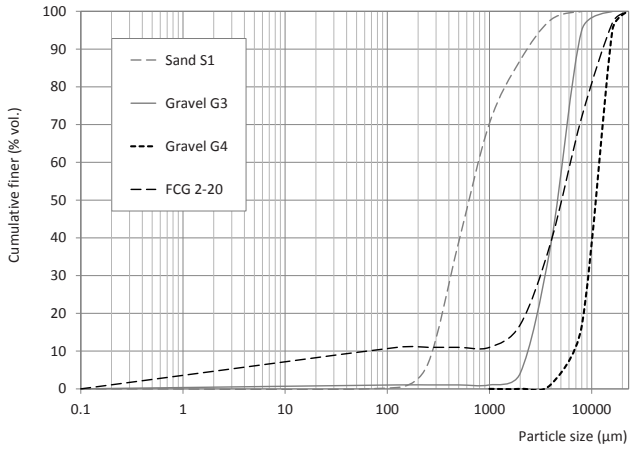

a.

b.

Figure 9.8. a. Particle size distributions of all used aggregates; **b.** The kerb stones produced during the pilot test.

The initial reference mix was composed of 13% cement (a CEM II/A-LL 42.5) and three types of aggregates: a 0-4 mm natural sand (termed N3) and two gravel types, a 2-8 mm (termed G3) and an 8-16 mm (termed G4), shown in Figure 9.8a. The ratio of the aggregates N3:G3:G4 by mass in the reference sample is 1:2:3. Out of the total volume of

the aggregates, 20% was replaced by FCG 2-20, and the recipe adjusted to keep the same cement/aggregates and water/cement ratios.

9.7.2 Mechanical strength results

The kerb stones produced had the dimensions of 1000 x 200 x 100 mm. The total production of this pilot test was of 5.5 m^3 of concrete- about 275 kerb stones. From these elements, cylinders of 100x100 mm were drilled and tested for compressive strength. The flexural strength was tested according to EN 1340 [180], except for the curing requirements.

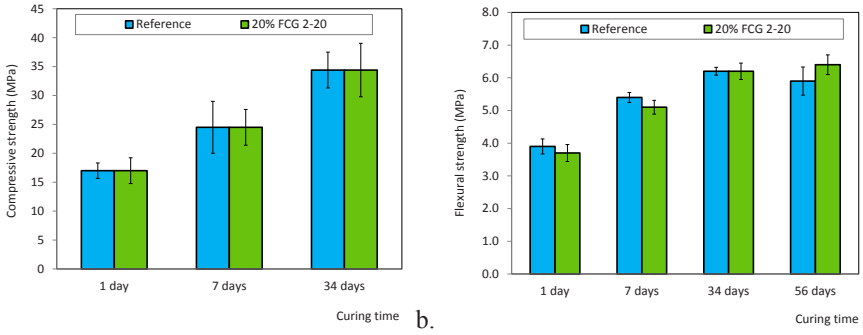

Figure 9.9. a. Compressive and **b.** flexural strength of the hardened samples.

The stones were kept in storage under usual factory conditions (15-18ºC, 47-67% relative humidity) until the test date. Figure 9.9 shows the strength development of the reference sample (termed "reference") and the FCG-containing stones (termed "sample").
At early ages (1 and 7 days), the compressive strength loss of the sample containing 20% vol. FCG was 17-18% of the reference concrete. However, after 35 days, this difference was of only 11%. The flexural strength, which is the most important parameter in the case of kerb stones, had an even more promising behaviour. At early ages, the loss of flexural strength was of only 5.1-5.5%, and after 35 days the FCG-containing kerbs reached the same flexural strength values as the reference concrete. After 56 days, the FCG-sample reached a flexural strength higher with ~ 10% than the reference sample.

9.7.3 Leaching results

The two designed earth moist kerb stone recipes were tested for leaching after 64 days, as required by [28]. Table 9.9 presents the obtained values on both the shaped kerb stones (in mg contaminant/m^2 sample) and the crushed blocks (in mg contaminant/kg sample).
The maximum values required by the SQR [28] can be found in Table 6.9.

Table 9.9. Leaching data of the kerb stones (reference mix and 20% FCG 2-20 mix).

Contaminant	Crushed reference (mg/kg d.m.)	Crushed sample (mg/kg d.m.)	Shaped reference (mg/m^2)	Shaped sample (mg/m^2)
Antimony (Sb)	0.017	0.01	0.4	0.4
Arsenic (As)	< 0.05	< 0.05	4.0	4.0
Barium (Ba)	4.5	6.6	19	20
Cadmium (Cd)	< 0.001	< 0.001	0.1	0.1
Chromium (Cr)	0.1	0.08	4.0	4.0
Cobalt (Co)	0.04	0.04	2.4	2.4
Copper (Cu)	< 0.05	0.33	4.0	4.0
Mercury (Hg)	< 0.0004	< 0.0004	0.0	0.0
Nickel (Ni)	< 0.05	< 0.05	4.0	4.0
Molybdenum (Mo)	0.012	0.021	0.8	0.8
Lead (Pb)	< 0.1	0.82	8.0	8.0
Selenium (Se)	< 0.007	< 0.007	0.6	0.6
Tin (Sn)	< 0.02	< 0.02	1.6	1.6
Vanadium (V)	< 0.1	< 0.099	8.0	8.0
Zinc (Zn)	< 0.2	< 0.2	16	16
Bromide (Br^-)	< 0.5	< 0.5	2	2
Chloride (Cl^-)	18	41	88	80
Fluoride (F^-)	3	3.2	128	96
Sulphate (SO_4^{2-})	30	26	960	960

The fact that the leaching of all contaminants was under the required legal limit, for both the shaped and the crushed samples confirms the fact that the combination of cleaning treatments and incorporation of the FCG 2-20 in a concrete matrix renders the bottom ash granulates as appropriate aggregate for such products.

9.8 Conclusion and discussion

Bottom ashes from Dutch incinerators were investigated in this chapter, with the scope of determining their suitability for use in concrete recipes. The study was divided into three parts, each concentrating on a different batch of bottom ash, generated in separate incinerators and in different years. Moreover, the three materials have undergone different treatment steps before they were tested as aggregate replacement in cement-based building materials. The complex treatment processes, as well as their influence on the removal of unwanted contaminants, were detailed in this chapter. Moreover, each of the three materials was applied as aggregates in concrete recipes.

In the first part of the study, a cleaned bottom ash fraction termed FCG 0-8 mm was applied as sand replacement in concrete recipes. It was shown that, using an optimized particle packing, the FCG 0-8 can be used to replace up to 25% of the sand and gravel in the concrete mix without significant loss of mechanical strength. Due to these promising results, research was continued on concrete scale.

In the second test program, the FCG 2-40 was used in concrete production as 100% replacement of aggregates. Six different mixes were prepared, using two types of cement, a fly ash and two types of sand, together with the FCG 2-40. A method based on particle size engineering was applied in order to improve the initial four mixes. Recipes with low cement content were designed for the FCG 2-40 with very promising results. Further optimization of the water to fines ratio in concrete mixes, together with the use of plasticizer, will be investigated, in order to optimize the replacement of natural aggregates with FCG without loss of mechanical properties. Results are promising, but swelling and cracking have been observed. This has been related to the aluminium content in the FCG 2-40. Further analysis showed that the Al is unevenly distributed in the granulates, so sieving out a fraction of the material could prevent the cracking.

When compared to the requirements of the Dutch standard Soil Quality Decree ("Besluit bodemkwaliteit"), the shaped concrete sample with FCG 2-40 mm meets the needed values. The FCG 2-40 has proven to be a promising replacement aggregate in concrete production. The fact that this is an upgraded secondary material makes it a feasible sustainable alternative to using natural gravel in concrete mixes.

In the third part of this chapter, the FCG has been treated in order to obtain a suitable building material for concrete mixes or prefab elements. Five separate treatment steps were used in order to achieve this, consisting, among others, of particle size separations, washing procedures and the removal of ferrous and non-ferrous metals. The resulting fraction is termed FORZ composite granulates 2-20 (FCG) and contains less than 0.3% non-ferrous metals and less than 0.1% metallic iron. The efficiency of the various treatment steps was investigated through the leaching analysis of the obtained material. Almost all the contaminant leaching values were under the legal limits after the whole treatment process. However, because chlorides and sulphates still had a slightly raised leaching value, the material was used in the production of shaped building blocks. Kerb

stones were produced using a 20% by volume replacement of the aggregates with FCG 2-20. The final aspect of the kerb units did not differ from the reference samples. The compressive strength was slightly lower than expected, which can be explained by the non-standard curing conditions. The low relative humidity during curing has affected the strength of the samples, since at low w/c ratios as employed in this study, the porous samples can easily dry out. Also, the cement used has a slow hydration rate, which will further delay the development of strength. The strength results were extremely positive, with a flexural strength after 35 days of the same level as the reference recipe. After 56 days the flexural strength of the FCG-containing sample reached a flexural strength 10% higher than the reference. This is an indication that the cement content of the recipe can be lowered when using FCG instead of natural aggregates, while keeping the flexural strength of the sample to the same level. The 20% replacement of aggregates is a sustainable option, by reducing the amount of natural sand and gravel and by decreasing the need for cement (and therefore the CO_2 footprint). All in all, the FCG produced from upgraded and treated MSWI bottom ash have proven to be suitable for the use in prefab concrete such as kerb units.

Chapter 10

Conclusions and recommendations

The main objective of this thesis was to combine several research directions in order to evaluate their benefits on improving the properties of cement-based recipes, while focusing on reducing their environmental impact. The durability of concrete is one of such approaches, which was attempted from a more chemical point of view. The traditional study method of the durability of concrete in chloride-exposed environments is through modelling the transport properties of the ions through the pore structure. In this research, the focus was chosen on the chemical and physical interaction mechanisms through which the hydration products can bind chloride ions.

A second approach was considering the reuse of recycled concrete (and thus closing its life cycle) and upgrading its properties through three different methods. The first method was to use smart recycling of concrete through a novel crushing technique in order to obtain an cement paste-enriched recycled concrete fraction and, at the same time, clean aggregates which can be applied in new recipes. The second method was thermally treating the recycled concrete fines in order to activate their hydraulic properties. Finally, the third method was blending the obtained optimized recycled concrete fines Portland cement and various pozzolanic materials in order to achieve the highest cement replacement level while retaining the initial mechanical properties of the mix or even surpass them.

The third considered method for lowering the environmental impact of concrete was the replacement of Portland cement and natural aggregates by industrial by-products. The focus was chosen on by-products of the incineration processes, which also have the advantage of producing clean energy- the more sustainable alternative. Such by-products which were investigated are bio-energy fly ashes from biomass incineration, paper sludge fly ash from the paper recycling process and municipal solid waste incineration ashes. Their application required investigating treatment options for removing certain unwanted contaminants, while at the same time upgrading the properties of these materials for their use in cement-based mixtures.

The more detailed conclusions of these three approaches will be detailed in the following sections.

10.1 The chloride binding ability of cement pastes

The chloride binding of hydrated pastes can be related to the individual binding ability of several steps: C−S−H, monosulphate, hydroxy-AFm, AFt, portlandite and Friedel's

salt. Each of these steps has the capacity to bind chlorides through either a chemical ion exchange or a physical process of adsorption on their surface. The first system to be studied was hydrated Ordinary Portland Cement (OPC), being the most produced binder worldwide. A number of factors were taken into consideration: oxide composition of the OPC, curing age, curing conditions, water/binder ratio. Based on these, the step assemblage of the hydration products was estimated in order to relate their amounts to the bound chlorides quantities.

Chloride binding isotherms were used to quantify the chloride binding ability of each hydrated step. A new isotherm is given for the AFm step, based on an extensive literature review. Similarly, a new relation is also proposed for $C-S-H$, taking into consideration the C_3S/C_2S ratio of the OPC. An extended model is also elaborated to include the contribution of other hydrated steps. A large range of external chloride concentrations was considered in order to cover the conditions of marine environments, salty lakes and the use of de-icing salts.

The final model made possible the evaluation of the contribution of each hydration product to the total bound chlorides quantity of the paste. The contribution of $HO-AFm$ was found to be the greatest for all considered external chloride concentrations, ranging from 60% at low concentrations to 30% at high ones. The contribution of $C-S-H$ is found to be lower, but almost constant throughout the whole external chlorides concentration, between 25 and 28% of the total bound chlorides. It can be concluded that, from an OPC composition point of view, a high aluminates content is beneficial for the chloride binding ability of the paste. At lower external chloride concentrations, for instance in coastal areas, the C_3A content is the most important parameter, while at higher concentrations, in salty lakes for example, the sulphate content of the OPC becomes of interest.

This model has also been extended to ground blast furnace slag-blended cements, as these are the most used within the Netherlands. In this case, the composition of the slag and its percentage in the cement blend are key factors in estimating the chloride binding ability of the hydrated pastes. The incorporation of alumina into the $C-S-H$ structure is also considered in this model, together with the variation of the C/S ratio of the $C-S-A-H$ step. The conclusions regarding the contribution of each step are different than the initial OPC model. While the A/S ratio of the initial slag plays an important role, it can be concluded that the $C-S-A-H$ step is responsible for binding approximately 67% of the chlorides, the rest being attributed to the AFm steps. The sulphate content of the slag is also found to play an important role, making the selection of the slag composition a crucial factor for increasing the total chloride binding capacity of the blended paste.

10.2 Concrete recycling and reuse

This part of the research focused on the concrete recycling process, by first considering the crushing method and its optimization. For this purpose, laboratory-made concrete was

crushed using a conventional jaw crusher, either directly or through multiple crushing cycles. A novel crusher prototype, termed the Smart Crusher, was employed for the same purpose, and the obtained material from these three methods was analysed and compared. During this study, a new method of quantifying the α-quartz content of the samples using a calibrated DSC signal was developed. The method was proven to be accurate by validating against XRF and XRD results, its relative error being under a few percentage. This is a fast method to determine the aggregate content of crushed concrete fractions; it is easy to implement and reliable, and has already been selected as quality control measure for a real-scale crushing installation. Also, an alternative method based on the specific density of the fraction has been developed.

A first conclusion of this part of the study is that, using the improved crushing technique, the recovery of the cement paste can be increased by 50%. At the same time, the obtained aggregates are cleaned of the attached mortar and more suitable for the re-use in concrete mixes. The use of recycled concrete sand obtained through this method leads to the same mechanical properties of mortars as in the case of the use of standard natural sand, while showing an increased early strength development.

Extending the research in the direction of the recycled concrete fines (RCF) obtained through smart crushing, a thermal treatment method was developed and optimized in order to increase the potential of this material. The results suggest that RCF treated at 800°C forms a calcium silicate step similar to the one in cement. Blending treated RCF with cement leads to mechanical properties of the mixes similar to the ones achieved by commercial fly ash-cement blends. Another interesting use of the RCFs was proven to be the activation of slag in RCF-slag-cement blends, which leads to better hardened properties.

10.3 The use of incineration by-products as building materials

In this research direction, a number of incineration by-products have been selected for treatment and application in cement-based recipes. The first of these were bio-energy fly ashes, collected from the boiler and cyclone of two Dutch biomass incineration facilities. A second type was paper sludge fly ash, which is the by-product of paper sludge incineration. A third type of material was Municipal Solid Waste Incineration (MSWI) ashes/slags.

The use of such materials is legislated in terms of environmental impact, which is quantified by the amount of leached contaminants through a standard test. In order to conform to these legal norms, most of these materials need to undergo pre-processing before being usable as building materials. The exception is the paper sludge fly ash, which is mostly contaminant-free, but poses other compositional challenges as an addition in cement-based mixtures.

A number of treatment options were investigated for each of these materials and their effects characterized through analytical techniques. The final optimized materials were

then tested in cement-based mixes. A few of the conclusions of these studies will be summarized here.
The bio-energy fly ashes were found to have a very different composition than coal combustion fly ash. Besides containing unburnt matter and a large amount of unwanted contaminants (heavy metals and salts such as chlorides and sulphates), their physical properties such as particle size and particle structure are different. A series of treatment steps- unburnt matter removal through air filtering or thermal treatment, washing using several liquid/solid ratios, shaking speeds, temperatures and treatment times, as well as a separate thermal treatment followed by grinding were analysed for their efficiency. Each of the bio-energy fly ashes was optimized using a combination of these treatment options in order to comply with both the environmental and building materials standards. Applying the final materials in cement-based mixes has shown that this new type of fly ash also presents pozzolanic properties and, when properly treated, can be used as a beneficial addition in mortars.
The investigated paper sludge fly ash comes from an already-optimized burning process that maximizes its potential as addition in concrete mixes. However, its high free lime content implies also a high water demand, which needs to be lowered. Two options for the increase of the use of this material were investigated- lowering its free lime content and blending with other supplementary cementitious materials such as fly ashes and recycled concrete fines. This part of the study brought together the use of a number of the investigated fine materials and has shown the benefit of their mixing in new recipes.
MSWI bottom ash was successfully applied in both ready-mix and earth-moist concrete recipes. A replacement level of 20% of natural aggregates lead to obtaining kerb stones with even improved flexural strength when compared to the reference recipe. Moreover, normally vibrated concrete recipes with reduced cement content incorporating large amounts of MSWI bottom ash were designed and proven to attain even better mechanical properties than the reference mixtures.

10.4 Recommendations for further research

This thesis has shown the benefits of combining various approaches in lowering the environmental impact of concrete and other cement-based mixtures. Further research topics which have emerged while conducting this study are summarized below.

1. The chloride binding modelling can be extended in two directions. The first logical continuation would be the investigation of the influence of fly ashes addition to the cement blend. Other supplementary cementitious materials, for instance recycled concrete fines, could also increase the chloride binding ability of cement-based blends and should be taken into consideration.
2. This research focused on the intrusion of chlorides from external media intro hardened pastes; the transition to the modelling of the internally mixed chlorides is the next logical

step. The benefits of such a model would extend to the chloride immobilization capacity of various cement-based blends, which would be useful when considering pozzolanic materials such as bio-energy fly ashes, which have a high chloride content.

3. The ability of hydrated cement pastes to bind other ions, such as alkalis, other halogens besides chlorides, or sulphates, can be investigated. The influence of supplementary cementitious materials such as ground granulated blast furnace slag or pulverized coal combustion fly ash on the binding of such ions could be estimated using binding isotherms.

4. Further investigation regarding the benefits of smart crushing of concrete should be conducted; the modelling of the crushing process and its influence on the properties of the obtained fractions would lead to obtaining materials optimized for the re-use in concrete mixes. Materials generated by the industrial scale Smart Crusher, recently commissioned, could be employed for this purpose.

5. The use of recycled concrete fines as clinker-kiln feed should be considered; the composition of this material is similar to the needed mix and has the advantage of not being carbonated, which would greatly lower the CO_2 generation of clinker production.

6. The optimization of the incineration process of a number of materials- biomass, municipal solid waste etc. - would lead to cleaner by-products, which would be easily applicable as building materials instead of being landfilled. The modelling of the incineration process and the influence of the waste feed would be useful in this direction.

7. Optimizing and implementing treatment lines (sieving, washing, removing of unburnt particles etc.) after the incineration processes would also contribute greatly to the quality of the incineration by-products, increasing their re-use as concrete constituents while at the same time ensuring their complying with existing environmental legislation.

8. A number of recycling and incineration by-products could have the potential be used as binders (either as cement replacement, or even as part of a geopolymer system), given a proper activation method. Such methods, which can be physical (thermal treatment, grinding etc.) or chemical (using activators or engineering their oxide composition to better mimic that of already-established secondary binders or even cements) merit further attention.

Bibliography

[1] Cement Association of Canada. [Online] Available at: http://ecosmartconcrete.com/?page_id=208 (2013).

[2] Marceau, M. L., Nisbet, M. A. & Van Geem, M. G. *Life Cycle Inventory of Portland Cement Concrete*. (2007).

[3] The European Cement Association. [Online] Available at: http://www.cembureau.eu/about-cement/key-facts-figures (2013).

[4] *Trends in Global CO_2 emissions 2012 report, PBL Netherlands Environmental Assesment Agency*. (2012).

[5] *Landfill Ban Decree - Besluit stortplaatsen en stortverboden afvalstoffen,VROM, Den Haag: Ruimte en Milieu. Ministerie van Volkshuisvesting, Ruimtelijke Ordeling en Milieubeheer.* (2012).

[6] Banse, M., Faaij, A., Hoefnagels, R. & Dornburg, V. Economic impact of large-scale deployment of biomass resources in the Netherlands. *12th Annu. Conf. Glob. Econ. Anal.* (2009).

[7] *Central Bureau voor de Statistiek, Renewable electricity 1991-2010, Den Haag*. (2011).

[8] Tam, V. W. Comparing the implementation of concrete recycling in the Australian and Japanese construction industries. *J. Clean. Prod.* **17**, 688–702 (2009).

[9] World Business Council for Sustainable Development, Concrete Recycling: The cement sustainability initiative. [Online] Available at: http://www.wbcsdcement.org/pdf/CSI-RecyclingConcrete-FullReport.pdf. (2009).

[10] Oikonomou, N. D. Recycled concrete aggregates. *Cem. Concr. Compos.* **27**, 315–318 (2005).

[11] EN 197-1 Cement – Part 1: Composition, specifications and conformity criteria for common cements. (2000).

[12] Neville, A. M. *Properties of Concrete*. (Pearson Education Limited: Edinburgh, 2002).

[13] Illston, J. M. & Domone, P. L. J. *Construction Materials, Their nature and behaviour.* (Taylor & Francis e-Library: New York, 2001).

[14] EN 15167-1 Ground granulated blast furnace slag for use in concrete, mortar and groutDefinitions, specifications and conformity criteria. (2006).

[15] ASTM C989 Standard specification for slag cement for use in concrete and mortars. (2001).

[16] Bernal, S. A., Mejía de Gutiérrez, R., Provis, J. L., Rodríguez, E. D. & Delvasto, S. Effect of binder content on the performance of alkali-activated slag concretes. *Cem. Concr. Res.* **41**, 1 (2011).

[17] Joshi, R. C. & Lohtia, R. P. *Fly ash in concrete: production, properties and uses*. (Gordon & Breach Science: 1997).

[18] *National Energy Technology Laboratory, History of coal use. [Online] Available at: http://www.netl.doe.gov/keyissues/historyofcoaluse.html (2011)*.

[19] *Dpcleantech. Biomass and waste to energy solution. [Online] Available at: http://www.dpcleantech.com/about-dpcleantech/past-a-future (2011)*.

[20] *CDEM. Company overview, Our History. [Online] Available at: http://www.cdem.nl/node/13 (2011).*

[21] Herbert, L. *The charted institution of waste management. [Online] Available at: http://www.ciwm.co.uk/web/FILES/About%20CIWM/100%20yrs%20London%20and%20SE%20center.pdf*. (2011).

[22] Tenerbaum, D. J. Recycling: Building on Fly Ash Waste. *Environ. Heal. Perspect.* **115**, A22 (2007).

[23] CUR 1992 *Vliegas als vulstof in beton. Gouda: Civieltechnisch Centrum Uitvoering Research en Regelgeving.*

[24] Vliegasunie *Jaarverslag Vliegasunie 2007*. 28 (2008).

[25] EN 450 Fly ash for concrete. Definition, specifications and conformity criteria. (2012).

[26] ASTM C618 Standard Specification for Coal Fly Ash and Raw or Calcined Natural Pozzolan for Use in Concrete. (2001).

[27] EN 12457 Characterisation of waste - Leaching - Compliance test for leaching of granular waste materials and sludges. (2002).

[28] *Soil Quality Regulation - Regeling bodemkwaliteit, VROM, Den Haag: Ruimte en Milieu. Ministerie van Volkshuisvesting, Ruimtelijke Ordeling en Milieubeheer.* (2013).
[29] EN 196-1 Methods of testing cement. Determination of strength. (2005).
[30] Neville, A. M. Chloride attack of reinforced concrete: an overview. *Mater. Struct.* **28**, 63–70 (1995).
[31] Justnes, H. A Review of Chloride Binding in Cementitious Systems, Cement and concrete. *Nord. Concr. Res.* **21**, 1–6 (1996).
[32] Yuan, Q., Shi, C., De Schutter, G., Audenaert, K. & Deng, D. Chloride binding of cement-based materials subjected to external chloride environment – A review. *Constr. Build. Mater.* **23**, 1–13 (2009).
[33] Ehtesham Hussain, S. & Al-Gahtani, A. S. Influence of sulfates on chloride binding in cements. *Cem. Concr. Res.* **24**, 8–24 (1994).
[34] Suryavanshi, A. K., Scantlebury, J. D. & Lyon, S. B. Mechanisms of Friedel's Salt Formation in Cements Rich in Tricalcium Aluminate. *Cem. Concr. Res.* **26**, 717–727 (1996).
[35] Arya, C., Buenfeld, N. R. & Newman, J. B. Factors influencing chloride-binding in concrete. *Cem. Concr. Res.* **20**, 291–300 (1990).
[36] Larsen, C. K. Chloride Binding in Concrete-Effect of Surrounding Environment and Concrete Composition, PhD thesis, The Norwegian University of Science and Technology. (1998).
[37] Zibara, H. Binding of External Chloride by Cement Pastes, PhD Thesis, University of Toronto. (2001).
[38] Luping, T. & Nilsson, L.-O. Chloride binding capacity and binding isotherms of OPC pastes and mortars. *Cem. Concr. Res.* **23**, 247–253 (1993).
[39] Al-Hussaini, M. J., Sangha, C. M., Plunkett, B. A. & Walden, P. J. The effect of chloride ion source on the free chloride ion percentages in OPC mortars. *Cem. Concr. Res.* **20**, 739–745 (1990).
[40] Tritthart, J. Chloride binding in cement I. Investigations to determine the composition of porewater in hardened cement. *Cem. Concr. Res.* **19**, 586–594 (1989).
[41] Neville, A. M. *Properties of Concrete: Fourth and Final Edition*. (Wiley: 1996).
[42] Spiesz, P. & Brouwers, H. J. H. Influence of the applied voltage on the Rapid Chloride Migration (RCM) test. *Cem. Concr. Res.* **42**, 1072–1082 (2012).
[43] Spiesz, P., Ballari, M. M. & Brouwers, H. J. H. RCM: A new model accounting for the non-linear chloride binding isotherm and the non-equilibrium conditions between the free- and bound-chloride concentrations. *Constr. Build. Mater.* **27**, 293–304 (2012).
[44] Spiesz, P. & Brouwers, H. J. H. The apparent and effective chloride migration coefficients obtained in migration tests. *Cem. Concr. Res.* **48**, 116–127 (2013).
[45] Jin, Z., Sun, W., Zhang, Y., Jiang, J. & Lai, J. Interaction between sulfate and chloride solution attack of concretes with and without fly ash. *Cem. Concr. Res.* **37**, 1223–1232 (2007).
[46] Mohammed, T. U. & Hamada, H. Relationship between free chloride and total chloride contents in concrete. *Cem. Concr. Res.* **33**, 1487–1490 (2003).
[47] Sandberg, P. Studies of chloride binding in concrete exposed in a marine environment. *Cem. Concr. Res.* **29**, 473–477 (1999).
[48] Ekolu, S. O., Thomas, M. D. A. & Hooton, R. D. Pessimum effect of externally applied chlorides on expansion due to delayed ettringite formation: Proposed mechanism. *Cem. Concr. Res.* **36**, 688–696 (2006).
[49] Theissing, E., Hest-Wardenier, P. & de Wind, G. The combining of sodium chloride and calcium chloride by a number of different hardened cement pastes. *Cem. Concr. Res.* **8**, 683–691 (1978).
[50] Delagrave, A., Marchand, J., Ollivier, J. P., Julien, S. & Hazrati, K. Chloride binding capacity of various hydrated cement paste systems. *Adv. Cem. Based Mater.* **6**, 28–35 (1997).
[51] Csizmadia, J., Balázs, G. & Tamás, F. D. Chloride ion binding capacity of aluminoferrites. *Cem. Concr. Res.* **31**, 577–588 (2001).
[52] Kuzel, H. & Pöllmann, H. Hydration of C_3A in the presence of $Ca(OH)_2$, $CaSO_4 \cdot 2H_2O$ and $CaCO_3$. *Cem. Concr. Res.* **21**, 885–895 (1991).
[53] Luo, R., Cai, Y., Wang, C. & Huang, X. Study of chloride binding and diffusion in GGBS concrete. *Cem. Concr. Res.* **33**, 1–7 (2003).
[54] Arya, C. & Xu, Y. Effect of cement type on chloride binding and corrosion of steel in concrete. *Cem. Concr. Res.* **25**, 893–902 (1995).

[55] Glasser, F. P., Kindness, A. & Stronach, S. A. Stability and solubility relationships in AFm phases: Part I. Chloride, sulfate and hydroxide. *Cem. Concr. Res.* **29**, 861–866 (1999).
[56] Matschei, T., Lothenbach, B. & Glasser, F. P. The AFm phase in Portland cement. *Cem. Concr. Res.* **37**, 118–130 (2007).
[57] Hirao, H., Yamada, K., Takahashi, H. & Zibara, H. Chloride Binding of Cement Estimated by Binding Isotherms of Hydrates. *J. Adv. Concr. Technol.* **3**, 77–84 (2005).
[58] Birnin-Yauri, U. A. & Glasser, F. P. Friedel's salt, $Ca_2Al(OH)_6(Cl,OH)\cdot 2H_2O$: its solid solutions and their role in chloride binding. *Cem. Concr. Res.* **28**, 1713–1723 (1998).
[59] Elakneswaran, Y., Nawa, T. & Kurumisawa, K. Electrokinetic potential of hydrated cement in relation to adsorption of chlorides. *Cem. Concr. Res.* **39**, 340–344 (2009).
[60] Hewlett P. *Lea's Chemistry of Cement and Concrete*. (Butterworth-Heinemann: 2004).
[61] Brouwers, H. J. H. The work of Powers and Brownyard revisited: Part 1. *Cem. Concr. Res.* **34**, 1697–1716 (2004).
[62] Brouwers, H. J. H. The work of Powers and Brownyard revisited: Part 2. *Cem. Concr. Res.* **35**, 1922–1936 (2005).
[63] Bentz, D. P. Influence of water-to-cement ratio on hydration kinetics: Simple models based on spatial considerations. *Cem. Concr. Res.* **36**, 238–244 (2006).
[64] Taylor, H. W. F. *Cement Chemistry*. (Academic Press Ltd.: London, 1992).
[65] Brouwers, H. J. H. *A hydration model of Portland cement using the works of Powers and Brownyard, Eindhoven University of Technology & Portland Cement Association. ISBN: 978-90-6814-184-9, Available on http://www.cement.org, 2011.*
[66] Beaudoin, J. J., Ramachandran, V. S. & Feldman, R. F. Interaction of chloride and C-S-H. *Cem. Concr. Res.* **20**, 875–883 (1990).
[67] Nagataki, S., Otsuki, N., Wee, T. & Nakashita, K. Condensation of Chloride Ion in Hardened Cement Matrix Materials and on Embedded Steel Bars. *ACI Mater. J.* **90**, 323–332 (1993).
[68] Wowra, O. & Setzer, M. J. *Frost Resistance of Concrete*. 147–153 (Taylor and Francis: 1997).
[69] Nielsen, E. P. The durability of white portland cement to chemical attack. (2004).
[70] Balonis, M., Lothenbach, B., Le Saout, G. & Glasser, F. P. Impact of chloride on the mineralogy of hydrated Portland cement systems. *Cem. Concr. Res.* **40**, 1009–1022 (2010).
[71] Glasser, F. P. Role of chemical binding in diffusion and mass transport. *Int. Conf. Ion Mass Transp. Cem. Mater.* (1996).
[72] Puntnis, C. V., Tsukamoto, K. & Nishimura, Y. Direct observations of pseudomorphism: compositional and textural evolution at a fluid–solid interface. *Am. Mineral.* **90**, 1909–1912 (2005).
[73] Jawed, I., Skalny, J. & Young, J. F. *Structure and performance of cements*. (Applied Science Publishers Ltd: Esses, 1983).
[74] Chatterji, S. & Kawamura, M. Electrical double layer. Ion transport and reactions in hardened cement paste. *Cem. Concr. Res.* **22**, 774–782 (1992).
[75] Laidler, K. J. & Meiser, J. H. *Physical Chemistry*. (The Benjamin Cummings Publishing Company:).
[76] Bockris, J., Conway, B. E. & Yeager, E. *The Double Layer*. (Plenum Press: New York, 1980).
[77] Helmholtz, H. V. Uber einige Gesetze der Vertheilung elektrischer Strome in korperlichen Leitem, mit Anwendung auf die thierischelektrischen Versuche. *Ann. Der Phys. Und Chemie* **89**, 211–233 (1853).
[78] Gouy G. Sur la constitution de la charge électrique a la surface d'un électrolyte. *J. Phys.* **4**, 457 (1910).
[79] Stern, O. The theory of the electrolytic double-layer. *Z. Elektrochem.* **30**, (1924).
[80] Guldbrand, L., Jönsson, B., Wennerström, H. K. & Linse, P. Electrical double layer forces. A Monte Carlo study. *J. Chem. Phys.* **80**, 2221–2228 (1984).
[81] Kjellander, R. & Marcelja, S. Attractive doublelayer interactions between calcium clay particles. *J. Colloid Interface Sci.* **126**, 194–211 (1988).
[82] Henocq, P. Modeling Ionic Interactions on the Surface of Calcium Silicate Hydrates. (2005).
[83] Grahame, D. C. Tte electrical double layer and the theory of electrocapillarity. *Chem. Rev.* **41**, 441–501 (1947).
[84] Nguyen, T. Q. Modélisations physico-chimiques de la pénétration des ions chlorures dans les matériaux cimentaires, PhD Thesis, L'Ecole Nationale Des Ponts Et Chaussees. (2007).

[85] Dhir, R. K., El-Mohr, M. A. K. & Dyer, T. D. Chloride binding in GGBS concrete. *Cem. Concr. Res.* **26**, 1767–1773 (1996).
[86] Xu, Y. The influence of sulphates on chloride binding and pore solution chemistry. *Cem. Concr. Res.* **27**, 1841–1850 (1997).
[87] Chen, W. & Brouwers, H. J. H. The hydration of slag, part 1: reaction models for alkali-activated slag. *J. Mater. Sci.* **42**, 428–443 (2006).
[88] Chen, W. & Brouwers, H. J. H. The hydration of slag, part 2: reaction models for blended cement. *J. Mater. Sci.* **42**, 444–464 (2006).
[89] Taylor, R., Richardson, I. G. & Brydson, R. M. D. Composition and microstructure of 20-year-old ordinary Portland cement–ground granulated blast-furnace slag blends containing 0 to 100% slag. *Cem. Concr. Res.* **40**, 971–983 (2010).
[90] Escalante, J. I., Gomez, L. Y., Mendoza, G., Mancha, H. & Mendez, J. Reactivity of blast-furnace slag in Portland cement blends hydrated under different conditions. *Cem. Concr. Res.* **31**, 1403–1409 (2001).
[91] Hill, J. & Sharp, J. H. The mineralogy and microstructure of three composite cements with high replacement levels. *Cem. Concr. Compos.* **24**, 191–199 (2002).
[92] Lothenbach, B., Scrivener, K. & Hooton, R. D. Supplementary cementitious materials. *Cem. Concr. Res.* **41**, 1244–1256 (2011).
[93] Florea, M. V. A. & Brouwers, H. J. H. Chloride binding related to hydration products. *Cem. Concr. Res.* **42**, 282–290 (2012).
[94] Revertegat, E., Richet, C. & Gégout, P. Effect of pH on the durability of cement pastes. *Cem. Concr. Res.* **22**, 259–272 (1992).
[95] Richardson, I. G., Brough, A. R., Groves, G. W. & Dobson, C. M. The characterization of hardened alkali-activated blast-furnace slag pastes and the nature of the calcium silicate hydrate (C-S-H) phase. *Cem. Concr. Res.* **24**, 813–829 (1994).
[96] Adolfsson, D., Robinson, R., Engström, F. & Björkman, B. Influence of mineralogy on the hydraulic properties of ladle slag. *Cem. Concr. Res.* **41**, 865–871 (2011).
[97] Puertas, F., Varela, M. T. B. & Domínguez, R. Hydration of $4CaO.Al_2O_3.Mn_2O_3$ in the absence and the presence of gypsum. A comparative study with the hydration of $4CaO.Al_2O_3.Fe_2O_3$. *Cem. Concr. Res.* **23**, 20–32 (1993).
[98] Stöber, S., Redhammer, G., Schorr, S., Prokhnenko, O. & Pöllmann, H. Structure refinements of members in the brownmillerite solid solution series $Ca_2Al_x(Fe_{0.5}Mn_{0.5})_{2-x}O_{5+\delta}$ with $1/2 \leq x \leq 4/3$. *J. Solid State Chem.* **197**, 420–428 (2013).
[99] Richardson, I. G. & Cabrera, J. G. The nature of C-S-H in model slag-cements. *Cem. Concr. Compos.* **22**, 259–266 (2000).
[100] Lumley, J. S., Gollop, R. S., Moir, G. K. & Taylor, H. F. W. Degrees of reaction of the slag in some blends with Portland cements. *Cem. Concr. Res.* **26**, 139–151 (1996).
[101] Kayali, O., Khan, M. S. H. & Ahmed, M. S. The role of hydrotalcite in chloride binding and corrosion protection in concretes with ground granulated blast furnace slag. *Cem. Concr. Compos.* **34**, 936–945 (2012).
[102] Ben Haha, M., Lothenbach, B., Le Saout, G. & Winnefeld, F. Influence of slag chemistry on the hydration of alkali-activated blast-furnace slag — Part I: Effect of MgO. *Cem. Concr. Res.* **41**, 955–963 (2011).
[103] Viallis-Terrisse, H. Interaction des Silicates de Calcium Hydratés, principaux constituants du ciment, avec les chlorures d'alcalins. Analogie avec les argiles, PhD Thesis, 1 Université de Bourgogne. (2000).
[104] Chen, W. Hydration of Slag Cement-Theory, Modeling and Application, PhD Thesis, University of Twente. (2006).
[105] Hansen, T. C. *Recycling of Demolished Concrete and Masonry*. (Chapman and Hall: RILEM report 6.: 1992).
[106] Hansen, T. & Lauritzen, E. Concrete waste in a global perspective, recycling concrete and other materials for sustainable development. *Am. Concr. Inst.* 35–45 (2004).
[107] Meyer, C. The greening of the concrete industry. *Cem. Concr. Compos.* **31**, 601–605 (2009).
[108] *Cement Sustaibability Initiative-Recycling Concrete. Geneva: World Business Council for Sustainable Development.* (2011).

[109] Etxeberria, M., Vazquez, E., Mari, A. & Barra, M. Influence of amount of recycled coarse aggregates and production process on properties of recycled aggregate concrete. *Cem. Concr. Res.* **37**, 735–742 (2007).
[110] Kou, S. & Poon, C. Properties of self-compacting concrete prepared with coarse and fine recycled concrete aggregates. *Cem. Concr. Compos.* **31**, 622–627 (2009).
[111] Padmini, A., Ramamurthy, K. & Mathews, M. Influence of parent concrete on the properties of recycled aggregate concrete. *Constr. Build. Mater.* **23**, 829–836 (2009).
[112] Lo, C., Kotrayothar, D., Tam, V. W. & Loo, Y. Comparison of recycled and natural aggregate properties. *3rd ACF Int. Conf.* 450–454 (2008).
[113] Corinaldesi, V., & Moriconi, G. Influence of mineral additions on the performance of 100% recycled aggregate concrete. *Constr. Build. Mater.* **23**, 2869–2876 (2009).
[114] Evangelista, L. & de Brito, J. Mechanical behaviour of concrete made with fine recycled concrete aggregates. *Cem. Concr. Compos.* **29**, 397–401 (2007).
[115] Sagoe-Crentsil, K., Brown, T. & Taylor, A. Performance of concrete made with commercially produced coarse recycled concrete aggregate. *Cem. Concr. Res.* **31**, 707–712 (2001).
[116] Shi-Cong, K. & Chi-Sun, P. Properties of concrete prepared with crushed fine stone, furnace bottom ash and fine recycled aggregate as fine aggregates. *Constr. Build. Mater.* **23**, 2877–2886 (2009).
[117] Meyer, C. The greening of the concrete industry. *Cem. Concr. Compos.* **31**, 601–605 (2009).
[118] Khatib, J. Properties of concrete incorporating fine recycled aggregate. *Cem. Concr. Res.* **35**, 763–769 (2005).
[119] Kim, H.-Y., Chun, B.-S., Park, T.-H. & Ryou, J.-S. An investigation of the recycling of waste concrete as a cementitious material. *J. Ceram. Process. Res.* **12**, 202–206 (2011).
[120] Sim, J. & Park, C. Compressive strength and resistance to chloride ion penetration and carbonation of recycled aggregate concrete with varying amount of fly ash and fine recycled aggregate. *Waste Manag.* **31**, 2352–2360 (2011).
[121] Hüsken, G. & Brouwers, H. J. H. Earth-moist concrete: application of a new mix design concept. *Cem. Concr. Res.* **38**, 1246–1259 (2009).
[122] EN 12390-3 Testing hardened concrete. Compressive strength of test specimens. (2009).
[123] Ning, Z. *Thermal Treatment of Recycled Concrete Fines*. (MSc Thesis, Eindhoven University of Technology: 2012).
[124] Schenk, K. J. WO 2011/142663. (2011).
[125] EN 933-1 Tests for geometrical properties of aggregates. Determination of particle size distribution. Sieving method. (2012).
[126] *Cement Sustaibability Initiative-Recycling Concrete. Geneva: World Business Council for Sustainable Development*. (2009).
[127] Husain, A. & Assas, M. M. Utilization of Demolished Concrete Waste for New Construction. *World Acad. Sci. Eng. Technol.* **73**, (2013).
[128] Li, X. 2008 Recycling and reuse of waste concrete in China: Part I. Material behaviour of recycled aggregates concrete. *Resour. Conserv. Recycl.* **53**, 36–44 (2008).
[129] Shui, Z., Xuan, D., Wan, H. & Cao, B. Rehydration reactivity of recycled mortar from concrete waste experienced to thermal treatment. *Constr. Build. Mater.* **22**, 1723–1729 (2008).
[130] Castello, M., Alonso, C., Andrade, C., Turrillas, X. & Campo, J. Composition and microstructural changes of cement pastes upon heating, as studied by neutron diffraction. *Cem. Concr. Res.* **34**, 1611–1644 (2004).
[131] Alonso, C. & Fernandes, L. Dehydration and rehydration processes of cement paste exposed to high temperature environments. *J. Mater. Sci.* **39**, 3015–3024 (2004).
[132] Handoo, S. & Agarwal, S. Physicochemical, mineralogical, and morphological characteristics of concrete exposed to elevated temperatures. *Cem. Concr. Res.* **32**, 1009–1018 (2002).
[133] Tayyib, A. The effect of thermal cycling on the durability of concrete made from local materials in the Arabian Gulf countries. *Cem. Concr. Res.* **19**, 131–142 (1989).
[134] Shui, Z., Xuan, D., Chen, W., Yu, R. & Zhang, R. Cementitious characteristics of hydrated cement paste subjected to various dehydration temperatures. *Constr. Build. Mater.* **23**, 531–537 (2009).
[135] Shui, Z., Yu, R. & Dong, J. Activation of fly ash with dehydrated cement paste. *ACI Mater. J.* **108**, 108–112 (2011).

[136] Alarcon-Ruiz, L., Platret, G., & Massieu, E. The use of thermal analysis in assessing the effect of temperature on a cement paste. *Cem. Concr. Res.* **35**, 609–613 (2005).
[137] Snellings, R., De Schepper, M., De Buysser, K., Van Driessche, I. & De Belie, N. Clinkering Reactions During Firing of Recyclable Concrete. *J. Am. Ceram. Soc.* **95**, 1741–1749 (2012).
[138] Illston, J., & Domone, P. *Construction Materials - their nature and behaviour*. (Spon Press: London, 2001).
[139] EN 1015-3 *Methods of test for mortar for masonry. Determination of consistence of fresh mortar (by flow table)*. (2007).
[140] HVC *Publicatie [Online] Available at: http://www.hvcgroep.nl/over_hvc/publicatie*. (2009).
[141] *DWMA. Jaarverslag 2009. Monitioring resstoffen van de verbranding van afval, biomassa zuiveringsslib [Monitoring residues from incineration of waste, biomass and sewage sludge]. Annual report.Bunnik. Libertas Dutch Waste Managment Association*. (2010).
[142] *National Waste Management Plan, "Landelijk afvalbeheerplan" 2009-2021. Naar een materiaalketenbeleid,VROM, Den Haag: Ruimte en Milieu. Ministerie van Volkshuisvesting, Ruimtelijke Ordeling en Milieubeheer.* (2010).
[143] Doudart de la Gree, G. C. H. Physical-chemical upgrading and use of bio-energy fly ashes as building material in the concrete industry, MSc Thesis, Eindhoven University of Technology. (2012).
[144] Joshi, R. C. Pozzolanic reaction in synthetic fly ashes, PhD Dissertation, Iowa State University. (1970).
[145] Joshi, R. C. & Marsh, B. K. Some Physical, Chemical and Mineralogical Properties of Some Canadian Fly Ashes. *MRS Proc.* **8**, 113–25 (1986).
[146] EN 12880 Characterization of sludges. Determination of dry residue and water content. (2000).
[147] EN 196-2 Methods of testing cement. Chemical analysis of cement. (2005).
[148] Heiri, O., Lotter, A. F. & Lemcke, G. Loss on ignition as a method for estimating organic and carbonate content in sediments: reproducibility and comparability of results. *Paleolimnology* **25**, 101–10 (2001).
[149] Van den Berg, P. *Beton technologie voor onderwijs en praktijk. Betonvereniging / Cement & Beton Centrum*. (2006).
[150] NEN 5950 Voorschriften Beton Technologie - Eisen, vervaardiging en keuring. (1995).
[151] van Eijk, R. J. *Hydration of cement mixtures containing contaminants.* (University of Twente, 2001).
[152] Yudovich, Y. E. & Ketris, M. P. Chlorine in coal: A review. *Int. J. Coal Geol.* **67**, 127–44 (2006).
[153] Fox, J. M. *Changes in fly ash with thermal threatment. Submitted for consideration in 2005 World of Coal Ash. Cleveland*. (2005).
[154] *CDEM. Folder Topcrete, binder properties. (2003)*.
[155] Murat, M. Hydration reaction and hardening of calcined clays and related minerals. *Cem. Concr. Res.* **13**, 259–66 (1983).
[156] Kinuthia, J. M., Wild, S., Sabir, B. B. & Bai, J. Self-compensating autogenous shrinkage in Portland cement-metakaolin-fly ash pastes. *Adv. Cem. Res.* **12**, 35–43 (2000).
[157] Wild, S., Khatib, J. & Roose, J. L. Chemical and autogenous shrinkage of Portland cement-metakaolin pastes. *Adv. Cem. Res.* **10**, 109–19 (1998).
[158] He, C., Osbaeck, B. & Makovicky, E. Pozzolanic reaction of six principal clay minerals: Activiation reactivity assessment and technological effects. *Cem. Concr. Res.* **25**, 1691–702 (1995).
[159] Zhang, M. H. & Malhotra, V. M. Characteristics of a thermally activated alumino-silicate pozzolanic material and its use in concrete. *Cem. Concr. Res.* **25**, 1713–25 (1995).
[160] Mehta, P. K. Testing and Correlation of Fly Ash Properties with Respect of Pozzolanic Behavior, EPRI, Palo Alto. (1984).
[161] Diamond, S. Fly Ash Concrete for Highway Use: Executive Summary. Publication FHWA/IN/JHRP-88/08-2. Joint High way Research Project, Indiana Department of Transportation a nd Purdue University, West Lafayette , Indiana. (1988).
[162] De Weerdt, K., Kjellsen, K. O., Sellevold, E. & Justnes, H. Synergy between fly ash and limestone powder in ternary cements. *Cem. Concr. Compos.* **33**, 30–38 (2011).

[163] De Weerdt, K., Ben Haha, Le Saout, G., Kjellsen, K.O., Justnes, H. & Lothenbach, B. Hydration mechanisms of ternary Portland cements containing limestone powder and fly ash. *Cem. Concr. Res.* **41**, 279–291 (2011).
[164] De Weerdt, K., Justnes, H., Lothenbach, B. & Ben Haha, M. The effect of limestone powder additions on strength and microstructure of fly ash blended cements. *Proc. 13th Int. Congr. Chem. Cem.* 219 (2011).
[165] Chimenos, J. M., Segarra, M., Fernandez, M. A. & Espiell, F. Characterization of the bottom ash in municipal solid waste incinerator. *J. Hazard. Mater.* **64**, 211–222 (1999).
[166] Müller, U. & Rübner, K. The microstructure of concrete made with municipal waste incinerator bottom ash as an aggregate component. *Cem. Concr. Res.* **36**, 1434–1443 (2006).
[167] Tang, P., Florea, M. V. A. & Brouwers, H. J. H. The characterization of MSWI bottom ash. *18th Int. Conf. Build. Mater. (IBAUSIL), Weimar* 2–1192–2–1199 (2012).
[168] Al-Rawas, A. A., Wahid Hago, A., Taha, R. & Al-Kharousi, K. Use of incinerator ash as a replacement for cement and sand in cement mortars. *Build. Environ.* **40**, 1261–1266 (2005).
[169] Pera, J., Coutaz, L., Ambroise, J. & Chababbet, M. Use of incinerator bottom ash in concrete. *Cem. Concr. Res.* **27**, 1–5 (1997).
[170] Siddique, R. Use of municipal solid waste ash in concrete. *Resour. Conserv. Recycl.* **55**, 83–91 (2010).
[171] Courard, L., Degeimbre, R., Laval, A.-L., Dupont, L. & Bertrand, L. Utilisation des mâchefers d'incinérateur d'ordures ménagères dans la fabrication de pavés en béton. *Mater. Struct.* **35**, 365–372 (2002).
[172] Sabbas, T., Polettini, A., Pomi, R., Klein, R. & Lechner, P. Management of municipal solid waste incineration residues. *Waste Manag.* **23**, 61–88 (2003).
[173] Santos, R. M., Mertens, G., Salman, M., Cizer, Ö. & Van Gerven, T. Comparative study of ageing, heat treatment and accelerated carbonation for stabilization of municipal solid waste incineration bottom ash in view of reducing regulated heavy metal/metalloid leaching. *J. Environ. Manage.* **128**, 807–821 (2013).
[174] Mangialardi, T. Disposal of MSWI fly ash through a combined washing-immobilisation process. *J. Hazard. Mater.* **98**, 225–240 (2003).
[175] Stekette, J. J., Duzijn, R. F. & Born, J. G. P. Quality improvement of MSWI bottom ash by enhanced aging, washing and combination processes. *Stud. Environ. Sci.* **71**, 12–23 (1997).
[176] Cioffi, R., Colangelo, F., Montagnaro, F. & Santaro, L. Manufacture of artificial aggregate using MSWI bottom ash. *Waste Manag.* **31**, 281–288 (2011).
[177] Cossu, R., Lai, T. & Pivnenko, K. Waste washing pre-treatment of municipal and special waste. *J. Hazard. Mater.* **207**, 65–72 (2012).
[178] EN 7375 Uitloogkarakteristieken - Bepaling van de uitloging van anorganische componenten uit vormgegeven en monolitische materialen met een diffusieproef - Vaste grond- en steenachtige materialen. (2004).
[179] Aubert, J. E., Husson, B. & Vaquier, A. Metallic aluminum in MSWI fly ash: quantification and influence on the properties of cement-based products. *Waste Manag.* **24**, 589–596 (2004).
[180] EN 1340 Concrete kerb units — Requirements and test methods. (2003).

List of symbols and abbreviations

Abbreviations

APC	Air Pollution Control
ASR	Alkali-Silica Reactions
BFB	Bubbling Fluidized Bed
C&DW	Construction and Demolition Waste
C&D	Construction and Demolition
CFB	Circulating Fluidized Bed
dcp	Dehydrated cement paste
DDSC	1st derivative of the Differential Scanning Calorimetry signal
DSC	Differential Scanning Calorimetry
DTG	1st derivative of the Thermogravimery signal
EDL	Electrical Double Layer
EDX	Energy-Dispersive X-Ray
FCG	FORZ Composite Granulates
GGBFS	Ground Granulated Blast Furnace Slag
HCP, hcp	Hardened Cement Paste
IBC	Insulation-, Management- and Control- (Isolatie-, Beheers- en Controle)
LOI	Loss On Ignition
MSWI	Municipal Solid Waste Incineration
NS	Norm Sand
OPC	Ordinary Portland Cement
PSD	Particle Size Distribution
PsFA	Paper Sludge Fly Ash
RCA	Recycled Concrete Aggregate
RCF	Recycled Concrete Fines
RCS	Recycled Concrete Sand
SEM	Secondary Electron Microscopy
SSA	Specific Surface Area
SQR	Soil Quality Decree
TG	Thermogravimery
XRD	X-Ray Diffraction
XRF	X-Ray Fluorescence

Symbols

Roman

a’	C/S ratio of C−S−A−H from slag pastes	-
$\bar{a}$	C/S ratio of C−S−A−H from slag-blended cement pastes	-
b’	A/S ratio of C−S−A−H from C−S−H from slag pastes	-
$\bar{b}$	A/S ratio of C−S−A−H from slag-blended cement pastes	-
c	Free chlorides concentration	[mol/l]
C_b^0	Chloride binding capacity of a hydration product	[mg Cl/g hydration product at 11% r.h.]
C_b	Chloride binding capacity of a hydration paste	[mg Cl/g sample at 11% r.h.]
d.m.	Dry matter	-
DW	Dry weight	[g]
d_{10}	Equivalent diameter of sieve on which passing is 10%	[µm]
d_{50}	Equivalent diameter of sieve on which passing is 50%	[µm]
d_{60}	Equivalent diameter of sieve on which passing is 60%	[µm]
d_{80}	Equivalent diameter of sieve on which passing is 80%	[µm]
d_{90}	Equivalent diameter of sieve on which passing is 90%	[µm]
D_{min}	Minimum particle diameter	[µm]
D_{max}	Maximum particle diameter	[µm]
K	material-dependent constant ; measure of the rate of leaching	-
L/S	Liquid to solid ratio	ml/g
M	Mass	[mg]
M	Molar mass	[g/mol]
N	Number of moles	[mol]
r.h.	Relative humidity	[%]
X	Mass fraction	-
w_0/b_0	Water to binder ratio	-

Greek

α	OPC degree of hydration	-
γ	Slag degree of hydration	-

α_F	Chloride binding capacity constant	$[l^{\beta_F}/mol^{\beta_F}]$
β_F	Binding intensity parameter	-
λ	Coefficient for chloride binding of $C-S-H$ from slag pastes	
δ_{C_3S}	C_3S mass fraction in the silicate clinker phases	-
δ_{C_2S}	C_2S mass fraction in the silicate clinker phases	-

Subscript

Cem	Cement
$C-S(-A)-H$	calcium silicate hydrate
E	Model by Elakneswaran et al. [59]
Ettr	Ettringite
H	Model by Hirao et al. [57]
Hp	Hydration product
Spl	Sample
UO	Unreacted Oxides
Z	Model by Zibara [37]

Superscript

Corr	Correction
Dhir	Model by Dhir et al. [85]
Diff	Difference
OPC	Ordinary Portland Cement
Sl	Slag
Total	Sum of OPC and slag components

Appendix 1

Notations in cement chemistry

Al_2O_3	A
CaO	C
CO_2	$\overline{C}$
H_2O	H
Fe_2O_3	F
MgO	M
SiO_2	S
SO_3	$\overline{S}$

Appendix 2

Minerals terminology

AH_3	gibbsite
A_2S	kaolin
$Al_2Si_2O_5(OH)_4$	metakaolin
A_3S_2	mullite
C	lime
CH	portlandite
$C\bar{C}$	calcite
$C\bar{S}$	anhydrite
$C\bar{S}H_{0.5}$	hemihydrate
$C\bar{S}H_2$	gypsum
C_2AS	gehlenite
C_2ASH_8	strätlingite
C_2S	belite
C_3A	tricalcium aluminate
$C_3A{\bullet}CaCl_2{\bullet}10H_2O$	Friedel's salt
$C_3A{\bullet}1/2CaCl_2{\bullet}1/2CaSO_4{\bullet}10H_2O$	Kuzel's salt
C_3AH_6	hydrogarnet
C_3S	alite
$C_4A\bar{S}H_{12}$	monosulphate tetracalcium aluminate hydrate (SO_4-AFm)
C_4AF	ferrite
C_4AH_{13}	tetracalcium aluminate hydrate ($HO-AFm$)
$C_6AFS_2H_8$	hydrogarnet
M_5AH_{13}	hydrotalcite
$C_6A\bar{S}_3H_{32}$	Ettringite (trisulphate tetracalcium aluminate hydrate, AFt)
FH_3	iron hydroxide
S	quartz

List of publications

Refereed Journal

Florea, M.V.A., Ning, Z. & Brouwers, H.J.H. Activation of liberated concrete fines and their application in mortars. *Constr. Build. Mater.* **50**, 1–12 (2014).

Florea, M.V.A. & Brouwers, H.J.H. Properties of various size fractions of crushed concrete related to process conditions and re-use. *Cem. Concr. Res.* **52**, 11–21 (2013).

Florea, M.V.A. & Brouwers, H.J.H. Chloride binding related to hydration products: slag-blended cements. *Under review in Constr. Build. Mater.* (2014).

Florea, M.V.A. & Brouwers, H.J.H. Chloride binding related to hydration products Part I: Ordinary Portland Cement. *Cem. Concr. Res.* **42**, 282–290 (2012).

Tang, P., Florea, M.V.A. & Brouwers, H.J.H. Investigation of municipal solid waste incineration bottom ash properties related to particle size. *To be submitted.*

Doudart de la Grée, G.C.H., Florea, M.V.A. & Brouwers, H.J.H. Upgrade and application of bio-energy fly ashes. *In preparation.*

Florea, M.V.A., Keulen, A. & Brouwers, H.J.H. The use of MSWI bottom ash in concrete mixtures. *In preparation.*

Professional

Florea, M.V.A. & Brouwers, H.J.H. Slim breken sluit materiaalkringloop. *Cement* 74 – 78 (2013).

Conference

Florea, M.V.A., Doudart de la Grée, G.C.H. & Brouwers, H.J.H. Paper sludge fly ash - From Industrial wastes to new cementitious mixes. *1st Int. Conf. Chem. Constr. Mater. Berlin* 479–482 (2013).

Doudart de la Grée, G.C.H., Florea, M.V.A. & Brouwers, H.J.H. Physical-chemical upgrading and use of bio-energy fly ashes as building material. *1st Int. Conf. Chem. Constr. Mater. Berlin* 23–26 (2013).

Florea, M.V.A. & Brouwers, H.J.H. The influence of crushing method on recycled concrete properties. *Int. Conf. Adv. Cem. Concr. Technol. Africa, Johannesburg.* 1041–1050 (2013).

Florea, M.V.A., Ning, Z. & Brouwers, H.J.H. Treatment and application of recycled concrete fines properties. *Int. Conf. Adv. Cem. Concr. Technol. Africa, Johannesburg.* 585–592 (2013).

Kumaran, G.S., Msinjili, N.S., Florea, M.V.A., Schmidt, W. & Nibasumba, P. A study on sustainable energy for cement industries in Rwanda. *Int. Conf. Adv. Cem. Concr. Technol. Africa, Johannesburg.* 1169–1175 (2013).

Buregyeya, A., Quercia Bianchi, G., Spiesz, P.R., Florea, M.V.A. & Nassingwa, R. Exploratory characterization of volcanic ash sourced from Uganda as a pozzolanic material in portland cement concrete properties. *Int. Conf. Adv. Cem. Concr. Technol. Africa, Johannesburg.* 97–104 (2013).

Tang, P., Florea, M.V.A. & Brouwers, H.J.H. The characterization of MSWI bottom ash. *18th Int. Conf. Build. Mater. (IBAUSIL), Weimar.* 1192–1199 (2012).

Florea, M.V.A. & Brouwers, H.J.H. Recycled concrete fines and aggregates : the composition of various size fractions related to crushing history. *18th Int. Conf. Build. Mater. (IBAUSIL), Weimar.* 1034–1041 (2012).

Keulen, A., Florea, M.V.A. & Brouwers, H.J.H. Upgrading MSWI bottom ash as building material for concrete mixes. *18th Int. Conf. Build. Mater. (IBAUSIL), Weimar.* 545–553 (2012).

Sabai, M.M., Florea, M.V.A., Mato, R.R.A.M. & Brouwers, H.J.H., Egmond - de Wilde De Ligny, E.L.C. & Lichtenberg, J.J.N. Investigation on the possibilities for recycling construction and demolition waste in to building materials in Tanzania. *Proc. EurAsia Waste Manag. Symp. Istanbul* 1–5 (2011).

Florea, M.V.A. & Brouwers, H.J.H. On the application of MSWI bottom ash as aggregate-replacement in concrete mixes. *Proc. EurAsia Waste Manag. Symp. Istanbul* 187–195 (2011).

Florea, M.V.A., Schmidt, W., Msinjili, N.S., Uzoegbo, H.C., Stipanovic,nuon Oslakovic, I., Brouwers, H.J.H., Kuehne, H.C. & Rogge, A. Recent developments and perspectives regarding the standardization and quality surveillance of cement in the East, Central and South African region. *12th Int. Congr. Chem. Cem. Madrid* (2011).

Florea, M.V.A. & Brouwers, H.J.H. Chloride binding related to hydration products Part I: Ordinary Portland Cement. *4th Int. RILEM PhD Student Work. Model. Durab. Reinf. Concr. Madrid* (2010).

Florea, M.V.A. & Brouwers, H.J.H. Free and bound chloride contents in cementitious materials. *8th fib Int. PhD Symp. Civ. Eng. Lyngby* (2010).

Florea, M.V.A. & Brouwers, H.J.H. Chloride binding in OPC hydration products. *17th Int. Conf. Build. Mater. (IBAUSIL), Weimar* (2009).

Florea, M.V.A. & Brouwers, H.J.H. Chloride binding in OPC hydration products. *3rd Int. RILEM PhD Student Work. Model. Durab. Reinf. Concr. Guimaraes* (2009).

Florea, M.V.A. & Jitaru, I. Ternary compounds of Cadmium with nucleobases. *Jr. Euromat Conf. Lausanne* (2004).

Florea, M.V.A. & Bogdan, D. Using educational software in teaching chemistry. *Int. Conf. South Eur. Chem. Soc. Belgrade* (2004).

Florea, M.V.A. & Bodgan, D. Volatile oils from Salvia Officinalis. *Rom. Conf. Chem. Chem. Eng. Bucharest* (2003).

Summary

The production of clinker in cement factories is a prominent source of CO_2 emissions; therefore, the replacement of cement with other supplementary cementitious materials in concrete mixes is beneficial for the environment. Moreover, using waste products to replace concrete components brings a new dimension by reducing the amount of natural raw materials needed. Examples of such replacement materials are recycled concrete aggregates and municipal solid waste incineration bottom ash for the larger particles needed for concrete, and fly ashes, ground slags, sludges and recycled concrete fines for the replacement of the cement. One of the drawbacks of using industrial by-products in concrete is their relatively high concentration in unwanted constituents, like chlorides, sulphates, or some heavy metals. While the latter are known to be bound by the cementitious matrix sufficiently, chlorides are the main cause of structural damage in reinforced concrete structures. Therefore, modelling the chloride binding ability of the cementitious matrix becomes of high importance, mainly in marine environments.

The first part of the research deals with modelling, correlating the total amount of chloride bound in concrete with the amounts bound by different hydration products. New insights in the quantities of the hydration products formed are used in order to predict the phase assemblage of hardened cement pastes. The two main chloride binding mechanisms are considered – through physical adsorption and through chemical reactions. An improved hydration model of slag-blended cements, taking into account new insights, is used to estimate and quantify the hydration products of slag-blended cements. Individual chloride binding isotherms are used to correlate these amounts of hydration products with the amount of bound chlorides.

The next part of the study focuses on replacing cement by other supplementary fine materials. The first aim is to use recycled concrete fines in new mortar recipes. A thermal treatment is employed to activate the material, which is then applied in mixtures containing plain ordinary Portland cement or fly-ash and slag-blended cements. Another investigation is conducted with the scope to apply four different bio-energy fly ashes from bio-energy power plants in concrete mixtures. The roles of this type of fly ash in a concrete mixture as a binder (partly or totally replacing cement) or filler are investigated. By using different treatment techniques like crushing, thermally and water treating bio-energy fly ash, the materials become comparable with commercial fly ash. Another type of incineration product that is studies is paper sludge fly ash. In this case, the challenges for use in concrete are the increased water demand and content of free lime, which reduce the properties of concrete. It is found that paper sludge fly ash has a positive effect on coal combustion fly ash and can by this increase its own utilization.

The final part of the study deals the replacement of larger-sized particles in mortar and concrete mixtures. The properties (particle size distribution, density, thermal treatment

reaction, oxide and mineralogical composition) of a large number of recycled concrete fractions, obtained through three crushing methods, are investigated. The use of recycled concrete sand, i.e. particle sizes between 150 μm and 2 mm, in new mortar is proven to be promising when the right crushing technique is adopted. The use of municipal solid waste incineration bottom ash with sizes between 2 and 40 mm is investigated in different types of concrete recipes and a pilot test is concluded with promising results.

Samenvatting

De productie van klinker in cementfabrieken is een belangrijke bron van CO_2-uitstoot. Hierdoor is de vervanging van cement door toegevoegde cementachtige materialen in betonmengsels gunstig voor het milieu. Bovendien zorgt het gebruik van afvalmaterialen voor de vervanging van betonbestandsdelen voor een additionele dimensie door het verminderen van de benodigde hoeveelheden natuurlijke grondstoffen. Voorbeelden van dergelijke vervangingsmaterialen zijn gerecyclede betonaggregaten en bodemassen van de huisvuilverbranding voor de grovere deeltjes in het beton, en vliegassen, bodemslakken, baggerspecie en fijne fractie van gerecyclede beton voor de vervanging van cement. Eén van de nadelen van het gebruik van industriële bijproducten in beton zijn hun relatief hoge concentraties van ongewenste bestandsdelen, zoals chlorides, sulfaten of sommige zware metalen. Terwijl van de laatste bekend is dat zij voldoende kunnen worden gebonden door de cementmatrix, chlorides zijn de belangrijkste oorzaak van constructieschade in gewapend betonconstructies. Daarom is de modellering van de chloride bindingscapaciteit van de cementmatrix van groot belang, vooral in maritieme omgevingen.

Het eerste deel van het onderzoek behandelt de modellering, met name de correlatie van de totale hoeveelheid gebonden chloride in beton aan de hoeveelheden gebonden door de verschillende hydratatieproducten. Nieuwe inzichten in de hoeveelheden van de gevormde hydratatieproducten zijn toegepast voor de voorspelling van de samenstelling van de uitgeharde cementpasta. De twee voornaamste chloride bindingsmechanismen die zijn beschouwd zijn fysische adsorptie en chemische reacties. Een verbeterd hydratatiemodel van slak cementen, dat rekening met deze nieuwe inzichten houdt, is toegepast voor het schatten en kwantificeren van de hydratatieproducten van slakcementen. Individuele chloride binding isothermen zijn gebruikt voor de correlatie van de deze hoeveelheden hydratatieproducten met het gebonden chloridengehalte.

Het volgende deel van de studie focust op de vervanging van cement door toegevoegde fijne materialen. Het eerste doel is om de fijne fractie van gerecyclede beton te gebruiken in nieuwe mortelrecepten. Een thermische behandeling is aangewend om het materiaal te activeren, waarna het is toegepast in mengsels die reguliere Portlandcement (CEM I) of poederkool vliegas- en slakcement bevatten. Een ander onderzoek is uitgevoerd met het doel om vier verschillende bio-energie vliegassen van bio-energiecentrales toe te passen in betonmengsels. De twee mogelijke rollen van dit type vliegas in een betonmengsel, als een binder (gedeeltelijk of volledige cementvervanger) of als een vuller, zijn onderzocht. Door het gebruik van verschillende behandelingstechnieken zoals breken, thermisch en nat behandelen van bio-energie vliegas, worden deze materialen vergelijkbaar met commerciële poederkoolvliegas. Een ander type verbrandingsproduct dat is bestudeerd is papierresidu vliegas. In dit geval zijn de uitdagingen voor de toepassing in beton de

verhoogde watervraag en de vrije kalk aanwezigheid, welke beide de eigenschappen van beton verslechteren. Het is naar voren gekomen dat papierresidu vliegas een positief effect heeft op poederkool vliegas en daarmee is de toepasbaarheid groter.
Het laatste deel van het onderzoek behandelde de vervanging van deeltjes met een grotere afmeting in mortelmengsels. De eigenschappen (korrelgrootteverdeling, dichtheid, thermische behandelingsreactie, oxiden- en mineralogische samenstelling) van een groot aantal gerecyclede betonfracties, verkregen door drie brekingsmethoden, zijn onderzocht. Van het gebruik van gerecyclede betonzand, d.w.z. korrelgrootte tussen 150 μm en 2 mm, in nieuw mortel is vastgesteld dat het veelbelovend is wanneer de correcte breekmethode is toegepast. Het gebruik van bodemas van huisvuilverbranding met een grootte tussen de 2 en 40 mm is onderzocht door middel van verschillende typen van betonrecepturen en een pilottest. Dit onderzoek is afgesloten met veelbelovende resultaten.

About the author

Personal data

Name:	Miruna Victoria Alexandra (Marinescu) Florea
Date of birth:	13 November 1984
Place of birth:	Bucharest, Romania

Education

2012-present	Researcher, Eindhoven University of Technology, Department of the Built Environment
2009 –2012	PhD student, Eindhoven University of Technology, Department of the Built Environment
2008 – 2009	PhD student, Twente University, Faculty of Engineering Technology

Research

2003 – 2008	Engineering Diploma at the Polytechnic University of Bucharest, Applied Chemistry and Materials Science Faculty
2007	SOCRATES/ERASMUS Student at Ecole Nationale Supérieure d'Ingénieurs de Limoges, Specialty: Material Science
1999 – 2003	"Mihai Viteazul" National College

Bouwstenen is een publikatiereeks van de Faculteit Bouwkunde, Technische Universiteit Eindhoven. Zij presenteert resultaten van onderzoek en andere aktiviteiten op het vakgebied der Bouwkunde, uitgevoerd in het kader van deze Faculteit.

Bouwstenen zijn telefonisch te bestellen op nummer
040 - 2472383

Kernredaktie
MTOZ

Reeds verschenen in de serie
Bouwstenen

nr 1
Elan: A Computer Model for Building Energy Design: Theory and Validation
Martin H. de Wit
H.H. Driessen
R.M.M. van der Velden

nr 2
Kwaliteit, Keuzevrijheid en Kosten: Evaluatie van Experiment Klarendal, Arnhem
J. Smeets
C. le Nobel
M. Broos
J. Frenken
A. v.d. Sanden

nr 3
Crooswijk: Van 'Bijzonder' naar 'Gewoon'
Vincent Smit
Kees Noort

nr 4
Staal in de Woningbouw
Edwin J.F. Delsing

nr 5
Mathematical Theory of Stressed Skin Action in Profiled Sheeting with Various Edge Conditions
Andre W.A.M.J. van den Bogaard

nr 6
Hoe Berekenbaar en Betrouwbaar is de Coëfficiënt k in x-ksigma en x-ks?
K.B. Lub
A.J. Bosch

nr 7
Het Typologisch Gereedschap: Een Verkennende Studie Omtrent Typologie en Omtrent de Aanpak van Typologisch Onderzoek
J.H. Luiten

nr 8
Informatievoorziening en Beheerprocessen
A. Nauta
Jos Smeets (red.)
Helga Fassbinder (projectleider)
Adrie Proveniers
J. v.d. Moosdijk

nr 9
Strukturering en Verwerking van Tijdgegevens voor de Uitvoering van Bouwwerken
ir. W.F. Schaefer
P.A. Erkelens

nr 10
Stedebouw en de Vorming van een Speciale Wetenschap
K. Doevendans

nr 11
Informatica en Ondersteuning van Ruimtelijke Besluitvorming
G.G. van der Meulen

nr 12
Staal in de Woningbouw, Korrosie-Bescherming van de Begane Grondvloer
Edwin J.F. Delsing

nr 13
Een Thermisch Model voor de Berekening van Staalplaatbetonvloeren onder Brandomstandigheden
A.F. Hamerlinck

nr 14
De Wijkgedachte in Nederland: Gemeenschapsstreven in een Stedebouwkundige Context
K. Doevendans
R. Stolzenburg

nr 15
Diaphragm Effect of Trapezoidally Profiled Steel Sheets: Experimental Research into the Influence of Force Application
Andre W.A.M.J. van den Bogaard

nr 16
Versterken met Spuit-Ferrocement: Het Mechanische Gedrag van met Spuit-Ferrocement Versterkte Gewapend Betonbalken
K.B. Lubir
M.C.G. van Wanroy

nr 17
De Tractaten van Jean Nicolas Louis Durand
G. van Zeyl

nr 18
Wonen onder een Plat Dak: Drie Opstellen over Enkele Vooronderstellingen van de Stedebouw
K. Doevendans

nr 19
Supporting Decision Making Processes: A Graphical and Interactive Analysis of Multivariate Data
W. Adams

nr 20
Self-Help Building Productivity: A Method for Improving House Building by Low-Income Groups Applied to Kenya 1990-2000
P. A. Erkelens

nr 21
De Verdeling van Woningen: Een Kwestie van Onderhandelen
Vincent Smit

nr 22
Flexibiliteit en Kosten in het Ontwerpproces: Een Besluitvormingondersteunend Model
M. Prins

nr 23
Spontane Nederzettingen Begeleid: Voorwaarden en Criteria in Sri Lanka
Po Hin Thung

nr 24
Fundamentals of the Design of Bamboo Structures
Oscar Arce-Villalobos

nr 25
Concepten van de Bouwkunde
M.F.Th. Bax (red.)
H.M.G.J. Trum (red.)

nr 26
Meaning of the Site
Xiaodong Li

nr 27
Het Woonmilieu op Begrip Gebracht: Een Speurtocht naar de Betekenis van het Begrip 'Woonmilieu'
Jaap Ketelaar

nr 28
Urban Environment in Developing Countries
editors: Peter A. Erkelens
George G. van der Meulen (red.)

nr 29
Stategische Plannen voor de Stad: Onderzoek en Planning in Drie Steden
prof.dr. H. Fassbinder (red.)
H. Rikhof (red.)

nr 30
Stedebouwkunde en Stadsbestuur
Piet Beekman

nr 31
De Architectuur van Djenné: Een Onderzoek naar de Historische Stad
P.C.M. Maas

nr 32
Conjoint Experiments and Retail Planning
Harmen Oppewal

nr 33
Strukturformen Indonesischer Bautechnik: Entwicklung Methodischer Grundlagen für eine 'Konstruktive Pattern Language' in Indonesien
Heinz Frick arch. SIA

nr 34
Styles of Architectural Designing: Empirical Research on Working Styles and Personality Dispositions
Anton P.M. van Bakel

nr 35
Conjoint Choice Models for Urban Tourism Planning and Marketing
Benedict Dellaert

nr 36
Stedelijke Planvorming als Co-Produktie
Helga Fassbinder (red.)

nr 37
Design Research in the Netherlands
editors: R.M. Oxman
M.F.Th. Bax
H.H. Achten

nr 38
Communication in the Building Industry
Bauke de Vries

nr 39
Optimaal Dimensioneren van Gelaste Plaatliggers
J.B.W. Stark
F. van Pelt
L.F.M. van Gorp
B.W.E.M. van Hove

nr 40
Huisvesting en Overwinning van Armoede
P.H. Thung
P. Beekman (red.)

nr 41
Urban Habitat: The Environment of Tomorrow
George G. van der Meulen
Peter A. Erkelens

nr 42
A Typology of Joints
John C.M. Olie

nr 43
Modeling Constraints-Based Choices for Leisure Mobility Planning
Marcus P. Stemerding

nr 44
Activity-Based Travel Demand Modeling
Dick Ettema

nr 45
Wind-Induced Pressure Fluctuations on Building Facades
Chris Geurts

nr 46
Generic Representations
Henri Achten

nr 47
Johann Santini Aichel: Architectuur en Ambiguiteit
Dirk De Meyer

nr 48
Concrete Behaviour in Multiaxial Compression
Erik van Geel

nr 49
Modelling Site Selection
Frank Witlox

nr 50
Ecolemma Model
Ferdinand Beetstra

nr 51
Conjoint Approaches to Developing Activity-Based Models
Donggen Wang

nr 52
On the Effectiveness of Ventilation
Ad Roos

nr 53
Conjoint Modeling Approaches for Residential Group preferences
Eric Molin

nr 54
Modelling Architectural Design Information by Features
Jos van Leeuwen

nr 55
A Spatial Decision Support System for the Planning of Retail and Service Facilities
Theo Arentze

nr 56
Integrated Lighting System Assistant
Ellie de Groot

nr 57
Ontwerpend Leren, Leren Ontwerpen
J.T. Boekholt

nr 58
Temporal Aspects of Theme Park Choice Behavior
Astrid Kemperman

nr 59
Ontwerp van een Geïndustrialiseerde Funderingswijze
Faas Moonen

nr 60
Merlin: A Decision Support System for Outdoor Leisure Planning
Manon van Middelkoop

nr 61
The Aura of Modernity
Jos Bosman

nr 62
Urban Form and Activity-Travel Patterns
Daniëlle Snellen

nr 63
Design Research in the Netherlands 2000
Henri Achten

nr 64
Computer Aided Dimensional Control in Building Construction
Rui Wu

nr 65
Beyond Sustainable Building
editors: Peter A. Erkelens
Sander de Jonge
August A.M. van Vliet
co-editor: Ruth J.G. Verhagen

nr 66
Das Globalrecyclingfähige Haus
Hans Löfflad

nr 67
Cool Schools for Hot Suburbs
René J. Dierkx

nr 68
A Bamboo Building Design Decision Support Tool
Fitri Mardjono

nr 69
Driving Rain on Building Envelopes
Fabien van Mook

nr 70
Heating Monumental Churches
Henk Schellen

nr 71
Van Woningverhuurder naar Aanbieder van Woongenot
Patrick Dogge

nr 72
Moisture Transfer Properties of Coated Gypsum
Emile Goossens

nr 73
Plybamboo Wall-Panels for Housing
Guillermo E. González-Beltrán

nr 74
The Future Site-Proceedings
Ger Maas
Frans van Gassel

nr 75
Radon transport in Autoclaved Aerated Concrete
Michel van der Pal

nr 76
The Reliability and Validity of Interactive Virtual Reality Computer Experiments
Amy Tan

nr 77
Measuring Housing Preferences Using Virtual Reality and Belief Networks
Maciej A. Orzechowski

nr 78
Computational Representations of Words and Associations in Architectural Design
Nicole Segers

nr 79
Measuring and Predicting Adaptation in Multidimensional Activity-Travel Patterns
Chang-Hyeon Joh

nr 80
Strategic Briefing
Fayez Al Hassan

nr 81
Well Being in Hospitals
Simona Di Cicco

nr 82
Solares Bauen: Implementierungs- und Umsetzungs-Aspekte in der Hochschulausbildung in Österreich
Gerhard Schuster

nr 83
Supporting Strategic Design of Workplace Environments with Case-Based Reasoning
Shauna Mallory-Hill

nr 84
ACCEL: A Tool for Supporting Concept Generation in the Early Design Phase
Maxim Ivashkov

nr 85
Brick-Mortar Interaction in Masonry under Compression
Ad Vermeltfoort

nr 86
Zelfredzaam Wonen
Guus van Vliet

nr 87
Een Ensemble met Grootstedelijke Allure
Jos Bosman
Hans Schippers

nr 88
On the Computation of Well-Structured Graphic Representations in Architectural Design
Henri Achten

nr 89
De Evolutie van een West-Afrikaanse Vernaculaire Architectuur
Wolf Schijns

nr 90
ROMBO Tactiek
Christoph Maria Ravesloot

nr 91
External Coupling between Building Energy Simulation and Computational Fluid Dynamics
Ery Djunaedy

nr 92
Design Research in the Netherlands 2005
editors: Henri Achten
Kees Dorst
Pieter Jan Stappers
Bauke de Vries

nr 93
Ein Modell zur Baulichen Transformation
Jalil H. Saber Zaimian

nr 94
Human Lighting Demands: Healthy Lighting in an Office Environment
Myriam Aries

nr 95
A Spatial Decision Support System for the Provision and Monitoring of Urban Greenspace
Claudia Pelizaro

nr 96
Leren Creëren
Adri Proveniers

nr 97
Simlandscape
Rob de Waard

nr 98
Design Team Communication
Ad den Otter

nr 99
Humaan-Ecologisch Georiënteerde Woningbouw
Juri Czabanowski

nr 100
Hambase
Martin de Wit

nr 101
Sound Transmission through Pipe Systems and into Building Structures
Susanne Bron-van der Jagt

nr 102
Het Bouwkundig Contrapunt
Jan Francis Boelen

nr 103
A Framework for a Multi-Agent Planning Support System
Dick Saarloos

nr 104
Bracing Steel Frames with Calcium Silicate Element Walls
Bright Mweene Ng'andu

nr 105
Naar een Nieuwe Houtskeletbouw
F.N.G. De Medts

nr 108
Geborgenheid
T.E.L. van Pinxteren

nr 109
Modelling Strategic Behaviour in Anticipation of Congestion
Qi Han

nr 110
Reflecties op het Woondomein
Fred Sanders

nr 111
On Assessment of Wind Comfort by Sand Erosion
Gábor Dezsö

nr 112
Bench Heating in Monumental Churches
Dionne Limpens-Neilen

nr 113
RE. Architecture
Ana Pereira Roders

nr 114
Toward Applicable Green Architecture
Usama El Fiky

nr 115
Knowledge Representation under Inherent Uncertainty in a Multi-Agent System for Land Use Planning
Liying Ma

nr 116
Integrated Heat Air and Moisture Modeling and Simulation
Jos van Schijndel

nr 117
Concrete Behaviour in Multiaxial Compression
J.P.W. Bongers

nr 118
The Image of the Urban Landscape
Ana Moya Pellitero

nr 119
The Self-Organizing City in Vietnam
Stephanie Geertman

nr 120
A Multi-Agent Planning Support System for Assessing Externalities of Urban Form Scenarios
Rachel Katoshevski-Cavari

nr 121
Den Schulbau Neu Denken, Fühlen und Wollen
Urs Christian Maurer-Dietrich

nr 122
Peter Eisenman Theories and Practices
Bernhard Kormoss

nr 123
User Simulation of Space Utilisation
Vincent Tabak

nr 125
In Search of a Complex System Model
Oswald Devisch

nr 126
Lighting at Work: Environmental Study of Direct Effects of Lighting Level and Spectrum on Psycho-Physiological Variables
Grazyna Górnicka

nr 127
Flanking Sound Transmission through Lightweight Framed Double Leaf Walls
Stefan Schoenwald

nr 128
Bounded Rationality and Spatio-Temporal Pedestrian Shopping Behavior
Wei Zhu

nr 129
Travel Information: Impact on Activity Travel Pattern
Zhongwei Sun

nr 130
Co-Simulation for Performance Prediction of Innovative Integrated Mechanical Energy Systems in Buildings
Marija Trčka

nr 131
Allemaal Winnen
M.J. Bakker

nr 132
Architectural Cue Model in Evacuation Simulation for Underground Space Design
Chengyu Sun

nr 133
Uncertainty and Sensitivity Analysis in Building Performance Simulation for Decision Support and Design Optimization
Christina Hopfe

nr 134
Facilitating Distributed Collaboration in the AEC/FM Sector Using Semantic Web Technologies
Jacob Beetz

nr 135
Circumferentially Adhesive Bonded Glass Panes for Bracing Steel Frame in Façades
Edwin Huveners

nr 136
Influence of Temperature on Concrete Beams Strengthened in Flexure with CFRP
Ernst-Lucas Klamer

nr 137
Sturen op Klantwaarde
Jos Smeets

nr 139
Lateral Behavior of Steel Frames with Discretely Connected Precast Concrete Infill Panels
Paul Teewen

nr 140
Integral Design Method in the Context of Sustainable Building Design
Perica Savanović

nr 141
Household Activity-Travel Behavior: Implementation of Within-Household Interactions
Renni Anggraini

nr 142
Design Research in the Netherlands 2010
Henri Achten

nr 143
Modelling Life Trajectories and Transport Mode Choice Using Bayesian Belief Networks
Marloes Verhoeven

nr 144
Assessing Construction Project Performance in Ghana
William Gyadu-Asiedu

nr 145
Empowering Seniors through Domotic Homes
Masi Mohammadi

nr 146
An Integral Design Concept for Ecological Self-Compacting Concrete
Martin Hunger

nr 147
Governing Multi-Actor Decision Processes in Dutch Industrial Area Redevelopment
Erik Blokhuis

nr 148
A Multifunctional Design Approach for Sustainable Concrete
Götz Hüsken

nr 149
Quality Monitoring in Infrastructural Design-Build Projects
Ruben Favié

nr 150
Assessment Matrix for Conservation of Valuable Timber Structures
Michael Abels

nr 151
Co-simulation of Building Energy Simulation and Computational Fluid Dynamics for Whole-Building Heat, Air and Moisture Engineering
Mohammad Mirsadeghi

nr 152
External Coupling of Building Energy Simulation and Building Element Heat, Air and Moisture Simulation
Daniel Cóstola

nr 153
Adaptive Decision Making In Multi-Stakeholder Retail Planning
Ingrid Janssen

nr 154
Landscape Generator
Kymo Slager

nr 155
Constraint Specification in Architecture
Remco Niemeijer

nr 156
A Need-Based Approach to Dynamic Activity Generation
Linda Nijland

nr 157
Modeling Office Firm Dynamics in an Agent-Based Micro Simulation Framework
Gustavo Garcia Manzato

nr 158
Lightweight Floor System for Vibration Comfort
Sander Zegers

nr 159
Aanpasbaarheid van de Draagstructuur
Roel Gijsbers

nr 160
'Village in the City' in Guangzhou, China
Yanliu Lin

nr 161
Climate Risk Assessment in Museums
Marco Martens

nr 162
Social Activity-Travel Patterns
Pauline van den Berg

nr 163
Sound Concentration Caused by Curved Surfaces
Martijn Vercammen

nr 164
Design of Environmentally Friendly Calcium Sulfate-Based Building Materials: Towards an Improved Indoor Air Quality
Qingliang Yu

nr 165
Beyond Uniform Thermal Comfort on the Effects of Non-Uniformity and Individual Physiology
Lisje Schellen

nr 166
Sustainable Residential Districts
Gaby Abdalla

nr 167
Towards a Performance Assessment Methodology using Computational Simulation for Air Distribution System Designs in Operating Rooms
Mônica do Amaral Melhado

nr 168
Strategic Decision Modeling in Brownfield Redevelopment
Brano Glumac

nr 169
Pamela: A Parking Analysis Model for Predicting Effects in Local Areas
Peter van der Waerden

nr 170
A Vision Driven Wayfinding Simulation-System Based on the Architectural Features Perceived in the Office Environment
Qunli Chen

nr 171
Measuring Mental Representations Underlying Activity-Travel Choices
Oliver Horeni

nr 172
Modelling the Effects of Social Networks on Activity and Travel Behaviour
Nicole Ronald

nr 173
Uncertainty Propagation and Sensitivity Analysis Techniques in Building Performance Simulation to Support Conceptual Building and System Design
Christian Struck

nr 174
Numerical Modeling of Micro-Scale Wind-Induced Pollutant Dispersion in the Built Environment
Pierre Gousseau

nr 175
Modeling Recreation Choices over the Family Lifecycle
Anna Beatriz Grigolon

nr 176
Experimental and Numerical Analysis of Mixing Ventilation at Laminar, Transitional and Turbulent Slot Reynolds Numbers
Twan van Hooff

nr 177
Collaborative Design Support: Workshops to Stimulate Interaction and Knowledge Exchange Between Practitioners
Emile M.C.J. Quanjel

nr 178
Future-Proof Platforms for Aging-in-Place
Michiel Brink

nr 179
Motivate: A Context-Aware Mobile Application for Physical Activity Promotion
Yuzhong Lin

nr 180
Experience the City: Analysis of Space-Time Behaviour and Spatial Learning
Anastasia Moiseeva

nr 181
Unbonded Post-Tensioned Shear Walls of Calcium Silicate Element Masonry
Lex van der Meer

nr 182
Construction and Demolition Waste Recycling into Innovative Building Materials for Sustainable Construction in Tanzania
Mwita M. Sabai

nr 183
Durability of Concrete with Emphasis on Chloride Migration
Przemysław Spiesz

nr 184
Computational Modeling of Urban Wind Flow and Natural Ventilation Potential of Buildings
Rubina Ramponi

nr 185
A Distributed Dynamic Simulation Mechanism for Buildings Automation and Control Systems
Azzedine Yahiaoui

nr 186
Modeling Cognitive Learning of Urban Networks in Daily Activity-Travel Behavior
Şehnaz Cenani Durmazoğlu

nr 187
Functionality and Adaptability of Design Solutions for Public Apartment Buildings in Ghana
Stephen Agyefi-Mensah

nr 188
A Construction Waste Generation Model for Developing Countries
Lilliana Abarca-Guerrero

nr 189
Synchronizing Networks: The Modeling of Supernetworks for Activity-Travel Behavior
Feixiong Liao

nr 190
Time and Money Allocation Decisions in Out-of-Home Leisure Activity Choices
Gamze Zeynep Dane

nr 191
How to Measure Added Value of CRE and Building Design
Rianne Appel-Meulenbroek

The production of clinker in cement factories is a prominent source of CO_2 emissions; therefore, the replacement of cement with other supplementary cementitious materials in concrete mixes is beneficial for the environment. Moreover, using waste products to replace concrete components brings a new dimension by reducing the amount of natural raw materials needed. Examples of such replacement materials are recycled concrete aggregates and municipal solid waste incineration bottom ash for the larger particles needed for concrete, and fly ashes, ground slags, sludges and recycled concrete fines for the replacement of the cement. One of the drawbacks of using industrial by-products in concrete is their relatively high concentration in unwanted constituents, like chlorides, sulphates, or some heavy metals. While the latter are known to be bound by the cementitious matrix sufficiently, chlorides are the main cause of structural damage in reinforced concrete structures. Therefore, modelling the chloride binding ability of the cementitious matrix becomes of high importance, mainly in marine environments.

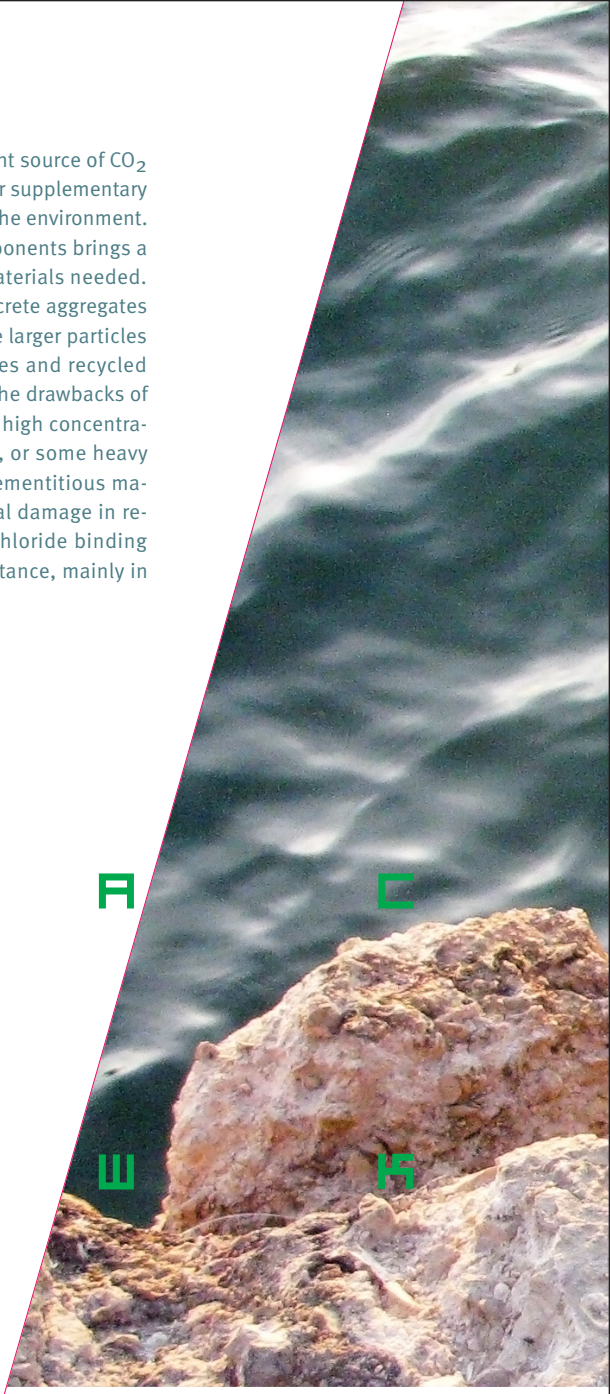

F A C

B W K

E H T

/ Department of the Built Environment

TU/e Technische Universiteit **Eindhoven** University of Technology